Technische Universiteit
Eindhoven
University of Technology

Department of Built Environment
Building Physics and Services

Den Dolech 2, 5612AZ Eindhoven
P.O. Box 513, 5600MB Eindhoven
The Netherlands
www.tue.nl

Cooling of a hot smoke layer by a sprinkler spray

Validation of a CFD-model

7S45M0 – Graduation project Building Physics and Services

Author
N.A.J. (Nick) Tenbült
0961996

Supervisors
Prof. ir. W. Zeiler
Ir. R.A.P. van Herpen FIFireE
Ir. N.J. van Oerle

Date
June 2018

Cooling of a hot smoke layer by a sprinkler spray

Validation of a CFD-model

Author

Name:	N.A.J. (Nick) Tenbült
Student ID:	0961996
Master program:	Architecture, Building and Planning (ABP)
Master track:	Building Physics and Services (BPS)

Supervisors

1st supervisor	Prof. ir. W. (Wim) Zeiler	(TU/e)
2nd supervisor	Ir. R.A.P. (Ruud) van Herpen FIFireE	(TU/e)
3rd supervisor	Ir. N.J. (Jur) van Oerle	(Peutz BV)

Department of Built Environment
Building Physics and Services

Den Dolech 2, 5612AZ Eindhoven
P.O. Box 513, 5600MB Eindhoven
The Netherlands
www.tue.nl

In collaboration with
Peutz BV

Lindenlaan 41, 6584AC Molenhoek
Postbus 66, 6585 ZH Mook
The Netherlands
www.peutz.nl

Eindhoven, June 14th, 2018

Preface

This master thesis is the final product of my graduation project to complete the master program Building Physics and Services at the University of Technology in Eindhoven. The research towards smoke layer cooling by a sprinkler spray has been done in collaboration with Peutz BV.

First of all, I want to thank Peutz BV for making this research possible. Before I started my graduation project I had the desire to perform experiments to validate a computational model and Peutz gave me this unique opportunity. Furthermore, I want to thank Jur van Oerle (Peutz) and David den Boer (Peutz) for their guidance and feedback during the project.

I want to thank Ruud van Herpen and Prof. Wim Zeiler for their feedback and pushing me to bring out the best in me.

Special thanks are for the people in the fire safety lab that supported me during the experiments. I did not only learn a lot from performing my own experiments but also, I learned a lot about performing fire experiments in general.

Finally, I want to thank everyone that supported me in the past year during this graduation project.

Enjoy reading,

Nick Tenbült

Eindhoven, June 2018

Abstract

In this study smoke layer cooling caused by a sprinkler water spray has been studied both experimental and numerical. Only the influence of the sprinkler spray on de smoke layer is studied, the fire is not affected by the sprinkler spray. Heptane pool fires of different sizes are used to obtain a stable smoke layer. The smoke is extracted mechanically by a fan and the dry gases are analysed. From oxygen and carbon dioxide concentrations the oxygen depletion is calculated. This is used to determine the fire's Heat Release Rate (HRR). Furthermore, temperatures of the smoke layer are measured throughout the smoke cabinet. In the centre of the smoke cabinet a sprinkler nozzle is located at a height of 2.9m. A commonly applied pendent sprinkler with a K-factor of 80.6 is activated manually after a stable smoke layer is formed. Different operating pressures were applied to study the cooling effect of an increased water flow rate.

Numerical simulation of a CFD-model is done with Fire Dynamics Simulator (FDS), developed by NIST. The measured HRR is applied in the models for simulating the pool fires. The sprinkler spray pattern that is implemented in the models, is based on the water distribution during bucket tests that have been performed. A spray pattern divides the spherical spray injection surface into more than 300 parts with each different directions and unique water mass fractions.

During the experiments a smoke layer with an average temperature of approximate 200°C was reduced with approximately 50°C, 70°C and 90°C for water flow rates of respectively 56 l/min, 71 l/min and 93 l/min. In all numerical simulations the temperature decrease caused by the sprinkler spray is underpredicted. This underprediction ranges between 30-50% of the measured temperature decrease. Regardless of the level of detail from the sprinkler spray, the models embedded in the FDS code are not capable to predict the temperature decrease of the smoke layer caused by water droplets.

Terminology

Air entrainment
Mixture of (ambient) air into the smoke plume, causing volume increase and dilution of the smoke.

Atomization process
The process of breaking-up a sprinkler water flow into small droplets.

Azimuth angle (ϕ)
The direction of an injected water droplet in the horizontal plane of the sprinkler.

Computational Fluid Dynamics (CFD)
Solving a fluid flow numerically by solving the Navier-Stokes equations within a computational domain of cells.

Cumulative Volume Fraction (CVF)
The fraction of the total water that has been carried by droplets of a specific size range.

Droplet size distribution
Defines the relative number of droplets according to size. Usually, the droplet diameter is used to define droplet ranges, expressed in micrometer.

Droplet trajectory
The path that a water droplet travels within the Cartesian coordinate system, from the sprinkler nozzle to the floor.

Elevation angle (θ)
The direction of an injected water droplet in the vertical plane of the sprinkler.

Fire Dynamics Simulator (FDS)
Open-source software to model low-speed, thermally-driven flows with an emphasis on smoke and heat transport caused by fires [1].

Heat release rate (HRR)
The rate at which energy is released by a fire, expressed in (kilo)Watts.

Large Eddy Simulation (LES)
The transport equations are solved for the large eddies and the small eddies are modelled with an eddy viscosity model (turbulence model).

Operating pressure
Water pressure at the sprinkler nozzle during activation expressed in bar. Lower than pump pressure.

Pump pressure
Water pressure at the sprinkler pump during activation expressed in bar. Higher than operating pressure.

Smoke logging
Diffusing and descending of a smoke layer by a water spray.

Soot yield
The soot yield is the mass ratio between the mass flow of soot particles in the smoke and the mass burning rate of the fuel.

Spray envelope
The outer surface of the volume at which water is injected by a sprinkler nozzle.

Volume median diameter (d_m)
The total volume of the droplets smaller than the median diameter that represents 50% of the total volume.

Nomenclature

Symbol	Unity	Property
A	m^2	Surface
A_f	m^2	Fuel surface
B	N	Buoyancy force
C	m	Approximated radius of wetted floor area
C_d	-	Discharge coefficient
C_D	-	Drag coefficient
C_{sp}	-	Sprinkler constant
D(x)	N	Drag force spherical droplet
d	µm	Diameter of a sphere
d_m	µm	Volume median diameter
d_n	m	Orifice diameter
E	kJ/m^3	Heat release per unit vol. consumed at 298 K
F_d `	N`	Total drag force
g	m/s^2	Gravitational acceleration
h	m	Height of smoke layer
h(d)	$W/m^2.K$	Convective heat transfer coefficient of droplet d
H	%	relative humidity
H_c	MJ/kg	Heat of combustion
k	kg/m	Drag constant of proportionality
k_t	-	Flow velocity profile
k_ρ	-	Reynolds correction for bi-directional probe
K	lpm√bar	K-factor
m	kg	Mass
$\dot{m}$	kg/s	Mass flow rate through sprinkler
$\dot{m}^{n''}$	kg/m^2s	Burning rate fuel per square meter
Nu	-	Nusselt number
p	bar	Pressure
Pr	-	Prandtl number
$\dot{Q}$	kW	Heat flow
Q_c	kJ	Heat transferred from smoke to droplets
Re	-	Reynolds number
RTI	$ms^{1/2}$	Response Time Index
T	K	Temperature (w=water, s=smoke, a=ambient)
U_{sp}	m/s	Velocity when water leaves sprinkler
v	m/s	Velocity
$\dot{V}$	m^3/s	Volumetric flow rate
V_{298}	m^3/s	Volumetric flow rate, normalized for 298K
Vol	m^3	Cone volume of sprinkler spray envelope
W_e	-	Weber number
$x_a{}^{02}$	-	Ambient mole fraction of oxygen
xO_2	-	Oxygen concentration in mole fraction
xCO_2	-	Carbon dioxide concentration in mole fraction

Greek symbols

ρ	kg/m^3	Density
σ_w	N/m^2	Surface tension water
ϕ	-	Oxygen depletion factor
χ	-	Combustion efficiency
υ	m^2/s	Kinematic viscosity

Table of Contents

1 Introduction

1.1 Problem statement

Nowadays, sprinkler systems are more often installed in Dutch buildings. According to the Dutch Building Code this kind of systems are not mandatory and are applied as an equivalent solution to the regulations of the Building Code to make fire compartments larger than 1000m^2, build higher than 70 meters, reduce the fire resistance of the main construction and to allow longer distances for escape routes. For the design of sprinkler systems usually NEN-EN 12845+A2+NEN 1073, FM standard and/or the NFPA 13 standard are used. The main objective of sprinkler systems is to suppress the fire and to keep it controllable. In particular cases, it is desired to even extinguish the fire. By suppressing a fire the fire growth and fire spread are reduced or stopped in order to make an offensive attack by the fire brigade possible, to protect property and to assure safe evacuation of building occupants [2].

Fire suppression by a sprinkler spray can be distinguished in three regions, namely the interference of water droplets with the fire plume (flame), smoke plume and smoke layer. The influence of water droplets on the smoke layer has been studied by several researchers with numerical models and experiments to validate the models. In 2010 Li et al. studied the drag effect of water droplets on the smoke layer in order to determine the effectiveness of natural smoke vents during sprinkler activation. The predictive models showed that increasing the water pressure of the sprinkler system results in less effective smoke venting, these results were validated with experiments [3]. The cooling effect of water droplets has been studied by Li et al. [4]. They concluded that the volumetric flow rate of smoke going upwards decreases under sprinkler spray due to the cooling effect of the water droplets [4]. Although both studies claim that their experimental results correspond well with their predictive models, CFD-models with sprinklers must be carefully used. A similar study performed by den Boer showed that with CFD-models the predicted smoke layer is too thick. Besides, cooling of the smoke layer is underpredicted and the flow patterns of the spill plume are inaccurate [5]. So far, numerical simulations are done with an evenly distributed water mass and velocity within the spray envelope. However, studies by Sheppard (2002) and van Venrooij (2016) indicate that for both elevation angle and azimuth angle irregular distribution of water occurs, which is strongly dependent on the nozzle's geometry [6], [7]. Further development of the CFD-models and gaining more experimental data is required to validate the CFD-models.

1.2 Research objective

The main objective of this graduation project is to gain insight in the cooling effects of a sprinkler spray on a smoke layer. Subordinate to the main objective numerical simulations in FDS are attempted to be validated by acquiring experimental data. In addition, this study aims to gain insight into the influence of different sprinkler spray patterns by varying the operating pressure. The gained insight must provide building designers and fire safety consultants strategies for a proper application of the mentioned systems and increase awareness of the consequences.

1.3 Research question

To what extent are the temperature, thickness, and flow patterns of a stable smoke layer affected by water droplets of the sprinkler system?

At what level of detail should the sprinkler spray pattern be modelled in a field model in terms of initial velocity, spray angles, droplet size and mass fractions to obtain reliable results for smoke layer cooling?

Can modelling of smoke layer cooling by a sprinkler spray be used in practice, considering the required computational time, level of detail and knowledge of the modeller?

1.4 Research relevance

The field of Fire (Safety) Engineering (FSE) is relatively young and there is still a lot of research that can be done on several subjects. This graduation project contributes to better understanding of smoke layer cooling due to activation of sprinkler systems. The use of Computational Fluid Dynamics for modelling fires and its effects is still in its infancy. Currently, modellers make unsubstantiated estimations of the initial size and velocity in order to compute droplet trajectories, which limits the use of application [8]. A validated CFD-model can contribute to the development of modelling fire suppression systems and help other researchers to validate their models and make substantiated choices within their models.

1.5 Research model

The research can be divided into four main parts as indicated in Figure 1(next page), namely Literature study, Experiments, Numerical simulation and Discussion. The goal of the first part, Literature study, is to get acquainted with the physical models of smoke layer cooling. Especially, smoke logging, cooling and drag effects by water droplets, droplet trajectories and combustion are necessary to get acquainted with before starting the simulations and experiments. The goal of the literature study is to determine which parameters are most influential for the numerical simulation, how a sprinkler spray can be modelled in a CFD model and which equations should be used.

The goal of the experiments is to obtain data that can be used to validate the results of the numerical simulation with experimental results. Peutz b.v. developed an experimental set-up in their laboratory that can be used for studying the effects of water droplets on the smoke layer. It contains two compartments, one smaller compartment where the fire is located and one adjacent larger compartment with a sprinkler head. The fire is not affected by the sprinkler spray in this configuration. A smoke layer is formed in the large compartment and both temperatures and height of the smoke layer can be measured. In the current set-up, smoke is extracted at the top and analysed in order to determine the heat release rate of the fire. The experiments will consist of multiple series, namely reference experiments and sprinkler experiments. During the first series, reference experiments, the sprinkler will not be activated and these experiments are used

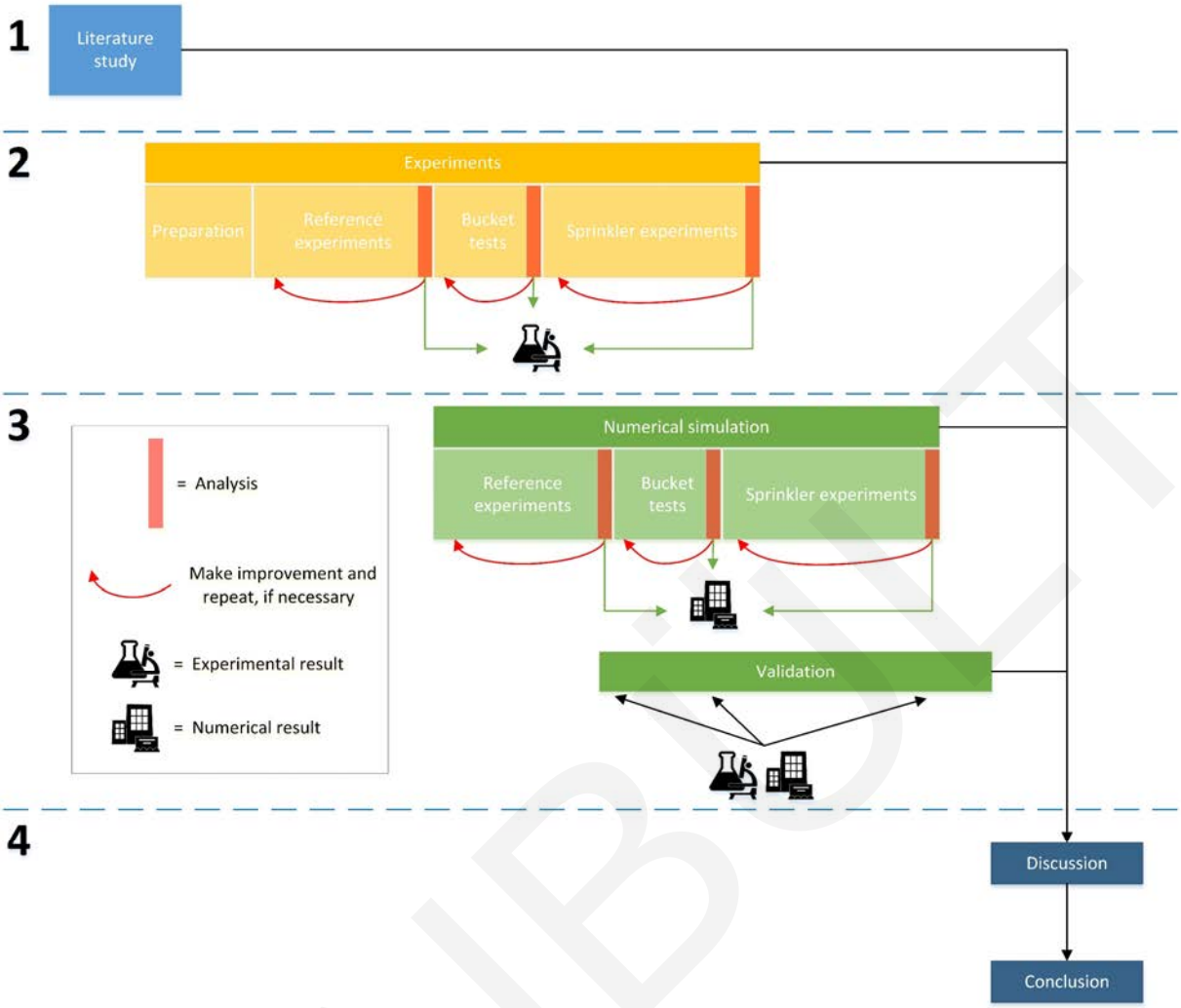

Figure 1 - Research model

to establish a zero condition. During the second series, sprinkler experiments, the sprinkler will be activated to measure the temperature decrease of the smoke layer. This will be compared with the zero condition where no sprinkler cooling is applied. In addition to these experiments bucket tests will be performed to measure the water distribution at the floor surface.

The third part of the graduation project, Numerical simulation, consist of three parts. For the numerical simulation, FDS, developed by NIST, is used. First, the reference experiments will be modelled in FDS to obtain a reliable model for the zero condition. Thereafter, the sprinkler spray pattern will be modelled and compared with the performed bucket tests to find the most suitable model configuration. Finally, the sprinkler test will be modelled by using the reference model and the sprinkler spray pattern model.

During the validation study, the experiments and numerical simulations will be compared to determine the reliability of the simulations. The results of this comparison will be discussed in the Discussion. Finally, the research questions will be answered in the conclusion.

1.6 Research limitations

- The experiments will be performed within the physical limits of the measurement set-up. This means that the maximum Heat Release Rate (HRR) of the fire will be limited based on the maximum hot gas temperature that the gas scrubber can endure. The set-up will be optimized but no significant changes will be made.

- During the experiments, smoke will be extracted by a mechanical fan to analyse the hot gases and to prevent smoke spread throughout the entire fire safety laboratory.

- Interaction of the sprinkler spray with the flame region is not considered in this study. Only the effects on the smoke layer are studied.

- Only one type of sprinkler nozzle will be used. Use of multiple sprinkler nozzle types is too extensive. Variation of sprinkler patterns will be done by using different operating pressures. To study the effect of a different sprinkler pattern in FDS a simple sprinkler model will be used in FDS to determine the differences between sophisticated and simplified spray patterns. However, the number of simulations that will be done with the simple spray pattern is limited.

1.7 Structure thesis

In chapter 2 a theoretical background is provided to create a better understanding of the problem, measurement methods and the occurring effects. In chapter 3 the measurement method and computational model that were used are further explained. In chapter 4 the measurement results are given along with the computational results. In chapter 5 a comparison is made between both types of results to conclude in chapter 6 and provide recommendations in chapter 7.

2 Theoretical background

2.1 Sprinkler system

Several different sprinkler systems can be distinguished from the above-mentioned standards such as wet pipe, dry pipe, pre-action and deluge systems. However, for this study the type of sprinkler system is less relevant and will not be further discussed. The different type of sprinkler heads, on the other hand, do have an impact on the sprinkler pattern and therefore have a more significant impact on the cooling of the smoke layer.

Sprinkler heads occur in many forms, have different specifications and can be assigned to specific building functions. For example, we can distinguish standard coverage sprinklers, residential sprinklers and storage sprinklers. Most crucial difference between those sprinklers is the discharge rate of water, for storage sprinklers the discharge rate is much larger since the potential energy release is often larger in storage rooms. Also, the direction of a sprinkler head may differ which result in different configurations of sprinkler heads such as pendent sprinklers, upright sprinklers and sidewall sprinklers. Other types of sprinklers are recessed sprinklers, flush-type sprinklers, concealed sprinklers and large drop sprinklers. [9]

Figure 2 - Left to right, Sidewall sprinkler, Upright sprinkler, Pendent sprinkler and Open sprinkler nozzle

In general, two different mechanisms can be used to activate a sprinkler system, namely a glass bulb or a fusible element. Under normal conditions, a cap or valve is held tightly against the orifice of the sprinkler head to prevent discharge of water. In case of a glass bulb sprinkler the cap is held against the orifice by a glass bulb that is filled with a liquid and a small air bubble. When the temperature rises the liquid expands and the bubble will be compressed. Further increase of the temperature results in a substantial pressure increase which makes the glass bulb shatter and the water starts flowing. The exact operating temperature of the sprinkler head can be regulated by adjusting the amount of liquid and changing the size of the air bubble. The activation temperature of sprinkler heads is usually indicated by a colour code of the glass bulb as given in Table 1. [9]

A fusible element sprinkler has a two-part metal element that is fused by a heat-sensitive alloy. The metal element holds the link in place that keeps the cap against the orifice. When temperature increases the fusible element will start to melt and eventually the two metal parts will be disconnected resulting in opening of the orifice. Alloys are usually composed of tin, lead cadmium and bismuth which have all sharply defined melting points. [9]

Despite the difference in operating mechanism the deflector is the most important element regarding the sprinkler spray pattern. Small differences in the deflector design result in major differences in the discharge characteristics [9]. The spray pattern of a sprinkler depends on the design of the deflector and velocity of the water when it hits the deflector. The impact velocity of water is dependent on the water pressure and the orifice of the sprinkler.

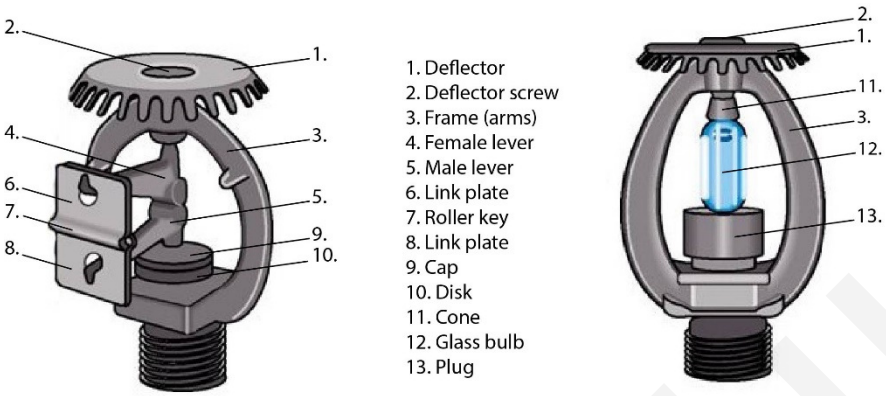

Figure 3 - Fusible link sprinkler vs. glass bulb sprinkler

Table 1 - Operating temperatures and corresponding colour codes of sprinkler heads

Fusible link sprinklers			Glass bulb sprinklers		
Nominal activation temperature [°C]	Color code		Nominal activation temperature [°C]	Color code	
57 – 77		Uncoloured	57		Orange
80 – 107		White	68		Red
121 – 149		Blue	79		Yellow
163 – 191		Red	93 – 100		Green
204 – 246		Green	121 – 141		Blue
260 – 302		Orange	163 – 182		Violet
320 – 343		Black	204 – 260		Black

The response time of a sprinkler nozzle is expressed in the Response Time Index, RTI according to UL199. The RTI is determined under regulated conditions. The sprinkler nozzle is exposed to a heated air stream in a so-called plunge oven with constant temperature and velocity. The time that is required to raise the temperature of the heat responsive element to approximately 63% of the temperature of the air stream is called the tau factor. The tau factor is then multiplied with the square root of the velocity to obtain the RTI (Equation 2.1.1). [10]

$$RTI = \tau \cdot \sqrt{v} \qquad 2.1.1$$

Sprinkler nozzles with a heat responsive element with an RTI-value smaller than or equal to 50(meter-seconds)$^{1/2}$ are called Fast Response Sprinklers (FSR). For sprinklers with

an RTI-value larger than or equal to 80(meter-seconds)$^{1/2}$ we speak of a Standard Response Sprinkler (SRS).

The coverage area of most sprinklers nozzles ranges between 9 and 12 m^2, therefore sprinkler nozzles are often placed in grids of 3x3m[1]. Extended coverage sprinklers can be applied in a larger grid according to the manufacturer's specifications. The volumetric flow rate of a single sprinkler nozzle is dependent on the operating pressure and the K-factor, this last parameter depends mostly on the nozzles orifice diameter.

$$\dot{V} = K\sqrt{p} \qquad 2.1.2$$

$\dot{V}$ = volume flow sprinkler [l/min]
K = sprinkler constant specified by manufacturer [lpm/√bar]
p = pressure of sprinkler head [bar]

The spray envelope of a sprinkler spray is not necessarily uniform for quantities as mass fraction and velocity. Due to the shape of the deflector these quantities can variate within the spray envelope. Therefore, a spherical coordinate system can be used to express these quantities for different elevation angles and azimuth angles. [11]

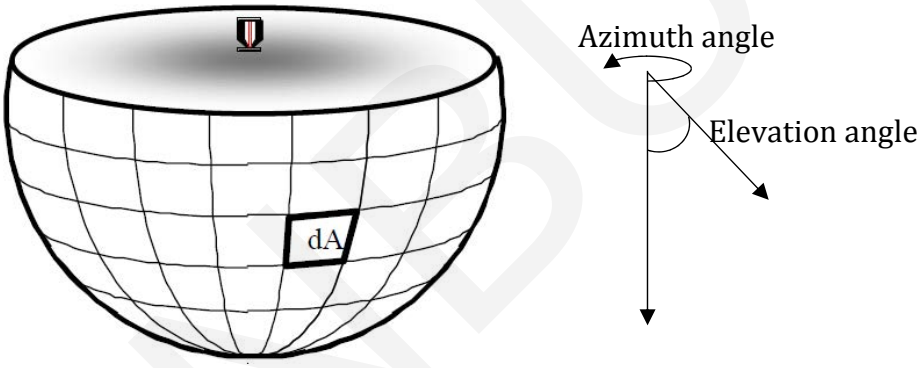

Figure 4 - Spherical coordinate system sprinkler spray envelope [11]

In paragraph 2.3 the sprinkler spray pattern will be further explained.

2.2 Smoke logging & Droplet trajectories

By spraying water directly into a smoke layer it may cause diffusing and descending of the smoke. This phenomenon is called smoke-logging and was introduced by Bullen in 1974. According to Bullen, the stability of the smoke layer depends on the ratio between the drag force (D) and buoyancy force (B) on the smoke layer. Smoke logging will occur when D>B, otherwise the smoke layer will remain stable [12].

The drag force on a single spherical droplet can be described by equation 2.2.1.

$$D(x) = -kv^2 \qquad 2.2.1$$

where

$$k = C_D \cdot \frac{1}{2} \cdot \rho_a \cdot A_{droplet} \qquad 2.2.2$$

With drag coefficient, C_D, being a constant. However, in practice C_D is a function of the Reynolds number based on the droplet diameter. The total drag force on the smoke layer according to Bullen's theory is described by equation 2.2.3.

$$D = \dot{m}\left(\frac{mg}{k}\right)^{\frac{1}{2}}\left(\frac{1}{2}ln\left(\frac{1+\left(1-e^{\frac{-2kh}{m}}\right)^{\frac{1}{2}}}{1-\left(1-e^{\frac{-2kh}{m}}\right)^{\frac{1}{2}}}\right)-\left(1-e^{\frac{-2kh}{m}}\right)^{\frac{1}{2}}\right) \qquad 2.2.3$$

The downward drag force on the layer will be countered by the upward buoyancy force B, which can be described by equation 2.2.4. Where Vol is the cone volume of the sprinkler spray.

$$B = (\rho_0 - \rho_s)gVol \qquad 2.2.4$$

$$Vol = \frac{\pi C h^2}{2} \qquad 2.2.5$$

Where C is the approximated radius of the wetted floor surface.

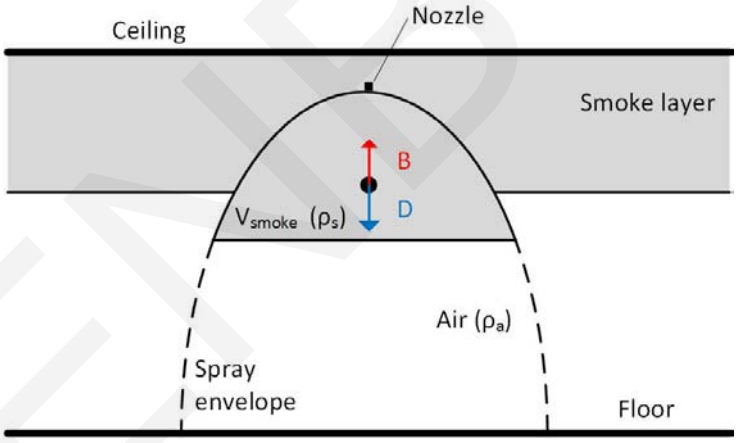

Figure 5 - Schematic instability criterion from Bullen theory [12]

A schematic of the instability criterion from the Bullen theory is shown in Figure 5. Equation 2.2.2 of Bullen's theory is only valid for smoke regions (V_{smoke}) that are entirely surrounded by ambient air [13]. The upward buoyancy is only applicable to the lower part of V_{smoke} since only this part is surrounded by ambient air. The buoyancy force on the other part of V_{smoke} works downward on smoke since it is cooled by sprinkler spray and surrounded by hot smoke. This means there is always some smoke descend and Bullen's theory is only valid for an initially thin smoke layer. [13]

Tang et al. revised the analytical model of Bullen and assume the smoke layer will descend in the spray envelope to a certain height once the sprinkler is activated. Then the smoke layer will maintain at that height meaning the downward forces and upward forces are

in balance. According to Tang et al. this phenomenon was observed in multiple experimental studies. [13]

Tang et al. divide their analytical model into three zones as can be seen in Figure 6. Zone I is the smoke layer outside the spray envelope which is not affected by the water droplets. This zone has the highest average temperature and it is assumed smoke layer temperature, T_s, is the same as for smoke layer without sprinkler activation. Zone II contains no smoke and therefore the temperature is equal to the ambient air temperature. Zone III within the spray envelope can be divided in an upper part (*Vi,s*) and a lower part (*Vi,a*). Due to entrainment of ambient air the temperature of the lower part can be lower than the temperature of the upper part. [13]

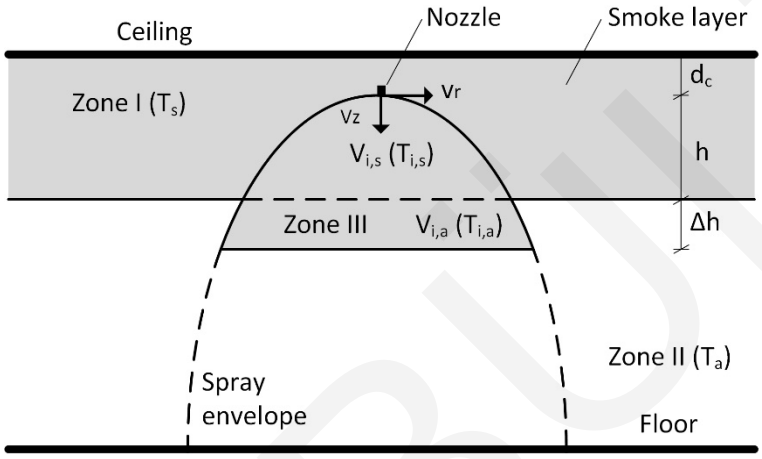

Figure 6 - Schematic of analytical model by Tang et al. [13]

$$F_D = \dot{m}_w\left(v_{z,in} - v_{z,out}\right) + m_w g \qquad 2.2.6$$

Droplet velocity v can be divided in a vertical component v_z and a radial component v_r.

$$v = \sqrt{{v_z}^2 + {v_r}^2} \qquad 2.2.7$$

By implementing equation *2.2.8-2.2.10* into Bullen's theory (equation *2.2.1* and *2.2.2*) the set of differential equations given in equation 2.2.11 is obtained, describing the single water droplet momentum equations.

$$C_D = \begin{cases} 24/Re & 0 \le Re < 1 \\ 12.6/Re^{0.5} & 1 \le Re < 800 \\ 0.44 & Re \ge 800 \end{cases} \qquad 2.2.8$$

$$Re = v d_m / v_{smoke} \qquad 2.2.9$$

$$v = 1.49 \cdot 10^{-5} \cdot 0.518 \left(\frac{T_i}{293}\left(\frac{T_i}{293} + 1.55\right)\right)^{0.7} \qquad 2.2.10$$

$$\begin{cases} \dfrac{d(v_z)}{dt} = g - \dfrac{3}{4} \cdot \dfrac{C_D \rho_i \sqrt{{v_z}^2 + {v_r}^2} \cdot v_z}{\rho_d d_m} \\ \dfrac{d(v_r)}{dt} = -\dfrac{3}{4} \cdot \dfrac{C_D \rho_i \sqrt{{v_z}^2 + {v_r}^2} \cdot v_r}{\rho_d d_m} \end{cases} \quad 2.2.11$$

By solving equations *2.2.11* and 2.2.12 numerically droplet trajectories can be determined along with $v_{z,out}$ which is necessary to compute the total drag force, F_D.

$$\begin{cases} \dfrac{dv}{dt} = v_z \\ \dfrac{dr}{dt} = v_r \end{cases} \quad 2.2.12$$

With equation *2.2.13* Δh, as mentioned in Figure 6 can be determined. When Δh is smaller than the height of the smoke-free layer, Δh is the distance of the smoke falling down. Otherwise, the smoke falls down to the floor. [13]

$$F_D + (\rho_{i,s} - \rho_s) g \int_0^h \pi r^2 \, dh = (\rho_a - \rho_{i,a}) g \int_0^{h+\Delta h} \pi r^2 \, dh \quad 2.2.13$$

2.2.1 Convective heat transfer

In 1979 Morgan and Baines extended Bullen's theory by including convective heat transfer. During the downfall of droplets heat is transferred from the buoyant smoke layer into the water droplets which have lower temperatures. The mathematical model introduced by Cooper in 1995 considered that the smoke layer beneath the sprinkler nozzle is pulled down by the drag force of the water droplets and pushed up by its own buoyancy[14]. A more recent heat transfer model is described by Li et al. based on earlier studies [15].

The convective heat transfer coefficient for a droplet with diameter d can be expressed by equation 2.2.14.

$$h(d) = \frac{Nu(d)k}{d} \quad 2.2.14$$

where k is the thermal conductivity of air and Nu is the Nusselt number for a spherical droplet as expressed by equation *2.2.15*.

$$Nu(d) = 2 + (0.4Re(d)^{0.5} + 0.06Re(d)^{\frac{2}{3}})Pr^{0.4} \quad 2.2.15$$

where Pr is the Prandtl number of air, which is often taken to be 0.7.

The energy exchange (convective heat transfer) between the droplets and the smoke layer can be obtained by equation *2.2.16* and is expressed in joules per second or Watt.

$$Q_c(i) = h(i)A(d)(T_s - T_w)N(i) \quad 2.2.16$$

The heat that is absorbed by droplets with diameter d is equal to equation *2.2.17* and is expressed in kilojoule.

$$Q_c(d) = m(d)c_w(T_f - T_0)N(d) \qquad T_f \leq 373K \qquad 2.2.17$$

where *m(i)* is the mass fraction of droplets with diameter *d* and T_f is the temperature of the droplet when it reaches the bottom. By summing up the absorbed heat of all droplets the total transferred heat from the smoke layer to the water droplets can be calculated and is equal to equation *2.2.18*, Q_c is expressed in kilojoule.

$$Q_c = \sum_{i=1}^{N} \frac{4}{3}\pi\left(\frac{d}{2}\right)^3 \rho_w c_w(T_f - T_0)N(d) \qquad T_f \leq 373K \qquad 2.2.18$$

The boiling point of water is 373K (100°C) and when the water droplets reach this temperature they will evaporate. In the above described mathematical model evaporation of water droplets is not considered. Therefore, the model is limited to the point where water droplets reach 373K. It is expected that the even if small droplets start to evaporate the mass fraction of those droplets is so small that it will not have much influence [15].

2.3 Droplet size

To determine the heat transfer between water droplets and surrounding air, the size and number of droplets for each diameter *N(d)* are required. *N(d)* depends on the water pressure, sprinkler type and the position in the sprinkler spray. The spray pattern of a sprinkler can be characterized by characteristic diameters and statistical size distributions. [6]

In mathematical models and numerical simulations, the water droplets are assumed to be spherical. However, in practices water droplets are not fully spherical, therefore the volume diameter d_v can be described as the diameter of a sphere having the same volume as a droplet. The volume median diameter d_m separates the higher half of the volume diameters from the lower half, in other words, the total volume of the droplets smaller than the median diameter represent 50% of the total volume. The volume median diameter differs for different types of sprinklers and water pressures. To estimate d_m equation *2.3.1* can be used [6]. In this equation, W_e is the dimensionless Weber number given by equation *2.3.2* [6].

$$d_m = \frac{C_{sp} d_n}{W_e^{\frac{1}{3}}} \qquad 2.3.1$$

$$W_e = \frac{\rho_w {U_{sp}}^2 d_n}{\sigma_w} \qquad 2.3.2$$

The sprinkler constant C_{sp} is experimentally determined and is highly dependent on the nozzle's geometry. For a Standard Sprinkler Pendent (SSP) with an orifice of 11mm Lawson determined that a sprinkler constant of 2.7 is appropriate [16]. The inner diameter of the sprinkler orifice, d_n, can be measured. The average droplet speed U_{sp} in

equation 2.3.2 can be calculated by dividing the volume flow by the orifice area of the sprinkler. The surface tension in water σ_w is equal to 72.8 mN/m.

When a sprinkler nozzle is activated and the water flow hits the deflector the water volume is scattered into small droplets, this process called sprinkler atomization is too complex to predict accurately in mathematical models and simulations. Therefore, a Eulerian-Lagrangian approach is used to introduce the water droplets into the computational domain with a prescribed distance, r_0, an elevation angle θ and azimuth angle ϕ [17]. This leads to a spherical surface of the spray boundary, see Figure 11. In Figure 7 the atomization process of a sprinkler spray is shown.

In numerical simulations, it is impractical to follow the motion of every single droplet in the sprinkler spray, therefore a particle injection rate N_p must be prescribed. A large group of real droplets is then represented by a computational Lagrangian particle [17].

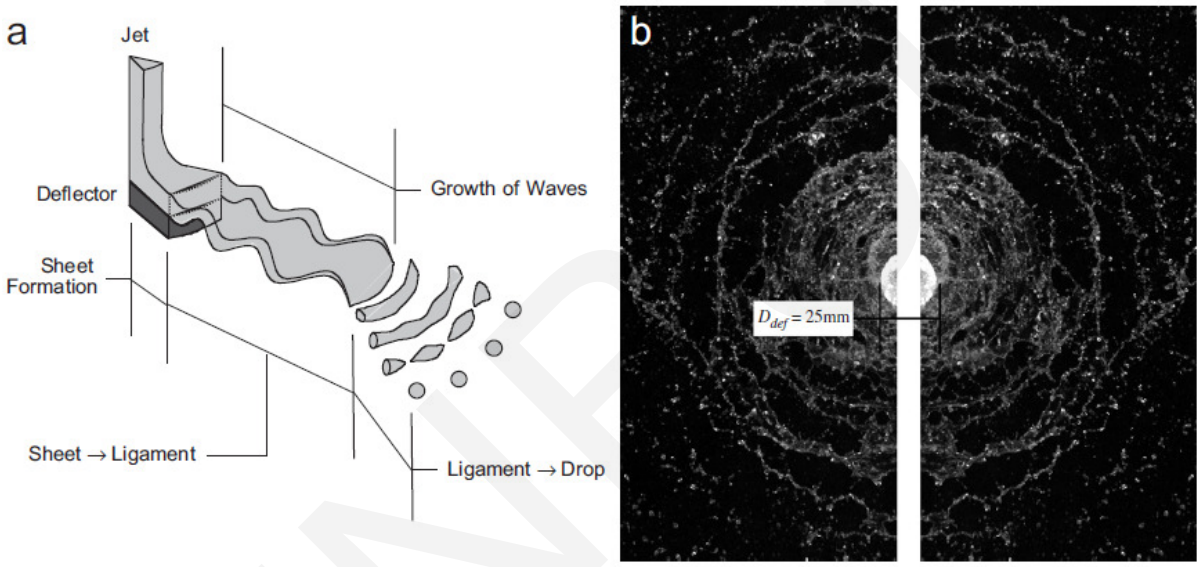

Figure 7 - (a) Illustration of the atomization process of a sprinkler spray, (b) photograph of atomization process [19]

It has been found that the distribution of droplet sizes can be described by a function in some cases. The most common droplet distribution functions currently used are the Rosin-Rammler function (*2.3.3*) and the log-normal function (*2.3.4*). With these functions the probability *y(d)* of a droplet size with diameter d can be calculated. [6]

$$y(d) = \frac{1}{\sqrt{2\pi}\sigma d} e^{-\left(\frac{(ln(d/d_m))^2}{2\sigma^2}\right)} \qquad 2.3.3$$

$$y(d) = \gamma\beta \frac{d^{\gamma-1}}{d_m^{\gamma}} e^{-\beta\left(\frac{d}{d_m}\right)^{\gamma}} \qquad 2.3.4$$

Here σ is the standard deviation of the log-normal distribution, usually around 0.6. Both γ and β are sprinkler constants usually taken to be 2.4 and 0.7 respectively. For a smooth transition at the volume median diameter σ =1.15/γ. [18]

The Cumulative Volume Fraction (CVF) is also often used to describe the sprinkler spray pattern and provides a method to determine the fraction of the total water that has been carried by droplets of a specific size range [6]. The CVF is equal to equation *2.3.5* and it has been found that for droplet sizes with a diameter smaller than the volume median diameter the log-normal distribution is best fitted and above the volume median diameter the Rosin-Rammler distribution is best fitted. However, a limited number of studies have been performed towards this relation. [19]

$$CVF(d) = \begin{cases} \frac{1}{2\pi}\int_0^d \frac{1}{\sigma d'} e^{-\left(\frac{(ln(d'/d_m))^2}{2\sigma^2}\right)} dd' & d \leq d_m \\ 1 - e^{-\beta\left(\frac{d}{d_m}\right)^\gamma} & d > d_m \end{cases} \qquad 2.3.5$$

A function or relationship for the creation of droplets by the deflector of the sprinkler nozzle is required to predict exactly the droplet distribution. Also, the exact values of the constants σ, γ and β used in equation *2.3.3* and *2.3.4* can at the moment only be determined by experiments for multiple locations and pressures. [6]

Zhou, D'Aniello and Yu performed laser-based shadow-imaging measurements to study the near-field and far-field spray patterns of a pendent fire sprinkler. They observed that the sprinkler frame arms and the configuration of the tines and slots of the deflectors affect the spray pattern in the near-field. In the far-field this influence is smaller and the droplet size is approximately constant with the azimuth angle. Near the centre of the sprinkler spray the maximum droplet size is reached. Approximately 0.5 meters from the centre the droplet size decreased to a minimum in order to again increase toward the edge of the sprinkler spray envelope. [20]

2.4 Heat Release Rate

The heat release rate, abbreviated with HRR, is the amount of heat energy released in time during combustion of a material and is often expressed in kW (kJ/s). The heat release rate of a fuel expressed in Watt can be calculated with equation *2.4.1*. This equation is based on the mass loss of the fuel and the energy release per kilogram of fuel.

$$HRR(t) = \dot{m}^{n\prime\prime} \cdot A_f \cdot \Delta H_c \cdot \chi \qquad 2.4.1$$

Here $\dot{m}^{n\prime\prime}$ is the mass loss rate in kg/m²s, A_f the area of fuel surface in m², ΔH_c the heat of combustion in case of complete combustion expressed in MJ/kg and χ is the combustion efficiency (1.0 for complete combustion). Since the heat of combustion and/or mass loss rate is not always known in advance another method is often used based on gas analysis. To calculate the heat release rate with Oxygen Consumption Calorimetry (OCC) the amount of oxygen used during combustion is measured. For this technique, it is required to collect all combustion products and remove them by an exhaust duct. In the duct a gas sampling probe is placed to be able to measure the concentration of oxygen (O_2), carbon dioxide (CO_2) and carbon monoxide (CO). With these concentrations the oxygen consumption factor can be determined with equation *2.4.3*. Inside the exhaust duct is also the temperature and pressure measured, in order to calculate the volumetric flow rate,

normalized to a temperature of 298 Kelvin, equation *2.4.4*. Subsequently, equation *2.4.2* is used to calculate the HRR.

$$HRR(t) = E \cdot \dot{V}_{298}(t) \cdot x_a^{O_2}\left(\frac{\Phi}{1+0.105\cdot\Phi}\right) \qquad 2.4.2$$

E, the heat release per unit volume consumed at 298K, often taken as ±17200 kJ/m^3 (complete combustion). The oxygen consumption factor is given by ϕ, the volumetric flow rate by $\dot{V}_{298}$ and $x_a{}^{O2}$ is the ambient mole fraction of oxygen including water vapour equal to equation *2.4.5* [21]. The constant 0.105 is the volumetric expansion factor minus 1. For complete combustion of carbon in dry air the volumetric expansion factor is 1, so the constant in equation *2.4.2* is zero. If the fuel is pure hydrogen the expansion factor is 1.21. A commonly used value is the average of combustion of carbon in dry air and combustion of hydrogen, resulting in a volumetric expansion factor of 1.105 and value of 0.105 in equation *2.4.2*. [22]

$$\Phi = \frac{\bar{x}O_2(30s \dots 90s)[1 - xCO_2(t)] - xO_2(t)[1 - \bar{x}CO_2(30s \dots 90s)]}{\bar{x}O_2(30s \dots 90s)[1 - xCO_2(t) - xO_2(t)]} \qquad 2.4.3$$

$$\dot{V}_{298}(t) = c \cdot A \cdot \frac{k_t}{k_\rho}\sqrt{\frac{\Delta p(t)}{T_{ms}(t)}} \qquad 2.4.4$$

$$x_a^{O_2} = \bar{x}O_2(30s \dots 90s)\left[1 - \frac{H}{100p}e^{\left(23.2 - \frac{3816}{\bar{T}_{ms}(30s \dots 90s) - 46}\right)}\right] \qquad 2.4.5$$

With

$xO_2(t)$	oxygen concentration in mole fraction [-]
$xCO_2(t)$	carbon dioxide concentration in mole fraction [-]
A	cross sectional area duct [m^2]
c	$(2T_0/\rho_0)^{1/2}$ = 22.4 [K$^{1/2}$m$^{3/2}$kg$^{-1/2}$]
p	ambient pressure [Pa]
$T_{ms}(t)$	temperature in general measurement section [K]
k_t	flow velocity profile [-]
k_ρ	Reynolds correction for bi-directional probe (1.08) [-]
H	relative humidity [%]

2.5 Heptane fire curve

After ignition of a heptane pool the maximum and constant burning rate is not immediately reached. Experiments at a small scale by Hayasaka (1997) indicate that three regions can be distinguished with different burning rates. In Figure 8 the three defined phases by Hayasaka are shown. After ignition the 'preheating phase' of the fuel starts and during this period the burning rate is constant while the fuel temperature starts to increase. The fuel can be divided into a vaporizing layer on top and a preheated

layer at the bottom. At the top surface of the vaporizing layer the temperature is equal to the boiling point, which is 98.4°C for heptane. During the preheating phase the temperature of the preheated layer starts to increase. In this phase the temperature increase of the fuel has no influence on the burning rate which is steady. In the 'transition phase' the top of the preheated layer starts to approach the boiling point and the burning rate starts to increase again. The burning rate increases as the 'boiling layer' thickens until the entire fuel layer is boiling or when an equilibrium is reached were further thickening of the fuel layer has no influence on the burning rate anymore. At this point the 'boiling phase' is reached, here the burning rate reaches its maximum value and remains constant at that level until all fuel is burned. [23]

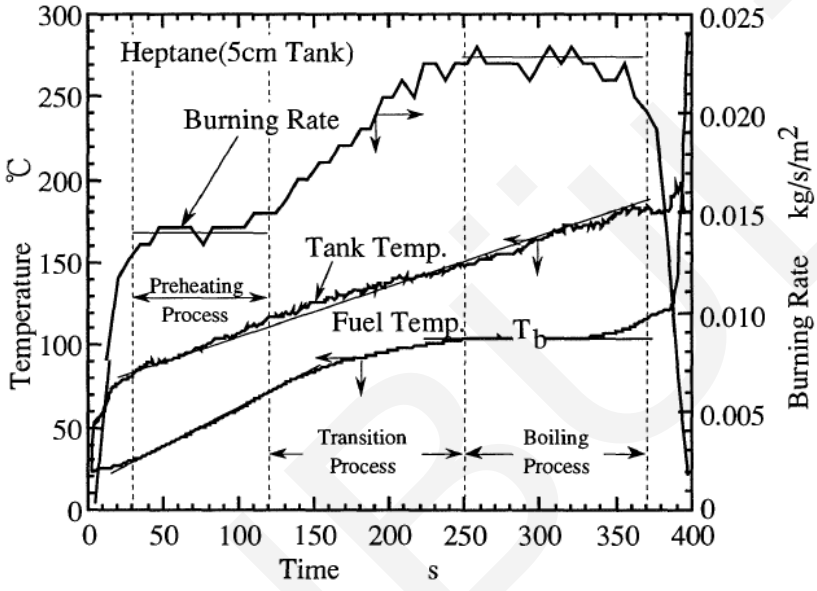

Figure 8 - Unsteady burning rate in time of small heptane pool fire (d=50mm) [23]

It is expected that these same principles will occur for larger heptane pool fires. When the fuel is poured on a water layer the burning surface of the fire remains constant from ignition till termination. Also, the water cools the fuel layer from beneath and the preheating phase will be extended.

3 Methodology

3.1 Experimental approach

3.1.1 Geometry of experimental set-up

The experimental set-up developed by Peutz BV is similar to the configuration used by several Chinese researchers [4], [15], [24]. Two cabinets of varied sizes were used namely, a burner cabinet and a larger sprinkler cabinet, see Figure 9. More extensive drawings of the measurement set-up are attached in Appendix 2.

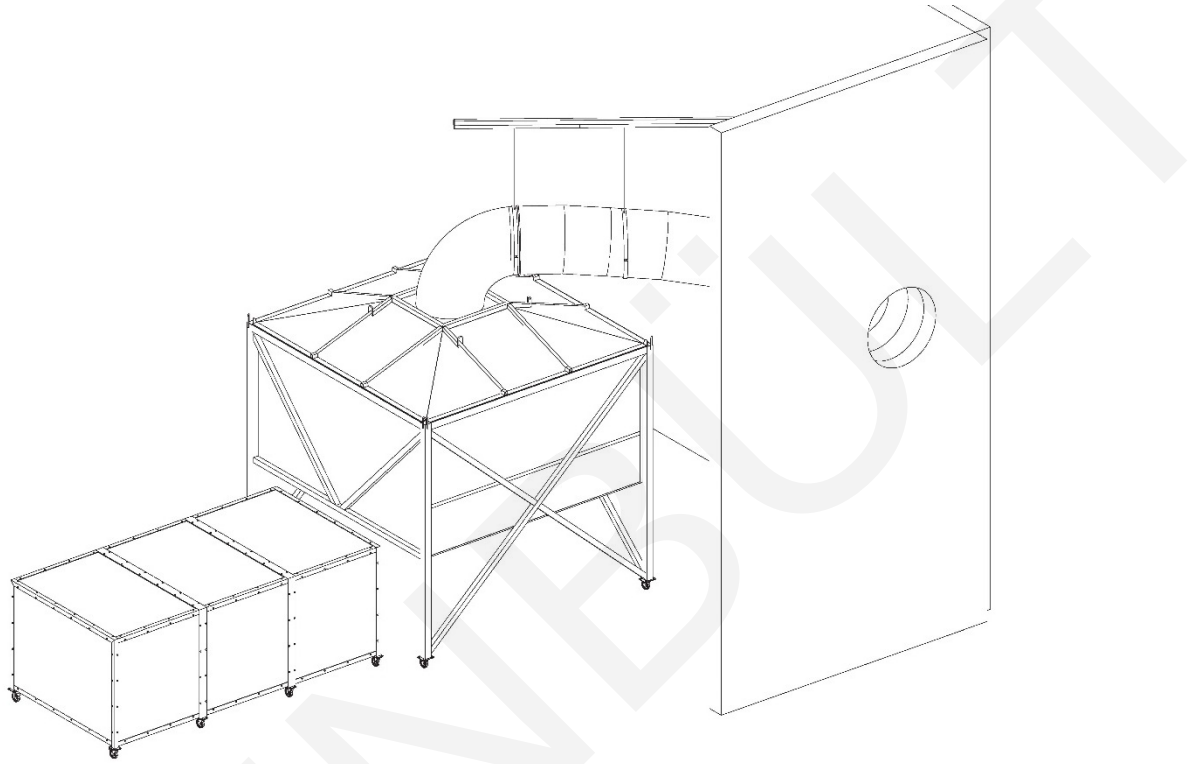

Figure 9 - 3D image of measurement set-up

The initially used fuel tray is a square tray with an open surface area of 0.25m^2 (0.5x0.5m) and is placed 0.65m from the back wall and 0.575m from the side walls. The steel walls of the fuel tray are 5mm thick and 0.15m high. Two supporters of 0.1m raise the fuel tank from the floor. With the fuel tray and heptane as fuel, an HRR of approximate 300kW is expected. The fuel is poured on a water layer to maintain a steady burning surface during the experiment. The water also 'cools' the fuel which slows down the increase of the evaporation rate during heating up.

Later, another fuel tray was used to obtain a higher HRR since not enough smoke was produced by the 300kW fire in relation to the minimum extraction capacity of the fan. Therefore, a fuel tray of 0.5x0.7m was used which results in an HRR of approximate 700kW. For this fuel tray additional cooling is required to keep the HRR constant until the end of the experiment. Therefore, the fuel tray is placed in a larger tray which is filled with water as cooling material.

The outer dimensions of the smoke cabinet are 3.0m x 3.0m x 3.46m and the side walls of the cabinet are open to a height of 1.65m. The side wall where the burner cabinet is placed is made of a steel plate. The other three side walls exist of calcium silicate board at the bottom (0.3m) with steel plates on top (1.075m). The calcium silicate boarding can be removed to differ the smoke layer height. The top of the smoke cabinet, also made of steel plates, has a trapezoidal form to guide smoke towards the middle where it is extracted by a mechanical fan. In Figure 12 a schematic overview of the measurement set-up is shown. In this figure the location of the measurement section and mechanical fan are indicated. The smoke outlet has a diameter of 0.7m and a volumetric air flow rate that can range between 1.4m^3/s and 5.0m^3/s for ambient conditions with a frequency controller.

In the middle of the smoke cabinet a sprinkler nozzle is placed at a height of 2.9m (deflector plate). A pendent sprinkler with a K-factor of 80.6L/min√bar and an orifice diameter of 11.1mm was used (VK102/12987AB), this is a commonly applied Standard Sprinkler Pendent (SSP). The exact dimensions of the sprinkler nozzle are given in Table 2. The glass bulb will be removed before the experiment, so the activation of the sprinkler can be controlled manually without delay of the glass bulb.

Figure 10 - Pendent sprinkler nozzle, VK102/12978AB

The output pressure of the water pump (DAB K55/100 T) is controlled by a frequency controller (DAB T/T 3). With the pump water is pumped from the water basin to the sprinkler nozzle. Due to the pumping height of approximate 3 meter and other pressure losses e.g. by conduit elbows, a working pressure at the pump of 0.25 bar is corresponding to an operating pressure of ±0.1 bar at the sprinkler nozzle. For setpoint pressures of 1.7, 3.1 and 4.8 bar at the pump it is determined with water volume flow tests that the pressure at the nozzle is 0.40, 0.79 and 1.34 bar. Original the operating pressure was aimed to be 0.5 bar (low value for this nozzle), 1.0 bar (average value), 1.5 bar (high value). However, volume flow tests at the end of this study indicated that earlier determined setpoints at the pump were inaccurate, resulting in lower operating pressures at the nozzle.

Table 2 - Dimension sprinkler nozzle, VK102/12987AB

Orifice	11.1 mm	Deflector Notch width	2 mm
Frame arm distance	19 mm	Deflector notch depth	5 mm
Frame arm thickness	3 mm	Number of notches	16
Frame arm width (1)	10 mm	Deflector Thickness	1 mm
Frame arm width (2)	3 mm	Height of deflector over orifice	31 mm
Deflector width	25 mm		

3.1.2 Measuring devices

The smoke cabinet contains three pillars with thermocouples to measure the gas temperature at multiple heights. The K-type thermocouples (GG220-2k-0.5M IEC Ki:1) have a temperature range of -270°C to 1372°C and both the inner and the outer insulator are made of fibreglass. The accuracy of the thermocouples is +/- 2°C. The positioning of the thermocouples is shown in Figure 11.

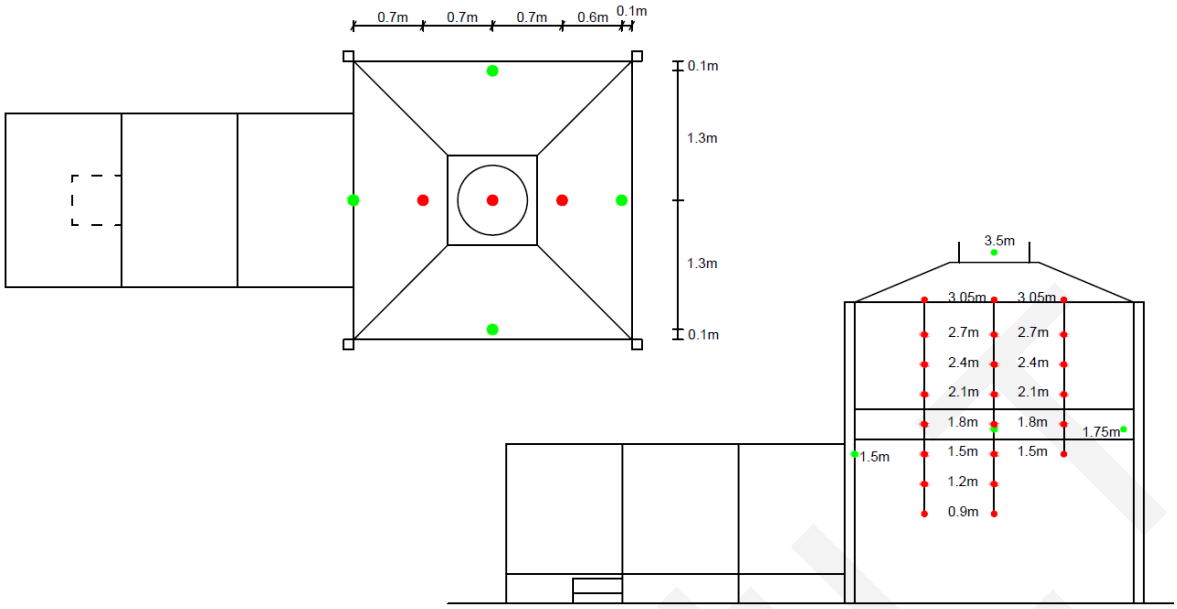

Figure 11 - Positions of thermocouples, Top view (left) and Side view (right)

Three thermocouple pillars are placed in the smoke cabinet on the centreline in the longitudinal direction. The first thermocouple pillar is placed 0.7m from the burner cabinet (smoke entrance) the second and third thermocouple pillar are placed on the centre point and 2.1m from the burner room. The vertical spacing between the thermocouples is 0.3m, except for the highest row of thermocouples which are located 0.35m apart from the second one. Also, a thermocouple is placed just below the ceiling of the burner cabinet at the interaction with the smoke cabinet to measure the gas temperature of the smoke that flows into the smoke cabinet. An additional three thermocouples are placed near the bottom of the other three side walls to show the temperature distribution at the bottom of the smoke layer once the smoke cabinet is filled. The last thermocouple is placed in the centre of the exhaust's inlet to monitor the gas temperature of the smoke extracted from the smoke cabinet.

The response time of a thermocouple is defined as the time that is required to reach 63.2% of an instantaneous temperature change. The smaller the diameter of the thermocouple the faster the response time will be. The 0.5mm, K-type, exposed thermocouples that are used have a relatively fast response time since they do not contain insulation material at the tip. The response time of a 0.5mm bare wire at room temperature and an air velocity of 18m/s is approximate 0.9 seconds [25]. For still air the response time is approximately 10 times larger. When the air velocity gradually increases the response time reduces exponentially resulting in an estimated response time during the experiments of 1.5 seconds.

Smoke is extracted from the smoke cabinet by a mechanical fan. The smoke is being analysed before it enters the gas scrubber. After a straight duct of approximately 30 meters, the differential pressure in the centre of the duct is measured with a bi-directional probe. Along with the velocity profile factor, as determined in Appendix 5, the volumetric flow rate can be calculated with equation 2.4.4. Behind the bi-directional probe, a gas sampling probe is placed. This gas sampling probe is connected to a gas analyser that is normally used for Single Burning Item (SBI) tests. For correction of the

air density with the temperature a thermocouple is placed behind the probes. With the differential pressure, oxygen concentration, carbon dioxide concentration and gas temperature the HRR of the fire can be calculated according to equation 2.4.2, explained in paragraph 2.4.

To prevent the thermocouples in the smoke cabinet from wetting during sprinkler activation, metal protection caps are placed above the thermocouples. In Appendix, 3 is explained why this method is chosen and is shown how the protective caps are placed.

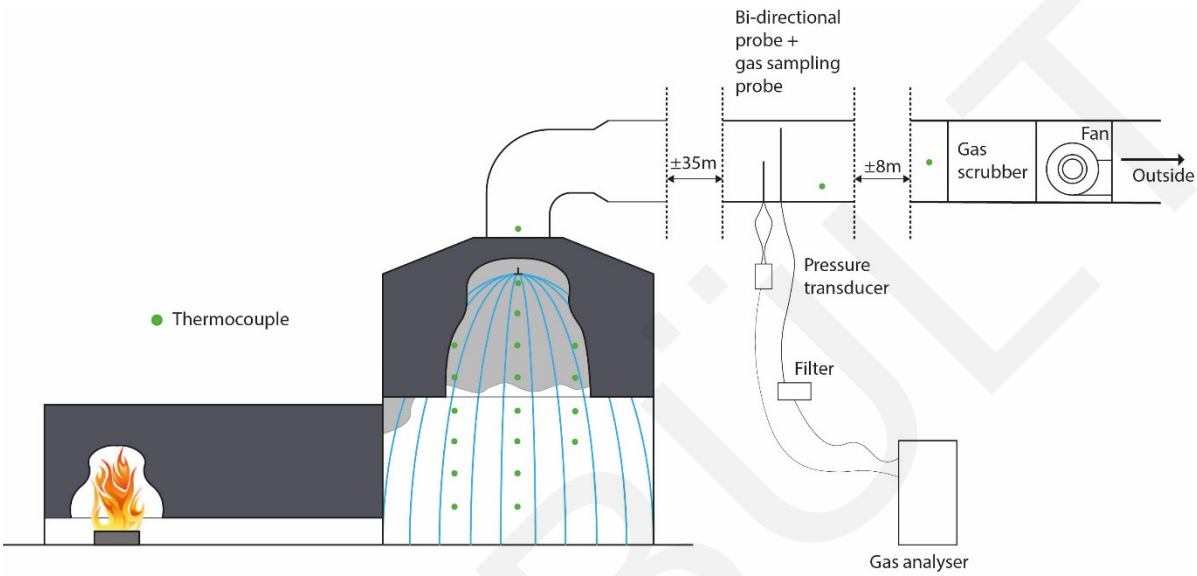

Figure 12 – Schematic overview measurement set-up

3.1.3 Output

With the measurement set-up described above the following parameters are measured:

- Gas temperature [°C]
  - Multiple locations throughout the smoke cabinet, see Figure 11.
  - Inlet extraction duct
  - Measurement section
- Differential pressure in exhaust duct [Pa]
- O_2 and CO_2 concentrations of the extracted smoke [mol fraction]

With these parameters, the following quantities are calculated:

- Volumetric air flow rate exhaust duct [m^3/s], normalized at 298K
- Oxygen depletion factor [-]
- Heat release rate [kW]
- Average smoke layer temperature [°C]

3.2 Numerical simulation

Field models or Computational Fluid Dynamics (CFD) models are complicated and require a high level of expertise from the modeller. The computational domain is divided into thousands of small volumes (cells), which can range from centimeters to meters. In general, a smaller cell size result in more reliable results. The Navier-Stokes equations are a system of partial differential equations that describe the flow of a fluid. The integrals in these partial differential equations can be replaced by discretized algebraic forms, which can be solved and result in numbers for the flow field values at discrete points in time and/or space. The transport equations are based on the basic physical principles of mass, energy and momentum conservation. Two approaches can be used to describe the transport equations of a fluid, namely a Eulerian and Lagrangian approach. With the Eulerian approach, the transport equations are written for a control volume. With the Lagrangian approach the transport equations are written for a moving particle.

This second approach can be used for modelling water droplets from sprinkler systems. [26]. The smallest vortices of a flow have the size of the Kolmogorov scale, but these vortices are mostly too small to be captured within the numerical grid and make it nearly impossible to solve the transport equations. Therefore, the transport equations will be filtered over a spatial interval (LES filter width) or averaged over a time interval. An example of filtering is Large Eddy Simulation (LES), these models solve the transport equations for the large eddies and the small eddies are modelled with an eddy viscosity model (turbulence model). Reynolds-Averaged Navier Stokes (RANS) models are an

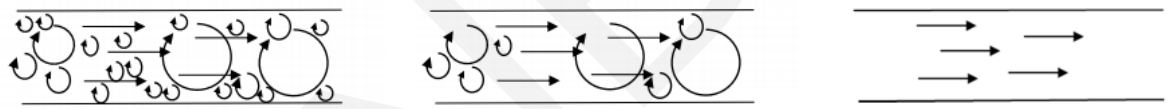

Figure 13 - Schematic view of solved flow for DNS (left), LES (middle) and RANS (right)

example of averaging over a time interval. For RANS models, only the mean flow is solved with the averaged Navier-Stokes equations and all eddies are modelled with a turbulence model. Choosing the appropriate turbulence model is a fundamental aspect of a CFD-model since it influences the distribution of the simulated flow variables, such as velocity, temperature and heat flow. Complete solving of the exact Navier-Stokes equations is called Direct Numerical Simulation (DNS) and all eddies are numerically solved. This makes it very time-consuming and it requires huge computational resources. A visual representation of the mentioned methods is shown in Figure 13. [26]

At the moment, there are several free software packages available for modelling fires with CFD. The most popular packages are Fire Dynamics Simulator (FDS), developed by the National Institute of Standards and Technology (NIST) and the open source FireFOAM, developed by FM Global.

3.2.1 Software

The Fire Dynamics Simulator (FDS, v6.6.0) is developed to model low-speed, thermally-driven flows with an emphasis on smoke and heat transport caused by fires unlike other

CFD software packages such as ANSYS Fluent [1]. FDS' core business is to simulate fire behaviour. For most cases in FDS, LES is used to model turbulent effects on the main flow. If the numerical mesh is fine enough it is also possible for FDS to use DNS. FDS is written in Fortran 90, and the core algorithm is second-order accurate [27].

The input code for FDS can be written with a text editor. To gain better insights into the model's geometry and input parameters the Graphical User Interface (GUI) PyroSim can be used. With PyroSim the code can be written easily for non-experienced users.

To maintain numerical stability and accuracy the time step should be well chosen. FDS uses constraints for the time step to maintain numerical stability. The Courant-Friedrichs-Lewy (CFL) constraint described in Equation 3.2.1 is used to determine the maximum time step. By applying this constraint, the fluid element cannot traverse more than one cell within a time step. In Equation 3.2.1 u is the velocity vector. [1]

$$CFL = \delta t \frac{\|u\|}{\delta x} < 1 \qquad 3.2.1$$

Since CFD-models can be time-consuming a simulation can run parallel by using Message Passing Interface (MPI). Therefore, the computational domain must be divided into multiple meshes. This way the workload can be divided over multiple cores or multiple processors. Parallel simulation at two computers does not necessarily mean a computational time reduction of 50%. To optimize the time reduction both workloads should be equal which means that both meshes should have the same numbers of cells. By dividing the workload into equal parts, the time that one of the cores or processors is in idle mode is minimized.

The finest computational domain in this study, with a total number of 620,868 cells, is divided into six almost equal parts with cell numbers ranging between 96,348 and 106,560 cells. The computational time for this model with 300 seconds of simulation time is approximate 25 – 30 hours.

3.2.2 Turbulent viscosity model

The turbulence model, gradient diffusion, is used in FDS for the closure of the sub-grid scale momentum and scalar flux terms. The turbulent (eddy) viscosity or turbulent (eddy) diffusivity is then required. The turbulent diffusivity can be obtained by using the Prandtl number or a constant Schmidt number. However, both turbulent transport equations depend on the turbulent viscosity, μ_t. FDS provides several methods for acquiring the turbulent viscosity. Since the release of FDS version 6 Deardoff's Model is used by default. [18]

Moya Ferero performed simulations with this model and the previous default turbulence model for a similar study and found no significant differences in the results [28]. Therefore the default Deardorff model was used in this study.

The turbulent viscosity by Deardorff's model is calculated according to Equation 3.2.2.

$$\mu_t = \rho C_v \Delta \sqrt{k_{sgs}} \qquad 3.2.2$$

Where k_{sgs} is the sub-grid scale kinetic energy and C_v is a model constant determined to have a value of 0.1. The LES filter width, Δ=(δxδyδz)^1/3 is the geometrical mean of the local mesh spacing at each direction. [18]

Deardorff's model is less suitable for near-wall turbulence. Therefore, FDS uses the constant Smagorinsky model with a damping function in the first off-wall grid cell. Damping is added so the viscosity goes to zero properly when the wall is approached.

3.2.3 Geometrical configuration

3.2.3.1 Computational domain

The computational domain contains the burner cabinet, the smoke cabinet and little free space around those cabinets. The free space is modelled minimalistic to limit the number of cells and reduce the computational time. Some free space is kept around the cabinets to allow air supply flows to develop (burner cabinet) and to allow smoke overflows (smoke cabinet). The sides and top of the domain are modelled 'open' and this allows 'free' air flows to develop in both positive and negative direction.

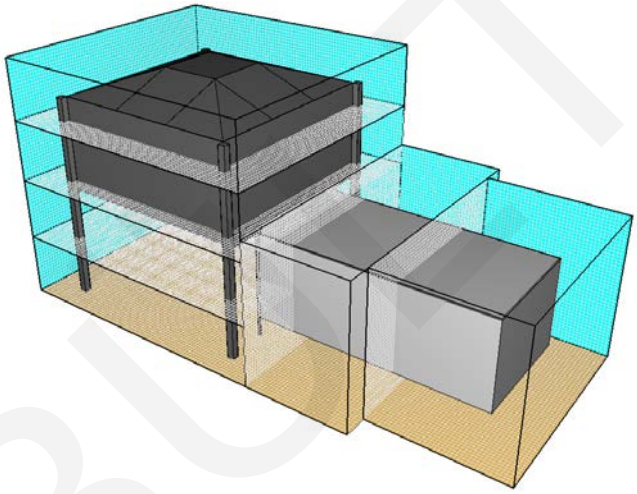

Figure 14 - Computational domain generated with PyroSim, (left) smoke cabinet, (right) burner cabinet

The domain is divided into six parts to make optimal use of the computer's capacity and to optimize the computational time. The domain around the smoke cabinet is divided into four equal parts with a size of 3.7 x 4.0 x 0.9 m. The two parts around the burner cabinet have sizes of 3.7 x 1.55 x 2.1m and 3.0 x 1.95 x 2.1m.

3.2.3.2 Grid & Cell size

As mentioned before the physical space that should be modelled is divided into a large number of rectangular cells to solve the low Mach number equations. It is assumed that within each cell quantities as the gas velocity, temperature, pressure etc. are uniform and only change in time. The mesh is restricted to rectangular Cartesian grids in FDS and objects/surfaces need to be placed on a cell's edge. Therefore, the computational grid must be generated with care, since FDS moves objects/surfaces to the nearest cell edge if this is not the case. Different cell sizes can be used, but nodes of different cell sizes should be aligned and the maximum aspect ratio is 2.

The FDS User Guide introduces a non-dimensional expression, D*/δx, to define the resolution of the grid. Here D* is a characteristic fire diameter given by Equation 3.2.3 and δx is the nominal size of a mesh cell.

$$D^* = \left(\frac{\dot{Q}}{\rho_\infty c_p T_\infty \sqrt{g}}\right)^{\frac{2}{5}} \qquad 3.2.3$$

The higher $D^*/\delta x$, the more computational cells span the diameter of the fire. A value of 4 is qualified as a coarse mesh, 10 can be seen as moderate and 16 as fine[1]. According to Ma and Quintiere, who studied numerical simulation of axisymmetric fire plumes in unconfined spaces the optimal resolution for a (small) pool fire is 20 cells within the characteristic diameter [29].

During the tests an HRR between 250 and 900 kW was measured. For ambient conditions with $\rho_\infty = 1.204\ kg/m^3$, $c_p = 1.005\ kJ/kg.K$ and $T_\infty = 293K$, Equation 3.2.3 result in a characteristic fire diameter (D^*) of 0.551 and 0.919 for 250kW and 900kW fires. With the above-mentioned criteria and Equation 3.2.3 the following cell sizes can be determined:

- Coarse $D^*/\delta x = 4$ → δx = 14 – 23 cm
- Moderate $D^*/\delta x = 10$ → δx = 5.5 – 9.3 cm
- Fine $D^*/\delta x = 16$ → δx = 3.6 – 5.8 cm
- Ma & Quintiere $D^*/\delta x = 20$ → δx = 2.8 – 4.6 cm

Because FDS moves edges of obstructions towards the closest cell edge and most dimensions of the measurement set-up are a multiplication of 5cm a three-dimensional grid size of 5cm is chosen as cell size for all heat release rates. For smaller fires this grid size can be considered as moderate and for the larger fires the grid size can be considered as fine. The total number of cells is 620,868 with a 5cm grid size.

3.2.3.3 Exhaust

To model a circular vent the exhaust is modelled with a duct and nodes. The volumetric air flow rate (m^3/s) is set variable in time by inserting a number of points in time with a defined flow rate. During the experiments the flow rate at the measurement section can be determined from the differential pressure and temperature. Since not the entire duct is modelled until the measurement section, the flow rate is corrected for the temperature drop between the extraction point and measurement section.

Leakage of the smoke cabinet is also modelled since the connection between the elevated top and adjacent walls is not completely closed. A leakage area of 336 cm^2 represents a 3-mm gap at this connection.

3.2.4 Combustion

The "simple chemistry" model is used by default in FDS for modelling of combustion. This single-step, mixing controlled chemical reaction contains three lumped species, namely air, fuel and products. A lumped specie is a group of primitive species, e.g. air consists of oxygen, nitrogen and insignificant amounts of water vapour and carbon dioxide. The model requires the number of carbon, hydrogen, oxygen and nitrogen atoms, along with the soot yield and carbon monoxide yield to determine the reaction products. [18]

Within the objective of this study the reaction products of the numerical simulations are no subject of interest.

3.2.5 Heat Release Rate

The HRR for a burning surface can be modelled with several methods. With the first method a maximum value of the heat release rate per surface area is defined. By defining a ramp-up time for multiple points the fire growth and extinction can be modelled. The

modelled HRR follows the defined ramp. The second method is based on the mass loss rate of the fuel which is also defined by a maximum value and a ramp-up time. The heat of combustion per kilogram of fuel should be chosen carefully since this is the most influential parameter for the estimated HRR. Since the HRR is measured during the experiments the first method will be used in this study to gain reliable results. A steel fuel tank is modelled with a top surface assigned as 'fire'. The top surface of every simulation has assigned a maximum HRR rate value and ramp-up time based on the performed experiments. The HRR ramp used in the simulations is shown in Figure 19.

3.2.6 Water droplets

The Lagrangian approach is used to model the trajectories of water droplets. Calculation of the droplet trajectories is explained in paragraph 2.2. The convective heat transfer model and trajectories described in paragraph 2.2 are slightly different from the embedded models in FDS. The droplet size distribution can be represented by different methods, but the most common method is a combination of the Rosin-Rammler and log-normal distribution. This method described in paragraph 2.3 is default in FDS.

The sprinkler spray envelope can be modelled with three different methods. Since the scattering of the water droplets by the nozzle's deflector is too complex the particles are injected in the model at a spherical surface around the nozzle that needs to be defined.

The first method defines a conical spray envelop and requires the injection velocity or orifice diameter. When the orifice diameter is given FDS determines the velocity with the equations in paragraph 2.2. A hollow spray envelope can be modelled by defining lower elevation angles that are larger than 0°. The particles are injected randomly with a Gaussian distribution.

With the second method an elliptical spray envelope can be modelled. This method is similar to the conical spray envelope and has an additional option to define the envelope for different azimuth angles.

The third method is the most sophisticated and divides the spherical injection surface into smaller surfaces by defining multiple elevation angles and azimuth angles. For every injection surface the velocity and mass fraction must be inserted to model a realistic spray pattern.

The median diameter that is inserted into the model is dependent on the water pressure and is determined for each pressure with equation 2.3.1. The water particles are injected at a spherical surface with radius 0.1m. The centre of the sphere represents the sprinkler nozzle.

To model a realistic spray pattern with the 'spray table' method detailed information is required which R&D departments of sprinkler manufacturers do not share. Particle Image Velocimetry is too extensive for this study and therefore bucket tests are performed to model a sprinkler pattern. The bucket tests and translation to a 'spray table' are explained in *Appendix 6 – Bucket test*. The 'spray table' is implemented in the FDS-model to model the sprinkler spray.

In Figure 15 until Figure 18 the results of the bucket tests are displayed for an operating pressure of 0.79 bar. The results are compared with the FDS predictions that are obtained with implementing the 'spray table'. As can be seen in the figures the relative error between the FDS model and measurements ranges between -34.5% (avg. underprediction) and +22.2% (avg. overprediction). The horizontal distance of the water droplets is smaller in the FDS model than was measured. This trend was observed in all numerical simulations. The spray table of the best-fitted results is used in the final simulations.

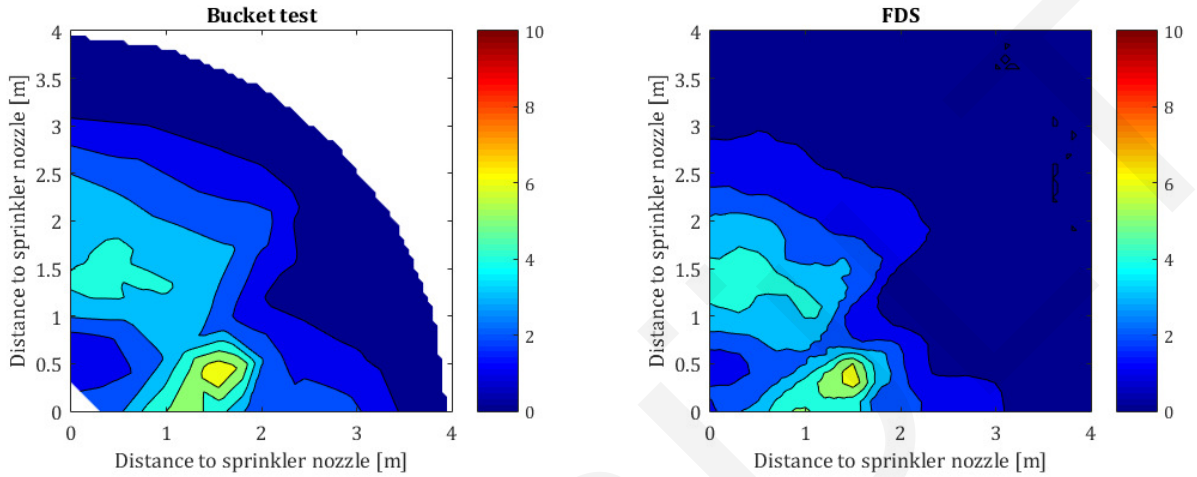

Figure 15 - Water collection at floor (lpm/m²) with operating pressure 0.79 bar, Bucket test (left), FDS (right)

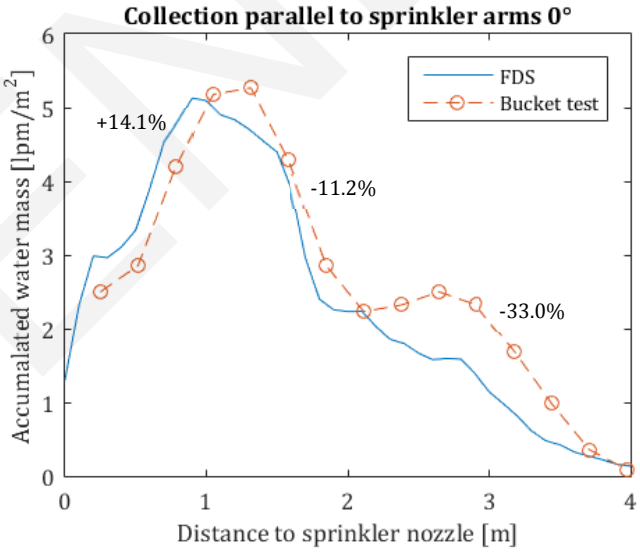

Figure 16 - Comparison Bucket tests & FDS (0.79 bar)

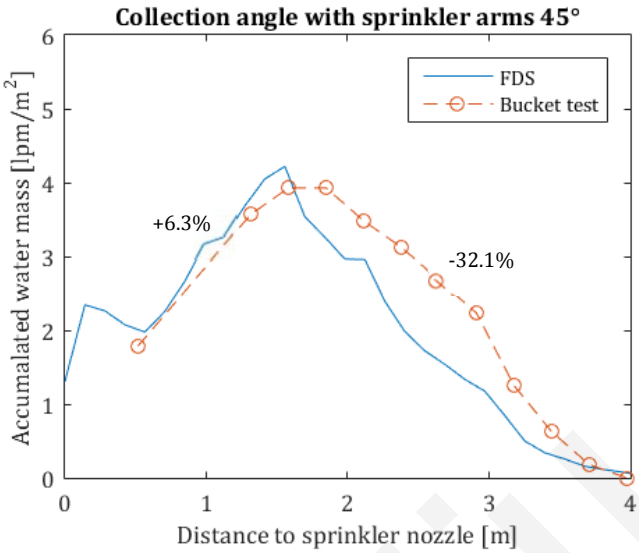

Figure 17 - Comparison Bucket tests & FDS (0.79 bar)

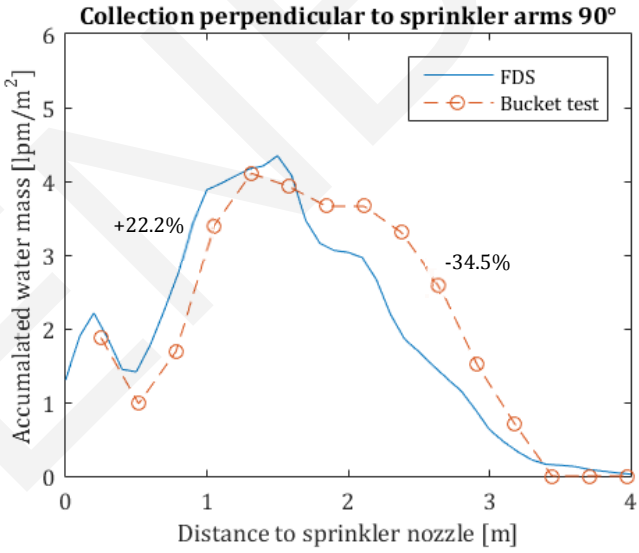

Figure 18 - Comparison Bucket tests & FDS (0.79 bar)

4 Results

4.1 Experiments

In Table 3 an overview is given of the (relevant) performed experiments. The reference tests are done to validate the computational model without applying a sprinkler system. In Appendix 7 the results of the individual tests are attached.

Table 3 - List of performed experiments

Name	Fuel	Weight [kg]	Pool size [m²]	Burning time [s]	Avg. HRR at peak [kW]	Theoretical THR [MJ]	Measured THR [MJ]
RH0	n-heptane	2.18	0.25	383	267	96.2	97.8 (+1.7%)
RH1	n-heptane	0.97	0.25	189	266	43.0	42.9 (-0.2%)
RHT2	heptane/toluene mixture 85/15	2.98	0.35(a)	202	650(c)	128.5	-
SHT1	heptane/toluene mixture 85/15	4.00	0.35(a)	221	978	172.4	165.3 (-4.1%)
SH1	Heptane	4.00	0.35(a)	242	875	178.2	198.7 (+11.5%)
SH2	Heptane	4.02	0.35(b)	290	730	179.1	178.3 (-0.5%)
SH3	Heptane	4.02	0.35(b)	260	785	179.1	171.1 (-4.5%)
SH4	Heptane	3.92	0.35(b)	250	948	174.7	174.8 (+0.1%)
SH5	Heptane	4.04	0.35(b)	226	916	180.0	167.3 (-7.1%)

(a) No additional fuel cooling
(b) Additional fuel cooling by larger fuel tray filled with water (0.7 x 1.0m)
(c) Measurement data HRR not stored. Recovered from fractions of data.

In Table 4 the applied sprinkler pressures and activation times are shown for the performed sprinkler experiments.

Table 4 - Sprinkler settings during sprinkler experiments

Name	Operating pressure [bar]	Sprinkler activated [s]	Sprinkler deactivated [s]	Water flow [l/min]
SHT1	0.79	154	250	71.6
SH1	0.79	96	186	71.6
SH2	0.40	118	223	51.0
SH3	1.34	120	250	93.3
SH4	0.79	123	223	71.6
SH5	1.34	121	221	93.3

4.1.1 Heat Release Rate & Total Heat Release

In Table 3 the theoretical and measured Total Heat Release (THR) are given to determine the reliability of the performed experiments. The theoretical THR is a product of the fuel weight and heat of combustion (H_c). For n-heptane and heptane H_c is 44.56 MJ/kg and for heptane/toluene H_c is 43.11 MJ/kg as determined in Appendix 4.

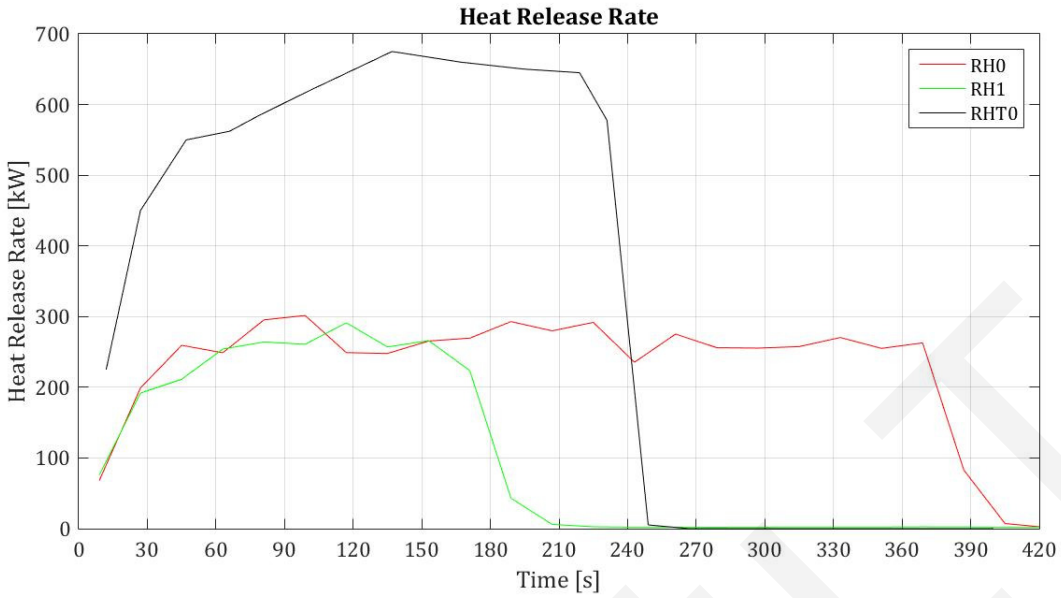

Figure 19 - Heat Release Rate reference tests n-heptane and heptane/toluene

In most experiments the measured THR agrees (within 10%) with the estimated THR. Except for SH1 where the measured THR is 11.5% higher than expected. In Figure 19 and Figure 20 the measured HRR of all experiments is shown. The measurement data is averaged in time to improve readability of the graphs.

The differences in burning time during the reference tests are caused by the different amounts of fuel that were used. When the burning rate is constant during the reference tests the HRR of the experiments (with similar pool size) is close together. For the sprinkler tests, on the other hand, the fuel weight and pool size were taken almost the same for each experiment but also for these tests differences in burning time were experienced. Experiments SH2, SH3, SH4 and SH5 are performed with additional cooling of the fuel tray to keep the evaporation rate of the fuel constant and thus the HRR constant.

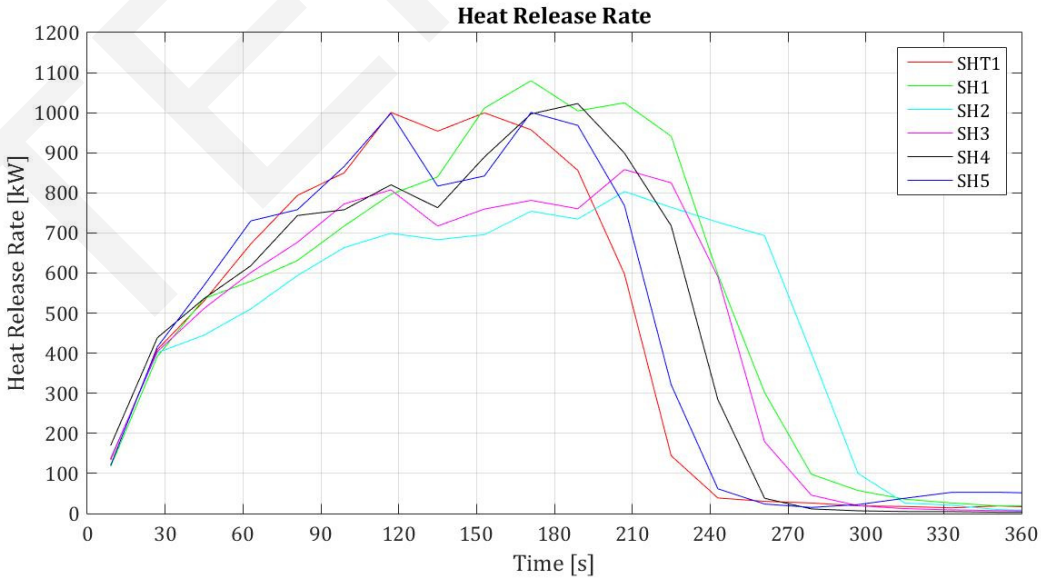

Figure 20 - Heat Release Rate sprinkler tests heptane/toluene and heptane

4.1.2 Smoke layer temperature

4.1.2.1 Reference experiments

The average smoke layer temperature is shown in Figure 21 for experiments RH0, RH1 and RHT2. The average smoke layer temperature is taken over the thermocouples that are in the smoke layer when a stable smoke layer is formed. For experiments RH0 and RH1 a smoke layer of approximate 1.0 – 1.4m formed in the smoke cabinet and the average is taken of the top 3 thermocouples of each pillar. After approximating 120 seconds a constant smoke layer temperature of 75°C was reached in both experiments. The temperature and height of the smoke layer were considered as insufficient for proper assessment of smoke layer cooling by a sprinkler spray and since the exhaust could not be reduced any further it was chosen to increase the pool size to generate more heat.

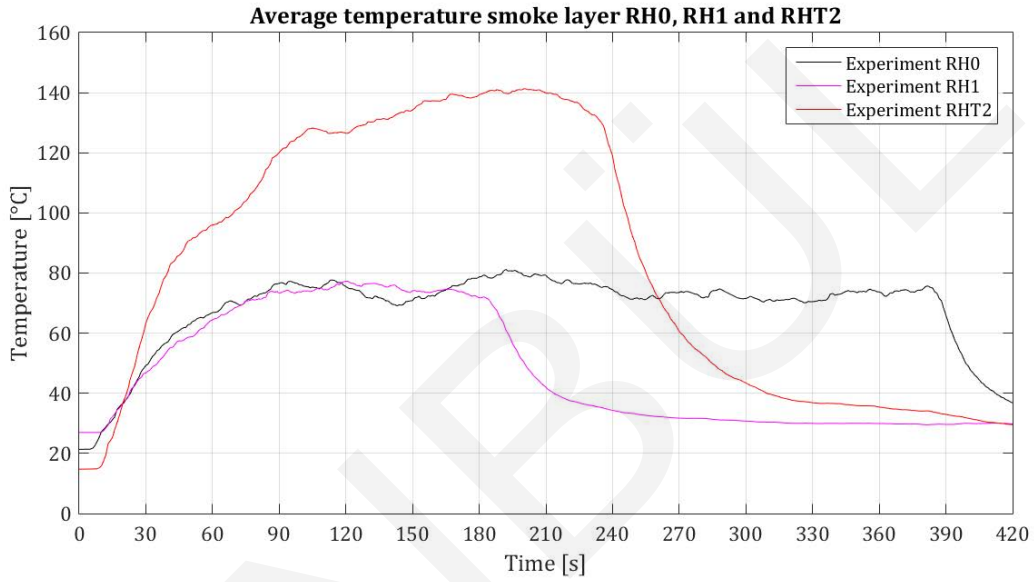

Figure 21 - Average smoke layer temperature reference tests (RH0, RH1, RHT2)

During RHT2 the smoke cabinet filled completely with smoke, meaning that the top 5 thermocouples of each pillar were in the smoke layer. The average is shown in Figure 21 is taken from these thermocouples. After 150 seconds a constant smoke layer temperature of 150°C was reached. The height and temperature of the smoke layer were found sufficient to perform the sprinkler test. During the first sprinkler test SHT1, the sprinkler will be manually activated after 150 seconds since it is expected that at this point a constant temperature is reached.

4.1.2.2 Sprinkler experiments (pressure 0.40 bar)

In Figure 22 the average smoke layer temperature is shown of experiment SH2. Between 118 and 223 seconds the sprinkler is active with an operating pressure of 0.40 bar. Heat is transferred from the hot gases to the water droplets and because of that the smoke layer temperature is reduced during the sprinkler activation. Once the sprinkler is deactivated after 223 seconds the temperature starts to increase again. Since the temperature is still increasing at the moment of sprinkler activation it is expected that the temperature would have kept raising if no sprinkler was activated. The expected temperature curve without sprinkler activation is shown by the blue, dashed line in Figure 22.

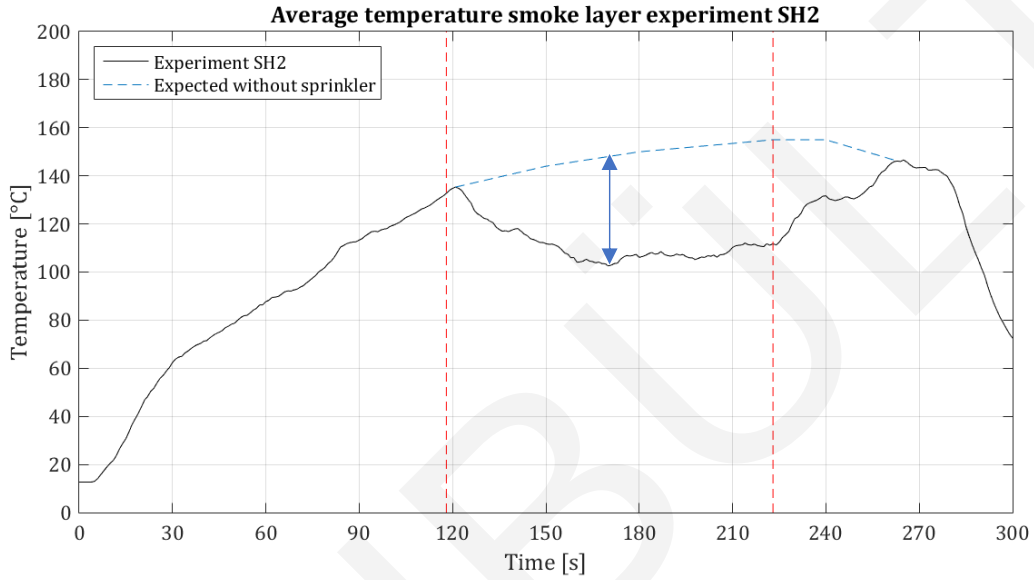

Figure 22 - Average smoke layer temperature sprinkler test heptane 2 (SH2)

It takes around 50 seconds for the smoke layer to reach its 'minimum' temperature and at this point the smoke layer is cooled down with 45 – 50 °C compared to the expected temperature without sprinkler activation. The HRR of the fire keeps slowly increasing during sprinkler activation, resulting in a small temperature increase of the smoke layer during sprinkler activation.

4.1.2.3 Sprinkler experiments (pressure 0.79 bar)

Three experiments with different sprinkler activation times were performed for an operating pressure of 0.79 bar. In Figure 23, Figure 24 and Figure 25 the average smoke layer temperature is shown of experiment SH1, SH4 and SHT1. In experiment SH1 the sprinkler is manually activated after 96 seconds, which is still in the developing phase of the fire. Approximate 30 seconds after sprinkler activation the minimum temperature is reached and then immediately starts increasing again. Cooling by the sprinkler spray is estimated at 60 – 65°C compared to no sprinkler. When the sprinkler is deactivated at 186 seconds the temperature is almost at the same level as at activation. The rapid increase of the temperature indicates that thermocouples were kept dry during the sprinkler activation and a better estimation can be made for the expected temperature curve without a sprinkler.

During experiment SH4 the sprinkler was manually activated after 123 seconds resulting in a higher temperature at that point. Again, it takes around 30 seconds before the minimum temperature is reached and thereafter it starts increasing again. The cooling is estimated at 70-75°C. Because the fire starts terminating at the same time as the sprinkler is deactivated the temperature does not rise again like in SH1.

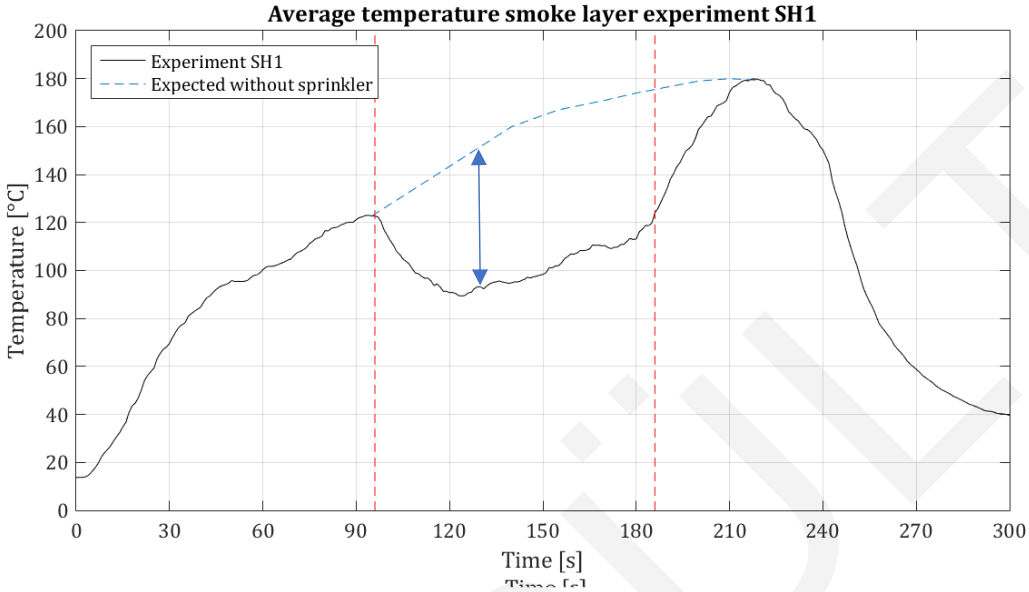

Figure 23 - Average smoke layer temperature sprinkler test heptane 1 (SH1)

SHT1 is the only sprinkler experiment performed with heptane/toluene and its sprinkler activation time is based on RHT2. However, during SHT1 the burning rate was high which resulted in a shorter burning period and an unexpected termination of the fire during sprinkler activation. Because no stability was reached with the activated sprinkler it is difficult to determine the cooling effect of the sprinkler spray. The small temperature increase at 180 seconds is too small to draw conclusions.

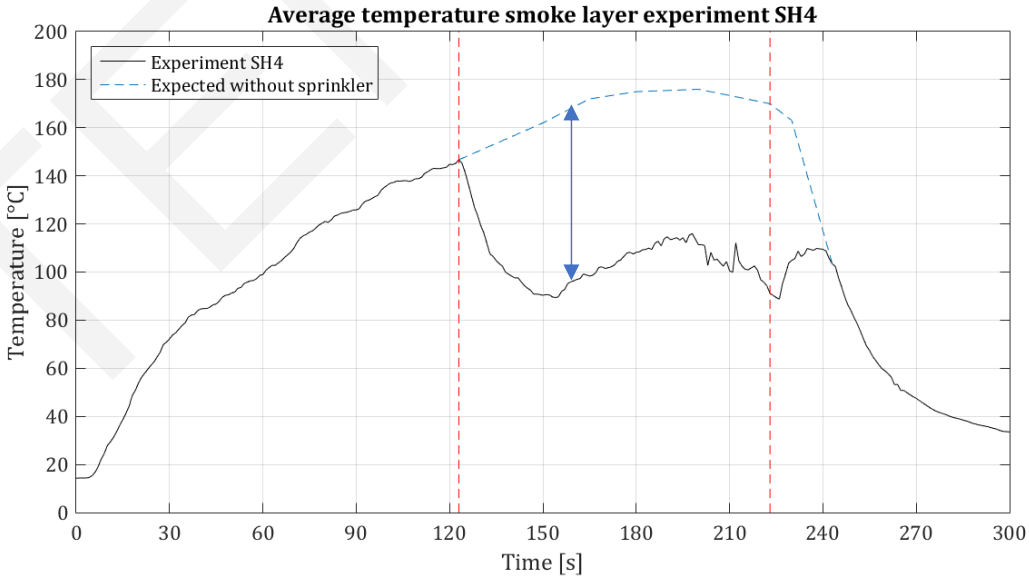

Figure 24 - Average smoke layer temperature sprinkler test heptane 4 (SH4)

4.1.2.4 Sprinkler experiments (pressure 1.34 bar)

The executed scenarios of SH3 and SH5 are almost identical. Nevertheless, the burning time of SH5 was 34 seconds shorter. In both experiments it takes around 40 seconds to reach the minimum smoke layer temperature. The higher HRR in SH5 results in a faster increase of the smoke layer temperature before and during sprinkler activation. After 190 seconds the fuel is almost depleted in SH5 and the temperature starts decreasing again as a result of the sprinkler and decreasing HRR. In SH3 the fire terminated directly after deactivation of the sprinkler, meaning the smoke layer did not heat-up anymore. For both experiments the sprinkler cooling is estimated to be 85 – 95 °C.

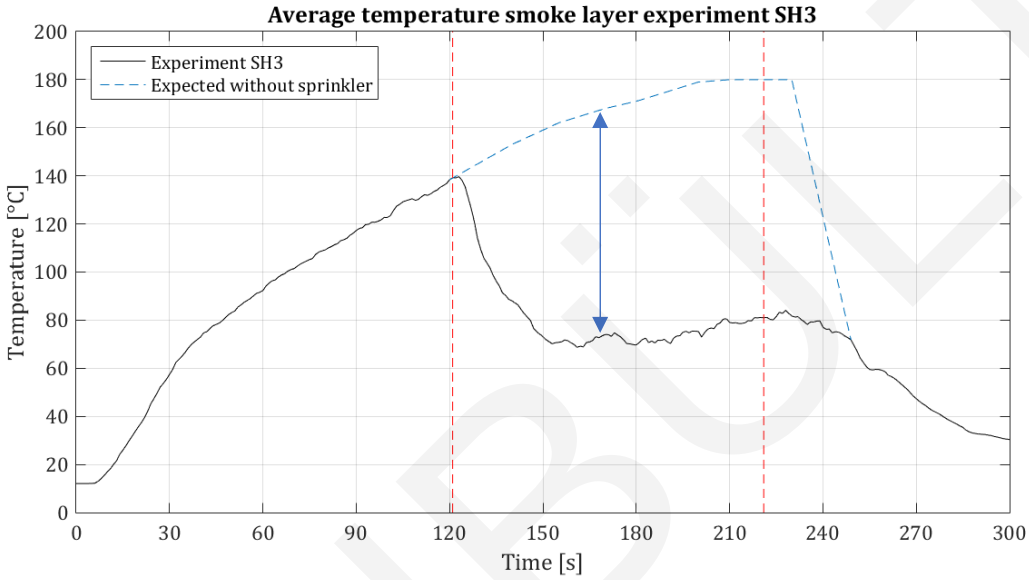

Figure 26 - Average smoke layer temperature sprinkler test heptane 3 (SH3)

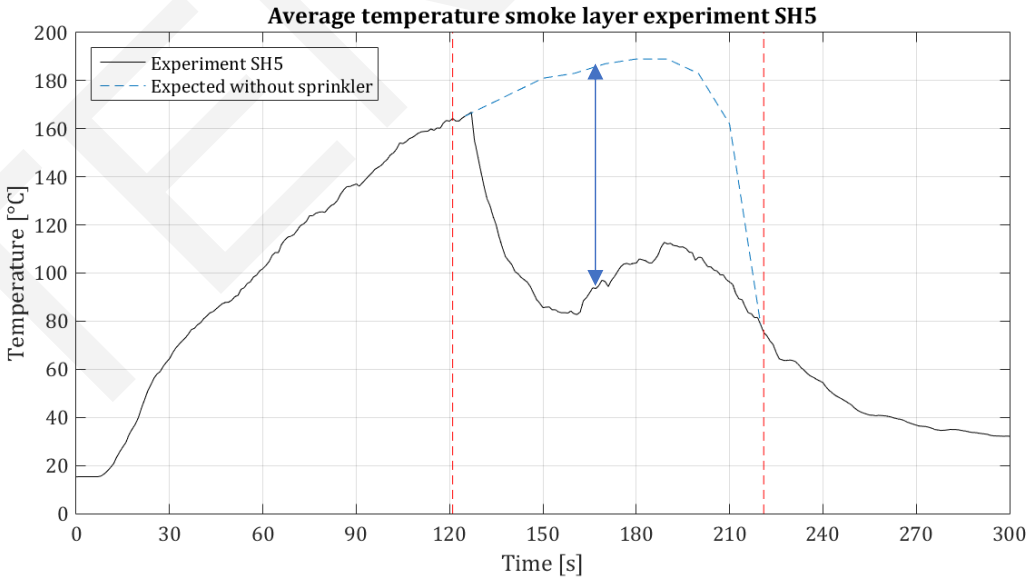

Figure 27 - Average smoke layer temperature sprinkler test heptane 5 (SH5)

4.2 Computational models

All experiments were modelled in FDS. For each simulation the same grid and method were used to solve the numerical problems. The HRR, sprinkler properties, exhaust rate and boundary conditions are deduced from the experiments.

4.2.1 Heat Release Rate

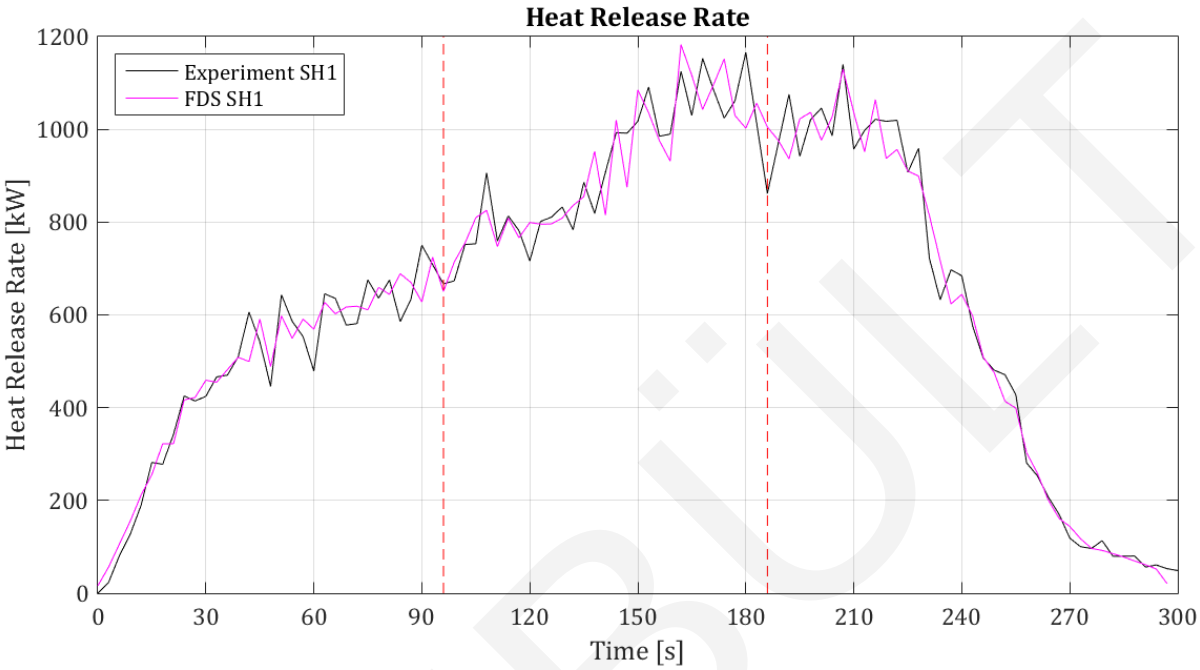

Figure 28 - Heat Release Rate as measured in SH1 and as modelled in FDS

In Figure 28 the modelled HRR by FDS(pink) and measured HRR (black) are shown for experiment SH1. The model prediction follows the imposed curve. Since there are no large deviations between the measurement and model further adjustments are not necessary for modelling the HRR.

4.2.2 Smoke layer temperature

4.2.2.1 Reference experiments

In Figure 29 the average smoke layer temperature of both experiment and simulation is shown. The measured and predicted temperatures show good agreement for RH0. However, the predicted smoke layer is thicker than was measured in the experiment. The larger smoke volume in the prediction with a similar smoke temperature compared to the measurement contains thus more energy. In other words, the smoke volume is overpredicted in FDS.

This is confirmed in RHT2 were the smoke cabinet is filled in both experiment and simulation. During the experiment the smoke is contained within the cabinet, but in the model prediction the smoke is spilt out of the cabinet, this results in a smoke layer with a higher temperature.

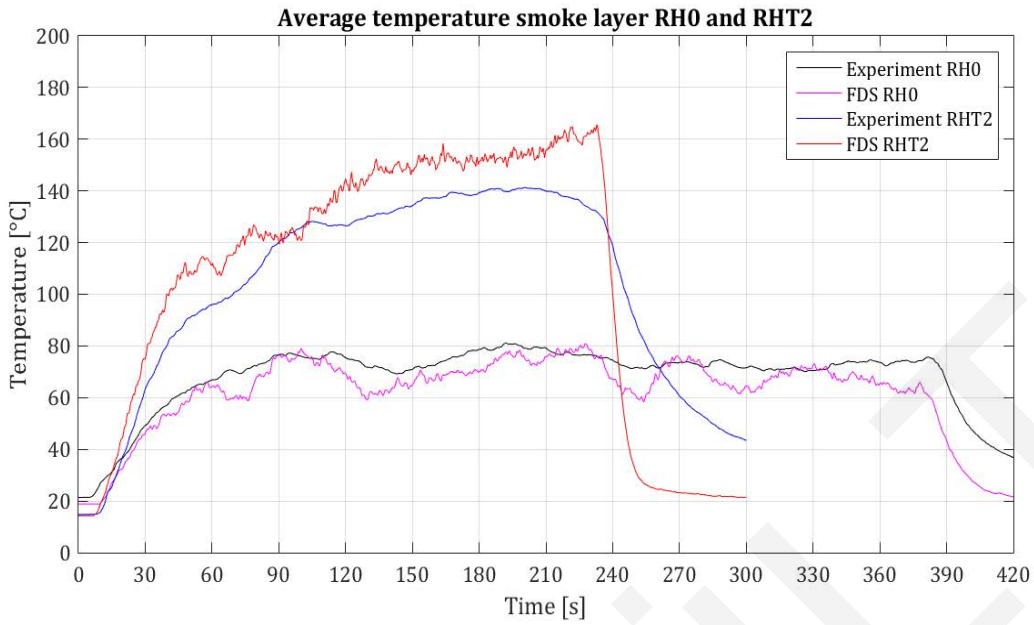

Figure 29 - FDS predictions of average smoke layer temperature RH0 and RHT2

4.2.2.2 Sprinkler experiments (0.40bar)

To examine cooling of the smoke layer in FDS the CFD-models were simulated two times. The first run includes the sprinkler spray as determined in Appendix 6 and according to the operating pressure. In the second run the same simulation is performed but without the sprinkler spray. In Figure 30 the simulation result with sprinkler spray is represented by the pink line (bottom line hatched area, between dashed lines) and the simulation without sprinkler spray is represented by the blue line (top line between dashed lines).

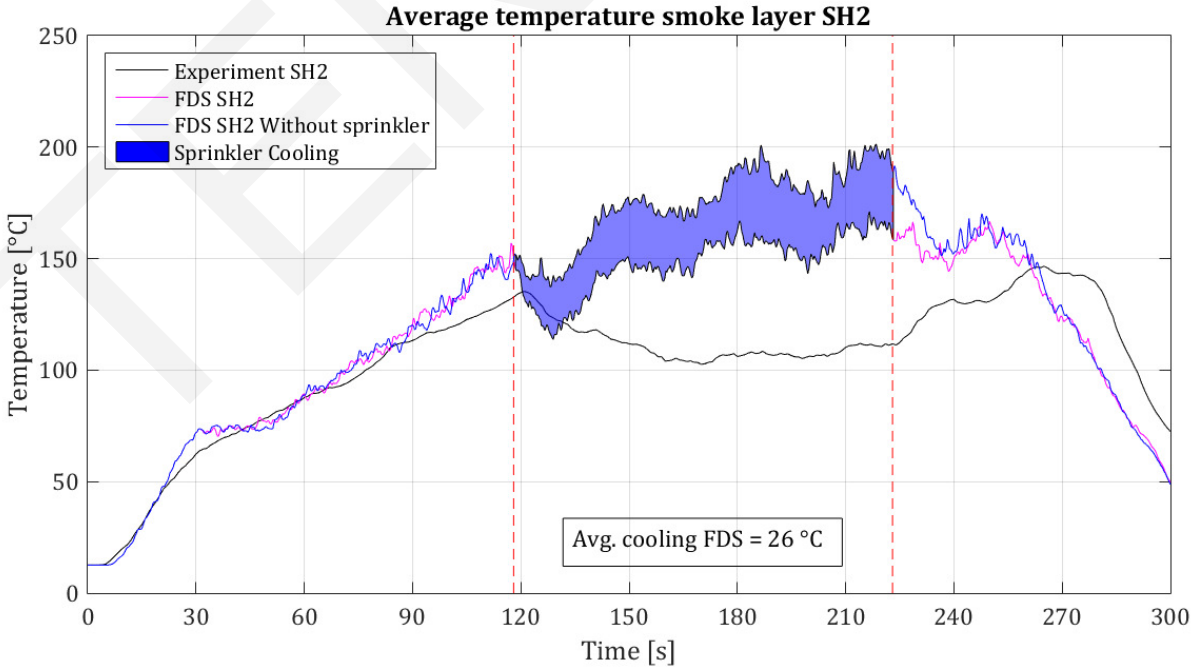

Figure 30 - FDS predictions of average smoke layer temperature SH2 (0.40 bar)

The experimental result is shown by the black line. Between the two red dashed lines the sprinkler is active.

Until 90 seconds the FDS models and the experiment show good agreement, thereafter the average temperature in the simulations is increasing faster and at sprinkler activation the temperature is approximately 20°C higher. The blue surface in Figure 30 shows the cooling of the smoke layer by the sprinkler spray in FDS. After 15 seconds of cooling the temperature starts rising again with the sprinkler still active. This effect is caused by the HRR which is increasing. During sprinkler cooling in FDS similar trends for temperature decrease and increase can be seen between the sprinkler model and model without a sprinkler. The temperature difference between those curves remains constant with an average cooling of 26°C. Where the temperature remains rather constant after its minimum is reached in the experiment, the predicted temperature in the model is higher at sprinkler deactivation than it was at activation.

4.2.2.3 Sprinkler experiments (0.79 bar)

In Figure 31, Figure 32 and Figure 33 the FDS results are shown for the sprinkler experiments with an operating pressure of 0.79 bar. Although, temperatures of the smoke layer and activation times are different between the experiments a consistent cooling of approximate 40°C is modelled with FDS.

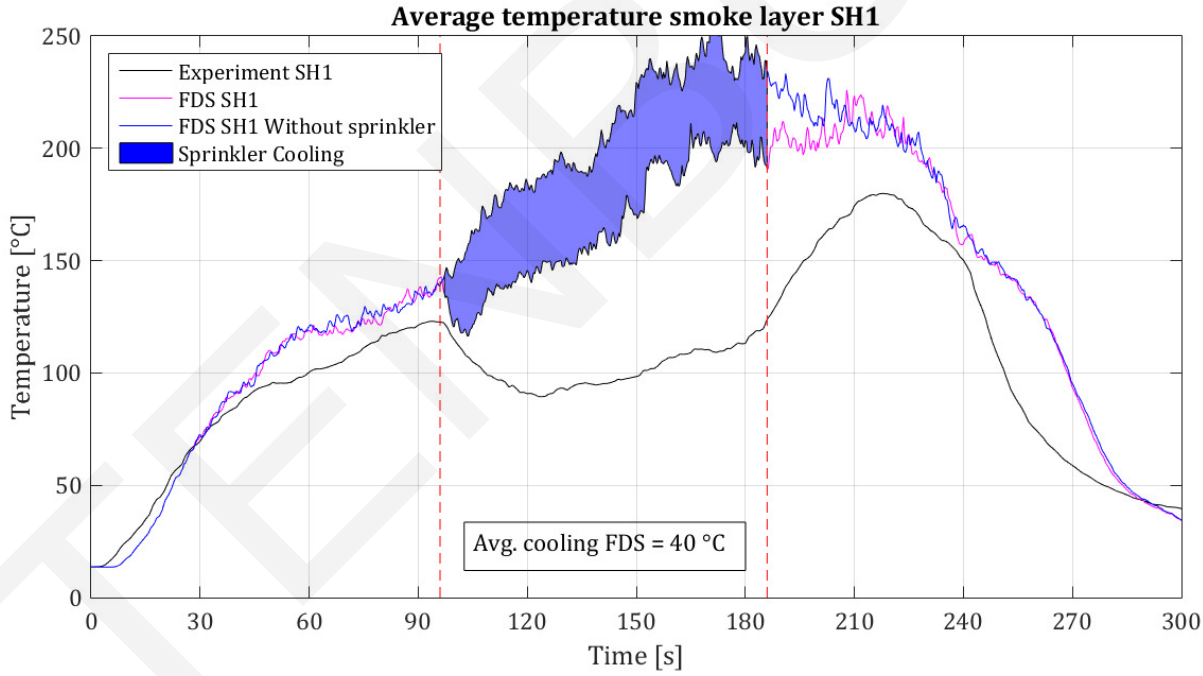

Figure 31 - FDS predictions of average smoke layer temperature SH1 (0.79 bar)

Compared to the measured cooling of 60 – 65°C for SH1 and 70 – 75°C for SH4 and SHT1 the cooling in FDS is underpredicted for an operating pressure of 0.79 bar.

In the model without sprinkler cooling the temperature increases rapidly after 96 seconds. Since the model without sprinkler is similar to the sprinkler model, also in this

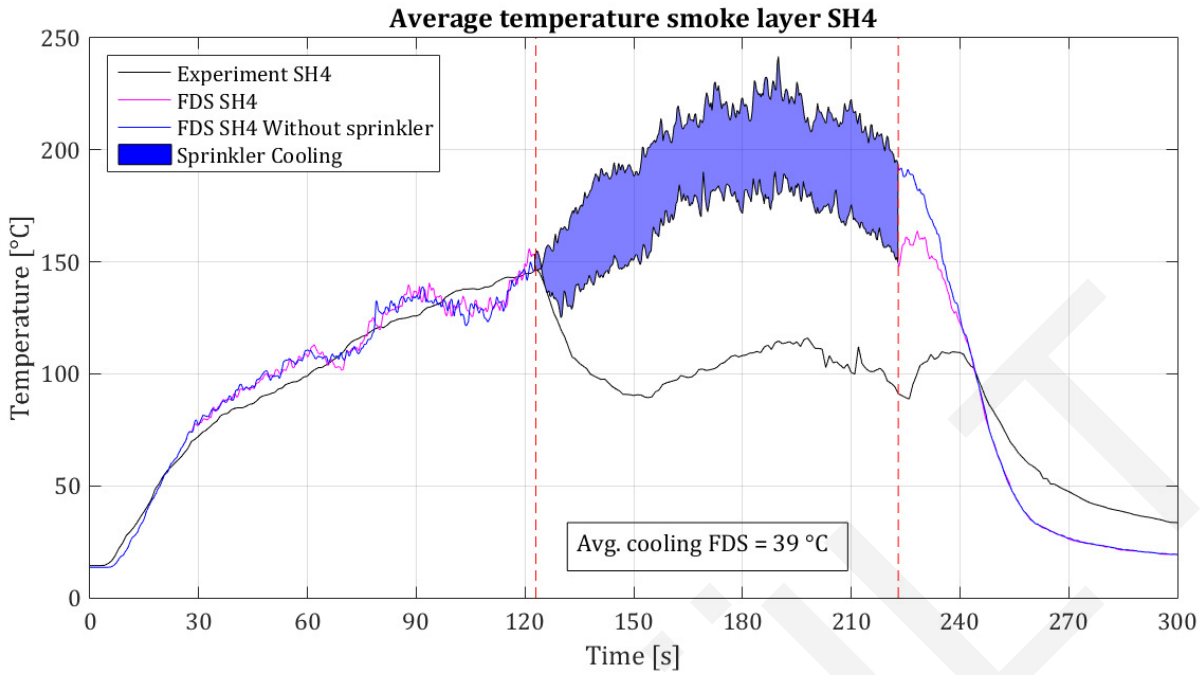

Figure 32 - FDS predictions of average smoke layer temperature SH4 (0.79 bar)

model the exhaust rate is reduced after 96 seconds, which results in more accumulation of heat in the smoke cabinet.

During experiment SHT1 the fire terminated during sprinkler activation. For the average cooling in FDS the temperature decay due to termination of the fire is not considered (only blue surface).

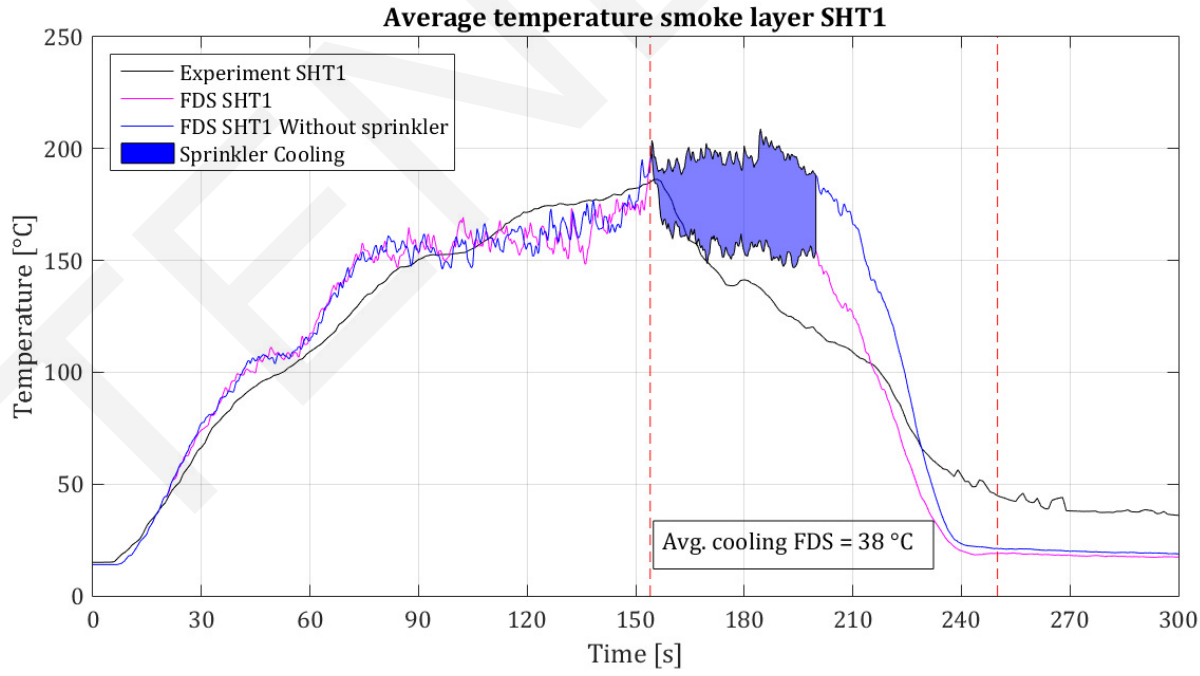

Figure 33 - FDS predictions of average smoke layer temperature SHT1 (0.79 bar)

4.2.2.4 Sprinkler experiments (1.34bar)

In Figure 34 and Figure 36 the FDS results are shown for the sprinkler experiments with an operating pressure of 1.34 bar. For both SH3 and SH5 the average smoke layer cooling predicted by FDS is approximate 60°C. As for operating pressures of 0.40 and 0.79 bar the cooling is underpredicted by FDS for an operating pressure of 1.34 bar

The temperature curve of FDS simulation SH3 without sprinkler gradually increases and a similar trend is followed by the sprinkler model after it reaches its minimum temperature. The smoke is cooled by 59°C during sprinkler activation. At sprinkler deactivation the temperature has already increased again with 40°C to 150°C as before sprinkler activation. In the experiment the smoke temperature only increased by 10°C and the temperature at deactivation is much lower than at activation.

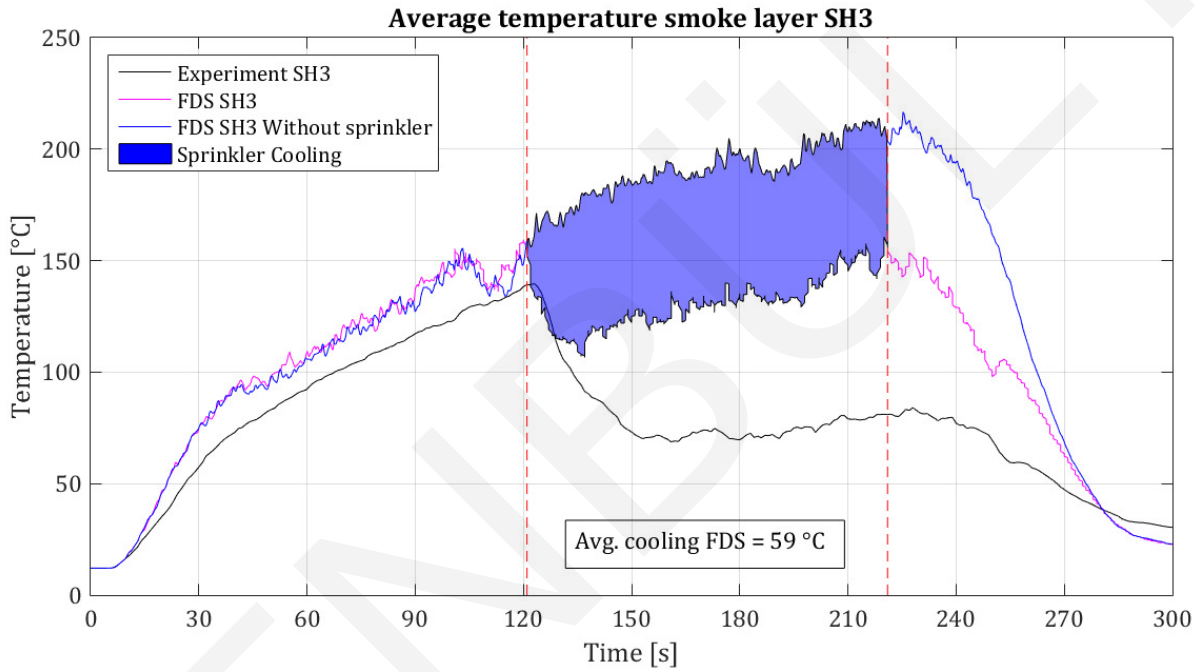

Figure 34 - FDS predictions of average smoke layer temperature SH3 (1.34 bar)

In Figure 35 a vertical section of the temperature is shown right before sprinkler activation and after 15 seconds of sprinkler cooling (temperature at minimum in FDS).

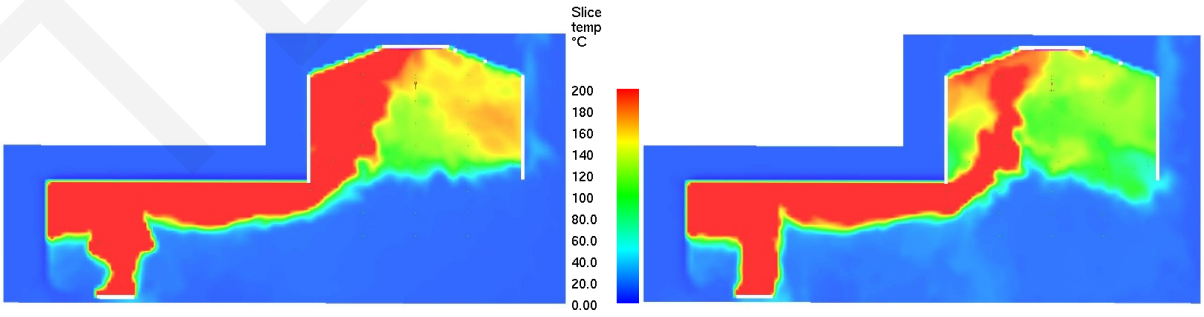

Figure 35 - Temperature FDS SH3, after 120.9 seconds (left) and 135.6 seconds (right)

In the plume region, the temperature is significantly reduced. At the opposite side of the plume, smoke is displaced downward when the sprinkler is active.

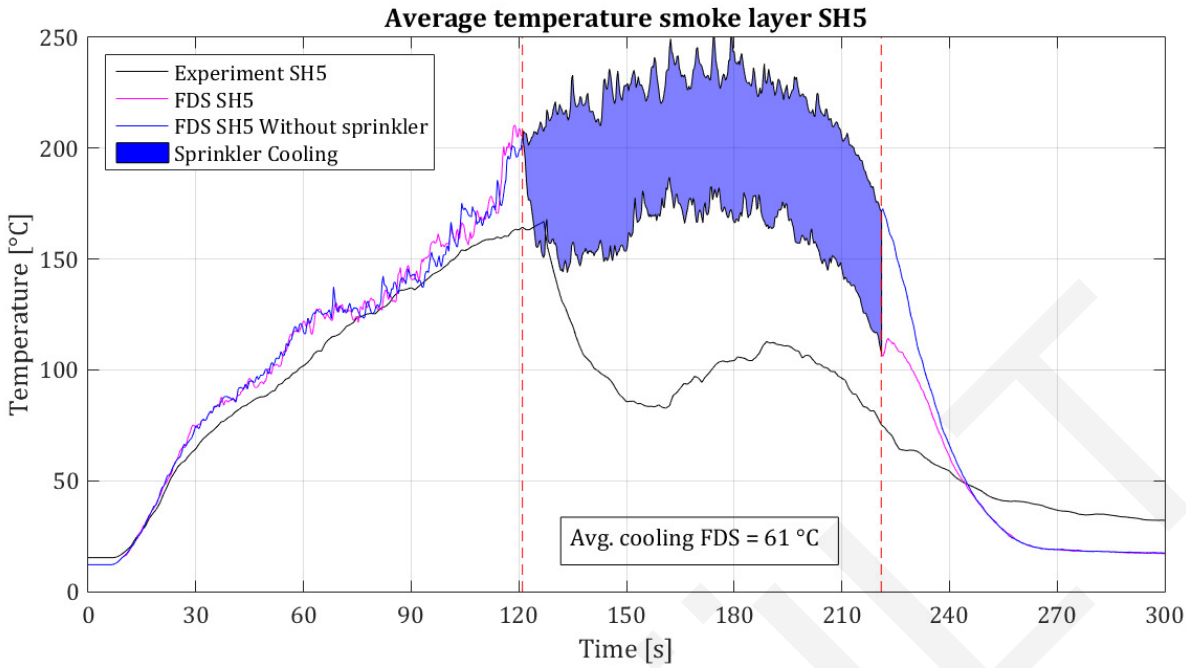

Figure 36 - FDS predictions of average smoke layer temperature SH5 (1.34 bar)

4.2.2.5 Overview results

In Table 5 the results for smoke layer cooling of all models and experiments are given. For all operating pressures the smoke layer cooling in the FDS models is underpredicted compared to the experiments. Despite accurate modelling of the sprinkler spray the predicted temperatures are higher than during the measurements.

Table 5 - Overview smoke layer cooling during experiments and in FDS

Experiment/ model	**Operating pressure [bar]**	**Water flow rate [l/min]**	**Measured temperature decrease [°C]**	**Modelled temperature decrease [°C]**
SH1	0.79	71.6	60 – 65 (-37%)	40 (-22%)
SH2	0.40	51.0	45 – 50 (-30%)	26 (-18%)
SH3	1.34	93.3	85 – 95 (-55%)	59 (-35%)
SH4	0.79	71.6	70 – 75 (-42%)	39 (-24%)
SH5	1.34	93.3	85 – 95 (-49%)	61 (-29%)
SHT1	0.79	71.6	70 – 75 (-30%)	38 (-21%)

5 Discussion

5.1 Experimental results

5.1.1 Measurement uncertainties

To determine the HRR several quantities are measured and a number of approximated constants are used. All these quantities and constants contain small errors which result in a total error for the HRR. From all individual errors a combined expanded relative standard uncertainty can be derived. When a coverage factor of 2 is applied a confidence level of approximately 95% is achieved. The standard uncertainty of the HRR can be calculated in two steps. At first the standard uncertainty for the normalized volumetric flow rate (V_{298}) is calculated (Table 6) since this quantity contains several constants and measured parameters. For constants C, k_t and k_p the same values are taken as determined in a study by Axelsson et al. [30]. The installed pressure transducer has an accuracy of 1% at a measurement range of 0-100Pa, resulting in a maximum error of 1Pa. During the measurements the differential pressure ranges between 5 and 10 Pascal. This means the relative error of the differential pressure is 10 – 20%. The K-type thermocouple has an error of 2.2°C. During the measurements the temperature is approximately 100°C at the measurement section, resulting in a relative error of 2.2%.

Table 6 – Derivation of combined expanded relative standard uncertainty for V_{298}

Quantity	**Relative error [%]**	**Relative standard uncertainty $u(x_i)/x_i$ [%]**	**Relative sensitivity coefficient $c_{r,i}$**	**Contribution to combined uncertainty of flow measurement $c_{r,i} \cdot u(x_i)/x_i = u_i(y)$**
A (area)	-	-	1	-
C (constant)		0.25[30]	1	0.25
k_t (velocity factor)		1.0 [30]	1	1.0
k_p (bi-probe factor)	2 [30]	1.15	1	1.15
Δp (pressure diff.)	10-20	5.78 – 11.56	0.5	2.89 – 5.78
T_s (temperature)	2.2	1.27	0.5	0.64
Combined expanded relative standard uncertainty				**6.7 – 12.0%**

The uncertainties for O_2 and CO_2 concentrations were determined by Axelsson et al. for a 150kW and 1MW fire [30]. For the 150kW fire a small relative error was found compared to the 1MW fire but the relative sensitivity coefficient is much larger than for a 1MW fire. It can be seen that for the smaller HRR the combined expanded relative uncertainty is slightly larger and that the differential pressure and the O_2 concentration are the most influential quantities.

Table 7 - Derivation of combined expanded relative standard uncertainty for HRR

Quantity (150kW – 1MW)	**Relative error [%]**	**Relative standard uncertainty $u(x_i)/x_i$ [%]**	**Relative sensitivity coefficient $c_{r,i}$**	**Contribution to combined uncertainty of flow measurement $c_{r,i} \cdot u(x_i)/x_i = u_i(y)$**
E-factor	5 [30]	2.0	1	2.0
V_{298}	-	-	-	6.7 – 12.0
O_2		0.08 – 0.3 [30]	-57 – -6.6 [30]	4.6 – 1.98
CO_2	2*	0.82	-0.18 – -0.13 [30]	0.15 – 0.11
Humidity (20%-80%) ambient conditions	5*	2.0	-0.0038 – -0.015 [30]	0.0076 – 0.03
Molecular weight of gas species	1*	0.58	1	0.58
Ambient pressure	-	-	-	negligible
Combined expanded relative standard uncertainty				**16.5 – 26.0% (150kW) 14.6 – 24.7% (1MW)**
*estimated values				

5.1.2 Heat Release Rate & Total Heat Release

In Table 3 the results for the measured HRR and THR are shown. The measured THR of SH1 is 11.5% higher than the estimated THR. The THR is a tool to determine the accuracy of the HRR measurement. Although, the deviation for SH1 is still within the relative uncertainty range as determined in Table 7 it is remarkable that the measured THR is larger than the estimated value. For the sprinkler tests the opposite effect was expected. Due to the sprinkler spray some of the smoke is pushed out of the sprinkler cabinet and not extracted through the exhaust duct. This effect would result in a lower value of the measured THR as occurred in SH2, SH3 and SH5. Therefore, the reliability of the measured HRR during SH1 is questionable. The HRR results of the other experiments seem to be reliable based on the expected and measured THR.

After analysis of SHT1 and SH1 it was found that the HHR kept increasing during the experiment. To reduce the evaporating of fuel and so the burning rate of the fuel the fuel tank was placed in a larger tank filled with water. The desired effect was achieved in SH2 and partially in SH3 but in SH4 and SH5 the cooling of the fuel tank did not seem to affect the HRR. Therefore, the HRR between the sprinkler tests differs more than in the reference tests, which make it more difficult to compare the sprinkler tests with each other.

5.1.3 Smoke layer temperature & energy content

During the experiments a smoke layer was formed in the smoke cabinet. Before sprinkler activation the volume of this smoke layer does not exceed the bottom edge of the cabinet. In an ideal situation the smoke volume remains equal during sprinkler activation, however smoke particles are dragged down by the water droplets causing more entrainment of air which results in a larger smoke volume. This enlarged smoke volume was often larger than the volume of the cabinet causing it to overflood. The flooded smoke volume could not be measured which makes it more difficult to determine all energy flows of the smoke layer.

During sprinkler activation the smoke layer can be distinguished into two zones, namely an upper zone within the enclosed parts of the smoke cabinet and a lower zone beneath the smoke cabinet. Due to the constant smoke volume of the upper zone, the energy required to heat up or cool down this smoke volume to a given temperature is easy to determine.

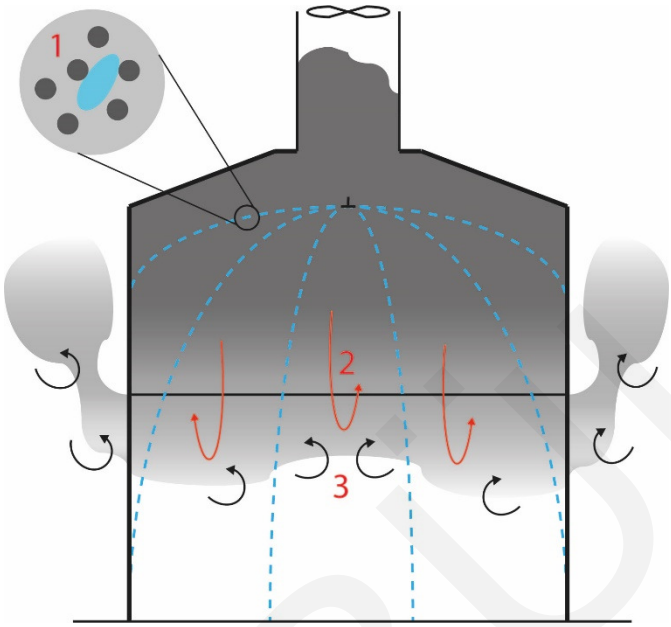

Figure 37 - Air entrainment during sprinkler activation

Figure 37 shows the upper and lower zone. In the upper zone (1) the smoke is cooled down by evaporation of water droplets and heat that is conducted to the water droplets when they fall through the smoke layer. The smoke particles in the upper layer 'stick' to the water droplets and are dragged down (2). Subsequently, ambient air is entrained into the descended smoke volume (3) which reduces the smoke temperature and increases its volume. The buoyant force of the smoke that was pushed out of the smoke cabinet and spray envelope was still dominant, causing it to rise again outside the cabinet.

It can be seen in Figure 38 that the smoke logging effect increases when the operating pressure is increased. For an operating pressure of 0.40 bar almost no smoke logging was observed where for 1.34 bar a diffuse smoke layer reduces the visibility significantly.

Figure 38 - Smoke logging during sprinkler experiments (multiple operating pressures)

5.1.3.1 Energy balance

In Figure 39 a simplification of the energy balanced is shown for a scenario without sprinkler activation (reference experiments) and a scenario with an activated sprinkler

(sprinkler experiments). In scenario 1 the energy loss to surroundings is equal to the inflow of energy ($\dot{Q}_{in}$) minus the outflow energy ($\dot{Q}_{out}$).

$$\dot{Q}_{walls}(t) = \dot{Q}_{in}(t) - \dot{Q}_{out}(t) \qquad 5.1.1$$

The energy flows $\dot{Q}_{in}$ and $\dot{Q}_{out}$ can be calculated from the measurements, which result in a value for $\dot{Q}_{walls}$.

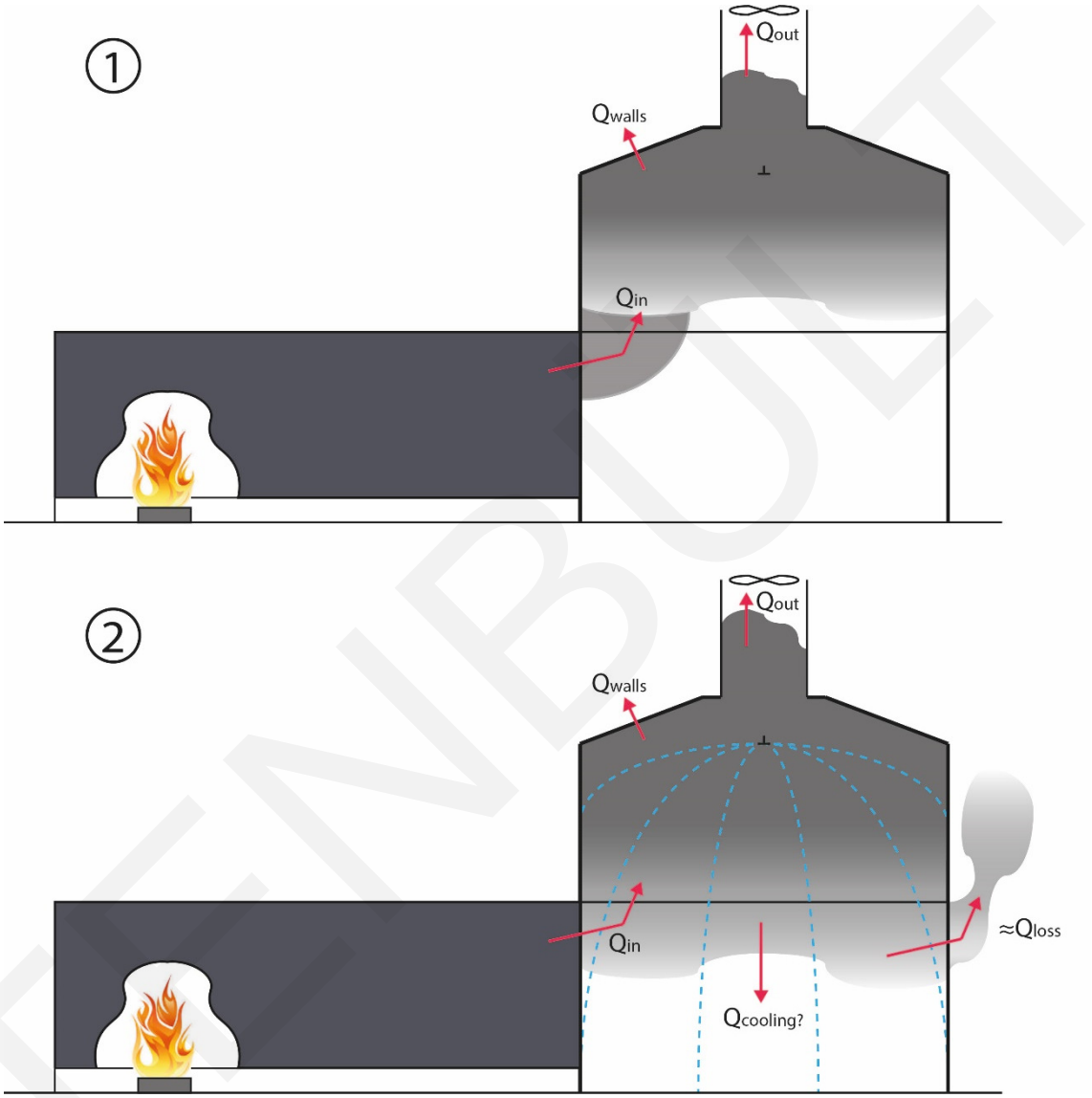

Figure 39 - Simplified energy balance, 1. No sprinkler, 2. Sprinkler activated

When the sprinkler is activated the cooling capacity of the water droplets is introduced in the energy balance. Again, $\dot{Q}_{in}$ and $\dot{Q}_{out}$ are known. A part of the energy is lost by smoke that flows out of the smoke cabinet ($\dot{Q}_{loss}$). For $\dot{Q}_{loss}$ an estimation must be made for the mass that flows out. The temperature of the lost smoke can be determined from the thermocouples at the bottom of the walls. The energy loss to the walls is not exactly known but can be estimated with the temperature difference between scenario 1 and 2. The temperature difference (ΔT) between the smoke and ambient air will be smaller resulting in less energy loss through the walls. Summing the positive energy flow and

negative energy flows results in an estimation of the cooling capacity of the sprinkler water ($\dot{Q}_{cooling}$).

$$\dot{Q}_{cooling}(t) = \dot{Q}_{in}(t) - \dot{Q}_{out}(t) - \dot{Q}_{walls}(t) - \dot{Q}_{loss}(t) \qquad 5.1.2$$

In Table 8 the cooling capacity is estimated for the performed sprinkler experiments. Scenario 1 is used to determine the energy loss to the wall just before the sprinkler activates. The cooling in scenario 2 is determined for the moment when the minimum smoke layer temperature is reached during sprinkler cooling.

Table 8 - Energy flows

	Scenario 1			Scenario 2					
Exp.	$\dot{Q}_{in}$ [kW]	$\dot{Q}_{out}$ [kW]	$\dot{Q}_{walls}$ [kW]	$\dot{Q}_{in}$ [kW]	$\dot{Q}_{out}$ [kW]	$\dot{Q}_{walls}$ [kW]	$\dot{Q}_{loss}$ [kW]	**$\dot{Q}_{cooling}$ [kW]**	$\dot{Q}_{cooling}/\dot{Q}_{in}$ x100%
SH1	420	289	131	480	151	97	48	**185**	38.5 %
SH2	438	345	93	438	201	78	24	**135**	30.9 %
SH3	471	370	101	471	145	44	73	**209**	44.5 %
SH4	540	413	127	570	201	78	48	**242**	42.5 %
SH5	550	421	128	525	127	66	67	**265**	50.5 %

For $\dot{Q}_{loss}$ an estimation has been done for the lost smoke volume, based on observations during the experiments. Smoke logging increased with increased water pressures. Smoke logging causes smoke to flow out of the smoke cabinet. The estimated volume is expressed in volume percentage of the exhaust hood, for an operating pressure of 0.40 bar this percentage is 5%, for 0.79 bar 10% and for 1.34 bar 15%.

Since several estimations and assumptions were done in the above-mentioned determination of the cooling capacity these results must be interpreted carefully.

5.2 Numerical results

5.2.1 Smoke layer temperature & energy content

In Appendix 8 can be seen that for most thermocouples the temperatures between experiment and simulation are different. Especially, for thermocouples close to the spill plume the measured and simulated temperature can differ significantly. Being in the middle of this plume or being at the edge of the spill plume can result in temperature differences of 100°C. The spill plume in the simulation results is rather vertical when it enters the smoke cabinet in FDS while during the experiments a more diagonal plume towards the exhaust was observed. Therefore, comparison of individual thermocouples does not provide a good representation of the accuracy of the simulation. The average smoke layer temperature and temperature of the smoke flowing in and out of the smoke cabinet are the most important indicators for model accuracy.

The response time of the model is faster than during the measurements. Due to the configuration of the thermocouple shields it is possible that hot smoke is accumulated below the shields where the thermocouple is located and it will take longer to cool it down.

In FDS the energy transferred to the water droplets is expressed as $\dot{Q}_{particles}$. The estimated cooling during the experiments is not purely heat transfer to the droplets, here also ambient air is entrained into the smoke volume causing it to cool down. Therefore, $\dot{Q}_{particles}$ and $\dot{Q}_{cooling}$ cannot be compared one-on-one.

Table 9 - Cooling by water particles in FDS compared with total cooling in experiment

Model/Exp.	$\dot{Q}_{particles}$ [kW]	Estimated exp. $\dot{Q}_{cooling}$ [kW]
SH1	82	185
SH2	48	135
SH3	94	209
SH4	97	242
SH5	124	265

Within $\dot{Q}_{cooling}$ the cooling by water droplets will be dominant and it is expected that this has a much larger share in the total cooling than air entrainment. Therefore, it can be concluded that the cooling by water droplets is underpredicted in the FDS model. The underpredicted cooling leads to less smoke logging and thus less entrainment of air. This consequence of underpredicted cooling by droplets results also in less cooling by air entrainment.

5.2.2 Effect of changing grid size and sprinkler spray pattern

To gain insight into the effect of different grid sizes and sprinkler spray patterns these two input parameters have been variated in the FDS model. In this paragraph the results of the numerical simulations are discussed.

5.2.2.1 Coarse grid

To study the influence of cell size a coarse grid is created in the sprinkler region with cells of 10x10x10 cm. The cell size in the burner region is maintained equal to the previous

Figure 40 - Coarse mesh in sprinkler region, horizontal section at 1m

models with a fine grid size of 5 cm. The number of cells in the coarse model is reduced to 142,425. In Figure 40 the coarse mesh is shown. No further changes were made to the model. Since the FDS results of model SH3 shows relative steady smoke layer cooling this model was used to study the influence of cell size and sprinkler spray pattern.

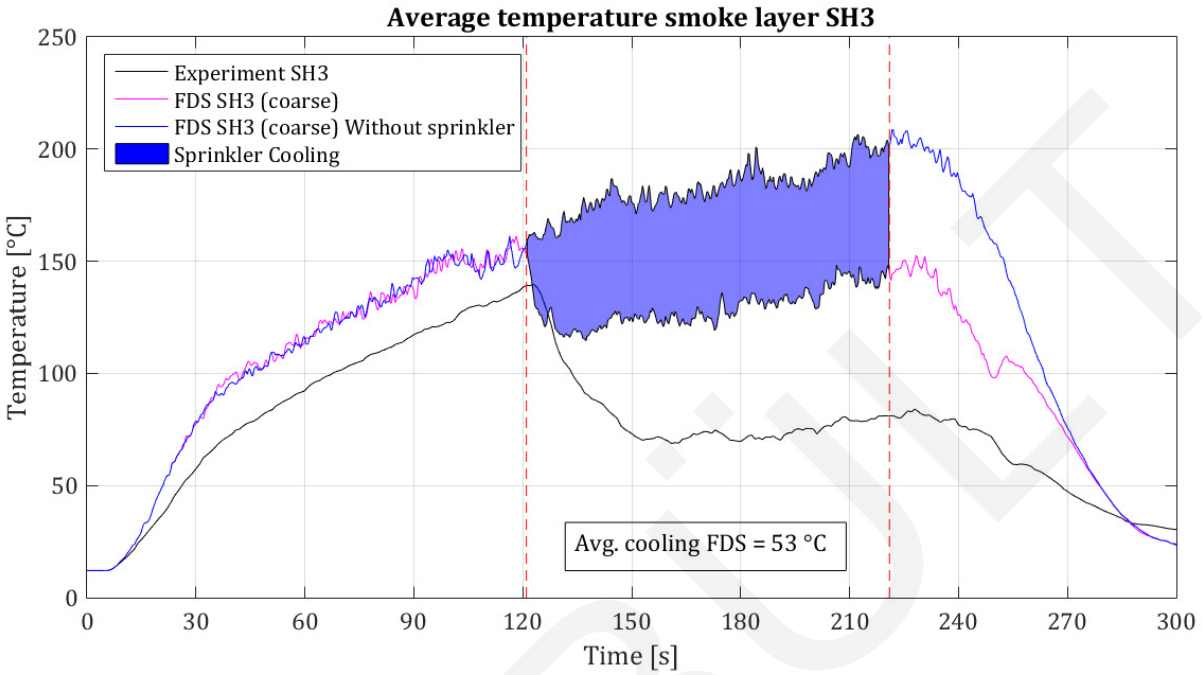

Figure 41 - FDS predictions of average smoke layer temperature SH3 (1.34 bar) with coarse mesh in sprinkler region

The results in Figure 41 show that the underprediction of the average smoke layer cooling is larger than for the model with a fine mesh with cell sizes of 5cm. In both the 'fine' model and the 'coarse' model the average smoke layer temperature at activation is just above 150°C. The minimum temperature reached in the 'coarse' model is slightly higher than for the 'fine' model, indicated that less cooling is present. However, at sprinkler deactivation the temperature in the 'coarse' model is slightly lower which can be explained by the lower temperature in the model without a sprinkler.

In the development phase of the fire (till approximate 90 seconds) the 'coarse' model has a larger overprediction of the average smoke layer temperature. This contradicts with the lower temperature at sprinkler deactivation. More coarse models must be simulated to find a clear explanation for these effects.

5.2.2.2 Simple spray pattern

The current sprinkler spray patterns are very complex and require a high level of knowledge and input, therefore a simple sprinkler spray pattern is used to see if the complex sprinkler spray model results in better predictions. In the simple spray pattern, the injection velocity is equal to the detailed model. Differences in the spray for azimuth angles are not considered and a Gaussian distribution is applied between an elevation angle of 0° and the maximum elevation angle in the detailed model.

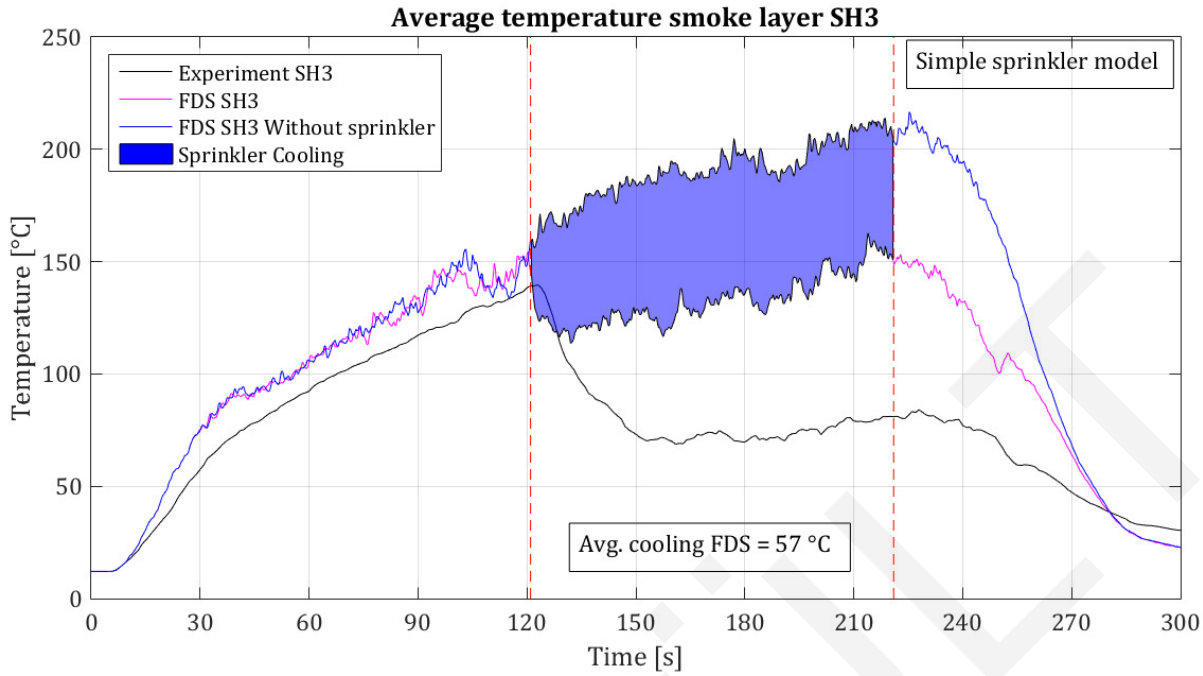

Figure 42 - FDS predictions of average smoke layer cooling SH3 (1.34 bar) with simple sprinkler spray model

The average smoke layer temperature is shown in Figure 42. The difference of 2°C in smoke layer cooling with the sophisticated sprinkler model for SH3 is negligible. However, as shown in Figure 43, the simple sprinkler spray pushes more smoke down meaning the average temperature of the smoke layer (above the purple line) is more difficult to compare to the measurements.

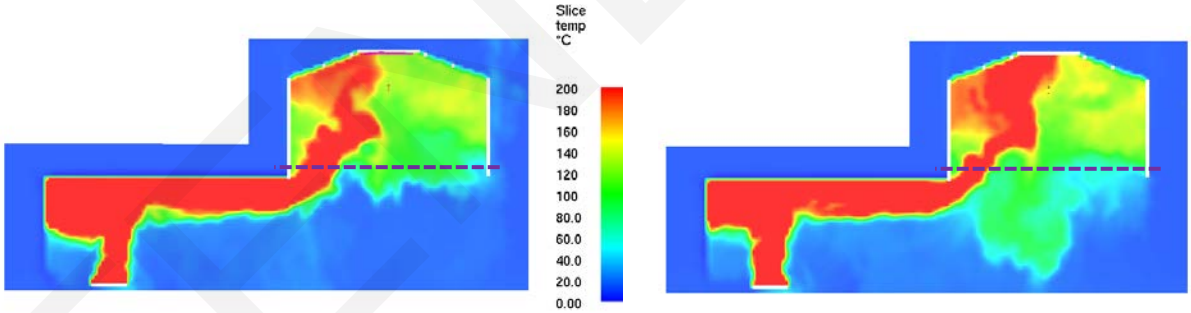

Figure 43 - Temperature slice after 130 seconds, sophisticated sprinkler pattern (left) and simple (uniform) sprinkler pattern (right)

5.2.2.3 Coarse grid & Simple spray pattern

Figure 44 shows the results of an FDS model where both the coarse grid and the simple sprinkler spray model are applied. Combining a coarse mesh with the simple spray model results in the largest underprediction of the smoke layer cooling so far for SH3. Again, it must be taken into account that a large quantity of smoke is pushed down and is not considered in the average smoke layer temperature in the hood.

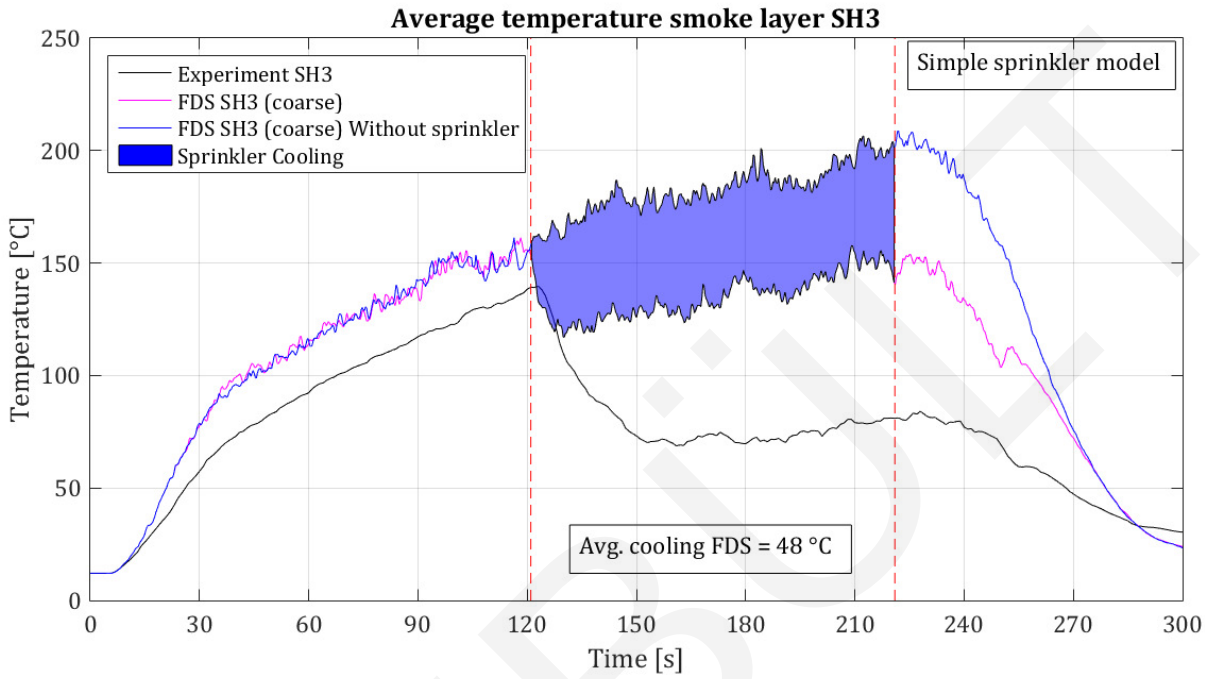

Figure 44 - FDS predictions of average smoke layer temperature SH3 (1.34 bar) with coarse mesh and simple sprinkler spray model

In Table 10 the energy transferred to the water droplets is given for the simulated variants. The given value is the average over the complete sprinkler activation time. For the original model with a fine grid and complex spray pattern the average cooling by water droplets is 102kW.

Table 10 - Average cooling by water droplets during sprinkler activation (SH3 variants)

SH3	$\dot{Q}_{particles}$ [kW]	Avg. cooling FDS [K]	Difference with Fine Grid + Complex pattern [kW]; [K]	
Coarse grid + Complex pattern	107	53	+5	-6
Fine grid+ Simple pattern	95	57	-7	-2
Coarse Grid + Simple pattern	108	48	+6	-9

The results for the models with coarse grids are contradictory. More energy is transferred to the water particles but the temperature decrease is smaller than for models with a finer grid and lower. This implies that with a coarse grid other forms of energy transport are underpredicted. Additional research is required to gain more insight into these effects.

6 Conclusion

During this graduation project, the effects of smoke layer cooling caused by an activated sprinkler nozzle, have been studied both experimental and numerical. Multiple experiments with and without sprinkler activation are performed and thereafter simulated with FDS. Three research questions have been formulated which will be answered here.

To what extent are the temperature, thickness, and flow patterns of a stable smoke layer affected by water droplets of the sprinkler system?

The injection of water droplets into the sprinkler spray reduces the smoke layer temperature. The experiments show that increasing the water flow rate of the sprinkler nozzle result in a larger temperature decrease. A smoke layer with an average temperature of approximately 200°C is reduced with 50°C, 70°C and 90°C for water flow rates of 56 l/min, 71 l/min and 93 l/min.

The thickness of the smoke layer increases within the sprinkler spray envelope. Smoke logging occurs and is caused by the downward drag forces of the water droplets that are exerted on the smoke particles. Again, increasing the water flow rate results in amplification of the effects. A water flow rate of 56 l/min, with relative large droplets, causes a very small amount of smoke logging, where a flow rate of 93 l/min, with smaller droplets, resulting in an unstable smoke layer and significantly reduced visibility. It can be concluded that smaller droplets amplify the downward smoke displacement.

Variant droplet distributions within a sprinkler spray cause different flow patterns. Spray angles with a high density of water droplets result in strong, local downward flows which will bend upward in regions with low droplet density or high buoyancy. Spray patterns with an evenly distributed droplet density result in weak downward flows within the entire spray envelope.

At what level of detail should the sprinkler spray pattern be modelled in a field model in terms of initial velocity, spray angles, droplet size and mass fractions to obtain reliable results for smoke layer cooling?

All simulations that have been done with FDS underpredicted cooling by the sprinkler spray. The spray pattern that was modelled, see paragraph 3.2.6, corresponded with a measured water distribution at the ground surface. The spherical spray injection surface was divided in a maximum of 360 surfaces, with each an individually assigned mass fraction. This can be considered as a very high level of detail, however, for all simulations the temperature decrease of the smoke layer is underpredicted. Simulations with a low-detailed, simple spray pattern did not result in significant differences for the smoke layer cooling. Regardless of the level of detail from the sprinkler spray, the models embedded in the FDS code to solve the numerical equations are not capable of predicting the smoke layer cooling by water droplets.

Can modelling of smoke layer cooling by a sprinkler spray be used in practice, considering the required computational time, level of detail and knowledge of the modeller?

The numerical simulations done in this study required 23 – 31 hours of computational time for a simulation time of 300 seconds and 620,868 cells. It is expected that in practice the desired simulation time and number of cells will be both larger, resulting in longer computational times.

Modelling of a sprinkler spray with a high level of detail requires information from the sprinkler manufacturer regarding spray angles and water mass distribution. This type of data is often not available. The workload of performing bucket tests is too high for individual projects.

The non-dimensional expression between the characteristic fire diameter and cell-size is often used to express a coarse, medium or fine grid. However, this ratio is dependent on fire size and results for large fires in a relatively large cell size, even for 'fine' meshes. The numerical simulations showed that in the sprinkler region coarsening of the mesh results in less accurate results. Therefore, the non-dimensional expression is not always applicable in the sprinkler region, meaning that the modeller needs to make a well-considered choice in this region.

Cooling of the smoke layer by a sprinkler spray is underpredicted in the FDS simulations, which results in a conservative outcome when studying the smoke layer temperature. In practice, the combination of conservative outcomes, high computational times, limited information about water droplet distributions and the required level of understanding, makes modelling sprinkler cooling with FDS inefficient.

7 Limitations & Recommendations

7.1 Limitations

There are several things the reader should bear in mind when interpreting and using the outcomes of this study. First, the overprediction of the smoke layer temperature (before sprinkler activation) by the simulations makes it more difficult to compare results between measurements and numerical simulations. Flow patterns in the model are slightly different than in the experiments meaning that individual thermocouple temperatures cannot be compared one-on-one, especially in the rising plume. For stratified locations in the smoke layer the results correspond better and comparison is possible.

Also, the use of different fuels complicates comparison of the experimental results, but for several reasons usage of different fuels was necessary. More important is the rather unstable HRR in several experiments and between experiments. In a few experiments the HRR kept growing resulting in shorter burning periods than anticipated and increasing temperatures during sprinkler activation. For this reason it is harder to estimate the smoke layer cooling by the sprinkler.

Although there is confidence that thermocouples were kept dry during the sprinkler experiments some of the thermocouples show deviant behaviour and indicated wetting of the thermocouples. Thermocouples that showed different behaviour were excluded from the average smoke layer temperature which may have affected the accuracy.

The effect of water droplets hitting the smoke cabinet is uncertain in the FDS model. After hitting the cabinet walls, the droplets fall straight down in the model, although the droplets do not disappear it is not entirely known what the remaining influence is of these droplets. This effect might contribute to the underprediction of smoke layer cooling by a sprinkler spray.

Only a limited number of numerical models are simulated for a coarse mesh and simple spray pattern. Although these results can be easily compared to the fine models with sophisticated sprinkler spray, more simulations are required to make solid statements about grid size and sprinkler spray. Equation 3.2.3 is developed for modelling the fire, with the current results it cannot be said yet if this ratio between characteristic fire diameter and cell size is the most suitable solution to model interference of sprinkler droplets with a smoke layer.

7.2 Recommendations

The gained experimental data in this study is sufficient for the further development of FDS and validation of numerical models. The underprediction of the smoke layer cooling by the sprinkler spray and overprediction of the smoke volume during the fire development are issues that need to be studied in further research.

Also, grid sensitivity in the sprinkler region and sprinkler sprays by different sprinkler nozzles are subjects for further research. In this study is indicated that changing the grid

size can influence the predicted smoke layer temperature. Especially, for relative large models that are used in practice it is valuable to know the minimum grid size, so no meshes are created with an excessive number of cells.

Further research should focus on numerical modelling. However, if one decides to gain more experimental data there are some improvements that can be done in the experimental set-up and measurement procedure. Some of these adjustments are also highly valuable for measuring HRR of large objects beneath the exhaust hood. Now, the uncertainty in measuring the HRR is relatively large which is caused by uncertainty in pressure measurements and determining the volumetric flow rate. The relative low pressures that are measured are a result of the duct size and volumetric flow rate that needs to be kept low to obtain a smoke layer in the smoke cabinet. A by-pass, parallel to the main duct and with a smaller diameter results in higher velocities in the parallel duct for the same volumetric flow rate. When the bi-directional probe and gas sampling probe are placed in the by-pass duct it is plausible the accuracy of the HRR measurements will increase. Also, it allows to further reduce the volumetric flow rate without measuring very small pressure differences (<5 Pa). Meaning a stable smoke layer can be obtained for smaller fires and the effects of large fires that keep growing will probably be ruled out.

Other small improvements that can be made are:

- Adding a thermocouple at the smoke inlet that is located further beneath the burner cabinet, so it will remain dry during sprinkler activation and temperature at this location can be monitored during the entire measurement.
- Adding a flow meter to measure the water flow during sprinkler activation.
- Prevent smoke from flowing directly into the outlet.

8 List of Figures

9 List of tables

10 References

[1] K. McGrattan, S. Hostikka, R. Mcdermott, J. Floyd, C. Weinschenk, and K. Overholt, *Fire Dynamics Simulator User ' s Guide*. 2017.

[2] Nederlands-Normalisatie-instituut, *NEN-EN 12845+A2+NEN 1073:2010 Vaste brandblusinstallaties - Automatische sprinkler installaties - Ontwerp, installatie en onderhoud*. The Netherlands, 2010.

[3] K. Y. Li, M. J. Spearpoint, J. Ji, R. Huo, Y. Z. Li, and L. H. Hu, "A Mathematical Model of the Drag Component of a Sprinkler Spray Adjacent to Horizontal Smoke Vents," *J. Fire Prot. Eng.*, vol. 20, pp. 27–54, 2010.

[4] S. C. Li, Y. Chen, and K. Y. Li, "A mathematical model on adjacent smoke filling involved sprinkler cooling to a smoke layer," *Saf. Sci.*, vol. 49, pp. 670–678, 2011.

[5] D. den Boer, "Validatie van een cfd sprinklermodel," *Bouwfysica*, vol. 1, pp. 32–35, 2013.

[6] D. T. Sheppard, "Spray Characteristics of Fire Sprinklers," Evanston, 2002.

[7] D. van Venrooij, "Validation of Fire Dynamics Simulation with sprinkler sprays," 2016.

[8] R. P. Fleming, "Automatic Sprinkler System Calculations," in *SFPE Handbook of Fire Protection Engineering*, 2016, pp. 1423–1449.

[9] NFPA, *FIRE PROTECTION HANDBOOK* ®, 20th ed. Quincy, Massachusetts: NFPA National Fire Protection Association, 2008.

[10] S. Martorano, "Automatic Sprinkler Thermal Sensitivity : Clarifying the Terms Fast Response and Quick Response," *Viking Tech. Artic.*, no. July, 2006.

[11] K. McGrattan and D. T. Sheppard, "Large scale tests of sprinkler, vent, draft curtain interaction," 1999.

[12] M. L. Bullen, "The effect of a sprinkler on the stability of a smoke layer beneath a ceiling," *Fire Technol.*, vol. 13, no. 1, pp. 21–34, 1977.

[13] Z. Tang, J. Vierendeels, Z. Fang, and B. Merci, "Description and application of an analytical model to quantify downward smoke displacement caused by a water spray," *Fire Saf. J.*, vol. 55, pp. 50–60, 2013.

[14] C. Zhang and W. Chow, "Numerical simulation on the interaction of sprinkler and smoke layer," in *The 9th Asia-Oceania Symposium on Fire Technology*, 2013, pp. 453–462.

[15] S. C. Li *et al.*, "Studies of Cooling Effects of Sprinkler Spray on Smoke Layer," *Fire Saf. Sci.*, pp. 861–872, 2008.

[16] J. R. Lawson, W. D. Walton, and D. D. Evans, "Measurement of Droplet Size in Sprinkler Sprays," Gaithersburg, 1988.

[17] T. Beji, S. E. Zadeh, G. Maragkos, and B. Merci, "Influence of the particle injection rate , droplet size distribution and volume flux angular distribution on the results and computational time of water spray CFD simulations," *Fire Saf. J.*, vol. 91, pp. 586–595, 2017.

[18] K. McGrattan, S. Hostikka, R. Mcdermott, J. Floyd, C. Weinschenk, and K. Overholt, *Fire Dynamics Simulator Technical Reference Guide Volume 1 : Mathematical Model*. 2017.

[19] D. Wu, D. Guillemin, and A. W. Marshall, "A modeling basis for predicting the initial sprinkler spray," *Fire Saf. J.*, vol. 42, pp. 283–294, 2007.

[20] X. Zhou, S. P. D'Aniello, and H.-Z. Yu, "Spray characterization measurements of a pendent fire sprinkler," *Fire Saf. J.*, vol. 54, pp. 36–48, 2012.

[21] Nederlands-Normalisatie-instituut, *NEN-EN 13823+A1:2014 Bepaling van het brandgedrag van bouwproducten*. The Netherlands, 2014.

[22] M. Janssens, "Calorimetry," in *SFPE Handbook of Fire Protection Engineering*, 5th ed., Springer, 2016, pp. 905–951.

[23] H. Hayasaka, "Unsteady Burning Rates of Small Pool Fires," in *Fire Safety Science - Proceedings of the fifth international symposium*, 1997, pp. 499–510.

[24] K. Y. Li, R. Huo, J. Ji, and B. B. Ren, "Experimental investigation on drag effect of sprinkler spray to adjacent horizontal natural smoke venting," *J. Hazard. Mater.*, vol. 174, pp. 512–521, 2010.

[25] OMEGA Engineering, "Thermocouples Response Time." [Online]. Available:

https://www.omega.com/techref/ThermocoupleResponseTime.html. [Accessed: 03-Apr-2018].

[26] A. Horvat, "Fire Modelling in Computational Fluid Dynamics (CFD)." 2010.

[27] A. Trouvé and Y. Wang, "Large eddy simulation of compartment fires," *Int. J. Comut. Fluid Dyn.*, vol. 24, no. 10, pp. 449–466, 2017.

[28] D. S. Moya Forero, "Numerical study on the interaction of sprinklers and heat vents," Ghent University, 2015.

[29] T. G. Ma and J. G. Quintiere, "Numerical simulation of axi-symmetric fire plumes : accuracy and limitations," *Fire Saf. J.*, vol. 38, pp. 467–492, 2003.

[30] J. Axelsson, P. Andersson, A. Lönnermark, P. Van Hees, and I. Wetterlund, "Uncertainties in measuring heat and smoke release rates in the Room / Corner Test and the SBI NT Techn Report 477," 2001.

11 Appendices

1. Literature study
2. Measurement set-up
3. Thermocouple shields
4. Heat of combustion and soot yield of heptane/toluene and heptane
5. Flow velocity factor
6. Bucket test & sprinkler spray pattern
7. Measurement log & experimental results
8. FDS results
9. FDS script
10. MATLAB script

Appendix 1 – Literature study

1.1 Experimental studies towards smoke layer cooling by sprinkler sprays

In the past decade, several experimental studies have been performed to study the cooling effect of sprinkler sprays on smoke cooling. An overview of these studies, including relevant details, is given in Table 1 till Table 3. To avoid suppression of the fire by the sprinkler spray the sprinkler head is located away from the fire, placed in an adjacent room or the spray is partially captured before interfering with the fire. Diesel pools of different sizes are often used as fuel to create a dark smoke layer for better visualization of the smoke layer height. Other fuels that are used in the experiments are alcohols like methanol or ethanol and hydrocarbons such as heptane or propane (gas). However, combustion of alcohols and hydrocarbons produce less soot which makes it more difficult to get a clear image of the smoke layer.

Ingason and Olsson [1]
This study by the Swedish National Testing and Research Institute consist of four major parts and the results are often used to validate field models (these field models will be discussed in section x.x). In the first part, experimental data is compared with calculated results for different fire growth rates and fire vent conditions to investigate the local effects of the vents. In the second part, the influence of the water spray on the ceiling jet was investigated and the third part focused on the influence of the water spray on the outflow of hot gases through the fire vents. In the last part, the influence of beam constructions near the ceiling was studied. The experimental set-up is located in a large test hall of 18 x 22.3 x 20m, where smoke can be mechanically extracted. The test room is 15 x 7.5 x 6m and has two open sides and two fire vents in the ceiling. With the propane gas burner, the heat release rate of the fire was regulated between 0 and 1.5MW.

In the test room the temperature and velocity were measured at multiple positions at different heights. Bi-directional probes were used to measure the differential pressures to calculate the velocity. The direction of the air flow was determined with air flow indicators. The most important conclusion of this study is that the impact of the water

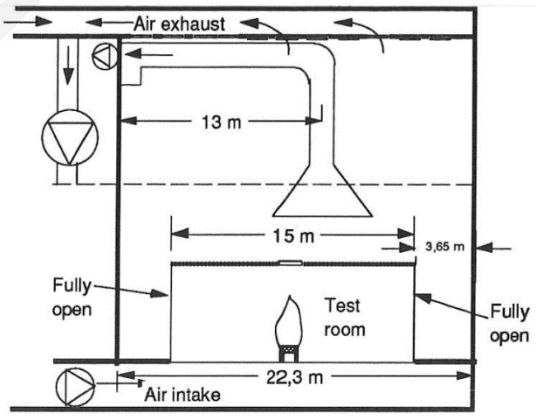

Figure 1 - Sectional view of experimental set-up Ingason and Olsson [1]

spray on the gas flow through the fire vent is the greatest when the sprinkler nozzle is close to the fire vent and this impact decreases with distance. [1]

Lougheed, McCartney, Taber (National Research Council Canada) [2]
The aim of this study was to investigate the impact of sprinklers on the smoke movement from a compartment into an adjacent room, e.g. an atrium. The two-story test room was placed into a much larger space which represented the atrium. The test room contained a propane burner to maintain a steady-state fire and two or four sprinklers were used to cool the smoke layer. Thermocouples were placed inside the test room and in front of the opening toward the 'atrium'. Smoke meters were used to determine if the smoke exiting the test room was non-buoyant (downward).

Depending on the heat release rate of the fire and a constant sprinkler density two scenarios were observed. For low heat release rates, the temperature distribution was uniform after sprinkler activation in the test room. This resulted in a non-buoyant smoke layer and accumulated near the opening towards the atrium. The temperature of the smoke was near ambient. For higher heat release rates a two-zone air stratification is maintained with a hot-smoke layer near the ceiling and flowing out of the test room through the opening. [2]

S.C. Li, Yang, Huo, Hu Y.Z. Li, K.Y. Li Wang [3]
Experiments were performed with two cabins, a burner cabin and a sprinkler cabin. A diesel pool fire is located in the burner cabin and the hot smoke flows towards the slightly higher sprinkler cabin. In the upper part of the sprinkler cabin, a stable smoke layer is formed. In total 16 experiments were performed with different heat release rates ranging from 52.5kW till 228kW and sprinkler working pressures ranging from 0.5 bar till 1.5 bar. In the sprinkler cabin, the gas temperature was measured by four trees with thermocouples. To prevent the thermocouples from wetting by the sprinkler spray a U-shaped thin metal shield was used to protect the thermocouples.

During the experiments sprinklers were active from the start. Cooling of the smoke layer was measured by the temperature increase of the smoke layer in time. A significant reduction of the temperature increase was observed for experiments with sprinkler

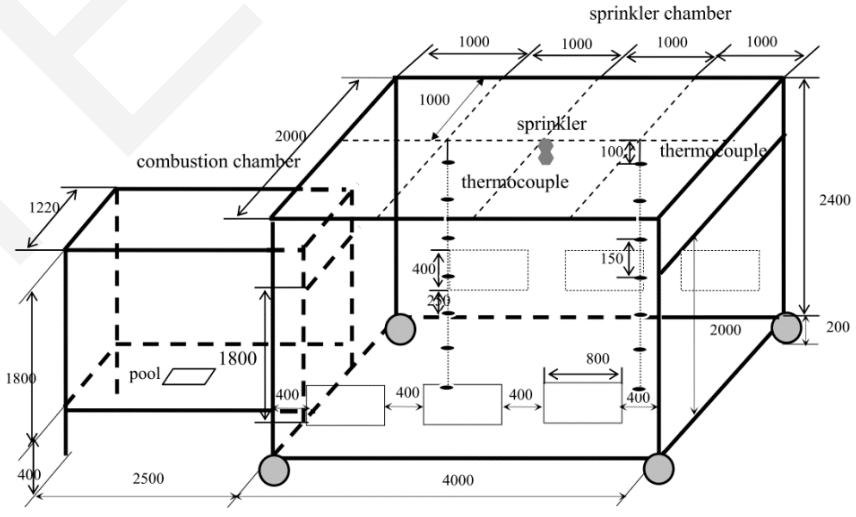

Figure 2 - Schematic overview experimental set-up S.C. Li et al. [3]

compared to experiments without a sprinkler. The effects of increasing the working pressure of the sprinkler were found to be smaller. [3]

Ota, Kuwana, Ohmiya, Matsuyama and Yamaguchi [4]
A single compartment was used for both the fire source as sprinkler location. To prevent extinguishment of the fire by the sprinkler system a water intake box was placed around the sprinkler head. This intake box captured the water that sprayed into the direction of the fire source so that no unusual sprinkler patterns occurred and the fire source is prevented from getting extinguished. The water flow rate of the sprinkler head is 80L/min and one-fourth is captured by the intake box which means that 60L/min is added to the smoke layer. The water intake box was extended for several experiments to reduce the flow rate of the water to 20L/min and 40L/min and keep the water pressure at the same level.
In the test room had one opening, represented by a door, to let the smoke flow out of the room. Inside the opening, the differential pressure was measured at three different points in height, in order to determine the air flow rate. Also, the CO2 concentration was measured and a method was introduced to determine the mass flow rate of the smoke plume. They found out that watering of the air flow influenced the fire plume and led to an increase of the entraining rate. [4]

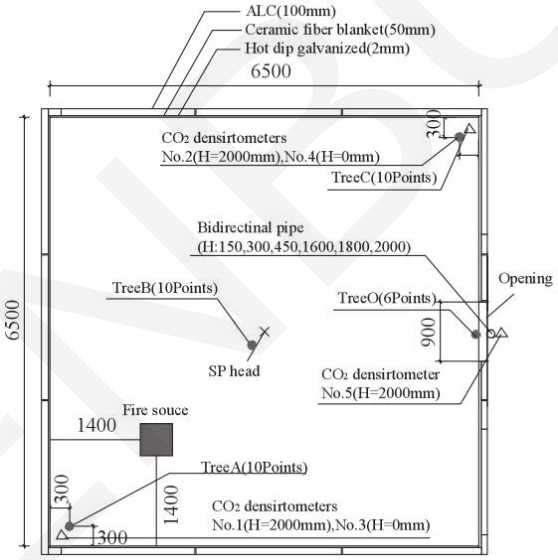

Figure 3 - Floor plan experimental set-up Ota et al. [4]

K.Y. Li, Huo, Ji and Ren [5]
The measurement set-up in this study is similar to that of an earlier performed study by S.C. Li et al. (2008). In addition to previous research natural smoke vents are added in the ceiling of the sprinkler cabin to study the effectiveness of natural smoke vents in combination with a sprinkler system. The velocity of the smoke flowing through the vents was measured with a target flow meter since the use of a pitot-tube, bi-directional probe or hot-wire anemometer were found not suitable due to condensed water or cover mesh. In total 36 experiments were done with two different heat release rates, various sprinkler pressures and different configurations of smoke vents.

By increasing the sprinkler pressure, the flow rate through the vents decreased and it was found that the sprinkler spray had a significant effect on the discharge rate of the smoke vents. For several cases, the direction of the flow reversed in the smoke vent and the air is 'sucked' into the sprinkler cabin. Increasing the area of the smoke vents resulted in a difference in velocities and reduction of the smoke layer temperature rise. When smoke-logging occurs no significant differences have been found for increasing the smoke vent area. [5]

Zhang, Chow, Huo, Zhong, Y.Z. Li [6]
The measurement set-up in this study is similar to that of an earlier performed study by S.C. Li et al. (2008). In addition, three different sprinkler heads were tested, wherefrom two upright sprinkler heads and one pendent sprinkler head. In total 25 experiments were conducted with different heat release rates and sprinkler pressures.

With an activated sprinkler, the maximum measured temperature rise was reduced till 30°C. It was observed that the smoke at the smoke-air interface layer loses its stability first. For relatively low sprinkler pressures of 0.5 bar, the smoke layer descends a little but remains stable. For higher sprinkler pressures the drag force of the water acting on the smoke layer was larger than its buoyancy resulting in the smoke layer descending to the floor. Besides experiments, the model of Bullen [7] was revised and compared with the measurements. It was found that smoke-logging will occur when the ratio between the drag force and buoyant force (D/B) greater is than 0.9. [6]

S.C. Li, Chen, K.Y. Li [8]
The Chinese researchers of this study have performed similar studies in the past towards cooling of the smoke layer by a sprinkler spray [3], [5]. Therefore, the basic principles of the measurement set-up show great similarities with these studies. The smoke vents that were applied by K.Y. Li, Ji and Ren (2010) are replaced by an additional cabin, called smoke filling cabin. The smoke flows from the sprinkler cabin into the larger smoke filling cabin where the smoke is stored and the height of the smoke layer is measured to determine the volumetric flow rate for sprinkled and non-sprinkled smoke layers. In each cabin, a vertical ruler is used to visually measure the height of the smoke layer and this is possible due to the dark smoke that is created by the diesel pool fire. For other fuels like pure hydrocarbons and alcohols which produce fewer soot particles, it is more difficult to visually determine the height of the smoke layer. The temperature of the smoke layer is measured by two trees of thermocouples in the sprinkler cabin, located at a distance of 1m from the sprinkler head. The thermocouples are protected by steel saddle caps to prevent wetting of the thermocouples.

During activation of the sprinkler, the smoke filling becomes slower due to a reduction of the volumetric flow rate. This reduction is caused by heat loss from the smoke to the water particles. Variations in sprinkler operating pressures had an insignificant effect on the smoke filling. Furthermore, a zone model was revised to include sprinkler cooling and subsequently compared with the experimental results. Agreements were found between the model predictions and experimental results. [8]

Tsuchiya [9]
This Japanese study is a continuation of the research by Ota et al. (2009). In both studies, the same measures were taken to capture a part of the sprinkler spray to prevent suppression of the fire. The main difference between both studies is the size of the test room, Tsuchiya's test room has a size of 3.2x3.2m where Ota et al. used a much larger test room of 6.5x6.5m. Tsuchiya's study is focused on the downward air flow that is caused by the sprinkler spray. The downward air flow is investigated by using Particle Image Velocimetry (PIV) and the fundamental parameters of the sprinkler nozzles like droplet distribution, droplet size and velocity were measured by using PIV.

With the data obtained from the PIV, the theoretical drag (D) was calculated and with the temperature difference the buoyancy (B) was calculated. The ratio D/B expresses the smoke layer's stability. Subsequently, the ratio between downward airflow rate (vs) and droplet velocity (vd) was related to D/B. Tsuchiya found out that the relationship between D/B and vs/vd is linear for the stable region and transition region of the smoke layer. [9]

Tang, Fang, Yuan, Merci [10]
Compared to the previously mentioned studies the scale of this study is smaller. The burner room is only 0.6x0.6x0.8m and smoke moves through a smoke duct towards the upper part of the smoke cabin, which is 2.0x2.0x3.4m. Again, the temperature is measured by two thermocouple trees. The distribution of the water droplets is measured by the microscopic measurement method. This means that the water droplets are collected at a vaseline-coated glass slide one meter below the sprinkler nozzle. Subsequently, the droplet diameters are measured by photomicrographs. A flattening coefficient is applied to correct for flattening of the droplets due to the impact of falling on the glass slide. The applied nozzle is a low-pressure water mist nozzle, therefore the obtained droplet diameters are relatively small compared to the size of water droplets distributed by regular sprinkler nozzles.

It was observed that for experiments with a smaller smoke layer thickness the downward smoke displacement is larger. Air entrainment is defined as an import factor in this effect. For a thin smoke layer, cold air is entrained into the spray envelope below the smoke layer which results in additional cooling and ultimately in more smoke-logging compared

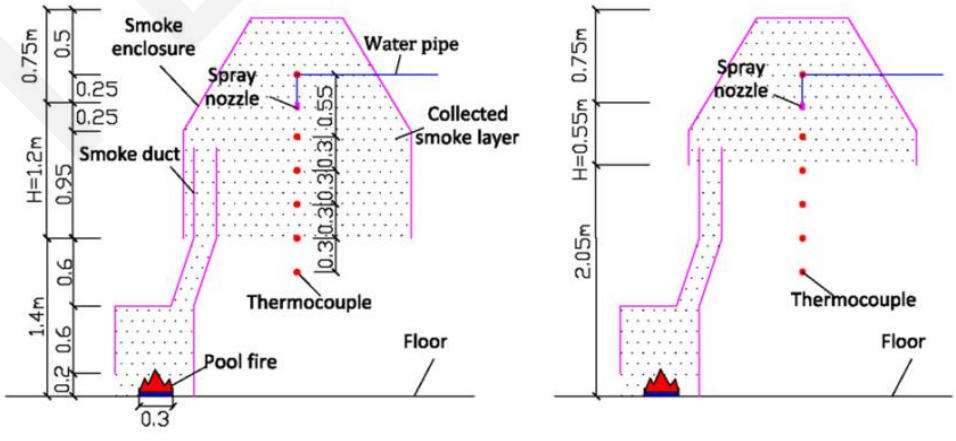

Figure 4 - Sectional view experimental set-up Tang, Fang, Yuan and Merci [10]

to thicker smoke layers. For a higher sprinkler operation pressure, this effect becomes more pronounced. [10]

Seo, Yoon, Koo, B.C. Kim, D.E. Kim, Matsuyama and Kwon [11]
The Korean researcher replicated the measurement set-up of Tsuchiya (2011) to investigate typically applied nozzles in Korea. The nozzles that were studied are a top-down nozzle, open nozzle, residential nozzle and flush nozzle. The particle diameter, particle velocity and spray distribution were measured by using PIV. Instead of the typically used diesel pool fires for this type of study, the Koreans used ethanol and n-heptane pool fires. The heat release rate of these fuels was determined by measuring the mass loss rate.

The measured temperatures in the upper layer decrease after sprinkler activation, while the temperature in the lower layer first decreases and after 60 seconds suddenly increases for a short period. According to the authors of this study, this decrease indicates that the smoke layer descended. However, this statement is based on the measurements of only one thermocouple. Descend of the smoke layer can be better explained by the measured CO2 concentrations near the ceiling and floor of the compartment. Near the ceiling, the CO2 concentration decreases after sprinkler activation and near the floor the concentration slightly increased. Furthermore, the researchers concluded that the fires source size should at least be 100kW or more to be able to analyze the smoke-logging phenomenon. [11]

Pretrel [12]
This recent, French study is different from most other performed studies in the past. First of all, the source that was used is a propane gas fire which is located in the corner of the test room. The test room is mechanically ventilated by a supply and exhaust vent. The test room has two sprinkler nozzles of the Deluge type. The variable parameters are the heat release rate of the fire, the sprinkler operating pressure and the sprinkler activation time. In total 17 experiments were conducted with a variation of these variable parameters. The air flow rate of the ventilation system was set to be constant during the measurements with a renewal rate of 15.4 per hour.

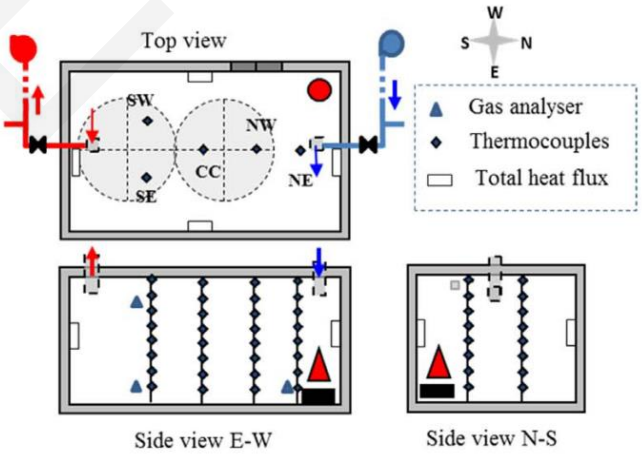

Figure 5 - Overview experimental set-up Pretrel [12]

During the experiments, two major behaviours were observed, namely chemical homogenization and cooling of the gases. Homogenization was investigated by measuring species concentrations, in this case, oxygen and carbon dioxide. It was measured that a larger number of droplets increased the mixing of the chemical species. With a sprinkler spray larger than 100l/min the concentration stratification disappears and the chemical concentrations are almost identical in the entire enclosure. It was observed that evaporation occurred mainly when the sprinkler is activated and thereafter gradually decreases. It was found that for fire scenarios with a sprinkler spray a significant part of the released energy is transferred to the droplet flow. For the examined cases this share could increase up to 65%. [12]

de Wilde [13]
The measurement set-up of this study is based on the set-up for Li et al. (2008) and has slightly different dimensions. The main difference between both studies is that de Wilde extracts air from the sprinkler cabin at the top. This is done mechanically and the extracted air/smoke passes a bi-directional probe and gas sampling probe in the exhaust duct before it leaves the laboratories. The bi-directional probe is used to measure the pressure difference in the centre of the duct, between the total pressure and the static pressure, in order to obtain the centre velocity. The gas sample probe is used to measure the oxygen and carbon dioxide concentration. Both the centre velocity as the species concentration are used to calculate the heat release rate of the fire.

In the sprinkler cabin, the temperature was measured by three thermocouple trees. However, the thermocouples were not sufficiently protected against water droplets which resulted in wetting of the thermocouples. This makes the results highly unreliable since it is most likely that the water temperature has been measured. The aim of the experiment was to validate a FDS-model, but at the end of the study, the FDS-model, as well as the experiments, were insufficient to gain reliable results.

1.1.1 Discussion & Conclusion

The geometry of the experimental set-ups can be divided in three groups, namely a large test space with a smaller test room within, a test space with two cabins (burner cabin and sprinkler cabin) and a single test space without additional rooms/cabins. The use of two different cabins has the advantage that the fire source cannot be affected by the sprinkler spray and a stable heat release rate can be maintained. Also, in the sprinkler cabin it is easier to create a stable smoke layer due to the reduced volume and ability to buffer the smoke. Different sizes of cabins are used, a sprinkler cabin of approximate 4x4x4m has been used multiple times. When the sprinkler cabin is to small the sprinkler spray bounces back from the cabin walls, which result in a different sprinkler spray pattern then for unbounded situations [13].

Diesel is often use as a fuel for pool fires, with different sizes. The main reason for using diesel is the thick dark smoke layer that is produced by combustion of diesel. However, the burning rate of diesel is irregular and the exact composition of diesel is not always known or may differ from time to time. Also, an additive is necessary to ignite the diesel. Another fire source that has been used, mostly for higher heat release rates (>1MW), is a

propane gas burner. By controlling the flow of the gas the size of the fire can be controlled. Disadvantage is the low soot yield which results in a low-density smoke layer which is less visible. The same effect occurs for alcohols such as methanol and ethanol and for hydrocarbons with a high purity like n-heptane >99.75%.

The type of sprinkler nozzle and operating sprinkler pressure can be chosen as desired and is dependent of the research objective and intensions of the research. A pendent sprinkler nozzle has often been used in the examined studies with operating pressures ranging from 0.5 to 2.0 bar.

The gas temperature is measured in all mentioned studies. In most cases, multiple thermocouple trees are used to determine the gas temperature at different positions and to determine the smoke layer height. Also, multiple thermocouple trees are used to calculate the average smoke layer temperature. The vertical spacing between the thermocouples ranges between 0.15 to 0.5 meter.

Studies that were interested in the effectiveness of smoke vents with simultaneously active sprinkler systems measured the air velocity near the smoke vents to determine the flow rate through the smoke vents. A bi-directional probe in combination with a manometer seems to be an appropriate method to measure the differential pressure in order to calculate the air velocity.

Gas analysis has been applied with different objectives. Pretrel measured the oxygen and carbon dioxide concentration at two different heights in his test room to study homogenization of the chemical stratification[12]. De Wilde measured the same parameters but measured them in the exhaust duct to calculate the heat release rate by using oxygen depletion [13].

In most studies it is mentioned that the smoke layer height has been measured. However, this is either done by temperature measurements or estimated visually with a ruler. More advanced measurement techniques e.g. to measure the optical density have not been applied in the mentioned studies.

The studies that protected thermocouples against water droplets used metal saddle caps or metal shields as protection [2], [3], [5], [8], [12]. According to the researchers the thermocouples were kept dry. Another method that was not very successful was a vertical metal profile to protect all thermocouples from the same thermocouple tree at once [13]. Therefore, the best option seems to be individual shields that cover the thermocouples.

Table 1 - Overview experimental studies smoke layer cooling by sprinkler Part 1 of 3

#	Autor(s)	Year	Scale of experiment	Fuel type	HRR [kW]
1	Ingason and Olsson [1]	1992	Full-scale	Propane burner	0 - 1500
2	Lougheed, McCartney and Taber (National Research Council Canada) [2]	2000	Full-scale	Propane burner (2x)	150 – 3000
3	S.C. Li, Yang, Huo, Hu Y.Z. Li, K.Y. Li and Wang [3]	2008	Full-scale	Diesel 0.25x0.25m, 0.3x0.3m, 0.5x0.5m, 0.6x0.6m	 52.5 72, 145 228
4	Ota, Kuwana, Ohmiya, Matsuyama and Yamaguchi [4]	2009	Full-scale	Methanol 0.32x0.32m, 0.45x0.45m, 0.9x0.45m	 54, 119, 235
5	K.Y. Li, Huo, Ji and Ren [5]	2010	Full-scale	Diesel 0.6x0.6m, 0.8x0.8m	 248, 476
6	Zhang, Chow, Huo, Zhong and Y.Z. Li [6]	2010	Full-scale	Diesel 0.5x0.5m, 0.6x0.6m, 0.7x0.7m (2x), 0.8x0.8m	 200, 248, 810, 476
7	S.C. Li, Chen and K.Y. Li [8]	2011	Full-scale	Diesel 0.25x0.25m, 0.3x0.3m, 0.5x0.5m, 0.6x0.6m	 52.5 72, 145, 228
8	Tsuchiya [9]	2011	Reduced-scale	Methanol 0.1m2, 0.25m2, n-heptane 0.1m2, 0.25m2	 67, 134 112, 290
9	Tang, Fang, Yuan and Merci [10]	2012	Reduced-scale	Diesel 0.3x0.3m (ignited with gasoline 1/10)	 -
10	Seo, Yoon, Koo, B.C. Kim, D.E. Kim, Matsuyama and Kwon [11]	2015	Reduced-scale	Ethanol 0.1m2, 0.25m2 n-heptane 0.1m2, 0.25m2	 50, 139, 99, 239
11	Pretrel [12]	2017	Full-scale	Propane burner	140 – 290
12	de Wilde [13]	2017	Reduced-scale	n-heptane 0.35m (circ.) 0.5x0.5m	 100 250

Table 2 - Overview experimental studies smoke layer cooling by sprinkler Part 2 of 3

#	Sprinkler head (number)	Flow coefficient [L/min√bar]	Operating pressure [bar]	Dimensions smoke cabin [m]	Dimensions burning cabin [m]	Smoke vents
1	Wormald A CU/P (1) Pendent	80	1.0 – 2.0	7.5x15x6	Burner cabin = Smoke cabin	Natural
2	Pendent (2 or 4)	4.1, 6.1, 8.1 L/min/m2	Unknown	13.1x17.2x12.2	5.2x9.2.6.4 (two-story), integrated in smoke cabin	Mechanical exhaust
3	ZSTP-15 (1)	80	0.5 – 1.0	4.0x2.0x2.6	2.5x1.2x2.2	No
4	Senju ZQRII Pendent (1)	80	1.0	6.5x6.5x3.9	Burner cabin = Smoke cabin	Natural (wall)
5	ZSTP-15 (1)	80	0.3 – 1.5	4.2x4.2x4.2	4.0x2.0x2.5	Natural smoke vents (1 or 3)
6	A upright B upright C pendent (1)	120 (A) 80 (B+C)	0.5 – 0.15	4.2x4.2x4.0	4.0x2.0x2.4	No
7	ZSTP-15 (1)	80	0.5 – 1.0	4.0x2.0x2.6 (sprinkler cabin) 4.2x4.2x4.0	2.5x1.2x2.2	No
8	I20 (fog) I40 (fog) I80 (fog) K80 Pendent(1)	6 12 24 80	1.0 – 3.0	3.2x3.2x3.2	Burner cabin = Smoke cabin	Natural (door)
9	Pendent (1) (water mist)	41-45	4.0 – 13.0	2.0x2.0x3.35	0.6x0.6x0.8	No
10	Pendent Open Residential Flush-type (1)	80 80 50 80	1.0	3.2x3.2x3.2	Burner cabin = Smoke cabin	Natural (door)
11	Pendent (2) (deluge)	26	1.0 – 5.5	4.9x8.7x3.9	Burner cabin = Smoke cabin	Mechanical exhaust and supply
12	VK102 (1) Pendent	80	0.5 – 1.5	2.8x2x8x3.4	1.75x3.5x1.6	Mechanical exhaust

Table 3 -Overview experimental studies smoke layer cooling by sprinkler Part 3 of 3

#	**Thermocouples protected**	**Measured parameters**	**Numerical simulation**
1	No	Temperature, velocity, (flow direction)	Yes
2	Thin metal shields	Temperature	No
3	Steel saddle caps	Temperature, smoke layer height, smoke flow velocity	Mathematical model
4	No	Temperature, differential pressure, CO2 concentration, mass loss rate	No
5	Steel saddle caps	Temperature, volume flow rate trough vents	Mathematical model in [14]
6	No	Temperature, sprinkler working pressure, smoke filling (regular camera)	No
7	Steel saddle caps	Temperature, smoke layer height	Mathematical model
8	No	Temperature, air flow rate	Yes, FDS model
9	No	Temperature, smoke layer height	No
10	No	Particle distribution, particle diameter, particle velocity, temperature, air velocity, CO2 concentration	No
11	Metal protective caps	Temperature, CO2 and O2 concentration, heat flux, ventilation flow rate	No
12	Metal L-profile (vertical)	Temperature, CO2 and O2 concentration, differential pressure	Yes, FDS model

1.2 Numerical simulation

In the field of fire safety engineering and science numerical models are more often applied to predict fire behavior. These models can be distinguished in zone-models and field models.

1.2.1 Zone models

A zone-model divides the computational domain into one or more zones and it is assumed that the conditions in each zone are well-mixed and therefore constant throughout the zone. Usually, a two-layer zone model is used for cases with a simplistic geometry, whereby a hot layer and cold layer are distinguished. The input of these models exists of room dimensions, building materials, size and location of openings, furnishing characteristics, heat release rate, fire location and size. The output that is generated by most zone models contains upper layer temperature, lower layer temperature, flash-over time and smoke interface height. Some models provide also the combustion gas concentrations and the average pressure throughout the compartment. Examples of zone models are OZone, CFAST and BranzFire.

1.2.2 Field models

Field models or Computational Fluid Dynamics (CFD) models are more complicated than zone models and require a higher level of expertise from the modeler. The computational domain is divided in thousands of small volumes (cells), which can range from centimeters to meters. In general, a smaller cell size result in more reliable results. The Navier-Stokes equations are a system of partial differential equations that describe flow of a fluid. The integrals in these partial differential equations can be replaced by discretized algebraic forms, which can be solved and result in numbers for the flow field values at discrete points in time and/or space. The transport equations are based on the basic physical principles of mass, energy and momentum conservation. Two approaches can be used to describe the transport equations of a fluid, namely a Eulerian and Lagrangian approach. With the Eulerian approach, the transport equations are written for a control volume. With the Lagrangian approach the transport equations are written for a moving particle. This second approach can be used for modeling water droplets from sprinkler systems. [15]

The smallest vortices of a flow have the size of the Kolmogorov scale, but these vortices are for most cases too small to be captured within the numerical grid and make it nearly impossible to solve the transport equations. Therefore, the transport equations will be filtered over a spatial interval or averaged over a time interval. An example of filtering is Large Eddy Simulation (LES), these models solve the transport equations for the large eddies and the small eddies are modeled with an eddy viscosity model (turbulence model). Reynolds-Averaged Navier Stokes (RANS) models are an example of averaging over a time interval. For RANS models only the mean flow is solved with the averaged Navier-Stokes equations and all eddies are modelled with a turbulence model. Choosing the appropriate turbulence model is a fundamental aspect of a CFD-model since it influences distribution of the simulated flow variables, such as velocity, temperature and

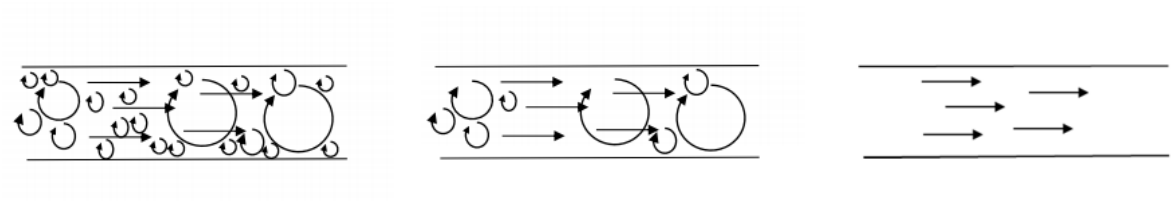

Figure 6 -Schematic view of solved flow for DNS (left), LES (middle) and RANS (right)

heat flow. Complete solving of the exact Navier-Stokes equations is called Direct Numerical Simulation (DNS) and all eddies are solved with this method. This makes it very time-consuming and it requires huge computational resources. A visual representation of the mentioned methods is shown in Figure 6. [15]

At the moment, there are several free software packages available for modeling fires with CFD. The most popular packages are Fire Dynamics Simulator (FDS), developed by the National Institute of Standards and Technology (NIST) and the open source FireFOAM, developed by FM Global.

1.2.2.1 FDS

The Fire Dynamics Simulator (FDS, release v6.6.0) is developed to model low-speed, thermally-driven flows with an emphasis on smoke and heat transport caused by fires unlike other CFD software packages such as ANSYS Fluent FDS' core business is to simulate fire behavior [16]. For most cases in FDS, LES is used to model turbulent effects on the main flow. If the numerical mesh is fine enough it is also possible with FDS to use DNS. FDS is written in Fortran 90, and the core algorithm is second-order accurate [17].

The turbulence model, gradient diffusion, is used in FDS for closure of the subgrid-scale momentum and scalar flux terms. The turbulent (eddy) viscosity or turbulent (eddy) diffusivity is then required. The turbulent diffusivity can be obtained by using the Prandtl number or a constant Schmidt number. However, both turbulent transport equations depend on the turbulent viscosity, μ_t. FDS provides several methods for acquiring the turbulent viscosity. Since FDS version 6 Deardoff's Model is used by default. In previous versions (1 to 5) the Constant Smagorinsky Model (C_s=0.2) was used for implementation of the turbulent viscosity. Other options in FDS are the Dynamic Smagorinsky Model, Vreman's Model and Renormalization Group (RNG) Model. [18]

The "simple chemistry" model is used by default in FDS and appropriate for most situations. This single-step, mixing controlled chemical reaction contains three lumped species, namely air, fuel and products. A lumped specie is a group of primitive species, e.g. air consists of oxygen, nitrogen and insignificant amounts of water vapor and carbon dioxide. The model requires the number of carbon, hydrogen, oxygen and nitrogen atoms, along with the soot yield and carbon monoxide yield to determine the reaction products. [18]

As mentioned before the physical space that should be modeled is divided into a large number of rectangular cells to solve the low Mach number equations. It is assumed that within each cell quantities as the gas velocity, temperature, pressure etc. are uniform and only change in time. The mesh is restricted to rectangular Cartesian grids in FDS and objects/surfaces need to be placed on a cell's edge. Therefore, the computational grid

must be generated with care, since FDS moves objects/surfaces to the nearest cell edge if this is not the case. Different cell sizes can be used, but nodes of different cell sizes should be aligned and the maximum aspect ratio is 2.

Results that are obtained with FDS can be viewed in another application developed by NIST called Smokeview. In Smokeview results in time for temperature, velocity, mass fractions etc. can be viewed for the preset (vector) slices, boundaries or surfaces.

1.2.2.2 FireFOAM

FireFOAM is based on the free, open-source CFD software package OpenFOAM. FireFOAM is object-orientated and based on C++ coding language. Like FDS the core algorithm of FireFOAM is second-order accurate. However, FireFOAM is a finite volume solver with implicit time integration. In contrast to FDS the FireFOAM solver supports advanced meshing options and is able to solve structured or unstructured polyhedral meshes. [17]

FireFOAM uses a different turbulence model in its LES simulations then FDS, turbulence is modeled by the Dynamic Smagorinsky model or the k-equation eddy viscosity model. Furthermore, an equilibrium chemistry model for combustion is used whereby the mixture composition is a single-variable function of the mixture fraction and flame extinction is neglected [17].

Results obtained with FireFOAM can be visualized in alternative programs, e.g. Paraview, FieldView, EnSight or Tecplot.

1.2.3 Numerical simulation of smoke layer cooling by sprinkler sprays

In the past decade, several numerical studies have been performed to study the cooling effect of sprinkler sprays on smoke cooling. An overview of these studies, including relevant details, is given in Table 4. In the next section, a summary will be given of each study and relevant conclusions will be pointed out. In general, a finer grid results in more accuracy of the simulation. The FDS User Guide introduces a non-dimensional expression, $D^*/\delta x$, to define the resolution of the grid. Here D^* is a characteristic fire diameter given by Equation *1.2.1* and δx is the nominal size of a mesh cell.

$$D^* = \left(\frac{\dot{Q}}{\rho_\infty c_p T_\infty \sqrt{g}}\right)^{\frac{2}{5}} \qquad 1.2.1$$

The higher $D^*/\delta x$, the more computational cells span the diameter of the fire. A value of 4 is qualified as a coarse mesh, 10 can be seen as moderate and 16 as fine[16]. According to Ma and Quintiere, who studied numerical simulation of axi-symmetric fire plumes in unconfined spaces the optimal resolution for a (small) pool fire is 20 cells within the characteristic diameter [19].

Chow and Cheung [20]

This numerical study was one of the first, using a field model, towards smoke layer cooling by sprinkler sprays. For the gas phase the conservation equations of mass, momentum and enthalpy were solved by the Pressure Implicit Splitting Operator (PISO)

algorithm. The liquid phase of the water spray was described by number of droplets with an initial velocity and calculated diameter, subsequently the trajectory of each droplet was calculated. The results were validated by experimental results by Ingason and Olsson (1992). A non-uniform grid was applied with finer cells near the ceiling and fire plume. The stability of the smoke layer was expressed by the D/B ratio which can be calculated from the field model. The cooling capacity of the water spray is only dependent of convection since evaporation is ignored in the model. No combustion model was included in the model which may have led to large deviations in results for positions close to the fire. [20]

Table 4 - Overview numerical studies smoke layer cooling by sprinkler

Autor(s)	**Year**	**Software**	**Q [kW]**	**D* [m]**	**Grid size [m] (finest mesh)**		**D*/dxyz**	**Grid sensitivity study**
					Plume region	**Other parts**		
Chow, Cheung	1994	PISO Algorithm	1000, 1500	0.959, 1.128	37*27*17 (cells) Non-uniform grid		variable	No
Hua, Kumar, Cheong, Khoo, Xue	2002	?	53	0.296	0.07	0.07	4.2	No
O'Grady and Novozhilov	2009	FDS v4.07	1500	1.128	0.075	0.1 – 0.2	15.0	Yes
Tsuchiya	2011	FDS	64 – 290	0.32 – 0.584	?	?	?	No
De Roeck	2013	FDS v5.5.3	5000 – 20000	1.83 – 3.18	0.25	0.5	7.3	Yes
Zhang and Chow	2013	FDS v5.5.3	1000, 1500	0.959, 1.128	0.077	0.077	12.5	Yes
Moya Forero	2015	FDS V6.1.1	1500	1.128	0.075	0.075	15.0	Yes
de Wilde	2017	FDS v6.5.3	300	0.592	0.25	0.25	2.4	No

Hua, Kumar, Cheong, Khoo and Xue [21]
The goal of this study was to introduce a numerical simulation approach to provide a quantitative analysis of the interactions between water spray and a fire plume. The sprinkler nozzle was located above the fire plume so the fire plume will be suppressed once the sprinkler is active. A relative small gas burner with a total heat release rate of approximate 53kW was studied with a coarse grid. The burning rate of the methane burner was estimated with the Arrhenius finite reaction rate model. Turbulence was modeled with a modified two-equation k-ε model to incorporate buoyancy effects. Various water droplet sizes were modeled ranging from 100μm to 270 μm for a hollow cone and solid cone spray pattern. [21]

O'Grady and Novozhilov [22]
Also for this numerical study the experimental results from Ingason and Olsson (1992) were used to validate the numerical results. Large Eddy Simulation (LES) was used since it was expected to have a major computational advantage compared to earlier RANS-models. In total six different grids were used with the non-dimensional expression $D^*/\delta x$, ranging from 5 to 15. It was found that reducing the cell size from 10cm towards 7.5cm had a significant negative effect on the computational time but only a small impact on the accuracy of the results. A combination of the log-normal and Rosin-Rammler droplet size distribution function were used to model the water spray. Evaporation of water droplets was considered in this study and the water vapor fraction at saturation conditions was calculated with the Clausius-Clapeyron equation. [22]

Tsuchiya [9]
This Japanese study performed in FDS contains little information about the applied techniques. A combination of the log-normal and Rosin-Rammler droplet size distribution functions were used for the water spray. Droplet size ranges between approximate 100µm and 1000µm. Further information was not given and it is assumed that default settings of FDS were used. [9]

De Roeck [23]
For this study, the default settings in FDS v5.5.3 were used to model turbulence, combustion and sprinkler spray distribution. No additional information is given on the use of different (sub)models.

Zhang and Chow [24]
Also for this numerical study the experimental results from Ingason and Olsson (1992) were used to validate the numerical results. The Fire Dynamics Simulater (FDS v5.5.3) was used for this numerical study. The core algorithm that is used to solve the Navier-Stokes equations is an explicit predictor-corrector that is second order accurate in space and time. The Smagorinsky model was used for turbulence model and Lagrangian particles are used to model smoke movement, sprinkler discharge and fuel sprays. In total four different grids were used with the non-dimensional expression $D^*/\delta x$, ranging from 3 to 12.5 centimeter. It was found that the 10cm cells ($D^*/\delta x$=9.5) were most suitable given the reduction of computational time and accuracy of the results. Evaporation of water droplets and water spray distribution are calculated with the same functions as used by O'Grady and Novozhilov [22]. [24]

Moya Forero [25]
Again, in this study is referred to the experimental results of Ingason and Olsson and used as reference for the numerical simulation. For the numerical study, a more recent version of FDS (v6.1.1) is used. It is pointed out that this version of FDS uses two different models for the turbulent viscosity, namely the default Deardoff model and the Constant coefficient Smagorinsky model. Both these models were tested. For both models a constant Prandtl and Schmidt number were used. The combustion model is similar to previous mentioned studies and is a single-step, mixing controlled combustion which considers the reaction of oxygen and fuel as infinitely fast. The water spray is modeled with the same functions as the previous mentioned study. [25]

de Wilde [13]
For this study FDS version 6.5.3 was used to model a burner room with an adjacent sprinkler room. Default settings of FDS were used to model turbulence, combustion and sprinkler spray distribution. The accuracy of the results is questionable given the low value of the non-dimensional expression $D^*/\delta x$ of 2.5. Also, the experimental results which were used to validate the numerical model are questionable since thermocouples were wetted during sprinkler activation. [13]

1.2.4 Discussion & Conclusion

For the numerical studies, performed in the last decade, NIST's Fire Dynamics Simulator (FDS) was the most frequent used software package. According to multiple of the mentioned study a cell size of 10cm is appropriate for modelling the smoke layer cooling by the sprinkler spray. Also, finer meshes of 3 to 10 cm were used in the studies, however, no significant improvements were found in the accuracy of the results and on the other side the computational times increased significantly. A $D^*/\delta x$ ratio of 10 seems to be appropriate for the defined problem.

By applying FDS as software package automatically large eddy simulations (LES) were applied. The default turbulence model in FDS changed with the introduction of FDS version 6. In version 1 to 5 a constant coefficient Smagorinsky model with Smagorinsky constant 0.2 was used for modelling the small eddies. This was changed to Deardorff's model in FDS version 6. Moya Ferero performed simulations with both turbulence models and found no significant differences in the results [25].

Since the water droplets will not be in contact with the fire hazard in the experiments that will be performed, the single-step, mixing controlled combustion seem to be suitable. With this method, the measured heat release can be fitted into the model and both soot as CO yields can be implemented.

Most of the above-mentioned studies applied a Rosin-Rammler-Lognormal droplet distribution and an equal distribution of water mass and velocity is assumed over the elevation and azimuth angles. Sprinkler experiments by Sheppard (2002) and van Venrooij (2016) indicate that a sprinkler spray envelope cannot be modeled that easily [26], [27]. For both elevation as azimuth angle an irregular distribution occurs and this is strongly dependent of the deflector's shape and geometry. By applying a sprinkler spray table in FDS different mass fractions and velocities can be assigned to parts of a spherical surface and a realistic sprinkler pattern can be modeled.

1.3 References

[1] H. Ingason and S. Olsson, “Interaction between Sprinklers and Fire Vents,” Boras, 1992.

[2] G. D. Lougheed, C. Mccartney, and B. C. Taber, “Smoke Movement for Sprinklered Fires,” *ASHRAE Trans.*, vol. 106, pp. 605–619, 2000.

[3] S. C. Li *et al.*, “Studies of Cooling Effects of Sprinkler Spray on Smoke Layer,” *Fire Saf. Sci.*, pp. 861–872, 2008.

[4] M. Ota, Y. Kuwana, Y. Ohmiya, K. Matsuyama, and J. Yamaguchi, “A Study on Smoke Behavior in a Compartment with Sprinkler System Activation - Simple Predictive Method on Mass Flow Rates Based on Experimental Study-,” *Fire Sci. Technol.*, vol. 28, no. 3, pp. 88–105, 2009.

[5] K. Y. Li, R. Huo, J. Ji, and B. B. Ren, “Experimental investigation on drag effect of sprinkler spray to adjacent horizontal natural smoke venting,” *J. Hazard. Mater.*, vol. 174, pp. 512–521, 2010.

[6] C. F. Zhang, W. K. Chow, R. Huo, W. Zhong, and Y. Z. Li, “Experimental Studies on Stability of Smoke Layer with a Sprinkler Water Spray,” *Exp. Heat Transf.*, vol. 23, pp. 196–216, 2010.

[7] M. L. Bullen, “The effect of a sprinkler on the stability of a smoke layer beneath a ceiling,” *Fire Technol.*, vol. 13, no. 1, pp. 21–34, 1977.

[8] S. C. Li, Y. Chen, and K. Y. Li, “A mathematical model on adjacent smoke filling involved sprinkler cooling to a smoke layer,” *Saf. Sci.*, vol. 49, pp. 670–678, 2011.

[9] M. Tsuchiya, “A Study on Smoke Behavior affected on Droplets of Sprinkler - Velocities of the droplets and smoke layer by PIV system,” Tokyo, 2011.

[10] Z. Tang, Z. Fang, J. P. Yuan, and B. Merci, “Experimental study of the downward displacement of fire-induced smoke by water sprays,” *Fire Saf. J.*, vol. 55, pp. 35–49, 2013.

[11] D. Seo *et al.*, “An Experimental Study on the Smoke-Logging Phenomenon Using Sprinkler for Performance-Based Evacuation Safety Design 88,” *Fire Technol.*, pp. 859–867, 2015.

[12] H. Pretrel, “Interaction between water spray and smoke in a fi re event in a con fi ned and mechanically ventilated enclosure,” *Fire Saf. J.*, vol. 91, pp. 336–346, 2017.

[13] P. de Wilde, “De Invloed van Sprinklers op een Stabiele Rooklaag - Validatie van een CFD sprinklermodel,” Saxion University of applied science, 2017.

[14] K. Y. Li, M. J. Spearpoint, J. Ji, R. Huo, Y. Z. Li, and L. H. Hu, “A Mathematical Model of the Drag Component of a Sprinkler Spray Adjacent to Horizontal Smoke Vents,” *J. Fire Prot. Eng.*, vol. 20, pp. 27–54, 2010.

[15] A. Horvat, “Fire Modelling in Computational Fluid Dynamics (CFD).” 2010.

[16] K. Mcgrattan, S. Hostikka, R. Mcdermott, J. Floyd, C. Weinschenk, and K. Overholt,

Fire Dynamics Simulator User ' s Guide. 2017.

[17] A. Trouvé and Y. Wang, "Large eddy simulation of compartment fires," *Int. J. Comut. Fluid Dyn.*, vol. 24, no. 10, pp. 449–466, 2017.

[18] K. Mcgrattan, S. Hostikka, R. Mcdermott, J. Floyd, C. Weinschenk, and K. Overholt, *Fire Dynamics Simulator Technical Reference Guide Volume 1 : Mathematical Model*. 2017.

[19] T. G. Ma and J. G. Quintiere, "Numerical simulation of axi-symmetric fire plumes : accuracy and limitations," *Fire Saf. J.*, vol. 38, pp. 467–492, 2003.

[20] W. Chow and Y. L. Cheung, "Simulation of Sprinkler-Hot Layer Interaction Using a Field Model," *Fire Mater.*, vol. 18, no. August, pp. 359–379, 1994.

[21] J. Hua, K. Kumar, B. C. Khoo, and H. Xue, "A numerical study of the interaction of water spray with a fire plume," *Fire Saf. J.*, vol. 37, pp. 631–657, 2002.

[22] N. O'Grady and V. Novozhilov, "Large Eddy Simulation of Sprinkler Interaction with a Fire Ceiling Jet," *Combust. Sci. Technol.*, vol. 181, pp. 984–1006, 2009.

[23] R. de Roeck, "Investigation of the influence of SHEVS on the activation time of sprinklers in an industrial building ." p. 3, 2013.

[24] C. Zhang and W. Chow, "Numerical simulation on the interaction of sprinkler and smoke layer," in *The 9th Asia-Oceania Symposium on Fire Technology*, 2013, pp. 453–462.

[25] D. S. Moya Forero, "Numerical study on the interaction of sprinklers and heat vents," Ghent University, 2015.

[26] D. T. Sheppard, "Spray Characteristics of Fire Sprinklers," Evanston, 2002.

[27] D. van Venrooij, "Validation of Fire Dynamics Simulation with sprinkler sprays," 2016.

Appendix 2 – Measurement set-up

- Drawings
  - 3D-view
  - Top view
  - Side view
- Photos
  - Side view
  - Fuel trays

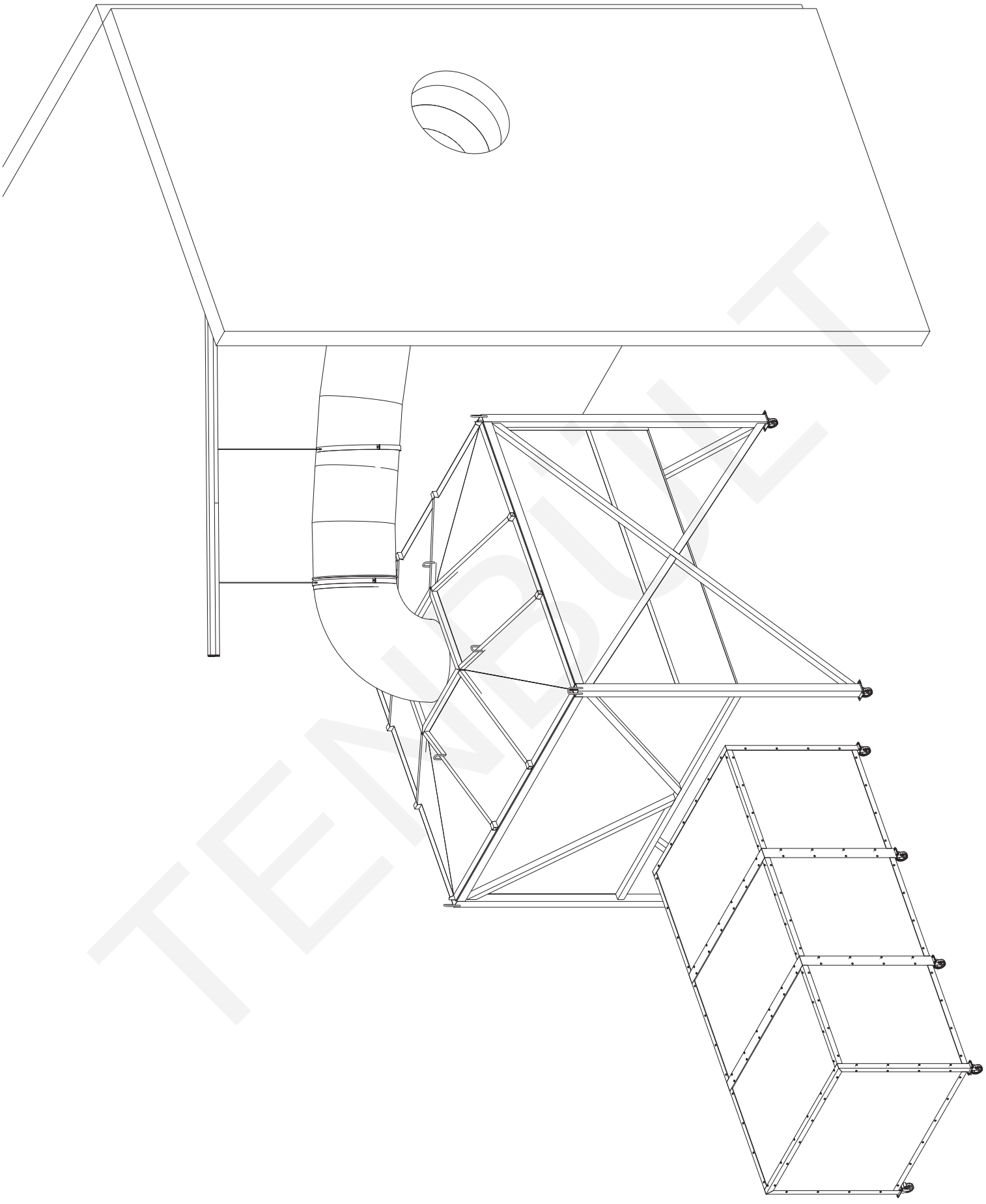

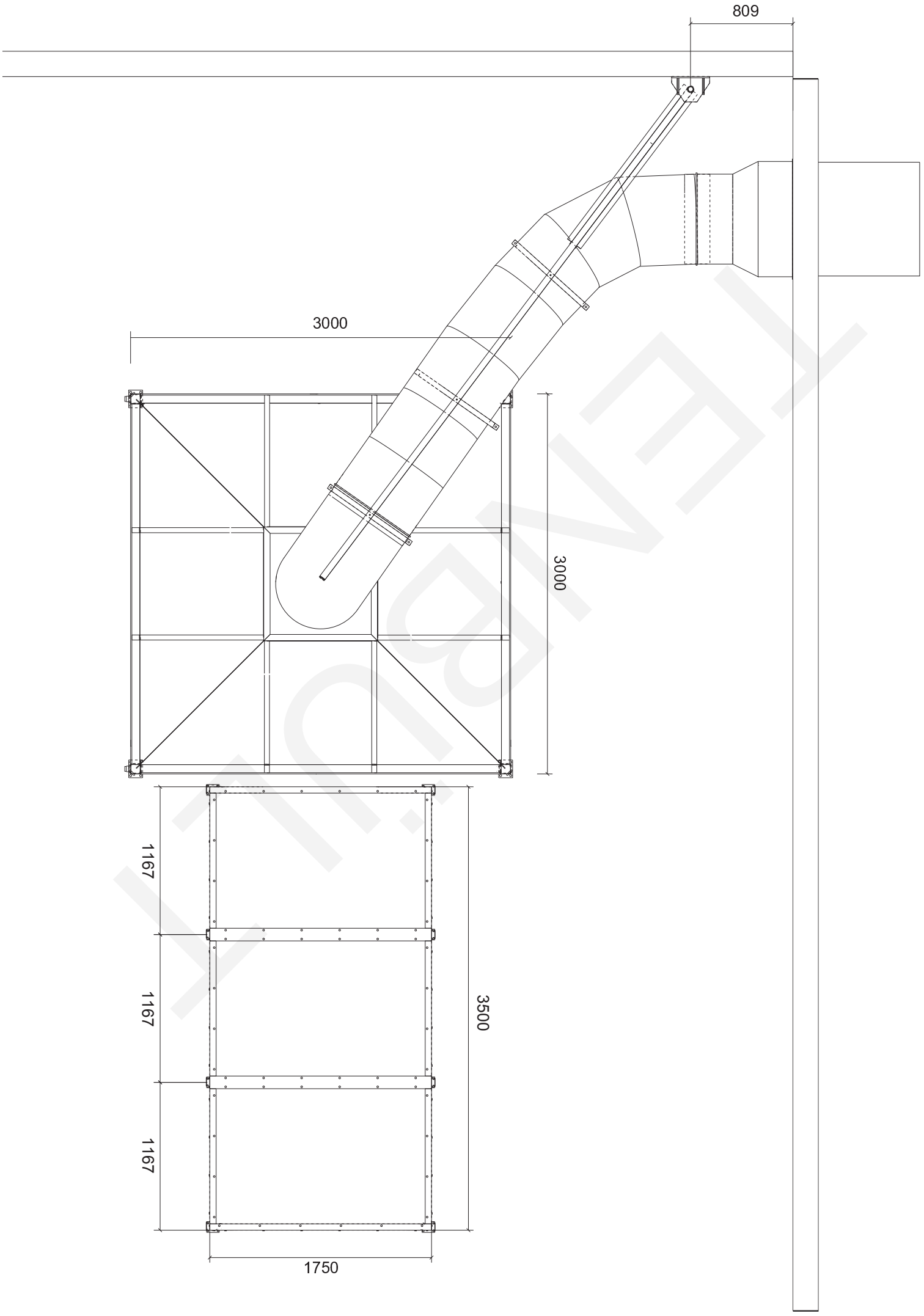
809
3000
3000
1167
1167
1167
3500
1750

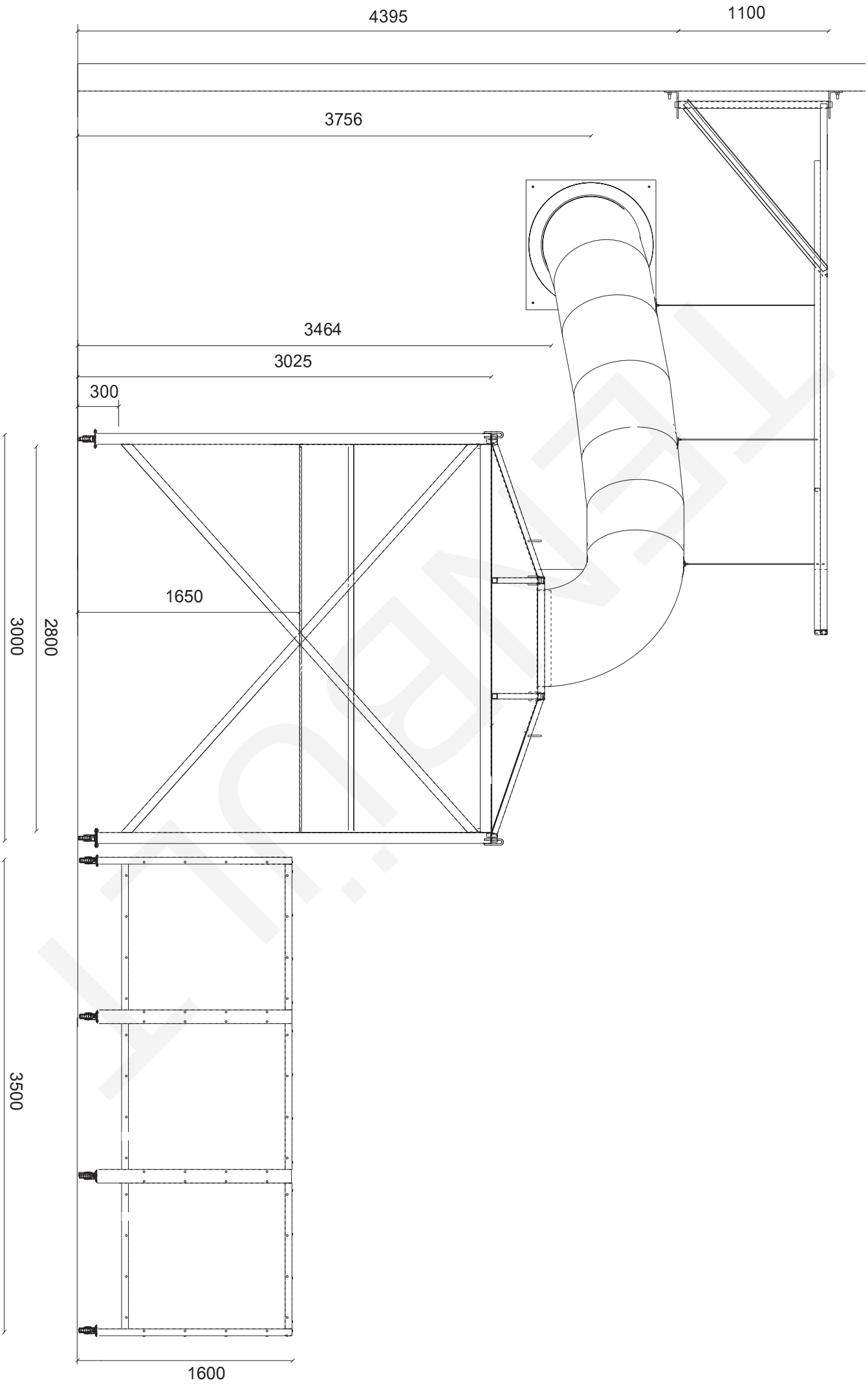
4395
1100
3756
3464
3025
300
1650
3000
2800
3500
1600

The outer dimensions of the burner cabinet are 3.5m x 1.75m x 1.60m and one side of the cabinet is left open to allow smoke movement towards the smoke cabinet. The bottom of the walls is raised 0.3m from the ground, so the fire is sufficed with enough oxygen to maintain an oxygen-controlled fire. The burner cabinet is made of a steel frame existing of L-profiles and T-profiles and is placed on wheels for easy movement of the cabinet. Between the steel profiles, single plates of calcium silicate are placed with a thickness of 15 millimetres.

Side view

Figure 2 - Side view measurement set-up, before RH0

Figure 1 - Side view measurement set-up, after SH3

Fuel trays

Figure 3 – Tray 1, 0.5 x 0.5m (0.25m²)

Figure 4 – Tray 2, 0.5 x 0.7m (0.35m²)

Figure 5 - Additional cooling of tray 2

Appendix 3 – Thermocouple Shields

3.1 Literature

To protect thermocouples from wetting by the sprinkler spray three different methods were tested by de Wilde, namely a nano silicone coating, a water suction system and a vertical metal profile [1]. The results of these methods were compared to a set-up without thermocouple protection. Coating of the thermocouples with a nano silicone spray had no significant effect on the results. Small-scale experiments with a suction tube near the thermocouples was also without a success. Eventually, a vertical protection shield was chosen to protect the thermocouples from wetting. The profile covered all thermocouples of one tree at once. A top view of the metal profile is shown in Figure 3. The thermocouples were placed in the circular part of the profile. Despite the vertical shield the thermocouples were still wetted during the sprinkler tests due to water droplets that bounced back from the hood and by very small droplets that swirl through the hood.

In earlier performed research thin metal shields were often applied to protect an individual thermocouple. Chinese researchers used steel saddle caps as depicted in Figure 1 and Figure 2 in different studies [2]–[4]. The sides of the saddle cap are open, so no heat accumulation takes place below the cap and hot gases can flow freely underneath the shield. This way the measurements are not affected by heat storage below the saddle caps and the thermocouples can respond quickly to a rapid decrease of the gas temperature when the sprinkler nozzle is activated. Although the shields were purposed to prevent the thermocouples from wetting it is indecipherable if the shields functioned properly. Given the experiences of de Wilde [1] with the vertical profile it is hard to believe that water can't reach the thermocouples through the open sides of the saddle cap.

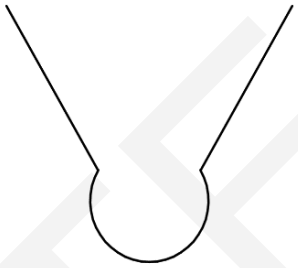

Figure 3 - Thermocouple protection, metal profile top view [1]

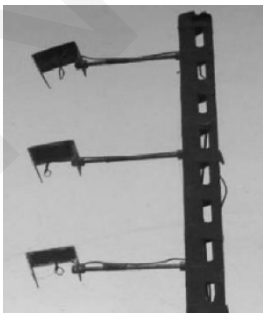

Figure 1 – Multiple saddle caps placed on a thermocouple tree with arms [4]

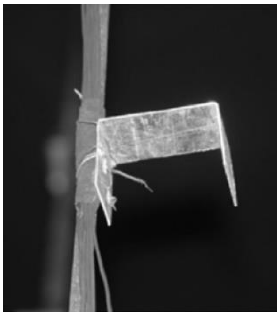

Figure 2 – Saddle cap placed close to the thermocouple tree [3]

Lougheed, McCartney and Taber used a different type of shield to prevent the thermocouples from wetting. They placed a shield with a diameter of 230 millimeter above each thermocouple to minimize direct water spray reaching the thermocouples [5].

3.2 Developed thermocouple shield

From the above-mentioned studies, it can be concluded that the ideal method for protection of the thermocouples has not been found yet. A physical shield seems to

perform better than a nano coating or suction system. The shield must protect the thermocouple from multiple directions and therefore needs to be sufficiently closed. However, by closing the shield there is a change of heat storage below the shield and this will result in a delay of temperature changes.

A new shield was developed that exists of two parts, a short plastic cylindrical tube and an aluminum cone shaped shield on top. A section of this new shield is shown in Figure 4. The thermocouple is placed in the lower have of the tube. Buoyant-driven flows can flow through the tube and can leave the shield at the top through the void between the shield and tube. The shield protects the thermocouple for direct spray from above. This will be the case for the lower placed thermocouples. The tube protects the thermocouple from direct water spray for more horizontal spray angles which is the case for higher placed thermocouples. Also, indirect water spray from the sides will be blocked by the tube. It is expected that heat will be stored just below the conical shield, therefore the thermocouple is placed in the lower half of the tube to prevent affection of the measured temperature by heat storage.

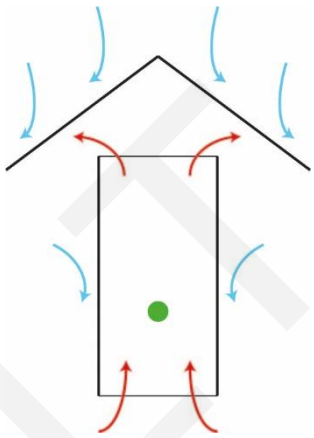

Figure 4 – Vertical section of thermocouple shield

3.3 Measurements

To test the new developed shield temperature measurements were performed with and without sprinkler activation under ambient conditions. First, a measurement was performed without protection shields. The measurement started in a normal situation without activation of the sprinkler. After approximating 150 seconds the sprinkler was activated, at that moment the average ambient air temperature was 22.6°C. The water temperature during sprinkler activation, T_w, was 15.9°C. All thermocouples below the sprinkler nozzle were wetted during sprinkler operation and measured within a few

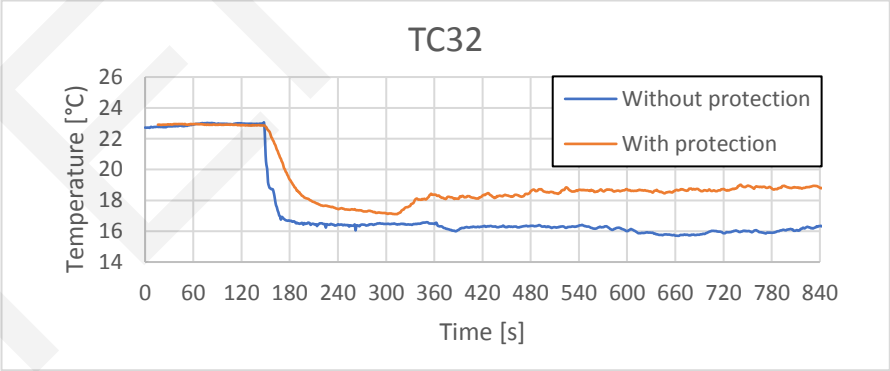

Figure 5 - Air temperature at thermocouple 32, sprinkler activation at 150s

seconds temperatures around 16.0°C (water temperature). The one thermocouple that was not wetted, located in the inlet of the exhaust, measured slightly higher temperatures of 16.6°C. This indicates that there is a difference between wetted and dry thermocouples, but also shows that the air temperature below the hood has dropped almost to the water temperature.

For the second measurement, protective shields were installed around the thermocouples. In Figure 5 the results for one thermocouple are shown (thermocouple 32) for both measurements. The temperature decrease is slower for thermocouples that are protected. This indicates that the thermocouple has not been in contact with water droplets. However, this also means that the temperature decrease is delayed since the thermocouple near the exhaust duct measures a faster decrease. In Figure 7 the temperatures are shown for the thermocouple that is in the inlet of the exhaust duct which remained dry during the sprinkler operation. This thermocouple gives the best indication of the actual air temperature beneath the hood. The relative fast recovery of the temperature after deactivation of the sprinkler nozzle indicates that the thermocouple is measuring the air temperature and this is desirable for all thermocouples. However, the recovery of the other thermocouples is much slower and for some thermocouples the temperatures remain lower than the ambient conditions.

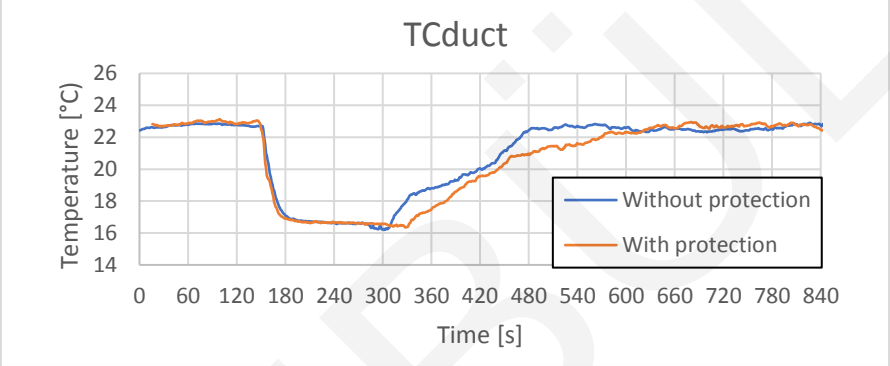

Figure 7 - Air temperature at inlet exhaust duct, activation of sprinkler at 150s

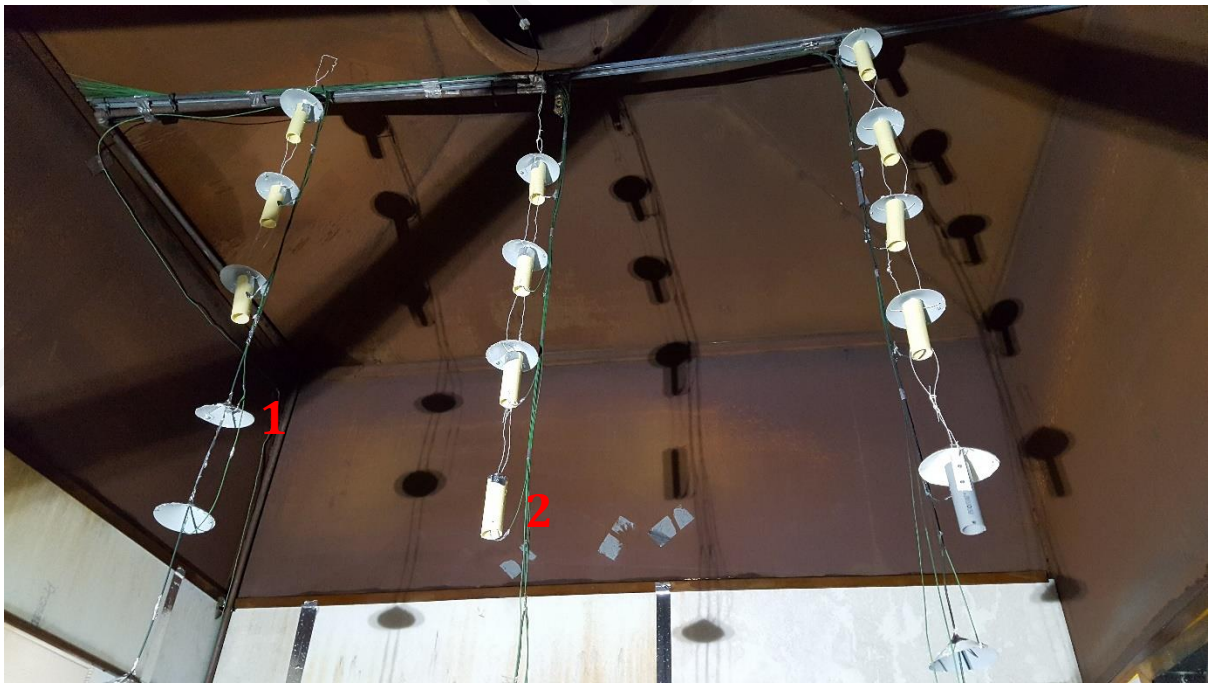

Figure 6 - Protective shields, different configurations at positions 1 (only shield) and 2 (top closed tube)

The delay in temperature decrease and delay in recovery time can be explained by entrapped air inside the plastic tube. When the sprinkler is activated the surrounding air cools down rapidly and a small volume of 'warm' air remains in the tube. Slowly this remaining volume cools down or flows out of the tube and the same temperature should be measured as by the dry thermocouple. However, the sprinkler was deactivated to early, because the temperature was still declining. Therefore, the experiment will be repeated. After deactivation of the sprinkler, the same effect occurs but this time 'cold' air is entrapped inside the tube which affects the recovery time. It can be concluded that the protective shields kept the thermocouples dry, but also had a negative effect on the temperature measurements.

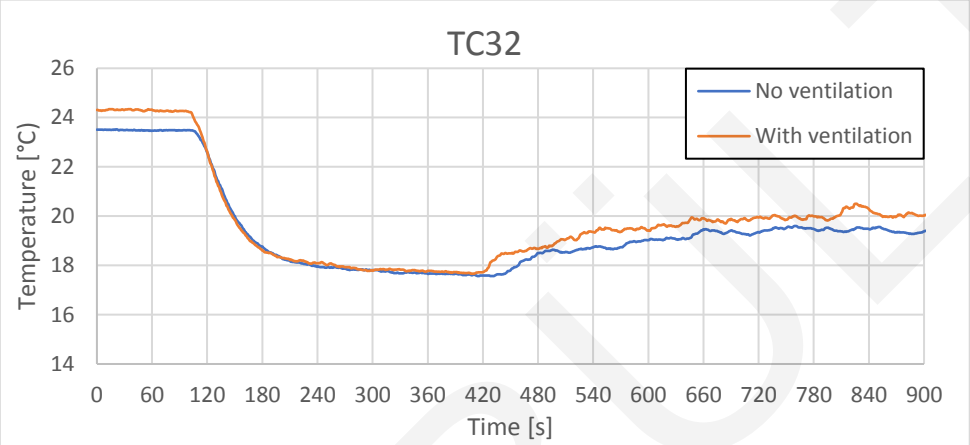

Figure 8 - Air temperature at thermocouple 32, sprinkler activation at 110s

During the second measurement day, also other configurations of protective shields were tested as can be seen in Figure 6. This time no measurement was done without protective shields. During this second measurement day two situations were examined. First the measurement was performed without activation of the exhaust system. Thereafter, the measurement was repeated with an activated exhaust system to see if this has a positive effect on the recovery time. The water temperature was 16.8°C and the ambient temperature was 23.3°C (in the top of the hood slightly higher temperatures were measured).

Again, the results are shown for thermocouple 32, see Figure 8. With an activated ventilation system, the temperature recovery is slightly larger, but the ambient temperature at the start of the experiment was also slightly higher.

A few thermocouples were only protected by the aluminum conical shield and the thermocouple was placed just beneath the shield. In Figure 9 the measured temperatures of one of those thermocouples is shown. For the measurement without ventilation the temperature decrease and recovery look similar to thermocouple 32. When the ventilation system is activated the temperature decrease is even more delayed than for thermocouple 32. Also, the decrease is capricious which seems to be caused by occasional air flows beneath the shield resulting in fluctuations of temperature. Recovery of the air temperature to ambient conditions seems to be better when the ventilation system is active, however the temperature does not reach the start value within 10 minutes after sprinkler deactivation.

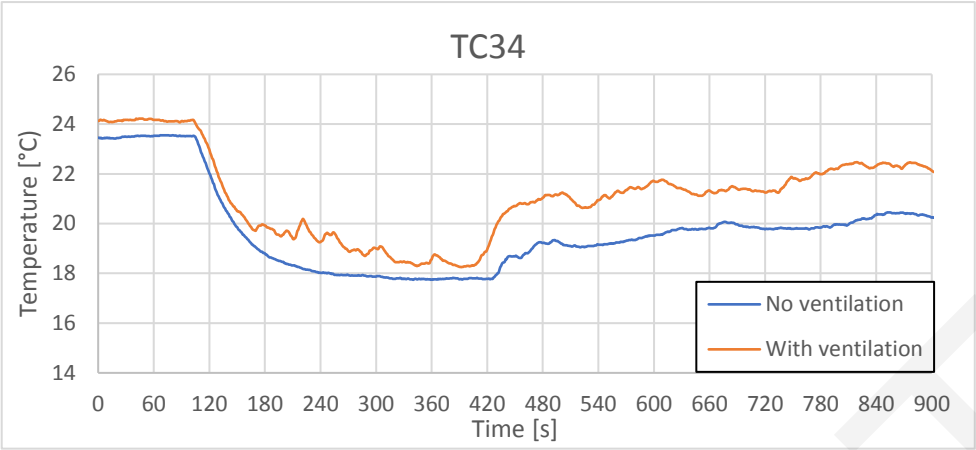

Figure 9 - Air temperature at thermocouple 34, sprinkler activation at 110s (only aluminum shield)

3.4 Conclusion

With the developed protection shields the thermocouples are prevented from wetting. However, the plastic tube forms a buffer for 'warm' air during the cool down and for 'cold' air during heat up. When only the aluminum shield is applied the heat up is faster, but the desired situation is not achieved. The measurements were performed with ambient conditions. It is expected that during the fire experiments the effects of buffering cold air will be smaller due to larger temperature differences and stronger buoyant forces that will 'push/drop' out the cold air. The buffering of warm air will remain and should be accounted for when reviewing the results of future experiments. For thermocouples that are less exposed to horizontal water spray (lower-placed thermocouples) the aluminum shield is sufficient to prevent the thermocouple from wetting.

3.5 References

[1] P. de Wilde, "De Invloed van Sprinklers op een Stabiele Rooklaag - Validatie van een CFD sprinklermodel," Saxion University of applied science, 2017.

[2] S. C. Li *et al.*, "Studies of Cooling Effects of Sprinkler Spray on Smoke Layer," *Fire Saf. Sci.*, pp. 861–872, 2008.

[3] K. Y. Li, R. Huo, J. Ji, and B. B. Ren, "Experimental investigation on drag effect of sprinkler spray to adjacent horizontal natural smoke venting," *J. Hazard. Mater.*, vol. 174, pp. 512–521, 2010.

[4] S. C. Li, Y. Chen, and K. Y. Li, "A mathematical model on adjacent smoke filling involved sprinkler cooling to a smoke layer," *Saf. Sci.*, vol. 49, pp. 670–678, 2011.

[5] G. D. Lougheed, C. Mccartney, and B. C. Taber, "Smoke Movement for Sprinklered Fires," *ASHRAE Trans.*, vol. 106, pp. 605–619, 2000.

Appendix 4 – Heat of combustion and soot yield of heptane/toluene and heptane

4.1 Introduction

The first tests were performed with n-heptane (>99.75) which resulted in 'clean' combustion with a very low soot yield. Consequence of the low soot yield is a poorly visible smoke layer due to the low concentration of smoke particles. A thick and visible smoke layer is desirable to study the effects of the sprinkler system. De Wilde (2017) performed a test with a mixture of n-heptane and diesel to create a thick smoke layer [1]. The volume ratio of the mixture was 20/80 with a total volume of 3.75L. A square fuel tank with a surface area of 0.25m^2 was used and the mixture was poured on a water layer to obtain a constant burning rate. The use of a small part of n-heptane is necessary to ignite the diesel. The experiment was not successful since the diesel started to separate and 'sinking' in to the water. The result of this effect was a longer burning time than expected at a lower and irregular heat release rate. Also, the fire started spattering due to interference with the water layer. Another disadvantage of diesel is the composition that may differ between manufacturers and over time.

Instead of using a heptane-diesel blend a heptane-toluene blend will be used. The blend is manufactured in a laboratory so a constant volume ratio of the chemicals is assured when different experiments are performed. The volume ratio of the heptane-toluene blend is 85/15 [%/%]. Toluene which is formerly known as toluol is a clear liquid with the typical smell of paint thinners. Toluene reacts as an aromatic hydrocarbon and is often used to increase the octane number of fuels. The molecular formula of toluene is $C_6H_5CH_3$ or C_7H_8.

In the past toluene has been used for fire experiments as a separate fuel. However, limited experiments have been performed with heptane-toluene blends and no experiments are known with an 85/15 volume ratio. Typical combustion parameters such as the heat of combustion and soot yield are therefore unknown for this specific blend. In a study by NIST towards hydrocarbon spray fires a heptane-toluene blend with volume fractions of 60% and 40% was tested. The heat of combustion, H_c, of the blend was estimated by taking the values of heptane and toluene and resulted in a value of 43.2MJ/kg [2].

In this study, also the soot, CO and CO_2 yields were determined. These yields were measured just above the visible fire and calculated by using the carbon balance method. The results are shown in Table 1 [2].

Table 1 - Combustion properties spray fire, n-heptane and heptane/toluene blend (60/40) [2]

Fuel	Combustion efficiency	Radiative fraction	Soot yield	CO yield	CO_2 yield
n-heptane	1.06±0.14	0.45±0.08	0.0108±0.0014	<0.008	3.04±0.12
Heptane/Toluene	0.70±0.13	0.35±0.08	0.114±0.022	0.042±0.016	2.70±0.15
Heptane	1.01±0.14	0.45±0.06	0.0149±0.0019	<0.008	3.03±0.12

It was concluded, as expected, that when the soot yield increased the combustion efficiency and radiative fraction decreased. Furthermore, the radiative fraction of heptane pool fires was compared with the experiments, it showed that spray fires have a higher radiative fraction and this is caused by the different structure of the fire, according to the researchers. [2]

Since there are no studies known with the 85/15 heptane/toluene blend a fuel calibration will be done with the Small Burning Item (SBI) measurement set-up. This method is usually used to determine the reaction to fire performance of construction products excluding flooring.

4.2 Soot yield

Combustion of a product (fuel) can be simplified to the following reaction:

Fuel + Oxygen → Products + Energy

To start this reaction a source of ignition (energy) is required or the temperature of the fuel needs to be increased to its ignition temperature. The combustion products are mostly hot gases consisting of CO_2, CO and H_2O. Due to the high temperatures of these gases air is entrained into the smoke plume which results in a large smoke volume. The visual impairment of smoke is caused by soot particles which are a result of incomplete combustion due to a lack of oxygen. The more soot particles are released the higher the density of the smoke is and the lower the visibility through the smoke [3].

A quantity to indicate the visibility is the optical density, OD, which can be obtained with equation *4.2.1* from the intensity of incident light in air (I_0) and intensity of light transmitted through smoke (I) [4].

$$OD = log_{10}(\frac{I_0}{I}) \qquad 4.2.1$$

A quantity to predict total smoke production is the mass optical density. For cellulose fires, the mass optical density is often taken as $100 m^3 m^{-1}/kg$, for products with high smoke production, such as car tires a value of $400\ m^3 m^{-1}/kg$ is more appropriate [3]. The mass optical density can also be determined by multiplying the soot yield, Y_s, with the mass extinction coefficient, K_m.

$$R = Y_s \cdot K_m \qquad 4.2.2$$

The soot yield is the mass ratio between the mass flow of soot particles in the smoke and the mass burning rate of the fuel.

$$Y_s = \frac{\dot{m}_s}{\dot{m}_f} \qquad 4.2.3$$

The mass flow of soot particles is a product of the volumetric flow rate, the mass concentration of smoke and a correction factor C_s, often taken as 0.97, for the slight radial decrease in the smoke concentration near surfaces [5].

$$\dot{m}_s = M_s \dot{V} C_s \qquad 4.2.4$$

$$M_s = \frac{\ln(I_0/I)}{\sigma_s L} \qquad 4.2.5$$

The mass concentration can be calculated with equation *4.2.5*, where σ_s is the relative smokiness of a fuel. A recommended value for σ_s by Mullholland et al. is 8.71 m^2/g with a standard uncertainty of 0.47m^2/g [5]. Furthermore, L is the path length of the light through the smoke from the transmitter to the receiver. Finally, the mass extinction coefficient can be determined with equation *4.2.6* and subsequently the mass optical density can be calculated with equation *4.2.2*. [3], [5]

$$K_m = \frac{OD \cdot \dot{V}}{\dot{m}_f} \qquad 4.2.6$$

4.3 Measurement set-up

To determine the heat of combustion of the heptane/toluene blend the heptane calibration procedure was followed of NEN-EN 13823+A1 *Reaction to fire tests for building products – Building products excluding floorings exposed to the thermal attack by a single burning item.*

For the calibration, a circular steel fuel tray was used with an internal diameter of 350mm, internal wall height of 152mm and wall thickness of 3mm. The fuel tray is then placed over the trolley platform on a calcium silicate board (400x400mm) which is raised 100mm by supports. The distance between the internal corner of the side walls and fuel tray is 500mm and the distance perpendicular on the side walls to the fuel tray is 300mm for both sides.

The volumetric flow rate of the exhaust system was set to 0.60 m^3/s and was kept between 0.65 m^3/s and 0.50 m^3/s during the experiment. The ambient temperatures were measured for 300 seconds before the start of the experiment. To obtain a constant burning rate 2000 grams of water were poured into the fuel tray and the measurement was started. Two minutes later, 2840 gram of the heptane/toluene blend were poured into the fuel tray. After one minute of waiting the fuel can be ignited. During the measurement, the following data is recorded every three seconds: m_{gas}, xCO_2, xO_2, Δp T_0 tot T_3 and the light receiver signal. After ceasing of the fire, the recording continued for at least five minutes.

Figure 1 - Heptane/Toluene calibration procedure

With the obtained data and the equations explained in Chapter 2, the heat release rate and soot yield can be determined. Subsequently, the heat of combustion can be calculated by dividing the total heat release by the weight of the burned fuel.

4.3.1 Results & Discussion

At the end of this appendix, the results of the heptane/toluene calibration are shown. In the first two graphs, the heat release rate and total heat release rate are given. The constant red line represents the average measured heat release rated between 300 seconds and 1380 seconds. The average heat release rate of the blend is 109.4kW and this is approximate 10% higher than for n-heptane which HRR is usually around 100kW. The heptane/toluene has a faster burning rate which results in a higher heat release rate. The total heat release rate is 122.4MJ which results in a heat of combustion of 43.11MJ/kg. This value is, as expected, in between the values for n-heptane, 44.56MJ/kg, and toluene, 41.2MJ/kg.

During the experiment, thick dark smoke was observed. With the light receiver, that is placed in the exhaust duct, the light extinction was measured. Subsequently, the soot yield and mass optical density were calculated. The visual observations were confirmed by a calculated soot yield of 0.071kg/kg which is almost five times higher than the soot yield for n-heptane (0.0149 [2]). The measured mass optical density of 371.5 m^3m^{-1}/kg is comparable to materials with a high smoke production such as rubbers, car tires and PVC. For these products a mass optical density of 400 m^3m^{-1}/kg is often applied [3].

4.3.2 Conclusion

As expected the heat of combustion of the heptane/toluene blend, 43.11MJ/kg, is within the values for n-heptane and toluene. Due to a slightly faster burning rate the heat release rate will be approximate 10% higher than for n-heptane. The smoke production by the blend with a mass optical density of 371.5 m^3m^{-1}/kg is more than sufficient to obtain a clearly visible smoke layer.

4.4 Repetition 1 (CHT1)

With the obtained data from test CHT0 the measurement section of the large set-up can be checked by performing a similar test in the smoke cabinet as in the SBI setup. The steel

Figure 2 - (left) set-up repetition SBI heptane/toluene calibration, (right) burning of heptane/toluene

fuel tray is placed beneath the exhaust hood and plasterboard walls are place around the tray to reproduce similar radiation conditions as in the SBI setup, Figure 2. The tray is filled with 2.00kg water and 1.00kg (±0.02) heptane/toluene is poured on the water. To

save fuel and to shorten the fire duration 1.00kg was used instead of 2.84kg. The expected heat release rate is 109.4kW and the expected total heat release is 43.11MJ.

The results of the test are shown on the next pages. When the fire reaches its steady-state the average heat release rate is 87.8kW which is lower than the expected 109.4kW. This can be explained by the lower burning rate of the fuel, 2.08 g/s compared to 2.50 g/s. The measured total heat release is 40.0MJ which is also lower than the expected 43.11MJ. The soot yield and mass optical density cannot be measured with this set-up because there are no light transmitter and receiver placed in the main exhaust duct.

4.5 Repetition 2 (CHT2)

Due to the different test results between CHT0 and CHT1 it was decided to repeat CHT1 in the SBI measurement set-up. In this test the same amounts of water and heptane/toluene are used as during CHT1. The objective of this measurement is to check which of the previous experiments can be reproduced. With similar conditions and set-up, it is expected that the results of CHT1 will be reproduced. The burning rate of CHT2 is with 2.17 g/s within an acceptable range compared to CHT1 (+4.3%). The increased burning rate should result in more energy that is released in a shorter period and thus a higher HRR. However, at the steady-state the HRR is lower with an average value of 83.4kW (-5.0%). Over the complete burning period this resulted in a THR of 36.8MJ, which is 8% lower than the obtained THR of test CHT1.

The soot yield measured during CHT2, 0.051 kg/kg, is lower than measured during CHT0, 0.071 kg/kg.

Table 2 - Comparison experiments CHT0, CHT1, CHT2 & CH1

Test		**CHT0** (SBI)	**CHT1**	**CHT2** (SBI)	**CH1**
Water	[kg]	2.00	2.00	2.00	2.00
Heptane/toluene	[kg]	2.84	1.00	1.00	2.84
Water/Fuel mass ratio	[-]	1 : 1.42	1 : 0.5	1 : 0.5	1 : 1.42
Fire duration	[s]	1137	482	462	1251
Burning rate	[g/s]	2.50	2.08	2.17	2.27
Total Heat Release	[MJ]	122.4	40.0	36.8	126.1
Heat of combustion	[MJ/kg]	43.11			44.4
Combustion efficiency	[-]	1.0	0.928	0.853	1.0
Heat Release Rate (at steady-state)	[kW]	109.4	87.8	83.4	105.6
Soot yield	[kg/kg]	0.071	NM	0.051	0.038
Mass optical density	[m^3m^{-1}/kg]	371.5	NM	247.9	149.8

4.6 Heptane (CH1, purity unknown)

Due to delivery problems of heptane/toluene a less pure form of heptane was used for the remaining experiments. The purity and exact composition of this fuel is unknown. For n-heptane with a high purity (>99.75%) it is commonly known that the heat of combustion is approximate 44.56MJ.

For heptane with the unknown purity, the same procedure as performed during CHT0 is repeated to determine heat of combustion and soot yield. The results are given in Table 2. The heat of combustion, 44.4MJ, is close to the expected value of 44.56MJ for heptane with high purity. Less soot is produced compared to heptane/toluene which means the visual effects will be less visible during the sprinkler tests.

4.7 Conclusion

It is assumed that the test results that are obtained with the SBI measurement set-up, which is accredited conform NEN-EN 13823+A1, are reliable and accurate. Since the equipment is maintained, checked and calibrated on a regular basis. The THR of CHT0 and CH1 have been used to determine the heat of combustion for heptane/toluene and heptane because this test is performed according to the calibration procedure of NEN-EN 13823+A1 and this test has the longest constant energy release.

The lower HRR of CHT1 compared to CHT0 can be explained by the slightly lower burning rate of the fuel which is most likely caused by a different water-to-fuel ratio. However, the heat of combustion should be equal in both measurements. This implies that the combustion of CHT1 is less efficient which resulted in incomplete combustion of the fuel that is extracted with the smoke. The results of CHT1 and CHT2 should be very similar, however the combustion efficiency is lower for CHT2 resulting in a lower HRR and THR.

From the test results of CHT0, CHT1 and CHT2 cannot be concluded if the measurement set-up in the main exhaust duct provides accurate results. The measured THR during CHT1 is within a 10%-range from both CHT0 as CHT2 and this is considered accurate enough to continue with the research.

4.8 References

[1] P. de Wilde, “De Invloed van Sprinklers op een Stabiele Rooklaag - Validatie van een CFD sprinklermodel,” Saxion University of applied science, 2017.

[2] A. Hamins, A. Maranghides, and G. Mulholland, “The Global Combustion Behavior of 1 MW to 3 MW Hydrocarbon Spray Fires Burning in an Open Environment,” 2003.

[3] R. A. P. van Herpen, “Rookdichtheid en zichtlengte,” in *Fire Safety Engineering*, 2007, pp. 1–10.

[4] A. Beard and R. Carvel, *The Handbook of Tunnel Fire Safety*. London: Thomas Telford, 2005.

[5] G. W. Mulholland, E. L. Johnsson, M. G. Fernandez, and D. A. Shear, “Design and Testing of a New Smoke Concentration Meter,” *Fire Mater.*, vol. 24, pp. 231–243, 2000.

Name experiment:	Calibration Heptane-Toluene 0 (CHT0)				
Date:	31-10-2017				
Ambient temperature:	15.4	°C			
Fire duration:	1137	s			
Fuel					
Name:	heptane-toluene (85/15)				
Surface:	0.078	m^2			
Weight:	2.84	kg			
Heat of combustion:	43.11	MJ/kg			
Theoretical THR:		MJ			
Mass burning rate	2.498	g/s	Measured THR:	122.4	MJ
Soot yield	0.071	kg/kg	Measured avg. HRR:	109.4	kW
Mass optical density	371.5	m3m-1/kg	Smoke layer height:	-	m

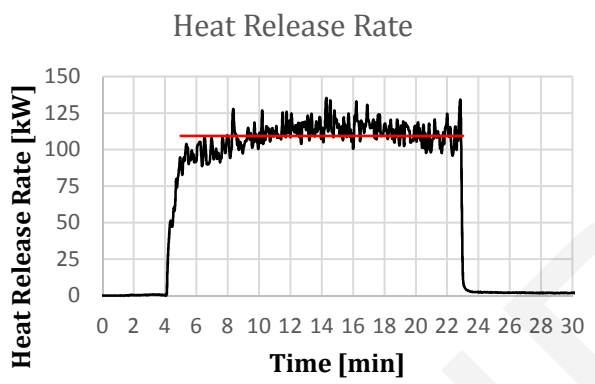

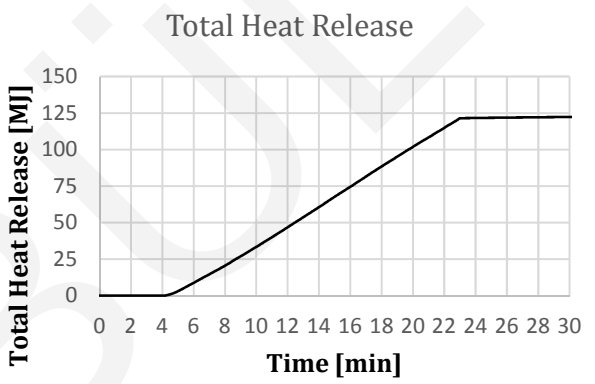

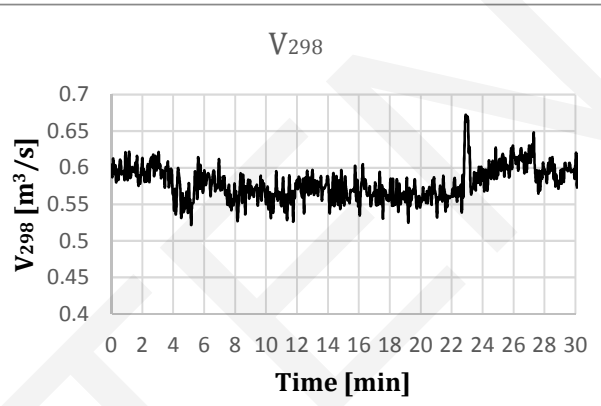

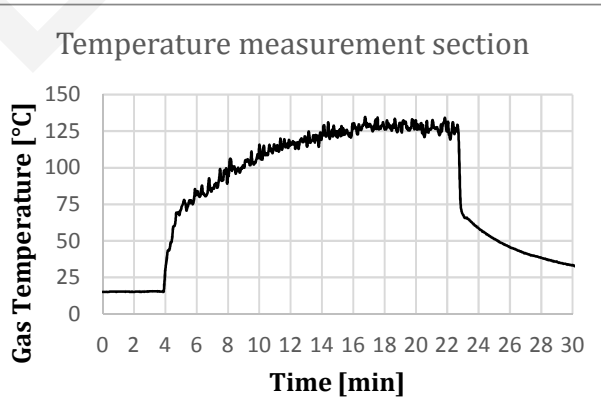

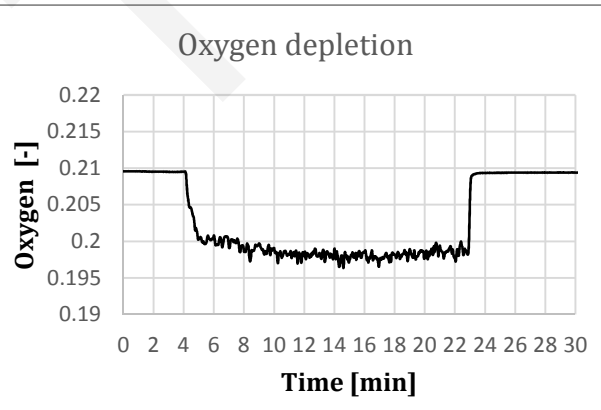

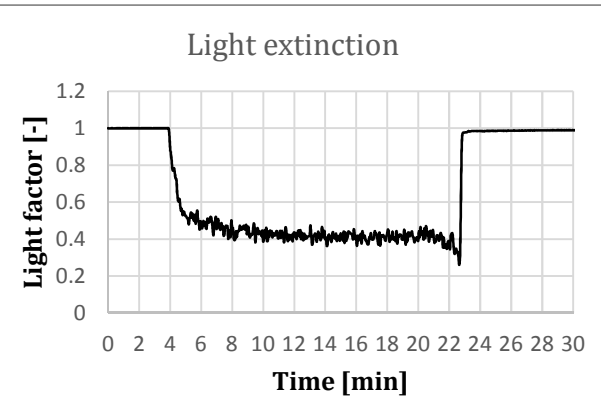

Name experiment:	Calibration Heptane-Toluene 1 (CHT1)				
Date:	20-12-2017				
Ambient temperature:	16.5	°C			
Fire duration:	482	s			
Fuel					
Name:	heptane-toluene (85/15)				
Surface:	0.096	m^2			
Weight:	1.00	kg			
Heat of combustion:	43.11	MJ/kg			
Theoretical THR:	43.11	MJ			
Mass burning rate	2.075	g/s	Measured THR:	40.0	MJ
Theoretical HRR	89.4	kW	Measured avg. HRR:	87.8	kW

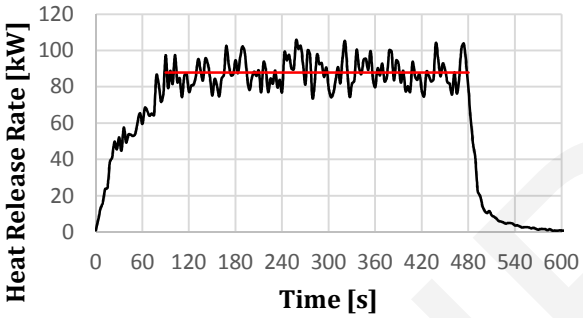

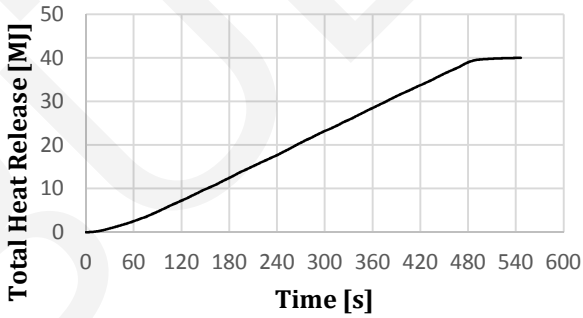

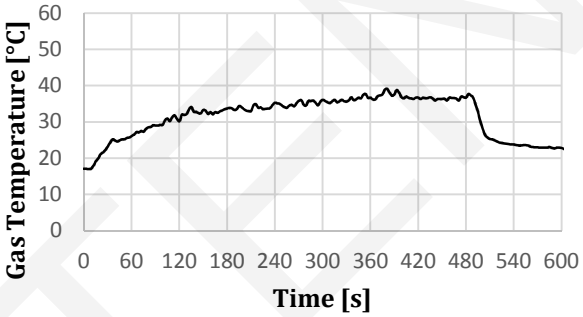

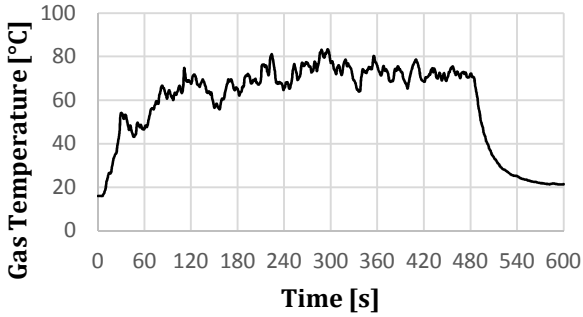

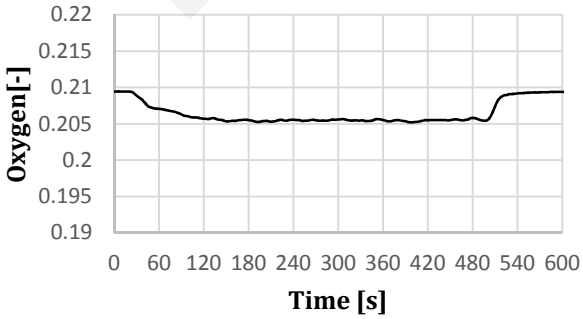

Name experiment:	Calibration Heptane-Toluene 2 (CHT2)				
Date:	11-1-2018				
Ambient temperature:	16	°C			
Fire duration:	462	s			
Fuel					
Name:	heptane-toluene (85/15)				
Surface:	0.096	m^2			
Weight:	1	kg			
Heat of combustion:	36.78	MJ/kg			
Theoretical THR:		MJ			
Mass burning rate	2.165	g/s	Measured THR:	36.8	MJ
Soot yield	0.051	kg/kg	Measured avg. HRR:	83.4	kW
Mass optical density	247.9	m3m-1/kg	Smoke layer height:	-	m

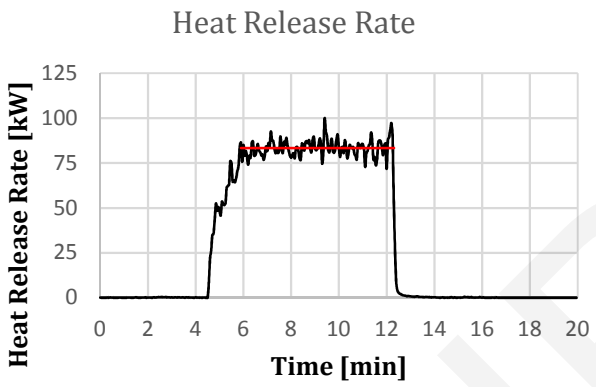

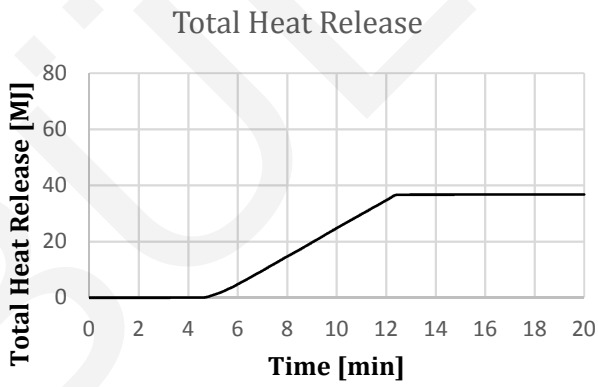

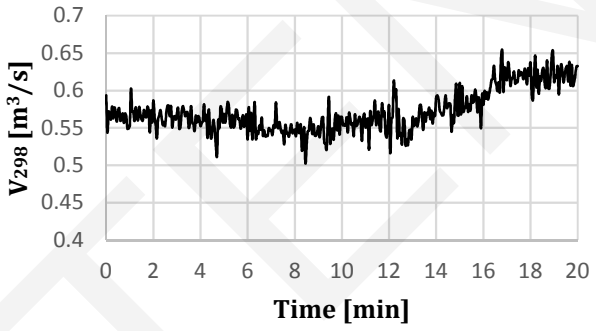

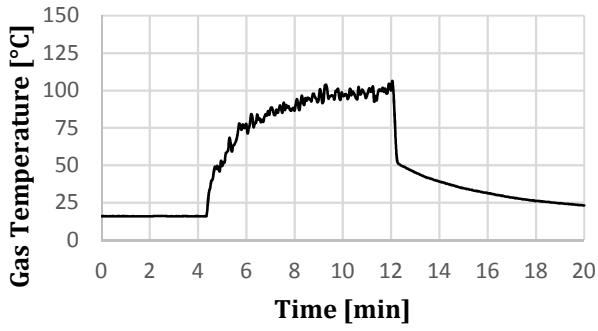

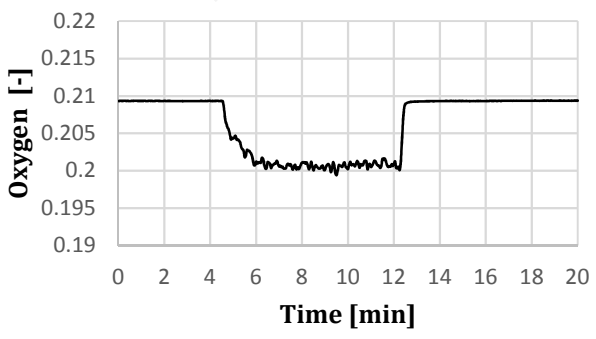

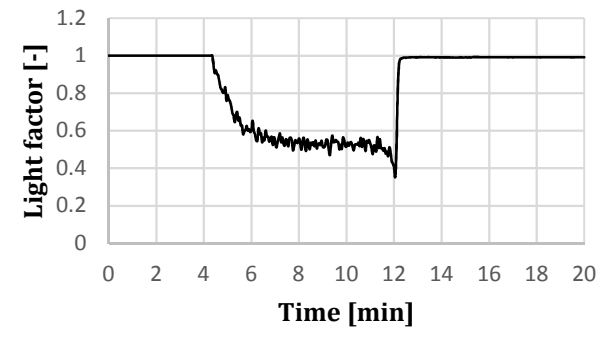

Name experiment:	Calibration Heptane 1 (CH1), purity unknown				
Date:	4-4-2017				
Ambient temperature:	15.85	°C			
Fire duration:	1251	s			
Fuel					
Name:	heptane (purity unknown)				
Surface:	0.096	m^2			
Weight:	2.84	kg			
Heat of combustion:	44.40	MJ/kg			
Theoretical THR:		MJ			
Mass burning rate	2.270	g/s	Measured THR:	126.1	MJ
Soot yield	0.038	kg/kg	Measured avg. HRR:	105.6	kW
Mass optical density	149.8	m3m-1/kg	Smoke layer height:	-	m

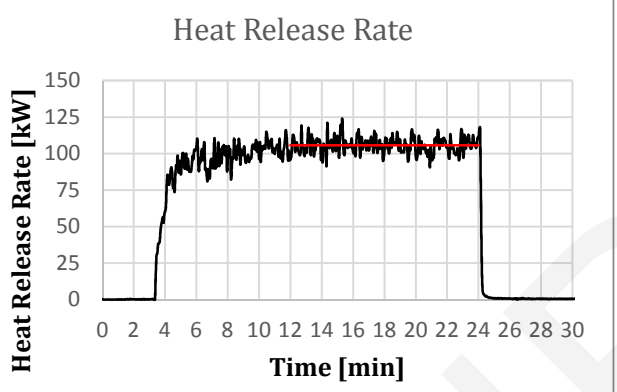

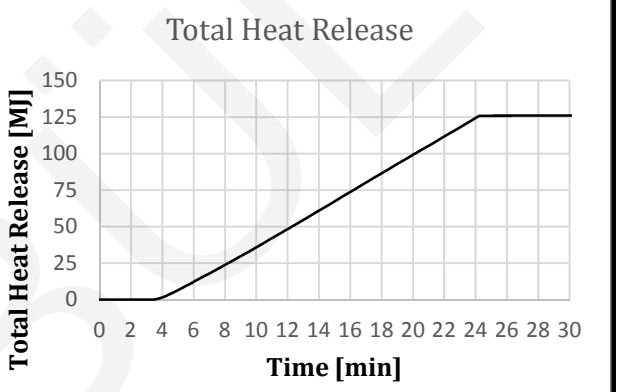

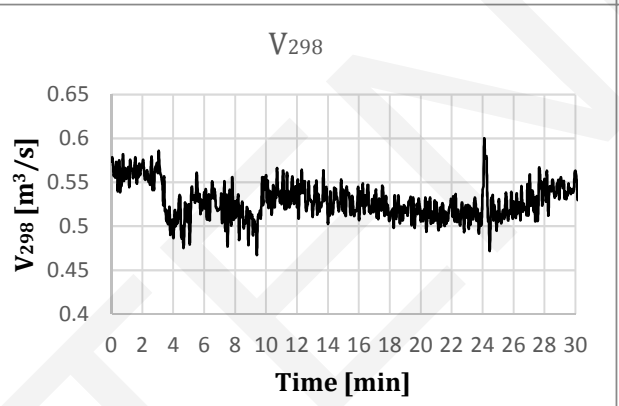

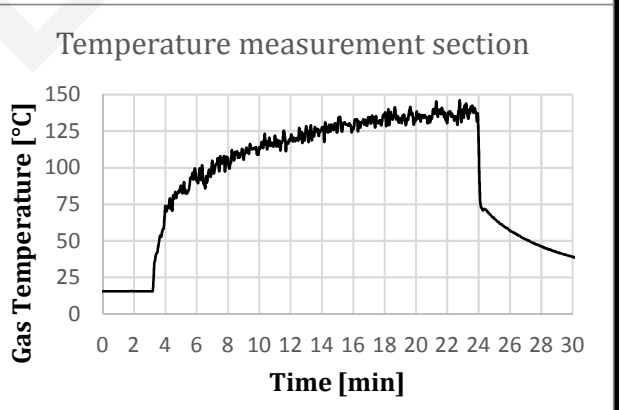

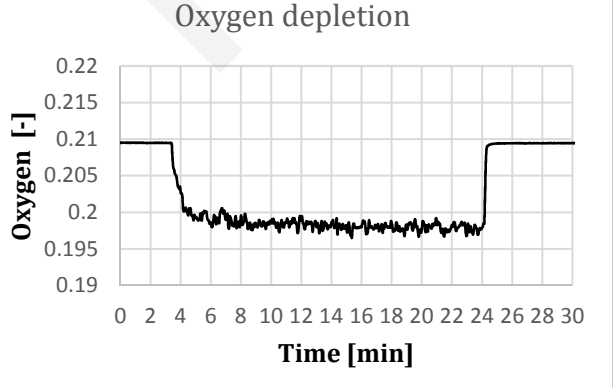

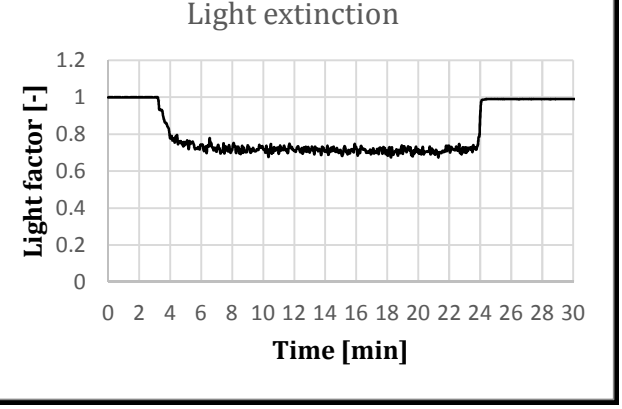

Appendix 5 – Velocity profile at measurement section

5.1 Velocity profile

To determine the heat release rate as accurate as possible with oxygen consumption calorimetry described in chapter 2 the volumetric flow rate is required. The volumetric flow rate is equal to equation 5.1.1. In this equation c, k_t, and k_ρ are constants, Δp and T will be measured and A is the cross-sectional area of the exhaust duct. For the current measurement set-up k_t of the main exhaust duct is unknown.

$$\dot{V}_{298}(t) = c \cdot A \cdot \frac{k_t}{k_\rho} \sqrt{\frac{\Delta p(t)}{T(t)}} \qquad 5.1.1$$

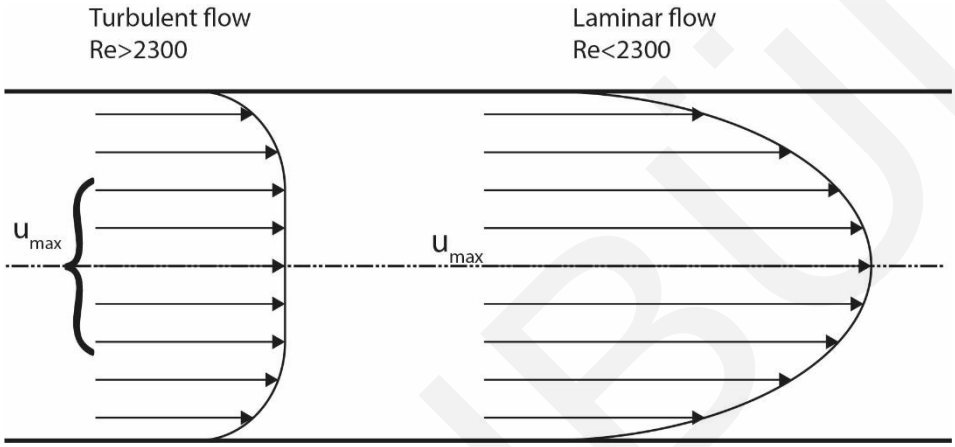

Figure 1 - Turbulent velocity profile vs. laminar velocity profile in smooth pipe

The velocity profile is a function of the Reynolds number. Laminar flows with low Reynolds number (Re<2300) have a parabolic velocity profile and low k_t. Turbulent flows with high Reynolds number have a smaller boundary layer thickness which means the velocity profile flattens and k_t is high. [1]

The velocity in a streamline can be determined by measuring both static and total pressure with a Pitot tube. Subsequently, the velocity can be calculated with Bernoulli's equation, equation 5.1.2. Assuming an isothermal flow, without friction (ideal fluid).

$$\rho v_1^2 + p_1 + g\rho h_1 = \rho v_2^2 + p_2 + g\rho h_2 = constant\ along\ streamline \qquad 5.1.2$$

If a streamline ends on a solid body e.g. the wall of an air duct, the velocity in that point $v_2 = 0$ and the friction and gravity can be neglected then equation 5.1.2 can be written as equation 5.1.3.

$$\rho v_1^2 + p_1 = p_2 \qquad 5.1.3$$

Subsequently, v_1 can be calculated with equation 5.1.4.

$$v_1 = \left(\frac{2(p_2 - p_1)}{\rho}\right)^{\frac{1}{2}} \qquad 5.1.4$$

The total pressure, p_1, and static pressure, p_2, can be measured with a Pitot tube as shown in Figure 2. Inserting these values into equation 5.1.4 results in the velocity of the air flow at the measuring point. By obtaining the velocity at different positions in the pipe the velocity profile of a streamline can be determined.

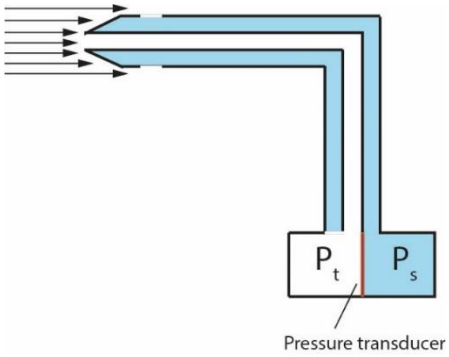

Figure 2 - Pitot tube (schematic)

The European standard NEN-EN 13823:2010+A1:2014 describes procedures that must be followed when conducting fire tests on building products that are exposed to a thermal attack by a single burning item. Annex C of this standard contains calibration methods for the required measuring equipment, including the flow factor k_t.

Flow factor k_t is determined by taking the mean value of $k_{t,qgas}$, $k_{t,heptane}$ and $k_{t,v}$. Here $k_{t,qgas}$ is the flow profile factor adjusted to the propane energy content, $k_{t,heptane}$ the flow profile factor adjusted to the heptane energy content and $k_{t,v}$ the velocity profile factor. Since no propane will be used during the experiments of this study this factor will not be considered. The value of k_t must meet the following criteria:

$$\left|(k_t - k_{t,v})/k_t\right| \leq 5\% \quad \text{and} \quad \left|(k_t - k_{t,heptane})/k_t\right| \leq 5\% \quad \text{and} \quad \left|(k_t - k_{t,qgas})/k_t\right| \leq 5\%$$

$k_{t,heptane}$ depends on the combustion efficiency of the fuel and since complete combustion is assumed $k_{t,heptane} = k_t$. And since propane is not considered in the experiments $k_{t,v} = k_t$. In this case the above-mentioned criteria cannot be checked and therefore the results of k_t should be handled with care.

5.2 Velocity profile factor according NEN-EN 13823:2010+A1:2014

The measurement positions on a single radius are expressed as a fraction of the radius with the following distances from the wall: 0.038; 0.153; 0.305; 0.434; 0.722 and 1.000 (center). For an air duct with a diameter of 900mm this results in the measurement positions as shown in Figure 3. For every measuring point the velocity should be measured 20 times, 10 times when traversing outwards from the center and 10 times when traversing inwards to the center. The measurement probe (Pitot tube) should be

mechanically fixed instead of held by hand and the horizontal/vertical positioning and the right angles to the duct shall be checked. [2]

The following steps must be performed [2]:

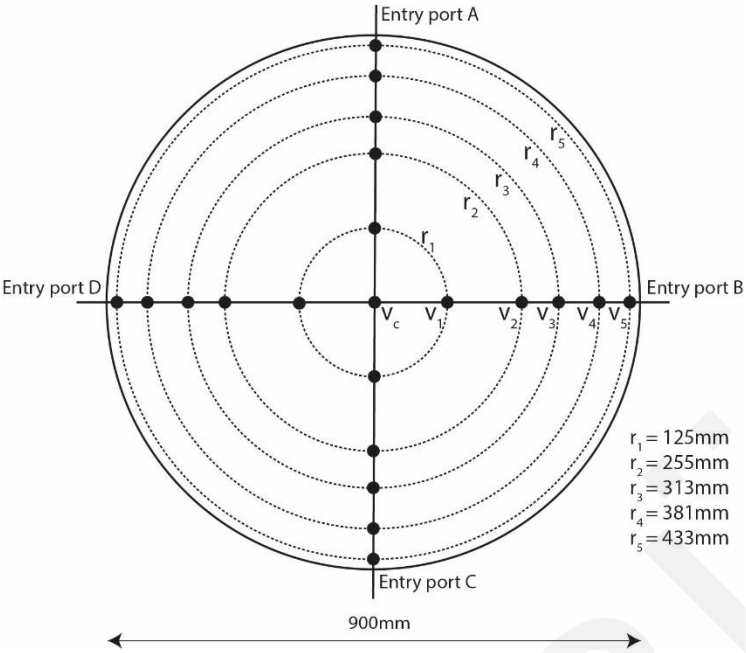

Figure 3 - Measurement points according NEN EN13823:2010+A1:2014

- Set the volume flow of the exhaust to V_{298} = 0.60 ± 0.05 m^3/s (not applicable to the measurement set-up since the duct size is different and the exact volume flow is unknown).
- Record the temperature at three positions in the general measurement section and ambient temperature for at least 300 seconds. The ambient temperature must be within the range 20 ± 10°C and the temperatures in the duct shall not differ by more than 4°C from the measured ambient temperature.
- Measure the differential pressure at six positions per entry point (5 points + center point) and calculate the velocity.
- Calculate the gas velocity per position as the mean value of the 20 measurements. This results in v_c for the center position and v_n for the other five positions for each entry port.

With the four velocity values for a given diameter v_n (distance between center and measurement point) the velocity at this radius v_N can be calculated by taking the mean value these four values. The same can be done for the center point. The velocity at the center point is given by v_C. Thereafter, the velocity profile factor can be computed by taking the mean value of the velocity ratios between the five measuring points and the center point. [2]

$$k_{t,v} = \frac{1}{5}\sum \frac{v_N}{v_C} \qquad 5.2.1$$

5.3 Measurements

The differential pressures are measured in vertical plane of the bi-directional probe as depicted in Figure 4. The bi-directional probe was removed during the experiment and the opening in the duct was used as entry point for the pitot tube. Due to the limited space around the duct, bounded by wall and ceiling, only one entry port could be used. All measurements were done from this entry point, as shown in Figure 5. To measure as accurate as possible a plate with guidance lines was fixed perpendicular to the flow direction of the pipe. The pitot tube can move in four directions and to measure accurate it is important to hold the pitot tube in the right direction for all four directions. The pitot tube is provided with lines that represent the distance from the wall to the measuring point to assure the appropriate depth of the pitot tube. Rotation of the pitot tube around its own axis is prevented by a guidance pin at the end of the pitot tube that must be kept horizontal. The height of the pitot tube's inlet is maintained by the guidance lines on the

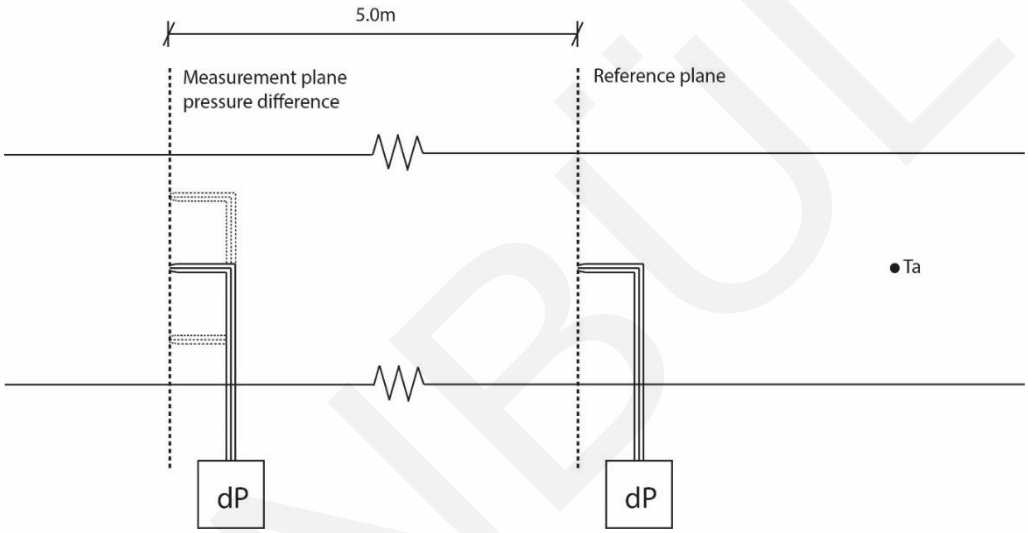

Figure 4 - Measurement set-up (horizontal section air duct)

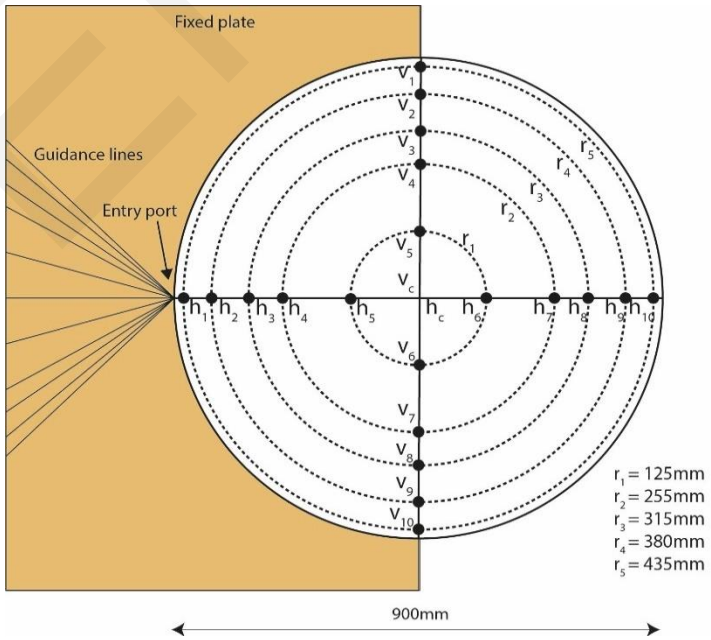

Figure 5 - Measurement points at measurement plane (vertical section)

fixed plated. The plate also prevents the pitot tube from horizontal rotation around the entry point, so the inlet is kept in the optimal air stream.

In Figure 4 and Figure 6 it can be seen that a second pitot tube is placed in the center of the duct. This second pitot tube is fixed and measures the pressure difference only in the center point. For every measurement in the measurement plane the pressure difference is also measured in the reference point, so sudden deviations in the air flow caused by the ventilator can be observed.

Behind the reference point the air temperature is measured by a thermocouple that was already in place.

5.3.1 DPM TT370S Digital manometer (without pitot tube)

Ranges: 199.9 Pa
1999 Pa
7kPa
Velocity range: 1.2 – 100 m/s
Accuracy differential pressure: 1%
Time constant: Slow 5 seconds
Fast 1 second

The micromanometer in Figure 6 measures the differential pressure between the static and total pressure. The manometer can directly calculate the velocity in m/s with the set air density factor on the device. The air density factor is dependent of the absolute pressure in millibar and the temperature. With these two values and the table printed on the manometer the correct air density factor can be determined. In Figure 6 the air density factor is set to 196 (200 standard conditions). The manometer has no logging function so the measured velocities will be read of the display and written down.

At the start of the measurements both manometers were connected to the reference pitot tube to see if both manometers measure the same values. No deviations were found between the manometers.

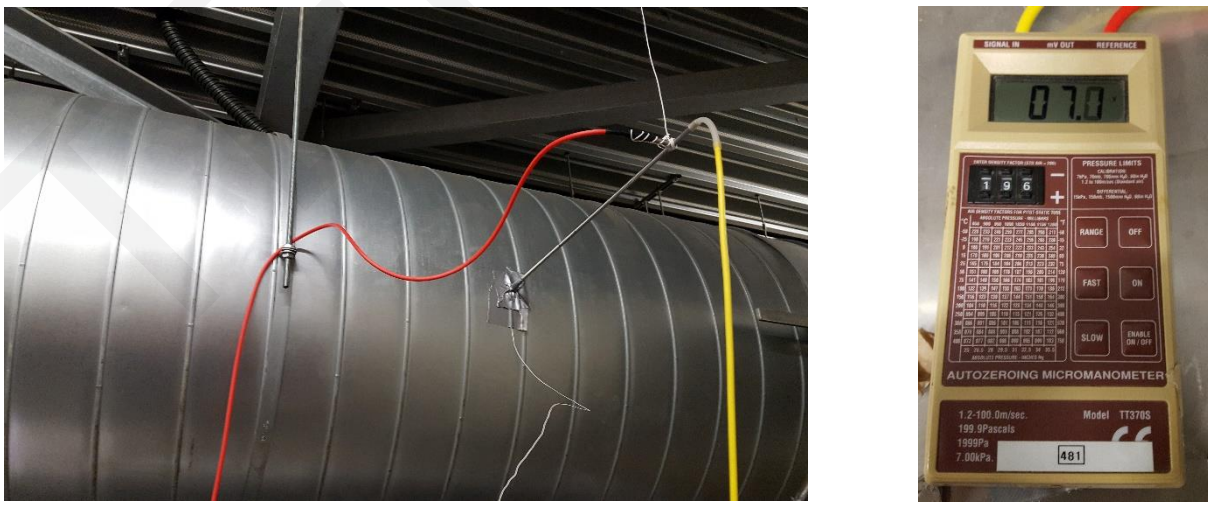

Figure 6 - Measurement set-up reference point (left), manometer (right)

5.3.2 Temperature

The thermocouple of type K, that is used to measure the temperature of the air flow is located further in the duct at approximate 10 meter from the measurement plane. The temperature is measured at the start and end of the measurements for each measured ventilation mode.

5.3.3 Ventilation modes

Ventilation is controlled by a frequency controller, the rotary knob ranges from 0 – 10. The experiment is repeated five times with different ventilation modes. The following modes were used during the experiment: 1, 3, 5, 7, 10. In contrast to the requirements of the SBI standard the volume flow cannot be controlled in m^3/s. The experiments provide insight in the volume flow for the different frequencies (modes) of the ventilator. The duct is only used to extract air and therefor only the velocity is measured in this direction.

5.3.4 Number of measurements

Every point is measured 4 times, 2 times while traversing towards the center and 2 times while traversing away from the center. The manometer has two modes, namely 'slow' and 'fast' with different time constants 1 second and 5 seconds respectively. All measurements were performed with the 'slow' time constant to average out small deviations.

5.3.5 Measurement conditions

In Table 1 the measurement conditions for each ventilation mode are given.

Table 1 - Conditions for different ventilation modes

Ventilation frequency [Hz]	Frequency ventilation mode [Hz]	Start Temperature	End Temperature
22.8 (1/10)	22.8	23.3	23.3
31.5 (3/10)	31.5	23.0	23.3
40.0 (5/10)	40.0	22.8	23.0
50.0 (7/10)	50.0	22.8	22.8
51.2 (10/10)	51.8	23.0	22.8

The multi-functional test room has two extraction points which can both be closed with a valve. The extractions points are in the wall and are located on top of each other. The highest located vent is aligned with the main exhaust duct and the bottom vent is connected to the main duct with in total three turns of 90 degrees. Later, during the fire experiments the bottom vent will be used as extraction point. Therefore, the velocity measurements in the duct were performed with the top valve closed and the other valve open. To get an indication in deviations between different configurations of the valves the center velocity was measured in the reference point at the maximum frequency. The result of this indicative measurement is shown in Table 2.

Table 2 - Maximum velocity with different valve settings

Setting of valves	Velocity in reference point [m/s]
Both valves open	7.7 – 8.0
Top closed, bottom open	7.1 – 7.3
Top open, bottom closed	7.6 – 7.8

5.4 Results

The results of the measurements are shown in Table 3. The center velocity is the average value of all measurements performed in the center point (h_c and v_c) for a certain ventilation mode. The average velocity at the radiuses 1 till 5 is the average value of all measurement points with the same radius, so R1 is the average value of h_5, h_6, v_5 and v_6. Eventually, the average velocity at the radiuses and center velocity result in the k-factor which can be used to calculate the average velocity and volume flow in the duct.

Table 3 – Results velocity measurements

Ventilation frequency [Hz]	Velocity center [m/s]	Average velocity R1 – R5 [m/s]					k-factor [-]	Average velocity [m/s]	Volume flow [m^3/s]
		R1	R2	R3	R4	R5			
22.8 (1/10)	3.06	3.12	3.08	3.04	2.88	2.47	0.953	2.92	1.86
31.5 (3/10)	4.13	4.17	4.15	4.02	3.65	2.98	0.919	3.79	2.41
40.0 (5/10)	5.30	5.28	5.28	5.08	4.66	3.79	0.909	4.82	3.06
50.0 (7/10)	6.49	6.44	6.43	6.20	5.66	4.48	0.900	5.84	3.72
51.2 (10/10)	6.68	6.62	6.63	6.36	5.69	4.93	0.906	6.05	3.85

5.4.1 Inaccuracies

Analysis of the results requires to consider several inaccuracies that occur during the measurements. The inaccuracies that occur are:

- the accuracy of the manometer, +/- 1%;
- wrong setting for air density factor, 0 - 1%;
- positioning of the pitot tube;
- reading of the values.

The accuracy of the manometer is given by its manufacturer and is estimated to be 1%. In other words, the measured values may differ 1% from the real values.

During the experiment the air density factor was set to 196. Hereby, the temperature was taken 23°C as measured and the absolute temperature was assumed to be 1000 mbar. During analysis of the results it turned out that the atmospheric pressure was 1015 mbar during the measurements. Therefore, the manometer slightly overestimates the calculated velocity due to the underestimated air density factor. The calculated overestimation of the velocity was found to be approximate 1%.

During the experiment the pitot tube was hold by hand, this may have caused misalignment of the pitot tube to the optimal air flow due to small rotations or deviating

angles of the tube. When the pitot tube is aligned with the air flow the maximum velocity will be measured in that point. So, when the pitot tube is not in the optimal flow a lower velocity will be measured. This means the actual velocity will be slightly higher than what was measured assuming not all positions were perfect. However, the range of this inaccuracy cannot be determined exactly.

The reading of the values was done by hand on two manometers, due to fluctuation of the values on the display it was difficult to read a value, even with the 'slow' time constant the values kept fluctuating, also for the fixed reference point. The average range of fluctuation for the reference point was 0.2–0.3 m/s. This inaccuracy can be solved by performing more measurements so the average of many points can be determined and a reliable value of the average velocity can be given.

5.4.2 Velocity profiles

On the next pages the horizontal and vertical velocity profile at the measurement plane are shown. The X-axis represents the air velocity and the Y-axis represents the distance from the ducts wall. For the horizontal velocity profile the entry point is located at y=0 and the opposite side of the duct is located at y=900. The vertical velocity profile ranges also from y=0 (bottom of duct) to y=900 (top of duct).

The blue lines indicate the average velocity of four measurements in a specific point. For each of the four measurements the velocity was measured in the reference point. The average of four reference measurements corresponding to a specific point is shown by the orange squares on the right side. All reference measurements were performed at the same distance and therefore the Y-axis is not applicable to these values. With the reference measurements it can be observed if an unexpected deviation in the velocity profile is caused by a change of velocity in the entire duct.

Measurement data of point h_{10} is missing in the graph since it was not possible to measure this point. Due to the fixed plate in combination with the length of the pitot tube and connected tube the pitot tube could not reach this point. The average velocity at radius R5 was determined by the average value of h_1, v_1 and v_{10}.

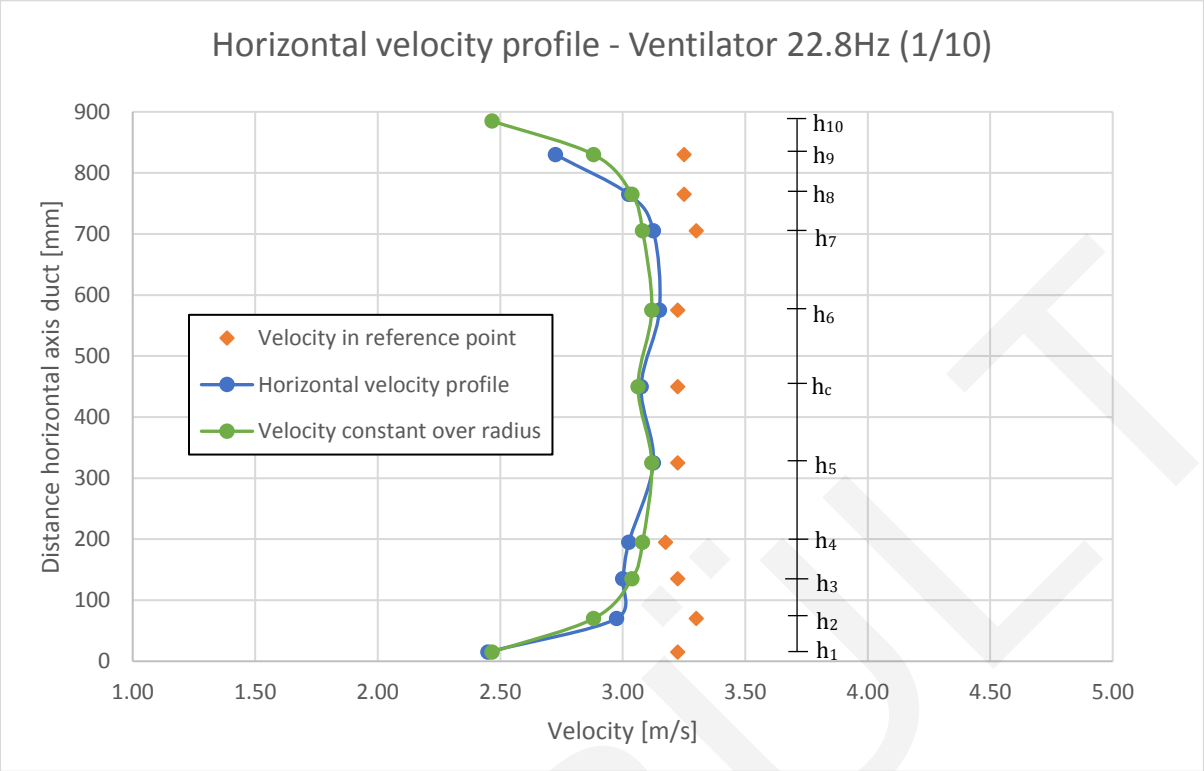

Figure 8 - Horizontal velocity profile with ventilator at 22.8Hz (1/10)

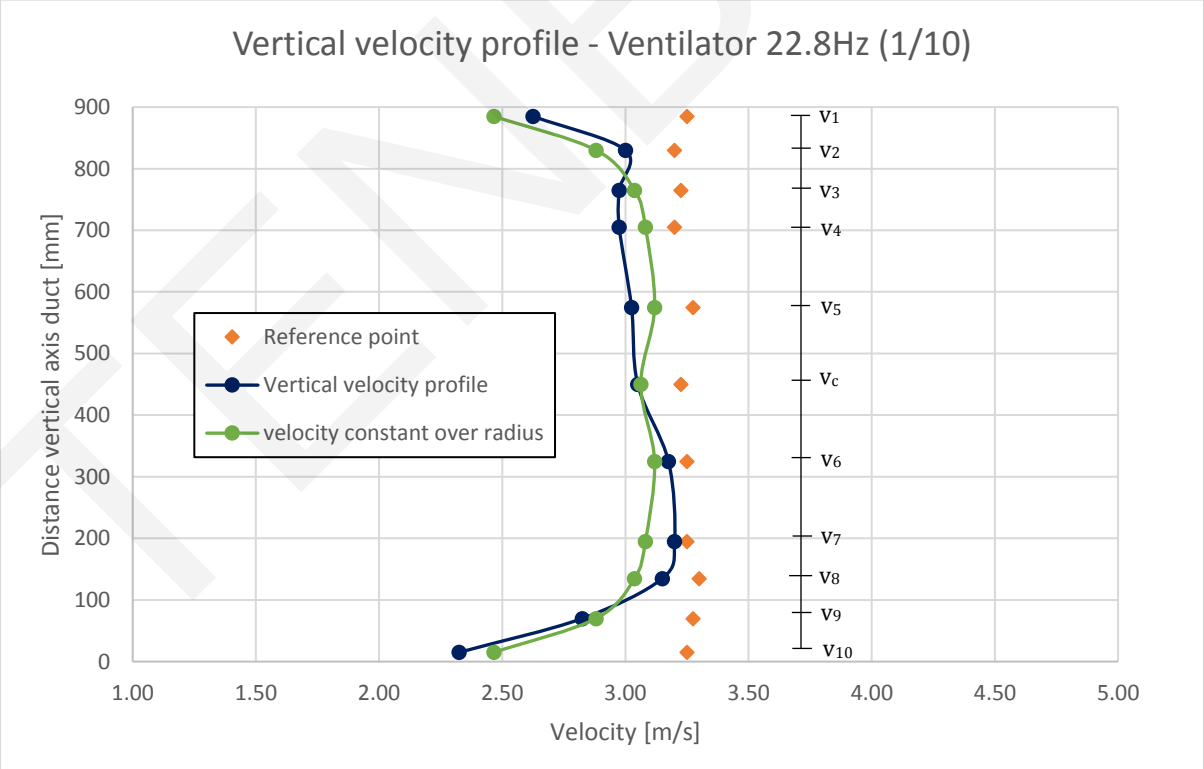

Figure 7 - Vertical velocity profile with ventilator at 22.8Hz (1/10)

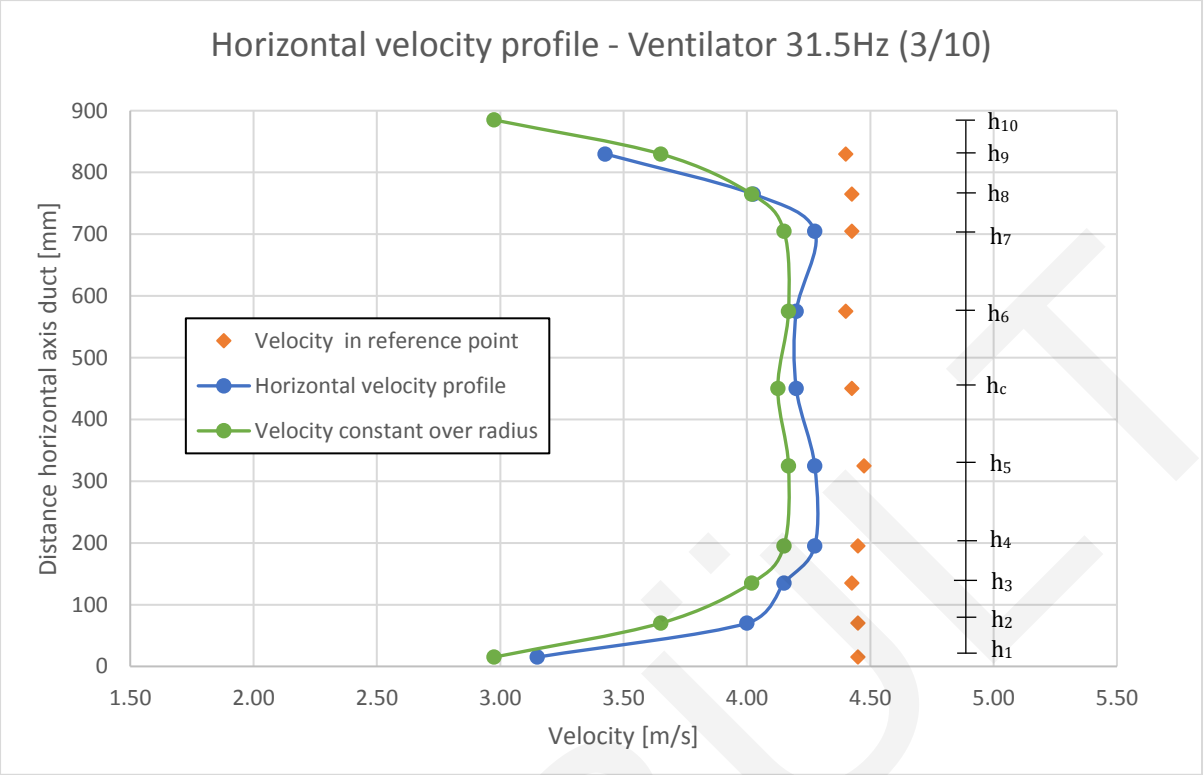

Figure 10 - Horizontal velocity profile with ventilator at 31.5Hz (3/10)

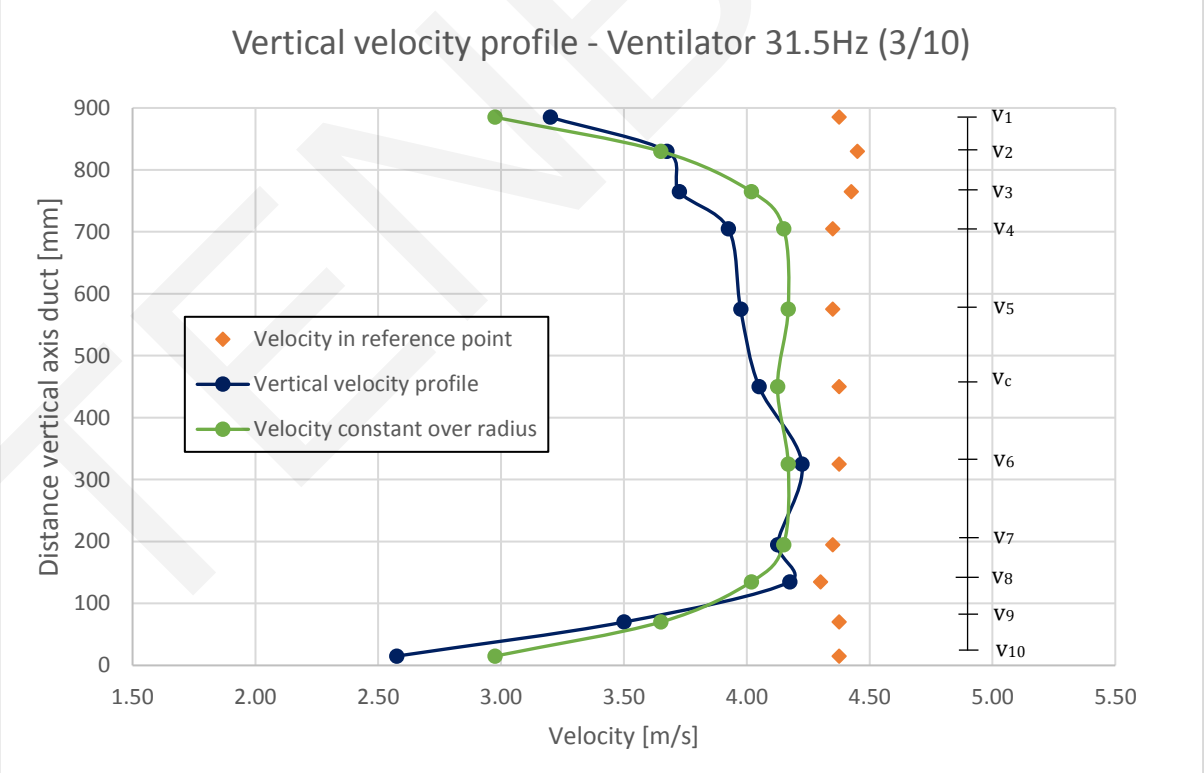

Figure 9 - Vertical velocity profile with ventilator at 31.5Hz (3/10)

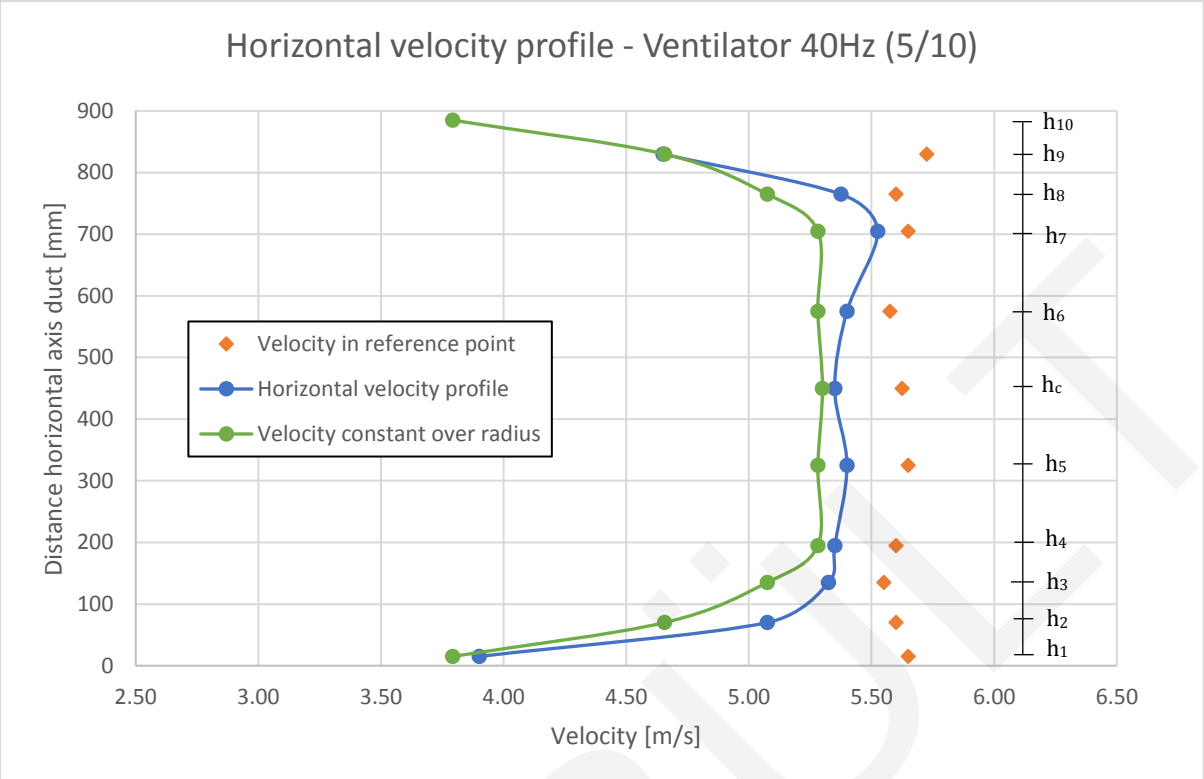

Figure 12 - Horizontal velocity profile with ventilator at 40Hz (5/10)

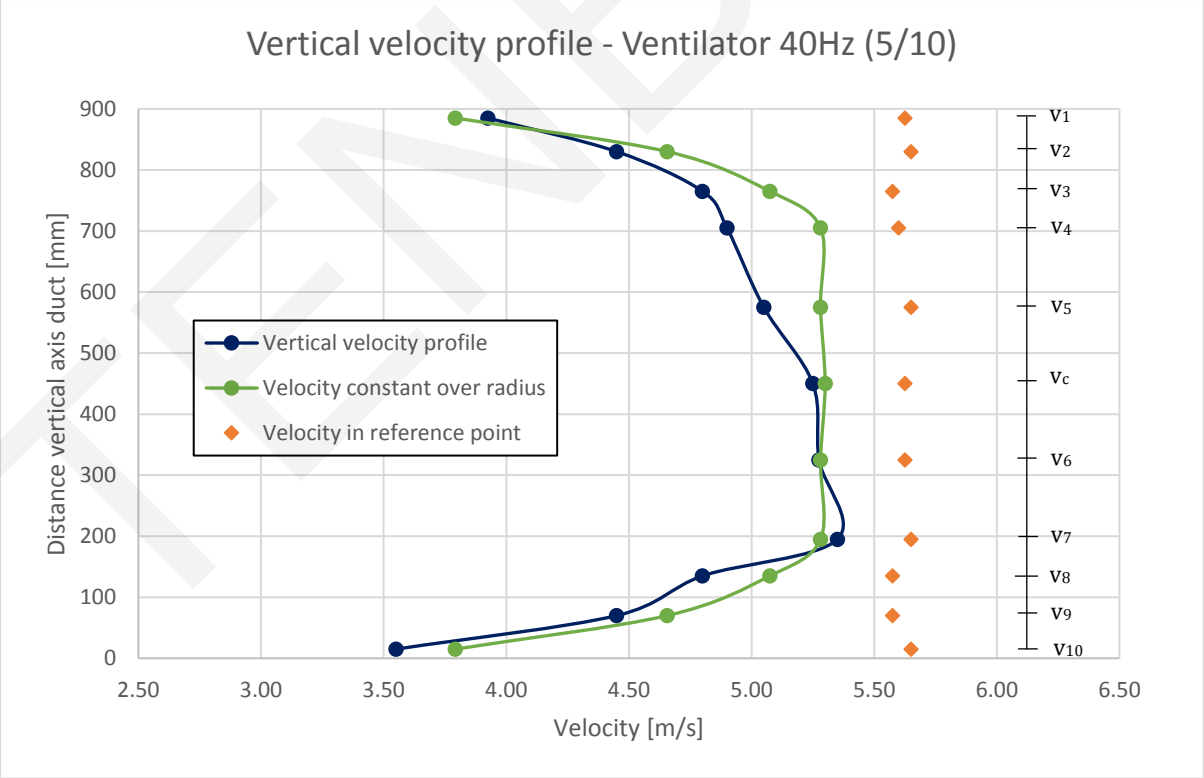

Figure 11 - Vertical velocity profile with ventilator at 40Hz (5/10)

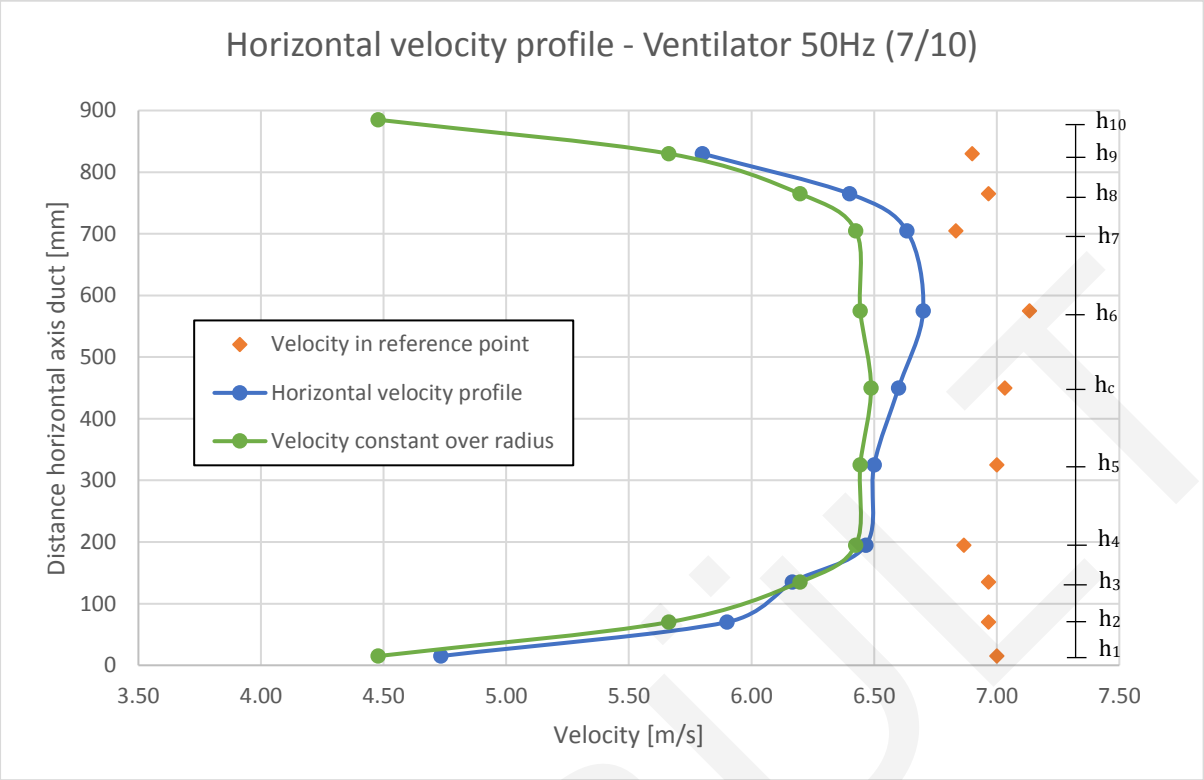

Figure 13 - Horizontal velocity profile with ventilator at 50Hz (7/10)

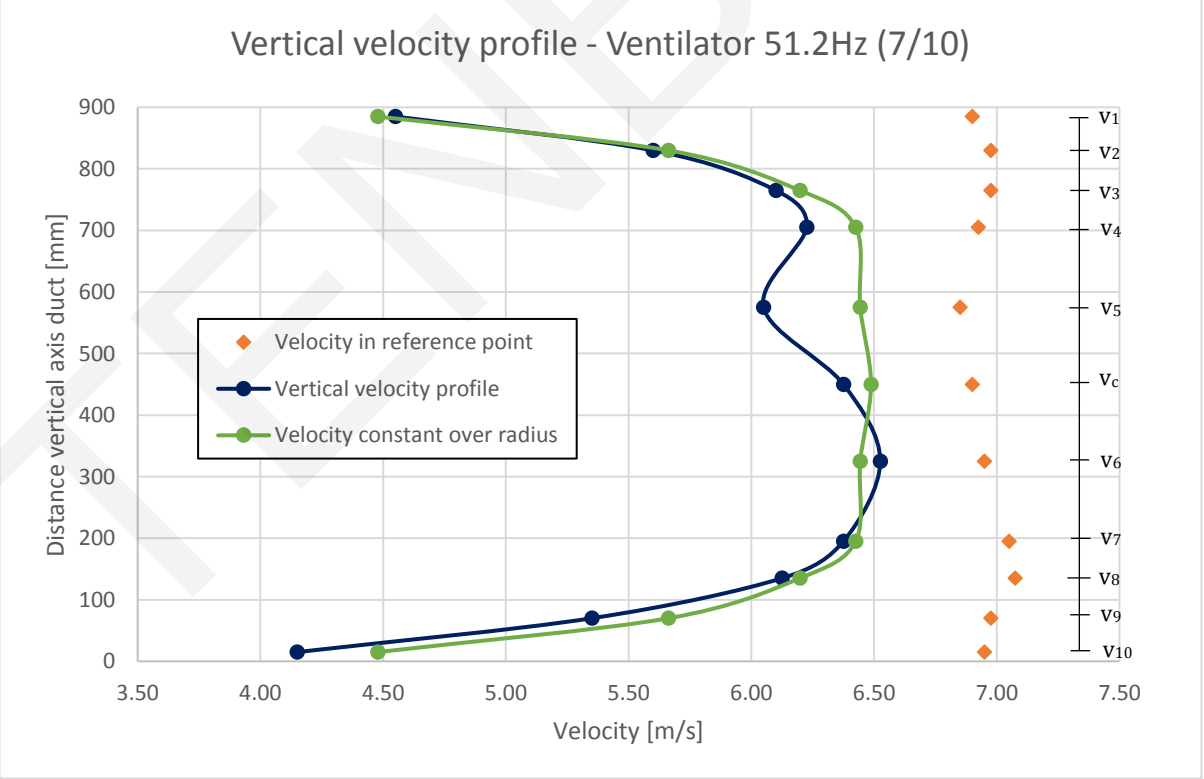

Figure 14 - Vertical velocity profile with ventilator at 50Hz (7/10)

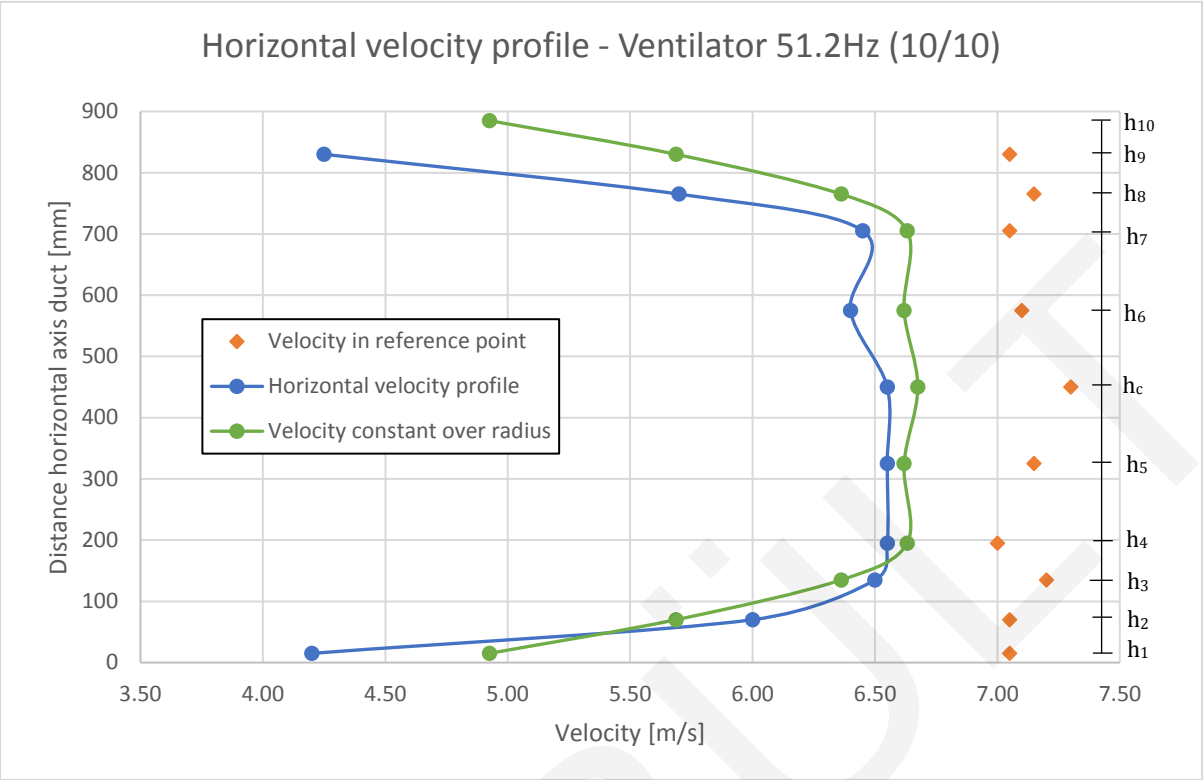

Figure 16 - Horizontal velocity profile with ventilator at 51.2Hz (10/10)

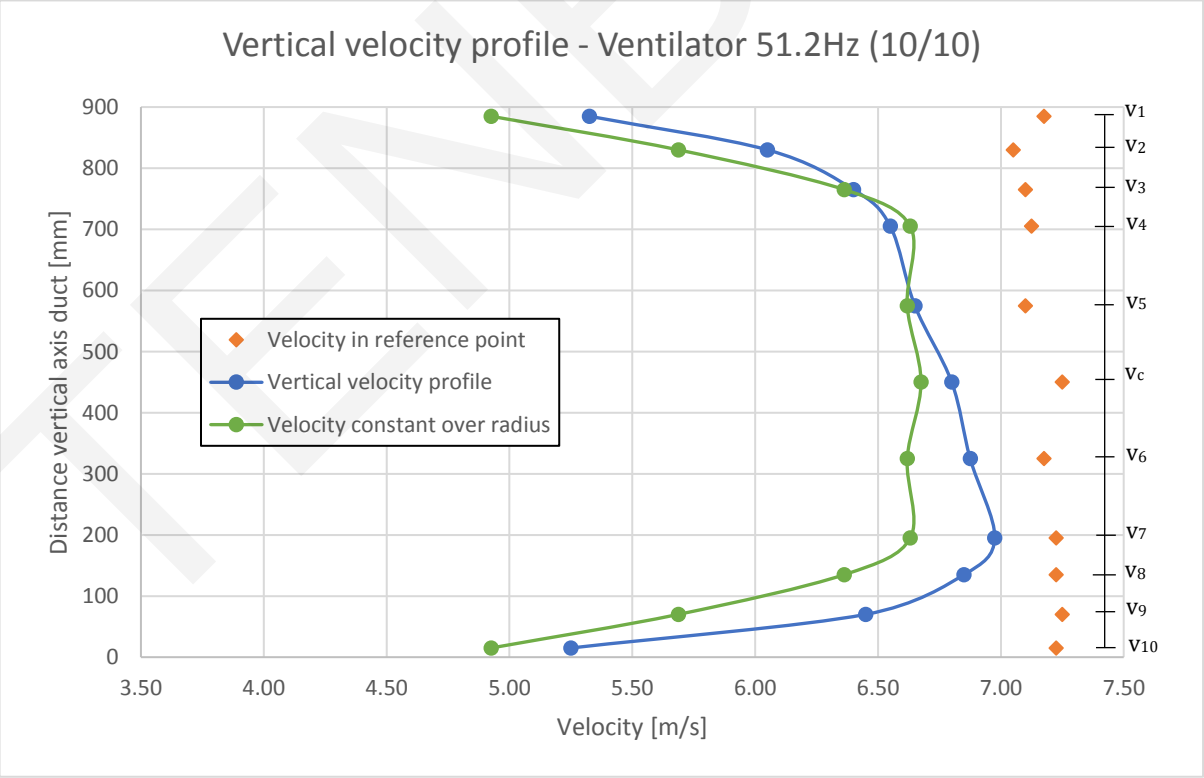

Figure 15 - Vertical velocity profile with ventilator at 51.2Hz

5.5 Discussion

The higher velocity in the reference point can be explained by the additional branch of the SBI-room that is connected to the main duct between the reference point and the measurement plane. The valve of this branch cannot be closed so a small amount of air is extracted through the 450mm duct of the SBI-set-up which result in a higher volume flow in the reference point.

The average velocity on a radius (v_N) can be obtained by adding the horizontal and vertical values and dividing by the number of measurements. By dividing v_N through the average center velocity (v_C) a dimensionless number is obtained which can be used to compare the velocity profile for the different ventilator frequencies. The dimensionless velocity factor is shown in Figure 17 for the measured ventilation modes.

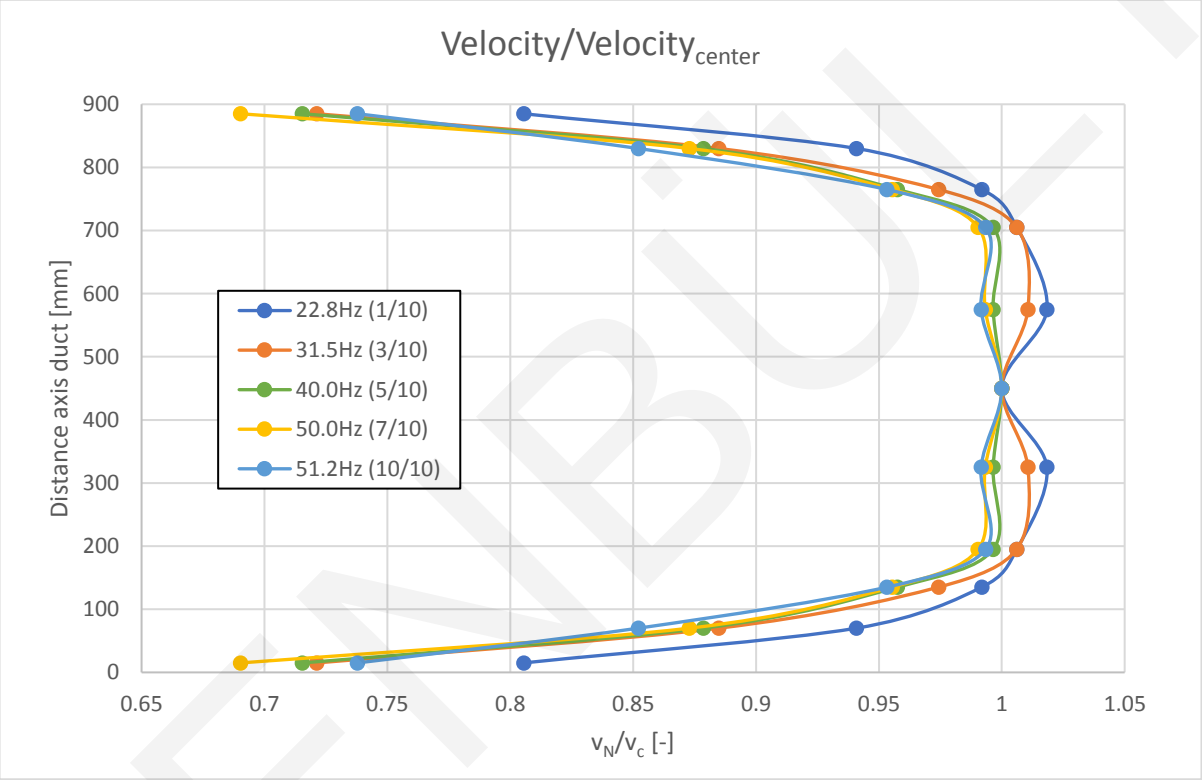

Figure 17 - Dimensionless velocity factor related to the center velocity

The k-factor as given in Table 3 is the average of all v_N/v_C values and can be used to calculate the average velocity in the exhaust duct. The velocity profiles for the highest three frequencies show many similarities. The two lowest frequencies show velocity factors larger than 1 which means the center velocity is not the maximum velocity in the exhaust duct.

Bi-directional probe

After the measurements with the pitot tube the bi-directional probe was installed back in the center of the exhaust duct. The tubes of the bi-directional probe were connected to the manometer that is permanently installed and can be connected to a logger (PC). Subsequently, measurements were performed for the different ventilator frequencies over a period of approximate two minutes per frequency. The resulting velocity of these measurements is shown in Figure 18. The dotted lines represent the average velocity

over time for the corresponding ventilator frequency. With the bi-directional probe, only the center velocity is measured. The velocity is corrected for the probe constant (k_p) of the bi-directional probe which is 1.08 according to its manufacturer. The probe constant of the pitot tube is 1.00, so no correction is required.

Table 4 the standard deviation of the center velocity is determined for the different ventilator frequencies along with its 95% confidence range (μ±2σ). In the last column of

Table 4 the bi-directional probe measurements are compared with the pitot tube measurements for the center position. For the frequencies 31.5Hz and 40.0Hz both velocities show similarity. For the other frequencies, the difference between both methods is larger. These differences in center velocity are also shown in Figure 19. In Figure 19 the velocity in the reference point is also shown since this is a fixed point just as the bi-directional probe that is not influenced by small movements. Also, there is a larger amount of data available in the reference point which result in a better representation of the average velocity.

In Figure 19 it can be seen that the slope of the regression lines is almost equal for the bi-directional probe and the reference point. This indicates that measurements with the bi-directional probe are accurate with an increase of the ventilator's frequency. The higher velocity in the reference point is caused by the additional air volume flow through the SBI-set-up.

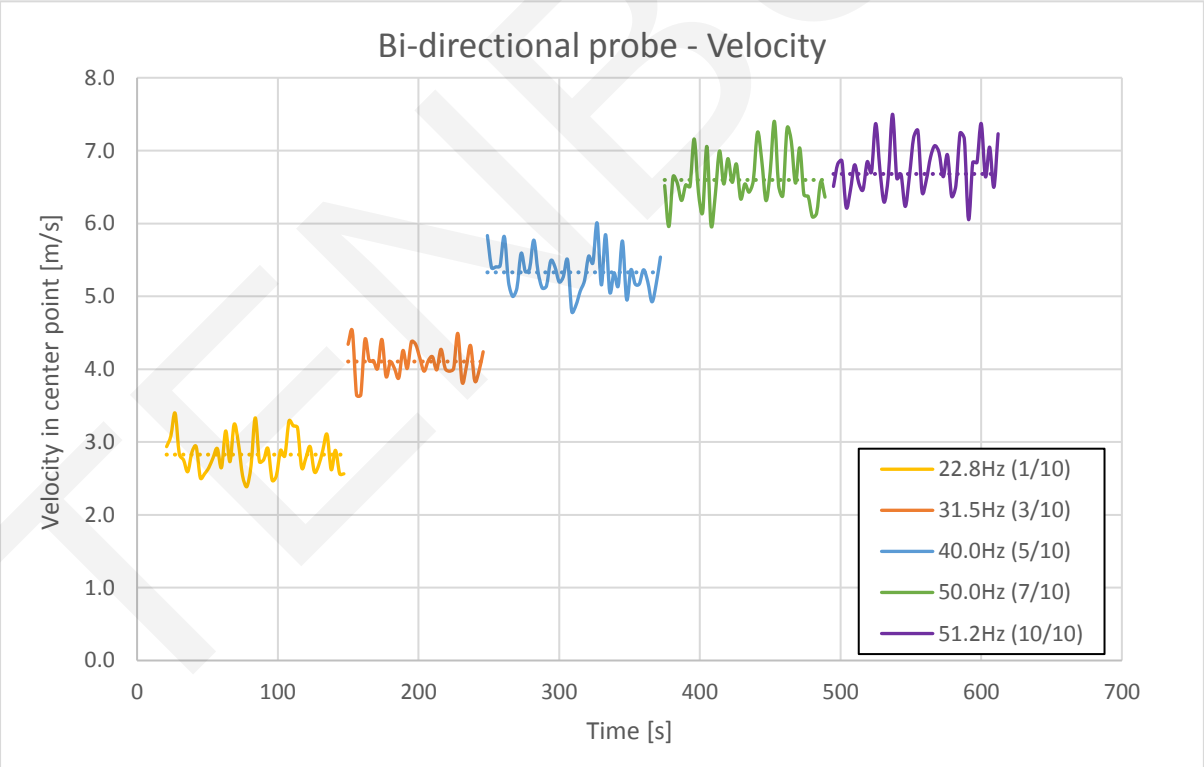

Figure 18 - Center velocity measured with bi-directional probe for different frequencies

Table 4 - Results bi-directional probe measurements

Ventilation frequency [Hz]	Average velocity in time [m/s]	Standard deviation [m/s]	95% confidence range [m/s]	Absolute deviation average center velocity with pitot tube measurements [m/s]
22.8 (1/10)	2.83	0.251	2.33 – 3.33	0.24
31.5 (3/10)	4.10	0.220	3.66 – 4.54	0.02
40.0 (5/10)	5.33	0.278	4.77 – 5.89	0.03
50.0 (7/10)	6.60	0.357	5.89 – 7.31	0.11
51.2 (10/10)	6.77	0.344	6.08 – 7.46	0.09

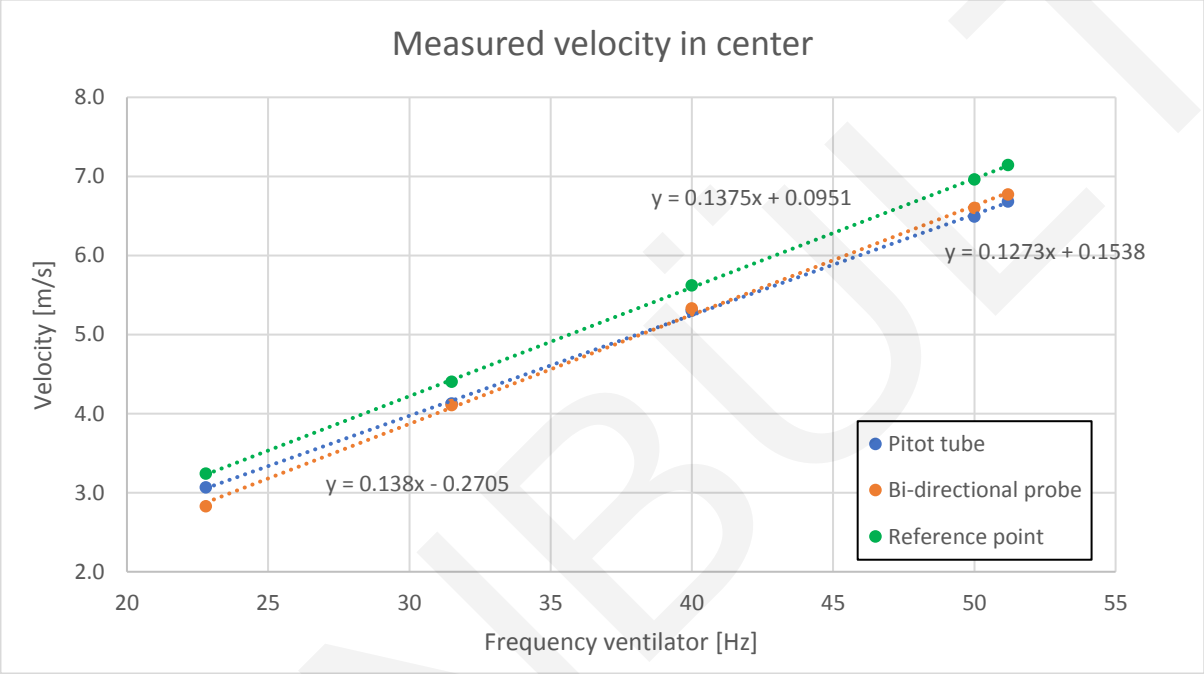

Figure 19 - Center velocity measured with bi-directional probe and pitot tube for multiple frequencies

5.6 Conclusion

By performing measurements with a pitot tube inside the exhaust duct the velocity profile factor was obtained. Different velocity profile factors were found for the different frequencies of the ventilator, which determines the total air flow, given in Table 3. The velocity profile factor is required to determine the volume flow rate which will be used for determination of the heat release rate.

During the measurements, it was observed that the pitot tube is very sensitive for small movement and deviations from the optimal measurement position. This made it more difficult to measure the correct air velocity and to make a statement about the total accuracy of the measurements. Therefore, the results of the measurement must be interpreted with care.

Comparison of the bi-directional probe measurements and pitot tube measurements show great similarity for two of the measured frequencies. For the lowest frequency, the measured center velocity was higher for the pitot tube which is difficult to explain since the bi-directional tube is less sensitive for small deviations in alignment to the flow and

its position is fixed in the center of the duct. For the highest frequencies, the opposite effect occurs and is the velocity measured by the bi-directional probe higher.

Based on only the center velocity the frequencies 31.5Hz and 40Hz result in the most reliable calculation of the velocity with the bi-directional probe and are therefore most suitable for the fire experiments.

5.7 References

[1] B. J. G. Sette, E. Theuns, B. Merci, and P. Vandevelde, "Temperature effects on the mass flow rate in the SBI and similar heat-release rate test equipment," *Fire Mater.*, vol. 31, no. May 2006, pp. 53–66, 2007.

[2] European committee for Standarization, *NEN-EN 13823+A1:2014 Bepaling van het brandgedrag van bouwproducten*. 2014.

[3] R. Van Mierlo and B. Sette, "The Single Burning Item (SBI) test method – a decade of development and plans for the near future," *HERON*, vol. 50, no. 4, pp. 191–207, 2005.

6 Appendix 6 – Bucket test & Sprinkler spray pattern

6.1 Earlier research

A TU/e graduate student, David van Venrooij, performed a number of bucket tests at Peutz in 2016 to study the water distribution of a sprinkler nozzle. The experiments were performed in an open area without obstruction of the smoke cabinet. A pendant sprinkler with a flow coefficient of 80.6L/min√bar and orifice diameter of 11.1mm was used. To include the effect of the sprinkler arms the test was repeated for different azimuth angles as shown in Figure 1, 0° (arms in line with buckets), 45° and 90° (arms perpendicular to buckets). [1]

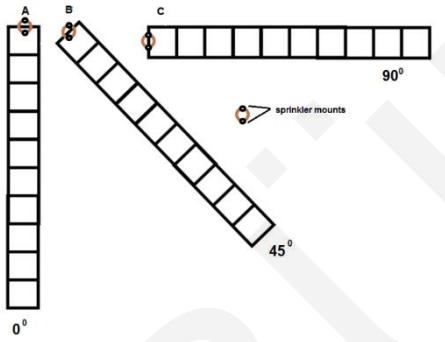

Figure 1 - Set-up bucket test (0°,45° and 90°) [1]

For each angle, three different operating pressures at the sprinkler nozzle were tested, 0.5 bar, 1.0 bar and 1.5 bar. Nine buckets were used to collect the water. The two buckets closest to the sprinkler nozzle were slightly larger with a collecting area of 0.24m² compared to the other buckets with a collecting area of 0.22m². The glass bulb in the sprinkler nozzle was removed to regulate activation of the sprinkler with the pump. For each measurement, the sprinkler nozzle at a height of 3m was activated for three minutes. The collected water was weighted to determine the water distribution over the ground surface. The results (1.0 bar) are shown in Figure 2.

The objective of the experiments was to gain information to reproduce a sprinkler spray pattern that can be used as input data for a CFD-simulation. However, the data that was

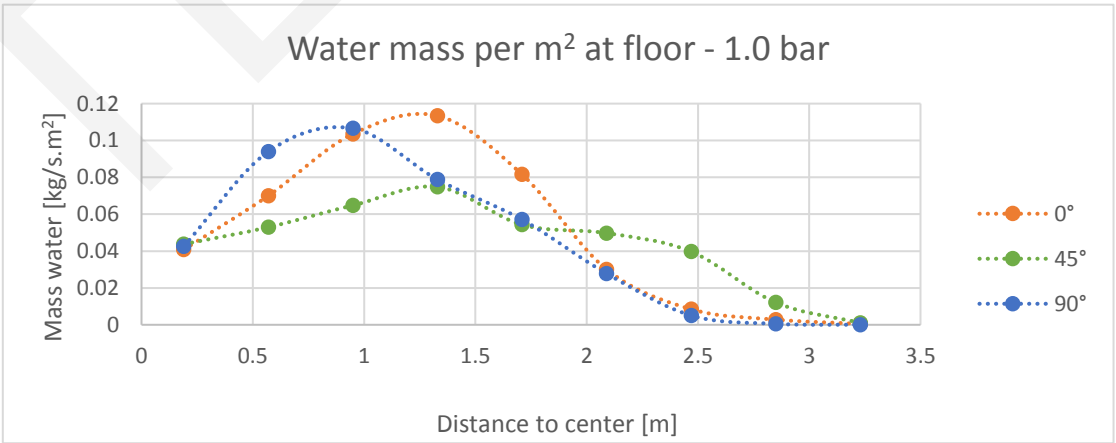

Figure 2 - Water mass distribution, operating pressure 1.0 bar [1]

gained was deficient to reproduce the sprinkler spray pattern. Therefore, a sprinkler spray pattern for a comparable sprinkler nozzle was chosen from another study which included Particle Image Velocimetry (PIV) measurements.

6.2 Measurement set-up

Earlier a series of bucket tests was performed beneath the smoke cabinet. During these tests buckets were placed at azimuth angles of 0°, 45°, 90° and 135°. However, the effect of the sprinkler arms was not very clear from this test. This was partly caused by the relative large interval between azimuth angles and partly due to the cabinet walls. Therefore, a second series of bucket tests was performed in a free field which will be described here. The first series of bucket tests will not be mentioned further.

Buckets with a size of 0.266 x 0.322 x 0.005m were placed in one quadrant of the sprinkler envelope. The buckets were placed at intervals of 15° ranging from -15° to 105° as depicted in Figure 3.

A pendent sprinkler nozzle was used, VK102 (12987AB), with a flow coefficient of 80.6L/min√bar and an orifice diameter of 11.1mm. A photo of this nozzle is shown in Chapter 2. The height of the sprinkler (2.90m) is equal to the height in the smoke cabinet. After sprinkler operation, each bucket is measured individually and the own weight of the bucket is extracted from the measured weight. The sprinkler activation time was 200 seconds (±2seconds). The test was performed for three different operating pressures (at pump), namely 1.7 bar, 3.1 bar and 4.8 bar.

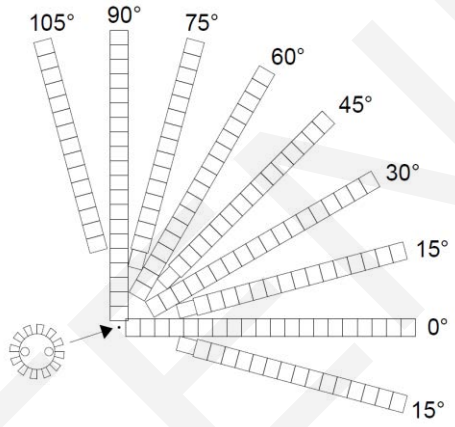

Figure 3 - Bucket placement (schematic)

Figure 4 - Bucket placement (photo)

The obtained data from the measurements is translated into a spray density (lpm/m^2) for the center of each bucket. To generate a contour plot these values are interpolated in a grid with cells of 5 x 5cm. The contour plot of each test is shown at the result pages at the end of this appendix.

6.2.1 Volume flow tests

Although the pressure at the sprinkler nozzle is measured with a manometer the flow rate over a certain time is measured to check the total water volume that needs to be used in the computational model. All water sprayed by the nozzle is collected in a vessel and weighted. The results of these tests are shown in Table 1. With the K-factor, provided by the nozzle manufacturer, the pressure at the nozzle can be calculated.

Table 1 - Setpoint pump and corresponding sprinkler pressure, K-factor = 80.6

Setpoint pump [bar]	**1.7 bar**		**3.1 bar**		**4.8 bar**	
	Test 1	Test 2	Test 1	Test 2	Test 1	Test 2
Water mass [kg]	101.9	101.2	72.2	101.0	93.8	97.1
Time [s]	120	120	60	85	60	63
Pressure [bar]	0.40	0.39	0.80	0.78	1.35	1.32
Flow rate [lpm]	51.0	50.6	72.2	71.3	93.8	92.5
Pressure at nozzle [bar]	**0.40**		**0.79**		**1.34**	

6.3 Modelling droplets in FDS

The bucket tests have been reproduced in NIST's Fire Dynamics Simulator (FDS) to validate such a sprinkler model. FDS requires the operating pressure and K-factor to determine the total water flow rate. The spray envelope and its corresponding water distribution can be modeled in three ways. The first approach, conical, is the simplest one and requires the velocity or orifice diameter and elevation angles as input parameters. The water droplets are distributed evenly between the given elevation angles. For the second approach, elliptical, also the azimuth angles are required as input parameters. The third approach is the most sophisticated method and exists of a spray table that needs to be inserted into the model. In this table, the injection of the water particles can be divided in small parts with individual properties. Every line represents a part of the water spray and contains two elevation angles, two azimuth angles, the mass fraction and velocity. The total mass fraction of all lines need to be ≤1. The elevation angle can differentiate between 0° and 180°, the azimuth angle between 0° and 360° (for all mentioned methods). Besides the injection properties of the water spray, also properties of the water droplets can be modeled. Most important input parameters are the volume median diameter, minimum and maximum diameter and the distribution type. Droplets can be distributed with the following functions: constant, Rosin-Rammler, Lognormal and Rosin-Rammler-Lognormal.

Given the complexity of a spray pattern and the aim to match the FDS model as accurate as possible with the bucket test the third model is most suitable to model the droplet injection along with the Rosin-Rammler-Lognormal size distribution.

6.4 Translate results bucket test into spray pattern table

Since no advanced measurements such as PIV were done the bucket test results need to be translated into a spray pattern table including mass fractions and velocity for multiple azimuth and elevation angles. The empirical equations, explained in Chapter 2, for predicting droplet trajectories and droplet size distribution are used in a mathematical model to calculate the injection angles for the corresponding bucket. The spray pattern table used in the FDS model is generated by translating data of all individual buckets and extrapolating it to the other quadrants of the spray envelope. The mathematical model that is made is given in Appendix 10 – MATLAB Script.

Since some parameters in the model are not undisputed and can be varied, the model cannot be applied directly to each nozzle type. By changing the parameters, a best fit need to be found.

6.4.1 Influence of (volume median) droplet size

The volume median diameter can be determined with equation 2.3.1. In this equation the sprinkler constant, C_{sp}, is an influential parameter which is little known about. The sprinkler constant depends on the geometrical properties of the nozzle and can be different for each nozzle type/model. In the FDS reference guide is mentioned that always a sprinkler constant of 2.33 is used in the underlaying model [2]. This implies that when using the simple methods of droplet modelling the volume median diameter is calculated wrong in FDS for nozzle types with a different sprinkler constant. In literature and from manufacturers little information can be found about the sprinkler constant. In a study by Lawson (1988) was found that the sprinkler constant of a Standard Sprinkler Pendent with an orifice diameter of 11mm is 2.7 [3]. This is the closest sprinkler type to the used sprinkler that can be found. Therefore, a sprinkler constant of 2.7 is used in the mathematical model.

In Figure 5 it can be seen what effect the droplet diameter has on the horizontal distance that is covered by the droplet. Small droplets with a lower mass are more affected by air friction and the horizontal velocity will slow down more rapidly resulting in a smaller horizontal distance.

In the mathematical model only the trajectories of droplets with the volume median diameter are calculated. By varying the droplet size distribution the effects of 'smaller' and 'larger' droplets can be accounted for. The applied volume diameter is always as calculated with empirical equations 2.3.1 and 2.3.2.

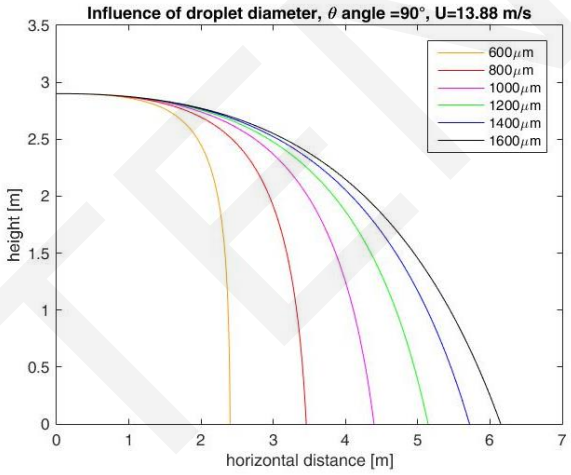

Figure 5 - Horizontal distance for different droplet sizes

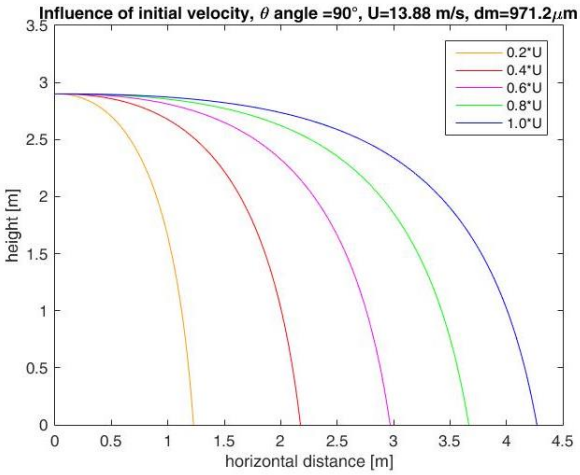

Figure 6 – Hor. distance for different injection velocities

6.4.2 Influence of initial velocity

The initial velocity is the velocity at which the droplets are injected in the model. By default it is assumed in the mathematical model that the initial velocity is equal to the velocity of water flowing out of the orifice. As can be seen in Figure 6 the higher the initial velocity the further the droplets will travel for an elevation angle of 90°. When it is observed in the FDS results that droplets are traveling to far the initial velocity can be

reduced to limit the horizontal distance. When this reduction is applied the velocity of water is reduced by the interaction with the deflector of the sprinkler nozzle.

6.4.3 Influence of size distribution

In the mathematical model the size distribution is not considered since only the trajectories for the volume median diameter are calculated. However, in FDS the spray pattern can be further fine-tuned by changing the empirical constants σ and γ in equation 2.3.3 and 2.3.4. To obtain a smooth transition between the two formula a mutual relation of σ =1.15/ γ is applied. The effects of changing σ and γ are shown in the result pages at the end of this appendix.

For example, when σ is increased there will be more 'larger' droplets that will travel a little further in horizontal direction.

6.4.4 Limitation of the model

The most important limitation of the mathematical model is the fitting of the buckets to elevation angles. When droplets are redirected by the deflector into an upward direction (elevation angle >>90°) there is a turning point in the maximum horizontal velocity. Meaning that some droplets with an elevation angle much larger than 90° will travel less far than droplets injected at a smaller elevation angle. The model links elevation angles to bucket edges. Since no distinction can be made in 'direct' and 'indirect' water during the bucket test 'indirect' water is left out of the model, Figure 7. When a sprinkler nozzle reflects much water in an upward direction the model is less accurate and needs more fitting.

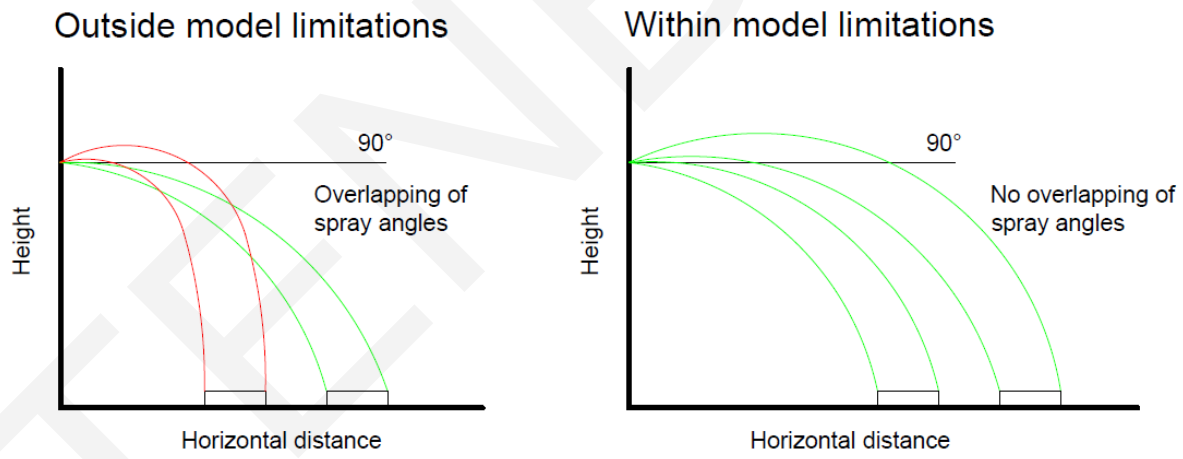

Figure 7 - Model limitations

6.4.5 Best fit

The spray pattern table generated by the mathematical model is implemented in a FDS model. Thereafter, the results of the water distribution at the ground surface in the FDS model and bucket test are compared. For sprinkler pressures of 0.40 and 0.79 bar the empirical equations and commonly used constants were found to be best fit. Changing the parameters did not result in better agreement with the bucket test results. Since no additional fitting had to be done the parameters are called 'default' in Table 2. For a sprinkler pressure of 1.34 bar the 'default' values result in slightly larger deviations between measurement and FDS model. Initial velocity, σ and γ were changed several

times until the best fit was achieved. Changing the values is based on the influences that are described in paragraph 6.4.2 until 6.5.4. In Table 2 the values of the best fitted models are given. On the next pages, the results of the bucket tests and FDS models are shown.

Table 2 - Parameters 'best fit'

	0.40 bar	**0.79 bar**	**1.34 bar**
d_m [μm]	1318.0 (default)	1050.6 (default)	881.0 (default)
U_0 [m/s]	8.78 (default)	12.34 (default)	14.46 (fitted)
σ [-]	2.4 (default)	2.4 (default)	3.0 (fitted)
γ [-]	0.48 (default)	0.48(default)	0.38(fitted)

6.4.6 References

[1] D. van Venrooij, "Validation of Fire Dynamics Simulation with sprinkler sprays," 2016.

[2] K. Mcgrattan, S. Hostikka, R. Mcdermott, J. Floyd, C. Weinschenk, and K. Overholt, *Fire Dynamics Simulator Technical Reference Guide Volume 1 : Mathematical Model*. 2017.

[3] J. R. Lawson, W. D. Walton, and D. D. Evans, "Measurement of Droplet Size in Sprinkler Sprays," Gaithersburg, 1988.

BT0.40 - Bucket Test Data

Date experiment: 14-3-2018

Sprinkler duration 201 seconds
Operating pressure (nozzle): 0.40 bar
Setpoint pump: 1.7bar

Nozzle: VK102
(theoretical) Flow rate = 51.0 L/min

Size distribution
σ = 2.4
γ = 1.15/σ = 0.48

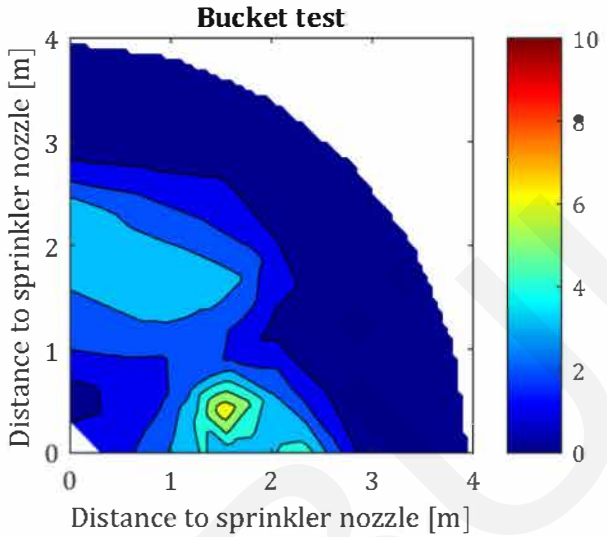

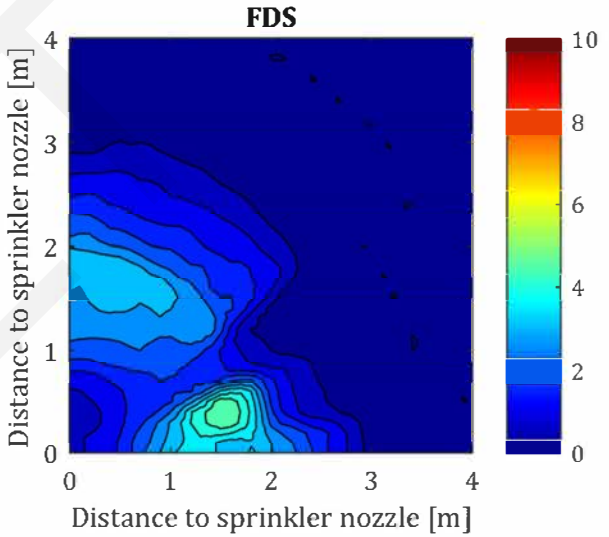

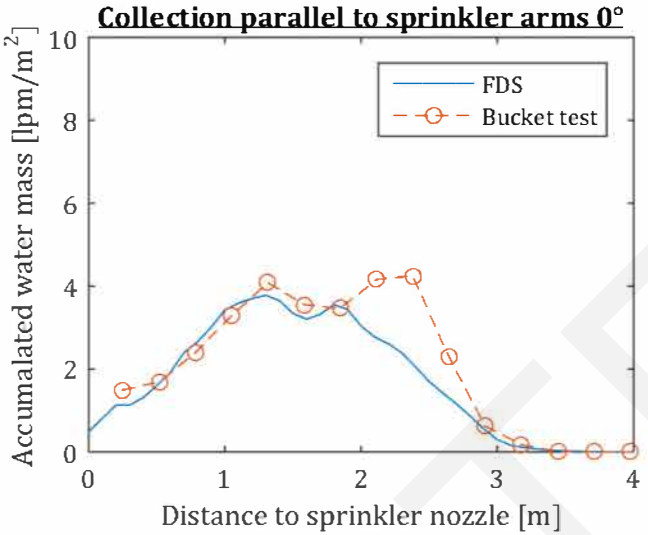

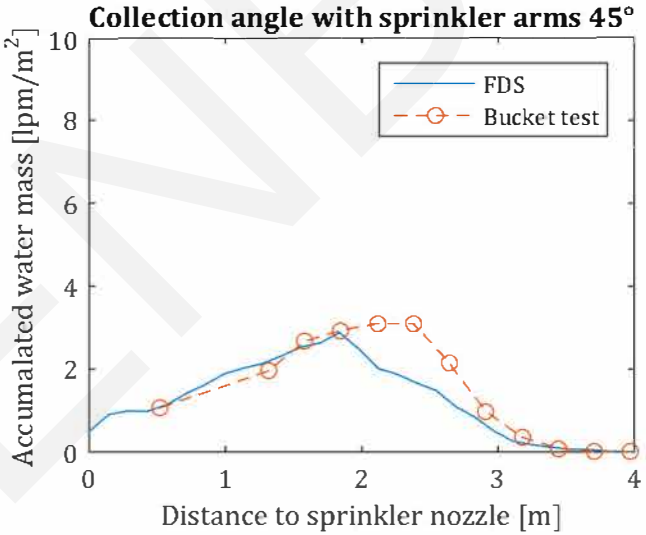

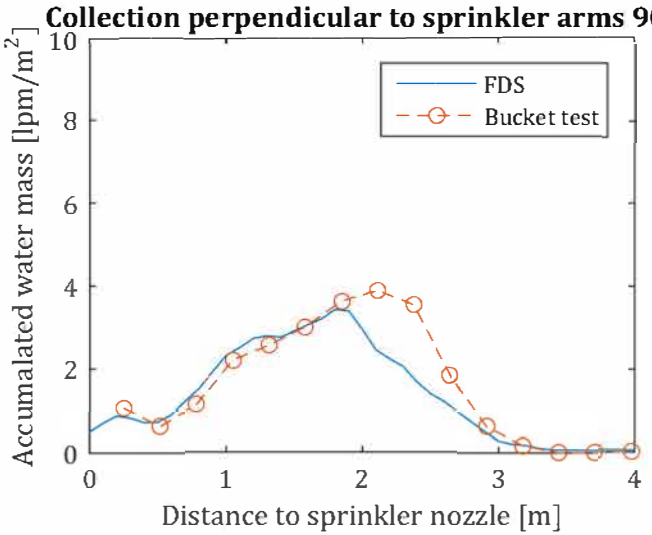

Changing γ and σ for 0.4 bar

Rosin-Rammler Lognormal distribution

$\beta = 0.693$
C = 2.7 (Lawson,1988)

Nozzle: VK102 (SSP)
Orifice diameter = 11.1mm
K-factor = 80.6 lpm/$\sqrt{\text{bar}}$
Flow rate = 50.98 lpm = 0.00085 m^3/s

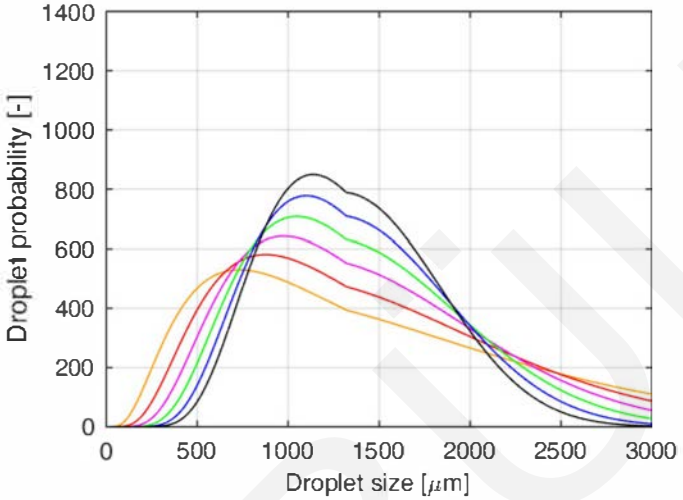

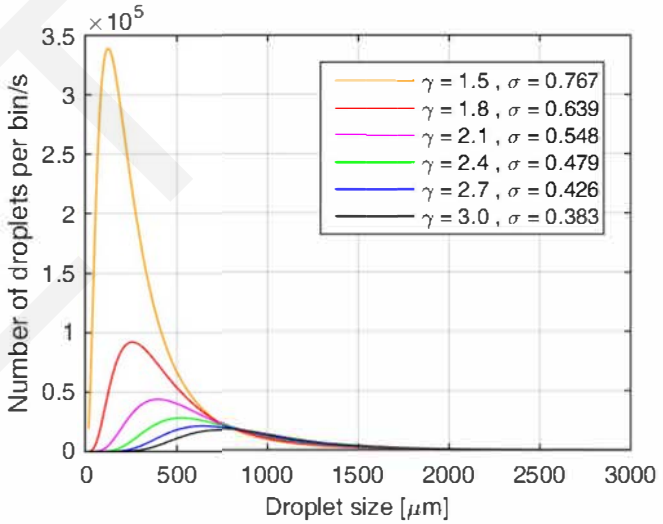

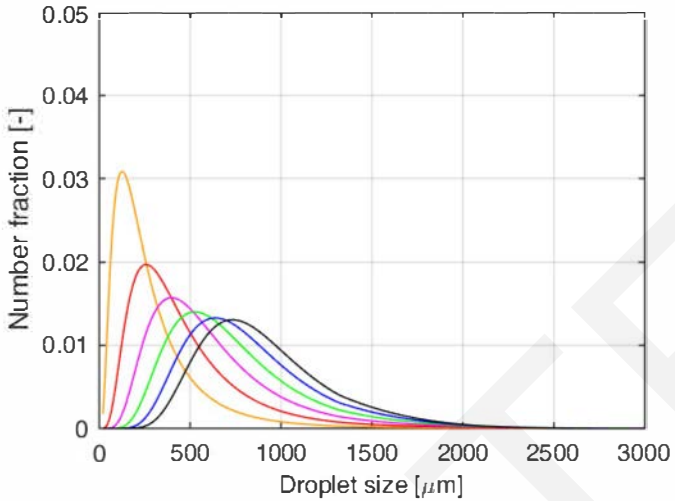

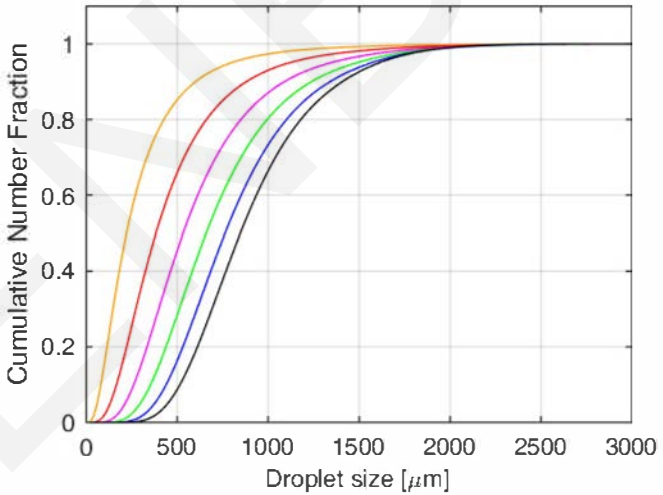

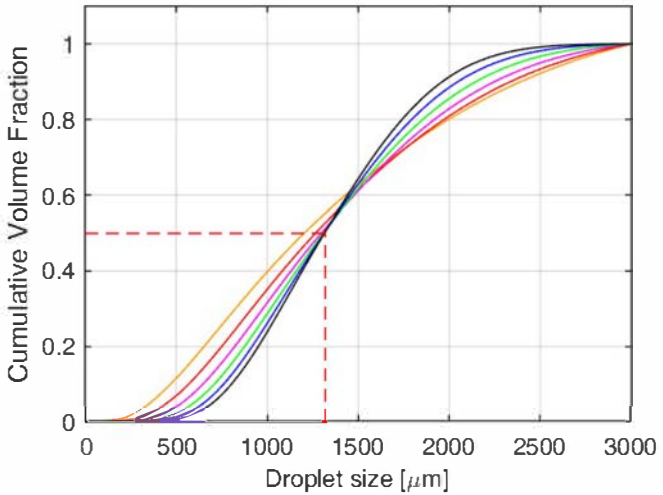

BT0.79 - Bucket Test Data

Date experiment: 16-3-2018

Sprinkler duration 200 seconds
Operating pressure (nozzle): 0.79 bar
Setpoint pump: 3.1bar

Nozzle: VK102
(theoretical) Flow rate = 71.64 L/min

Size distribution
σ = 2.4
$\gamma = 1.15/\sigma$ = 0.48

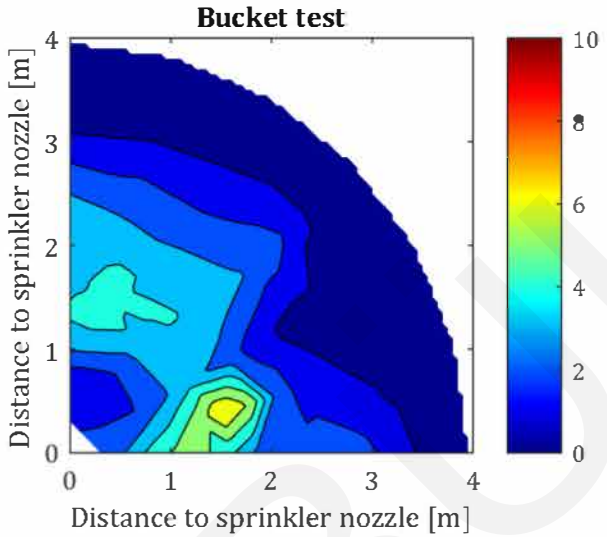

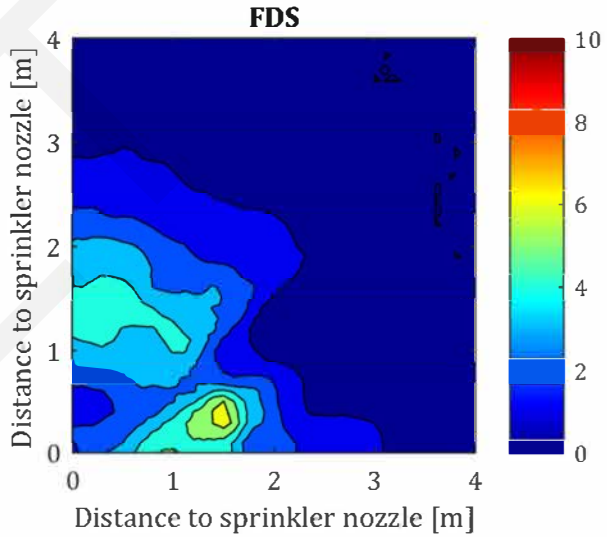

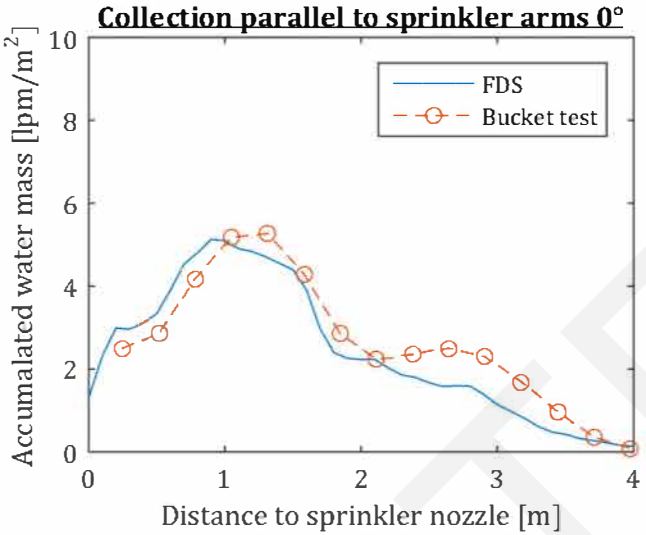

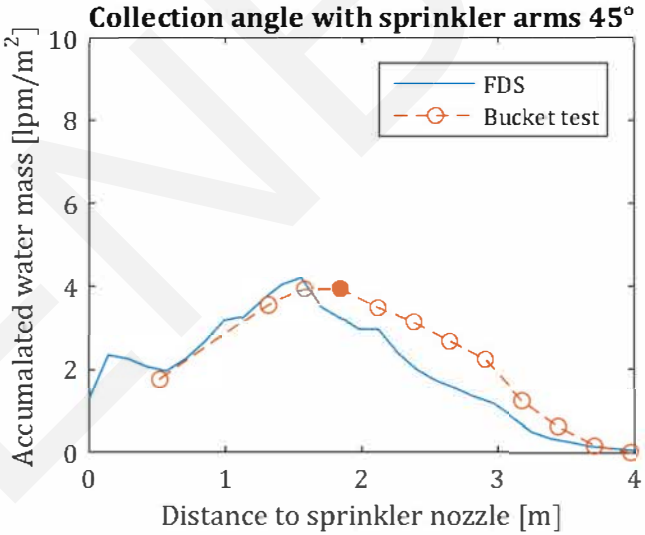

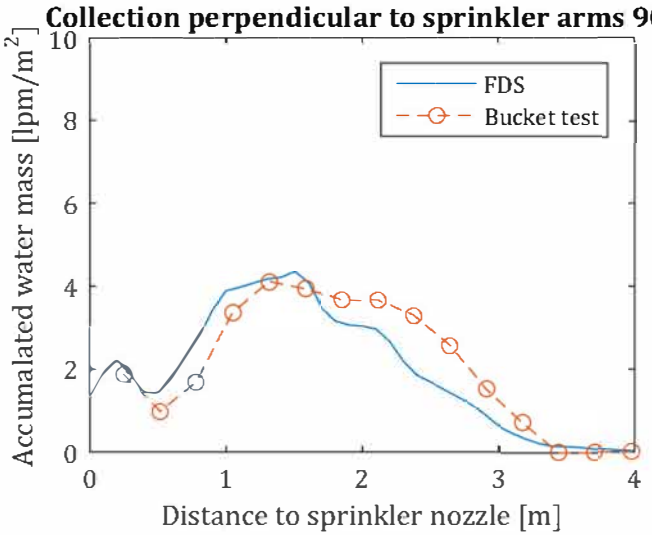

Changing γ and σ for 0.79 bar

Rosin-Rammler Lognormal distribution

$\beta = 0.693$
C = 2.7 (Lawson,1988)

Nozzle: VK102 (SSP)
Orifice diameter = 11.1mm
K-factor = 80.6 lpm/$\sqrt{\text{bar}}$
Flow rate = 71.64 lpm = 0.00120 m^3/s

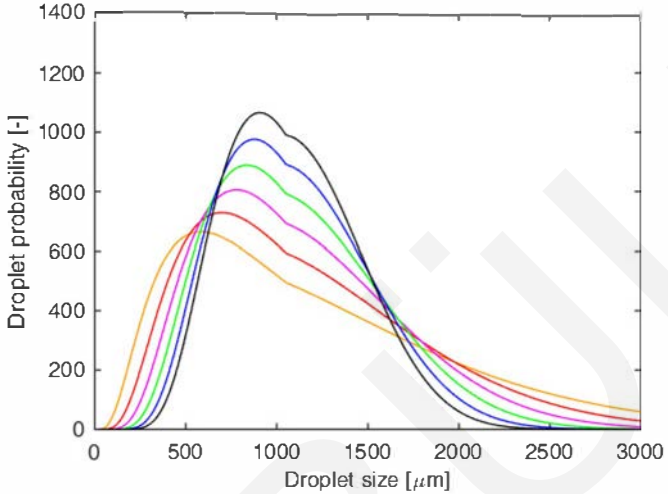

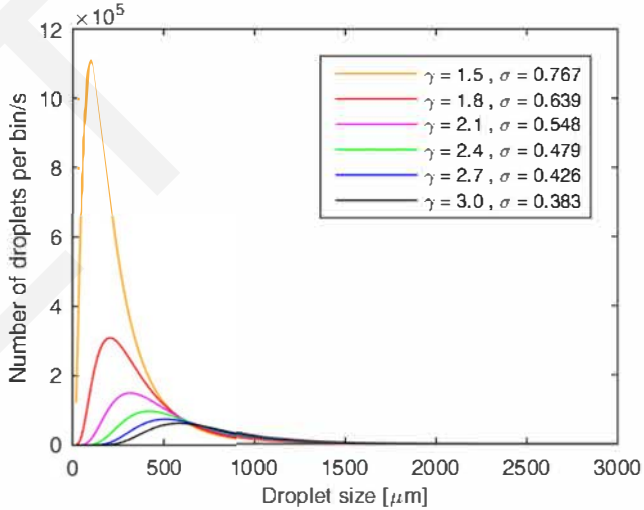

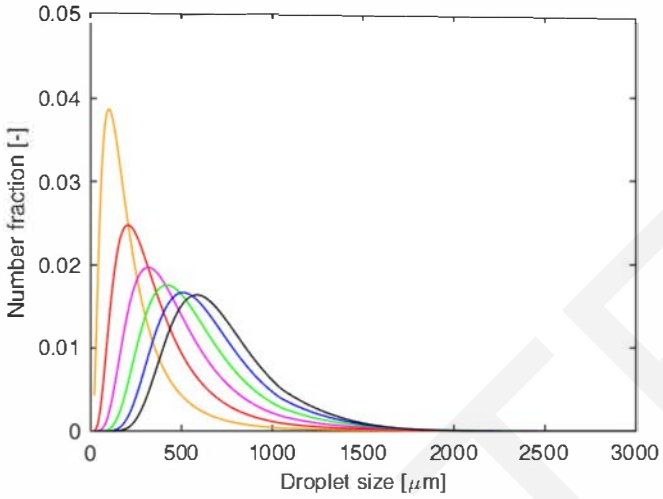

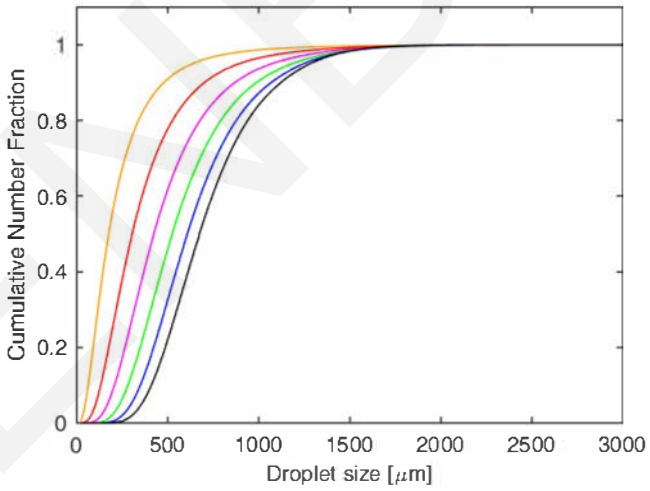

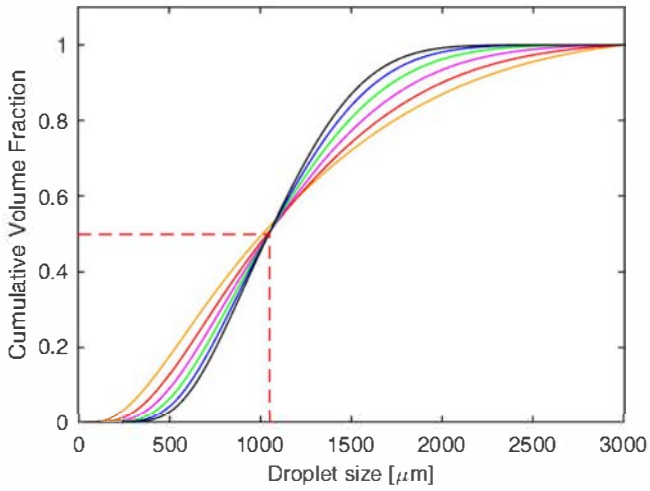

BT1.34 - Bucket Test Data

Date experiment: 16-3-2018

Sprinkler duration 200 seconds
Operating pressure (nozzle): 1.34 bar
Setpoint pump: 4.8bar

Nozzle: VK102
(theoretical) Flow rate = 93.30 L/min

Size distribution
σ = 3.0
γ = 1.15/σ = 0.38

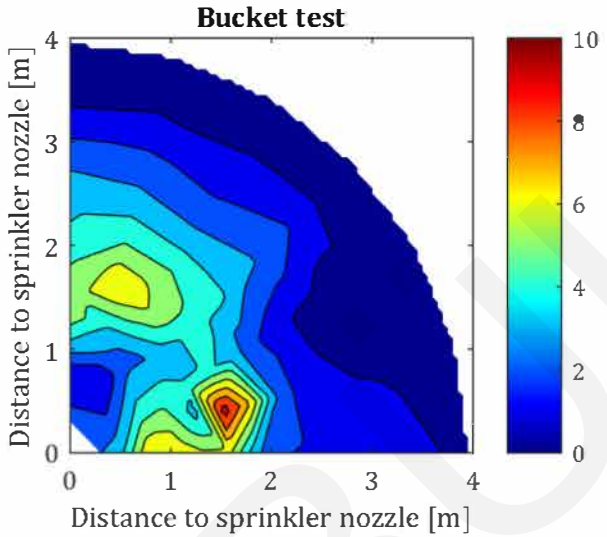

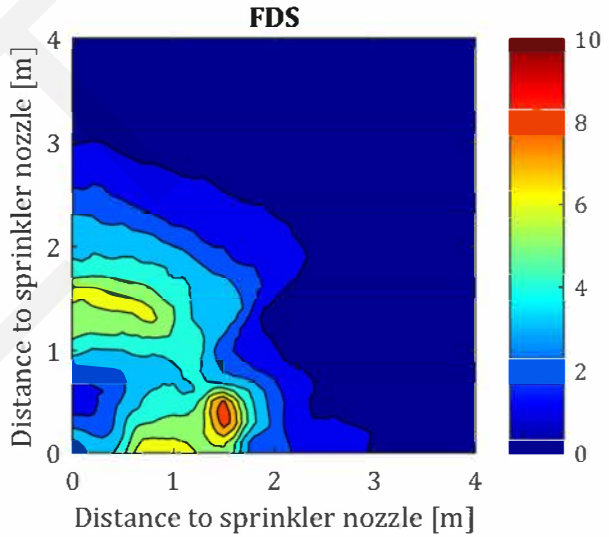

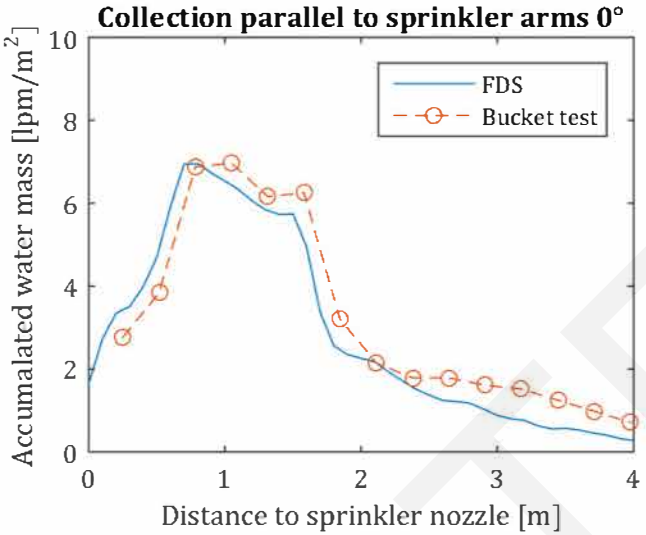

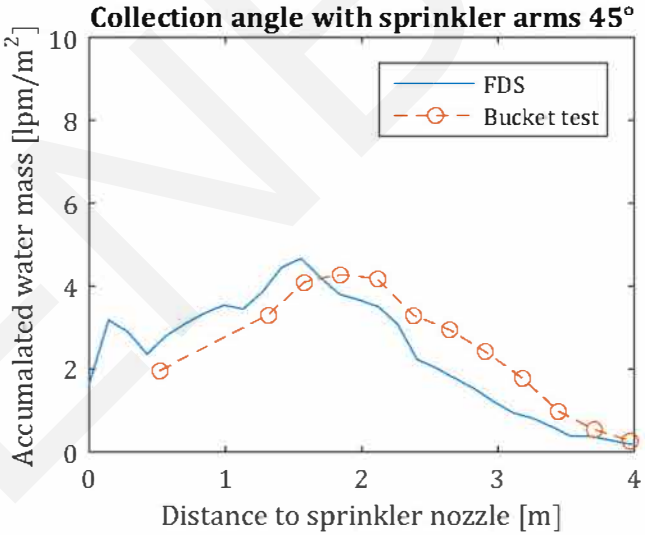

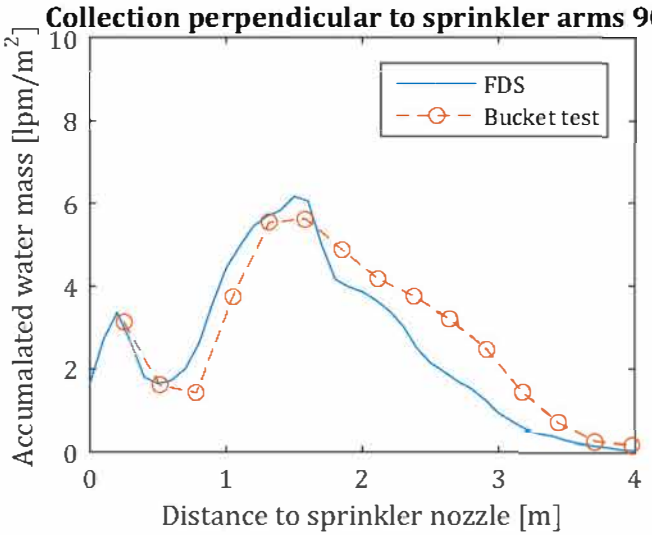

Changing γ and σ for 1.34 bar

Rosin-Rammler Lognormal distribution

$\beta = 0.693$
C = 2.7 (Lawson,1988)

Nozzle: VK102 (SSP)
Orifice diameter = 11.1mm
K-factor = 80.6 lpm/$\sqrt{\text{bar}}$
Flow rate = 93.30 lpm = 0.00155 m^3/s

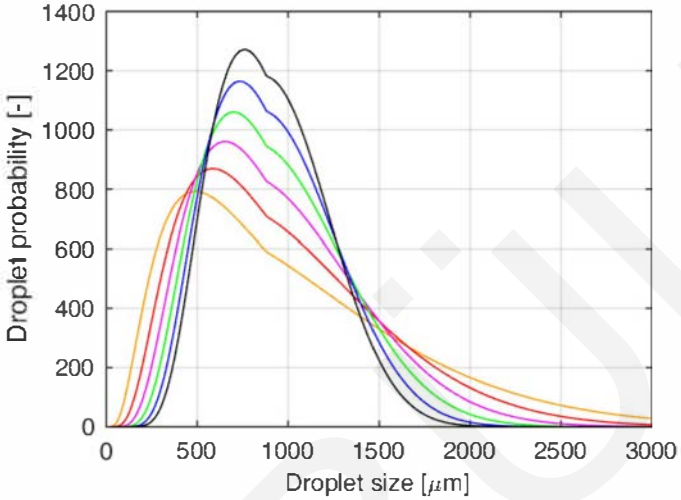

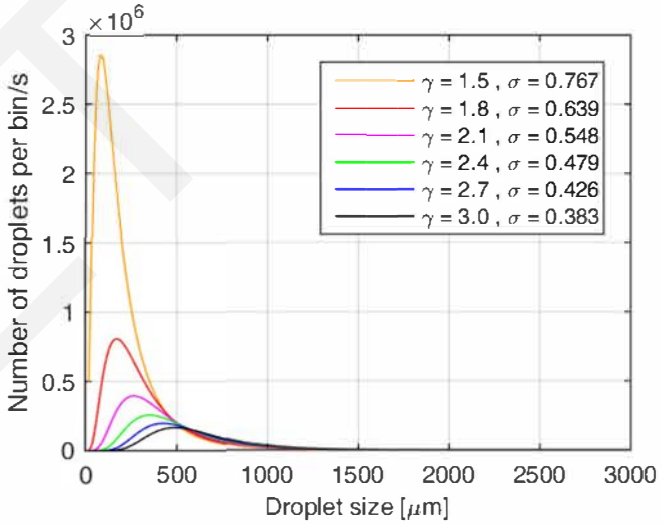

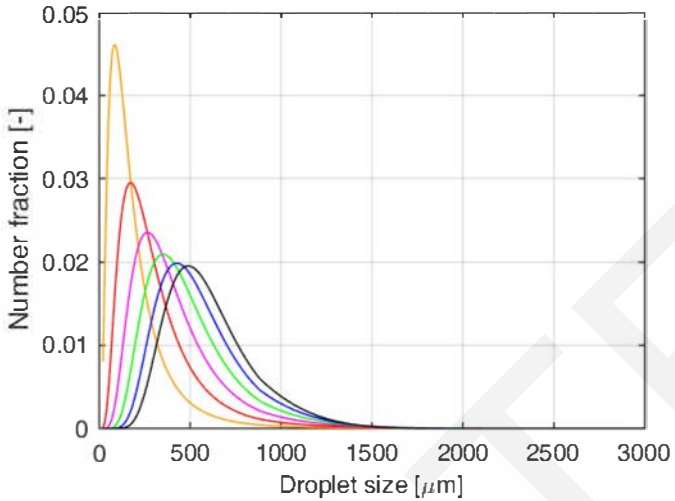

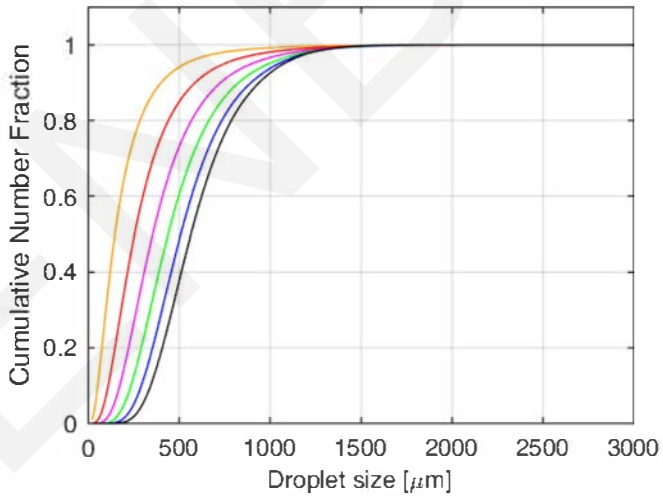

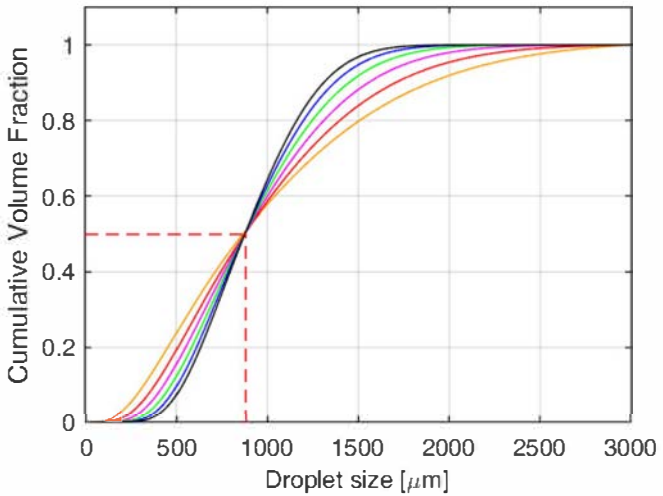

Appendix 7 – Measurement log & Experimental Results

This appendix contains a brief explanation for each fire experiment that has been performed with the measurement set-up. Also, a sheet is added with the measurement results. This sheet contains graphs with the following measured parameters:

- Heat release rate (HRR);
- Total heat release (THR);
- Inlet temperature (gas temperature of smoke that flows into the smoke cabinet, T_{inlet});
- Outlet temperature (gas temperature at outlet of smoke cabinet, T_{duct})
- Average gas temperature smoke cabinet (average of $T_{11\text{-}15}$, $T_{21\text{-}25}$, $T_{31\text{-}35}$ and T_{duct});
- Gas temperature thermocouples T_{31} till T_{35}.

Information such as the fuel weight, fire duration, sprinkler activation times, ambient conditions etc. are given in the added sheets.

7.1 RH0

Scenario: At t=0 a n-heptane pool fire is ignited (0.25m^2). The fuel is poured on a water layer to achieve a steady burning rate. Gas temperatures in the smoke cabinet are measured to determine the average smoke layer temperature. At the measurement section in the exhaust duct four quantities are measured to determine the heat release rate of the pool fire. The measured quantities are temperature, differential pressure, oxygen concentration and carbon dioxide concentration. The sprinkler system is not activated during this measurement. The measurements were continued 5 minutes after ceasing of the fire. The positioning of the thermocouples for this experiment is slightly different from the positions mentioned in the experimental approach. Instead, the same thermocouple positions as de Wilde (2017) were used. Hereby, the highest thermocouple is placed at 2.8m with a spacing of 0.3m.

Measurement objective: The main objective of this first reference experiment is to measure the heat release rate of the fire, since this was not being done properly before. Also, the experiment is used to see when a steady state is reached for the smoke layer and what its properties are. This data will be used to validate the FDS model without sprinkler.

Configuration exhaust: The frequency controller is set to 1/10 (22.8Hz) which corresponds to an average volumetric flow rate (V_{298}) of 1.68 m^3/s.

Observations: It was observed that no smoke layer was buffered in the smoke cabinet. The smoke and hot gases flow directly towards the exhaust once the smoke is spilled into the smoke cabinet. In the thermocouple results can be seen that only higher temperatures are measured for thermocouples that are in the air stream and a few thermocouples at the top of the threes.

7.2 RH1

Scenario: Reproduction of the firs experiment, RH0. For this experiment the burning time was shorter, because no more fuel was available.

Measurement objective: Reproduction of the first experiment, RH0.

Configuration exhaust: The frequency controller is set to 1/10 (22.8Hz) which corresponds to an average volumetric flow rate (V_{298}) of 1.62 m^3/s.

Observations: The same observations were made as for experiment RH0. No stable smoke layer was formed within the smoke cabinet. Observation of the spill plume showed that the hot gases flow directly towards the smoke outlet where hot gases are extracted by the mechanical fan. This indicates that too much gases are extracted from the smoke cabinet.

7.3 RHT0

Scenario: At t=0 a heptane-toluene pool fire is ignited (0.25m^2). The fuel is poured on a water layer to achieve a steady burning rate. In addition to RH0 and RH1 thermocouples are added near the walls of the smoke cabinet. Furthermore, a thermocouple is added at the smoke inlet to measure the gas temperature of the smoke that flows into the smoke cabinet. The other thermocouples were moved up and are located at the positions as mentioned in the experimental approach. Determination of the heat release rate is similar to RH0 and RH1.

Measurement objective: The main objective of this experiment is to measure the heat release rate and to find an exhaust system configuration which results in a stable smoke layer.

Configuration exhaust: The frequency controller is set to 0/10 (18.0Hz) which corresponds to an average volumetric flow rate (V_{298}) of 1.36 m^3/s. During the measurement was observed that the smoke layer was not descending far enough, so an additional valve was opened 45° (half open) to reduce the volume flow at the extraction point. Through the open valve extra 'fresh' air is admixed in the main exhaust duct. Due to smaller pressure losses in this section of the exhaust duct the total volume flow increased slightly. Because of the exhaust reduction in the smoke cabinet the smoke layer descended, but not the entire hood was filled.

Observations: Combustion of the heptane/toluene blend resulted in thick, dark smoke production which forms a clearly visible smoke layer in the smoke cabinet. However, with the current configuration of the exhaust system the hood is not filled with smoke completely.

7.4 RHT1

Scenario: The fire scenario of RHT was reproduced with a different configuration of the exhaust system.

Measurement objective: The main objective of this experiment is to measure the heat release rate of the heptane/toluene pool fire and to find an exhaust system configuration which results in a stable smoke layer.

Configuration exhaust: The frequency controller is set to 0/10 (18.0Hz) and the additional valve is opened 90° (completely open). The total volumetric flow rate (V_{298}) at the measurement section is 1.54 m^3/s.

Observations: During the experiment, the smoke cabinet filled completely with smoke and incidental the hood flooded and pulses of smoke were pushed out of the smoke cabinet.

7.5 RHT2

Scenario: At t=0 a heptane-toluene pool fire is ignited (0.35m^2). The fuel (2.98kg) is poured on a water layer to achieve a steady burning rate. The expected heat release rate is 500kW and expected fire duration is 300 seconds.

Measurement objective: The main objective of this experiment is to measure the heat release rate of the heptane/toluene pool fire and to find an exhaust system configuration which results in a stable smoke layer.

Configuration exhaust: The frequency controller is set to 1.5/10 (24.8Hz) and all air is extracted from the smoke cabinet (additional valves closed). The total volumetric flow rate at the measurement section is 1.95m^3/s as determined with a volume flow measurement.

Observations: During the experiment, the smoke cabinet filled completely with smoke without flooding. The configuration of the exhaust system seems to be appropriate for the applied fire size. The fire duration was with 202 seconds shorter than was expected. The increased burning rate resulted in a higher heat release rate than expected.

7.6 SHT1

Scenario: At t=0 a heptane-toluene pool fire is ignited (0.35m^2). The fuel (4.00kg) is poured on a water layer to achieve a steady burning rate. The expected heat release rate is 500kW and expected fire duration is 400 seconds.

Measurement objective: The main objective of this experiment is to measure the heat release rate of the heptane/toluene pool fire and to measure the smoke layer temperatures before, during and after sprinkler activation. Downward smoke displacement will be visually observed.

Configuration exhaust: The frequency controller is set to 1.5/10 (24.8Hz) at the start of the experiment. The total volumetric flow rate (V_{298}) at the measurement section is 1.95 m^3/s. During the experiment the frequency controller was changed two times. After 90 seconds to 2/10 (26.7Hz) and after 120 seconds to 3/10 (31.0Hz) in order to control the smoke layer.

Observations: During the experiment, the smoke cabinet filled completely with smoke and the hood started to flood after 70 seconds. Therefore, the exhaust flow was increased after 90 seconds and 120 seconds. To cool the smoke layer the sprinkler was activated after 154 seconds with an intended duration of 120 seconds and operating pressure of 0.79 bar. The downward smoke displacement ranged between 0.6 and 0.9 meters. After

221 seconds the fire extinguished with the sprinkler still operating. Therefore, no smoke layer temperatures could be measured after sprinkler activation.

7.7 SH1

Scenario: At t=0 a heptane pool fire is ignited (0.35m^2). The fuel (4.00kg) is poured on a water layer to achieve a steady burning rate. The expected heat release rate is 800kW and expected fire duration is 240 seconds.

Measurement objective: The main objective of this experiment is to measure the heat release rate of the heptane pool fire and to measure the smoke layer temperatures before, during and after sprinkler activation. Downward smoke displacement will be visually observed.

Configuration exhaust: The frequency controller is set to 1.5/10 (24.8Hz) at the start of the experiment. The total volumetric flow rate (V_{298}) at the measurement section is 1.95 m^3/s.

Observations: During the experiment, a stable smoke layer was formed within the smoke cabinet with an interface height of approximate 2.0m. After 96 seconds the sprinkler system is activated with an operating pressure of 0.79 bar at the sprinkler nozzle. The sprinkler was activated for 90 seconds. Especially, at the edges of the spray envelope downward displacement of the smoke was observed. In the center of the envelope almost no downward displacement occurred. Compared to SHT1 the displacement of smoke is much more difficult to determine. After deactivation of the sprinkler the interface height of the smoke layer is lower than before activation. This indicates the fire has still grown during sprinkler operation resulting in a higher smoke production. This is possible because the fire hazard is not directly affected by the sprinkler spray. The heat release rate measurements also indicate that the fire further developed during sprinkler operation.

7.8 SH2

Scenario: At t=0 a heptane pool fire is ignited (0.35m^2). The fuel (4.02kg) is poured on a water layer to achieve a steady burning rate. The fuel tray is placed in another tray of 0.7m x 1.0m filled with water to cool the fuel. Cooling of the fuel is done to reduce evaporation of the fuel resulting in a lower pyrolis rate and a steadier HRR. The expected heat release rate is 750kW and expected fire duration is 275 seconds.

Measurement objective: The main objective of this experiment is to measure the heat release rate of the heptane pool fire and to measure the smoke layer temperatures before, during and after sprinkler activation. Downward smoke displacement will be visually observed.

Configuration exhaust: The frequency controller is set to 1.5/10 (24.8Hz) at the start of the experiment. The total volumetric flow rate (V_{298}) at the measurement section is 1.68 m^3/s at that moment. After 70 seconds the frequency controller is set to 1.0/10 (22.8Hz) to increase the smoke layer thickness.

Observations: During the experiment, a stable smoke layer was formed within the smoke cabinet with an interface height of approximate 2.0m (at the separation between

the steel and calcium silicate plates). After118 seconds the sprinkler system is activated with an operating pressure of 0.40 bar at the sprinkler nozzle. The sprinkler was activated for 105 seconds. At the placed rulers smoke displacement cannot be measured. What can be seen is that the smoke layer descended approximate 30 centimeters within the smoke cabinet (height of the calcium silicate plates). Almost no diffusing of the smoke layer was observed. At the floor less soot particles are observed indicating that less soot particles are 'washed' from the smoke layer.

7.9 SH3

Scenario: At t=0 a heptane pool fire is ignited (0.35m^2). The fuel (4.02kg) is poured on a water layer to achieve a steady burning rate. The expected heat release rate is 750kW and expected fire duration is 275 seconds. It is expected that from all the sprinkler tests this test will result in the largest downward smoke displacement since the flow rate will be larger and thus has in theory more cooling capacity.

Measurement objective: The main objective of this experiment is to measure the heat release rate of the heptane pool fire and to measure the smoke layer temperatures before, during and after sprinkler activation. Downward smoke displacement will be visually observed.

Configuration exhaust: The frequency controller is set to 1.0/10 (22.8Hz) at the start of the experiment. The total volumetric flow rate (V_{298}) at the measurement section is 1.68 m^3/s.

Observations: During the experiment, a stable smoke layer was formed within the smoke cabinet with an interface height of approximate 2.0m. After 120 seconds the sprinkler system is activated with an operating pressure of 1.34 bar at the sprinkler nozzle. The sprinkler was activated for 130 seconds. Also, for this experiment no downward displacement of the entire smoke layer can be observed as during SHT1. In the vicinity of the third thermocouple tree the smoke layer is diffusing until approximate 1.0 to 1.2m below the smoke layer. The smoke is partly pushed down and mixing with air and water droplets. Although some smoke is pushed out of the smoke cabinet by the sprinkler spray the expected displacement did not occur. A possible explanation for this is the increased water pressure which results in a higher injection velocity causing more droplets to bounce to the hood and fall down.

7.10 SH4

Scenario: At t=0 a heptane pool fire is ignited (0.35m^2). The fuel (3.92kg) is poured on a water layer to achieve a steady burning rate. The expected heat release rate is 750kW and expected fire duration is 275 seconds. The operating pressure of the sprinkler is 0.79 bar as within SH1 and SHT1. The activation and deactivation times of the sprinkler are set similar to SH2 and SH3 to be able to compare the results of the different operating pressures.

Measurement objective: The main objective of this experiment is to measure the heat release rate of the heptane pool fire and to measure the smoke layer temperatures before, during and after sprinkler activation. Downward smoke displacement will be visually

observed. This experiment is done to make appropriate comparisons with operating pressures of 0.40 and 1.34 bar.

Configuration exhaust: The frequency controller is set to 1.0/10 (22.8Hz) at the start of the experiment. The total volumetric flow rate (V_{298}) at the measurement section is 1.68 m^3/s.

Observations: During the experiment, a stable smoke layer was formed within the smoke cabinet with an interface height of approximate 1.9m. After 123 seconds the sprinkler system is activated with an operating pressure of 0.79 bar at the sprinkler nozzle. The sprinkler was activated for 100 seconds. During this experiment similar effects as during SH3 were observed regarding smoke diffusing and smoke descendance. The burning period of 250 seconds was a little shorter than the expected 275 seconds. The resulted in shorter heat-up phase after sprinkler deactivation, meaning that the temperatures did not increase till the desired levels.

7.11 SH5

Scenario: At t=0 a heptane pool fire is ignited ($0.35m^2$). The fuel (4.04kg) is poured on a water layer to achieve a steady burning rate. The expected heat release rate is 750kW and expected fire duration is 275 seconds. The activation and deactivation of the sprinkler is set similar to SH2 and SH3 to be able to compare the results of the different operating pressures.

Measurement objective: The main objective of this experiment is to measure the heat release rate of the heptane pool fire and to measure the smoke layer temperatures before, during and after sprinkler activation. Downward smoke displacement will be visually observed. It is assumed that during SH3 the thermocouples in the exhaust outlet were wetted (TC duct), although this is very unlikely given the position of the thermocouple, right above the sprinkler nozzle. Since the data obtained at TC duct is very valuable SH3 is repeated.

Configuration exhaust: The frequency controller is set to 1.0/10 (22.8Hz) at the start of the experiment. The total volumetric flow rate (V_{298}) at the measurement section is 1.68 m^3/s.

Observations: During the experiment, a stable smoke layer was formed within the smoke cabinet with an interface height of approximate 1.7m. Some pulsing flooding of the hood is observed before the sprinkler activates. After 121 seconds the sprinkler system is activated with an operating pressure of 1.34 bar at the sprinkler nozzle. The sprinkler was activated for 100 seconds. Within the entire spray envelope smoke diffusing is observed. In the vicinity of the third thermocouple tree this effect can be seen most obvious. At this location the diffused smoke reaches the ground surface. Also, excessive amounts of smoke are pushed out of the smoke cabinet. The fire ceased almost simultaneously as the sprinkler was deactivated. The burning period was 50 seconds shorter than expected and by this no heat-up after sprinkler deactivation took place.

On the following pages an overview is given of the experimental results.

Name experiment:	Reference n-Heptane 0 (RH0)				
Date:	22-8-2017				
Ambient temperature:	21.2	°C			
Fire duration:	383	s			
Fuel			**Sprinkler**		
Name:	n-heptane (>99.75%)		Sprinkler activated at:		s
Surface:	0.25	m^2	Sprinkler deactivated at:		s
Weight:	2.175	kg	Operating pressure:		bar
Heat of combustion:	44.56	MJ/kg	K-factor:		L/min√bar
Theoretical THR:	96.92	MJ	Water flow rate:	0	L/min
Mass burning rate	5.679	g/s	Measured THR:	97.8	MJ
Theoretical HRR	253.0	kW	Measured avg. HRR:	267.3	kW
			Smoke layer height:	2.2-2.5	m

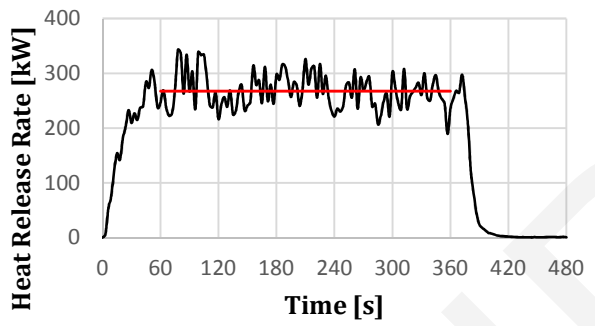

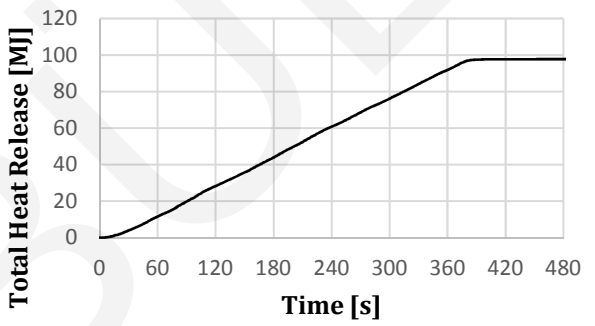

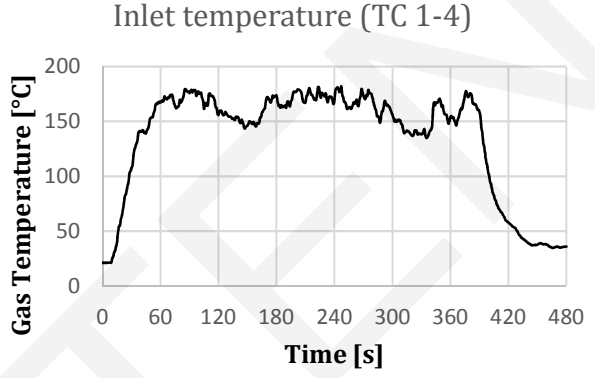

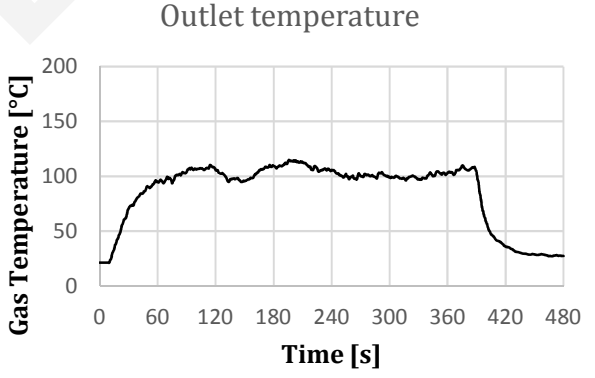

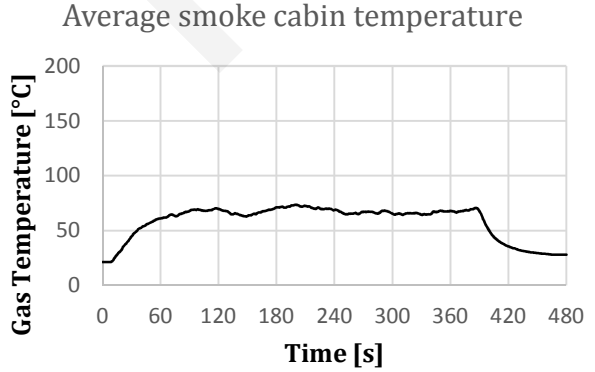

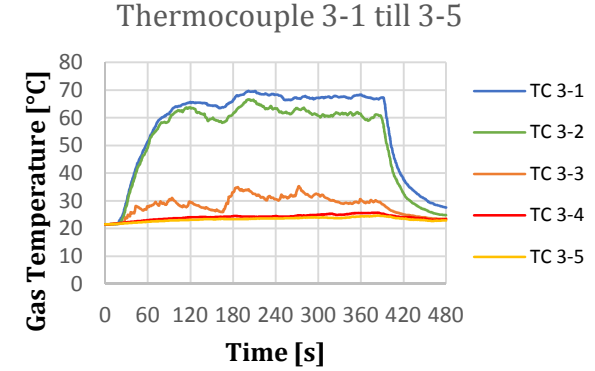

Name experiment:	Reference n-Heptane 0 (RH0)
Date:	22-8-2017
Ambient temperature:	21.2 °C
Fire duration:	383 s

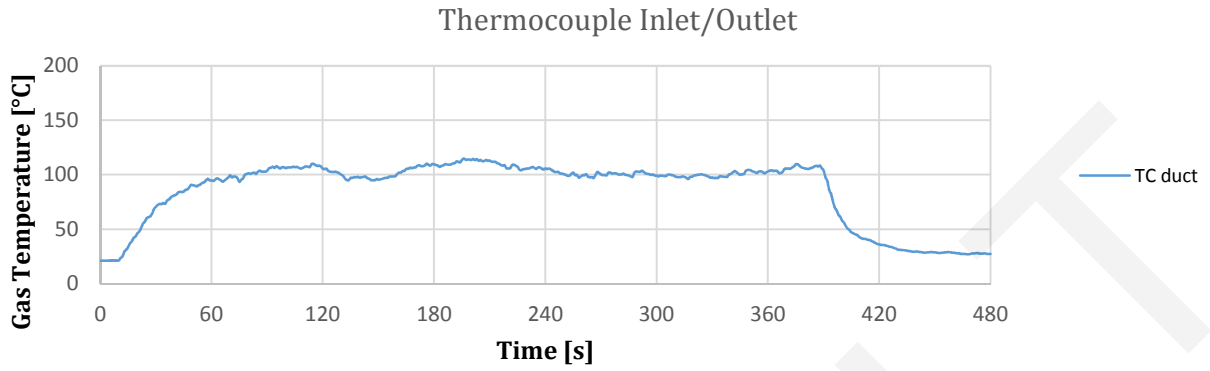

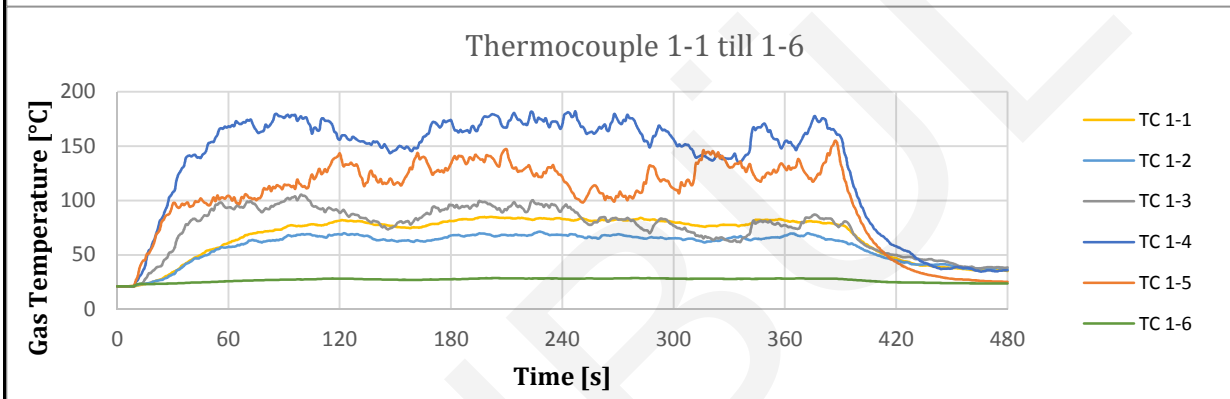

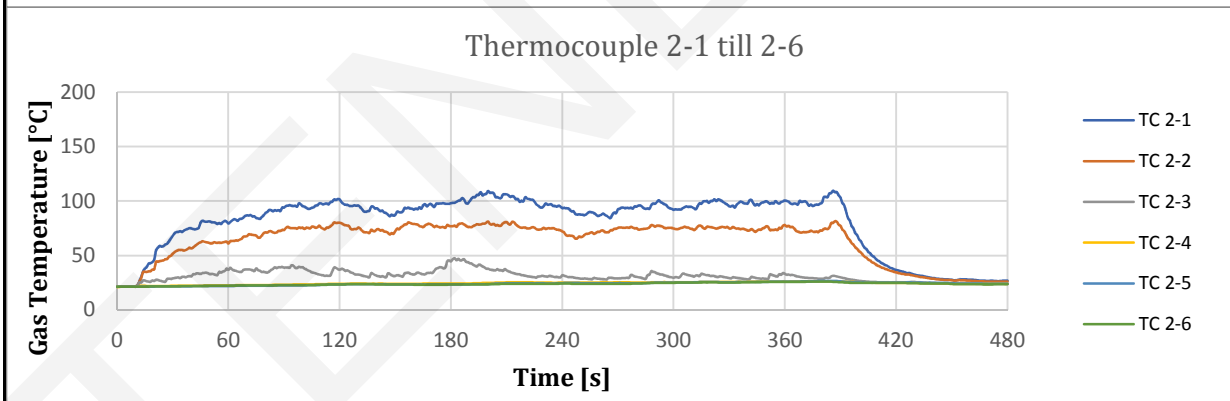

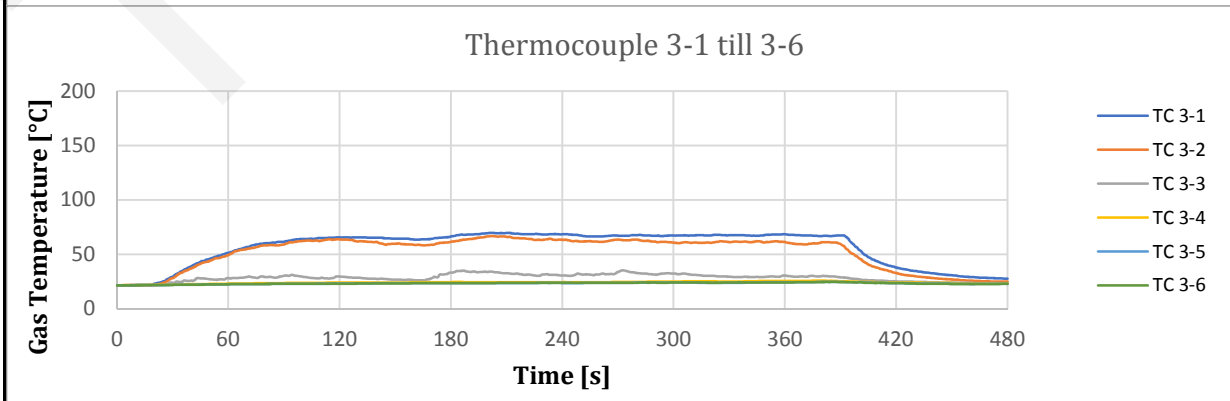

Name experiment:	Reference n-Heptane (RH1)				
Date:	29-8-2017				
Ambient temperature:	26.3	°C			
Fire duration:	189	s			
Fuel			**Sprinkler**		
Name:	n-heptane (>99.75%)		Sprinkler activated at:		s
Surface:	0.25	m^2	Sprinkler deactivated at:		s
Weight:	0.965	kg	Operating pressure:		bar
Heat of combustion:	44.56	MJ/kg	K-factor:		L/min√bar
Theoretical THR:	43.00	MJ	Water flow rate:	0	L/min
Mass burning rate	5.106	g/s	Measured THR:	42.9	MJ
Theoretical HRR	227.5	kW	Measured avg. HRR:	266.4	kW
			Smoke layer height:	2.2-2.5	m

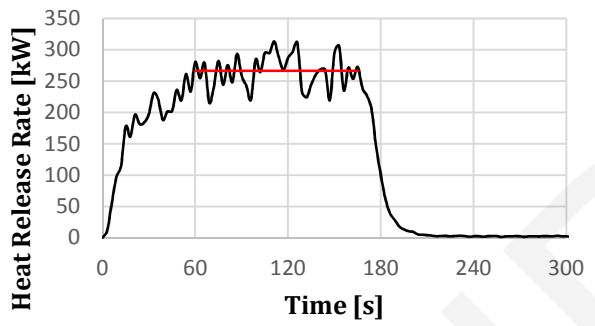

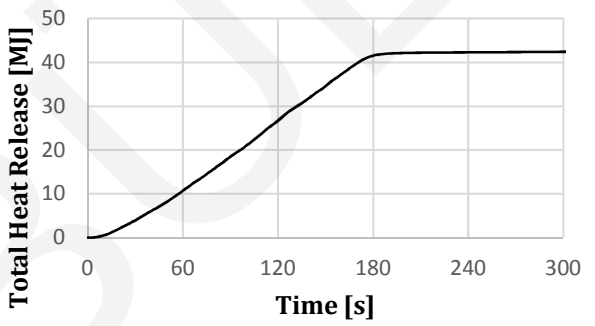

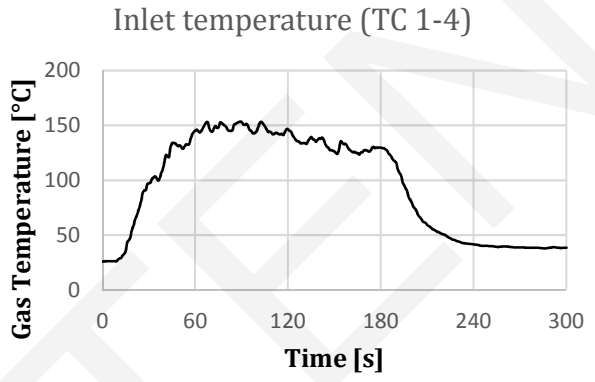

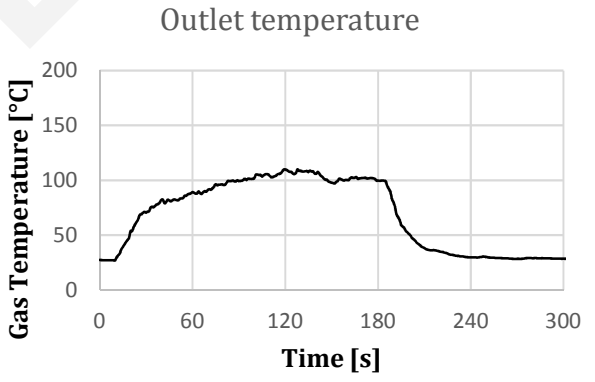

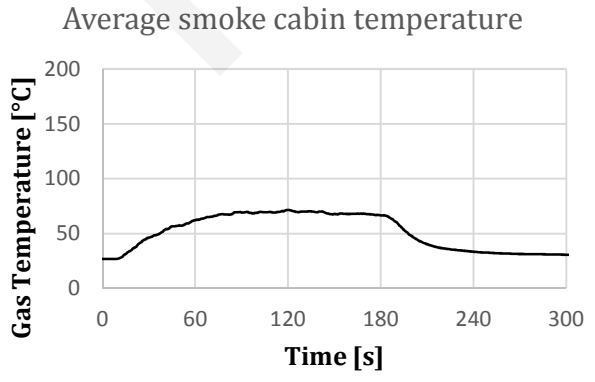

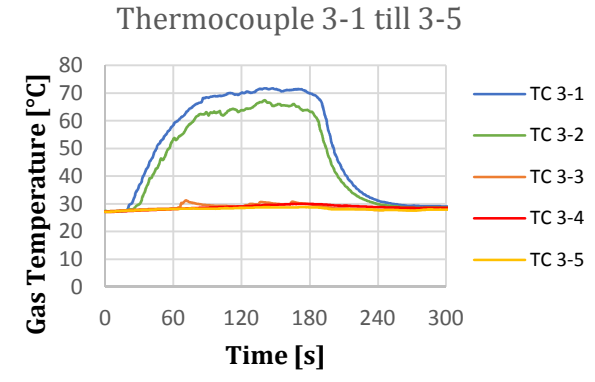

Name experiment:	Reference n-Heptane (RH1)
Date:	29-8-2017
Ambient temperature:	26.3 °C
Fire duration:	189 s

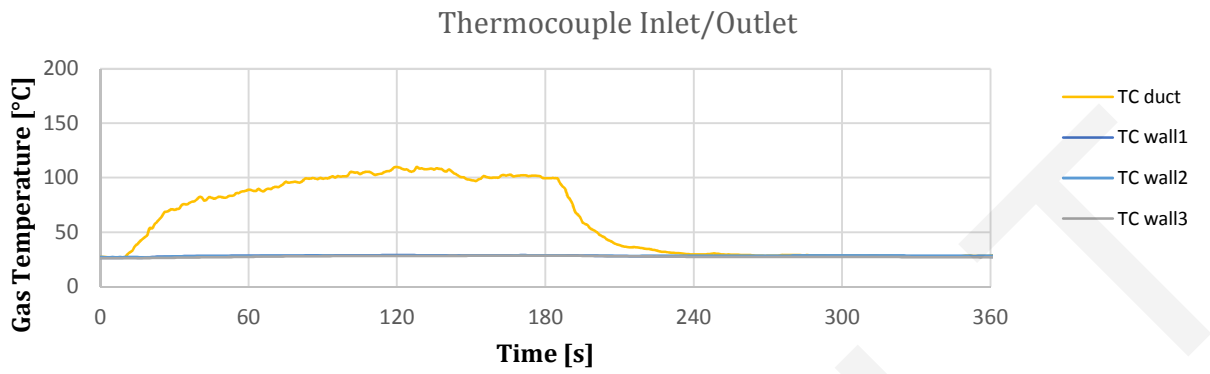

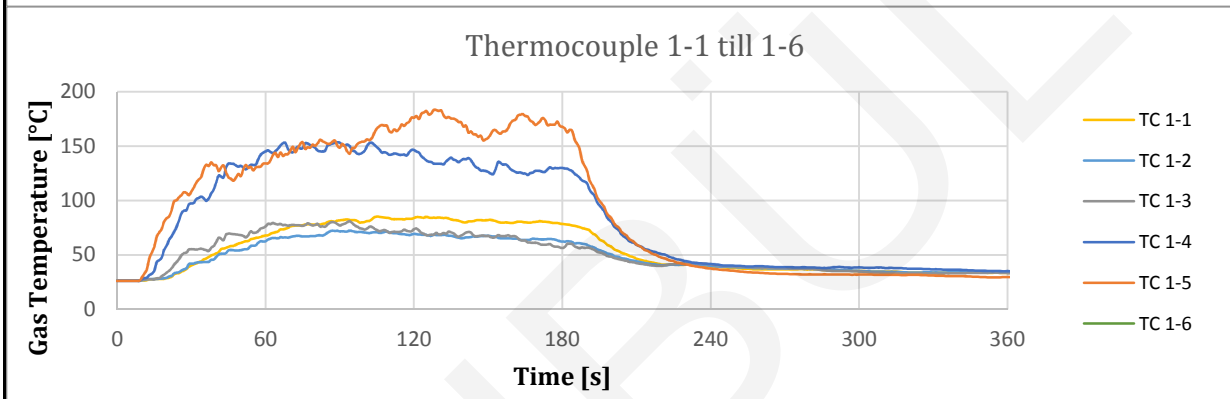

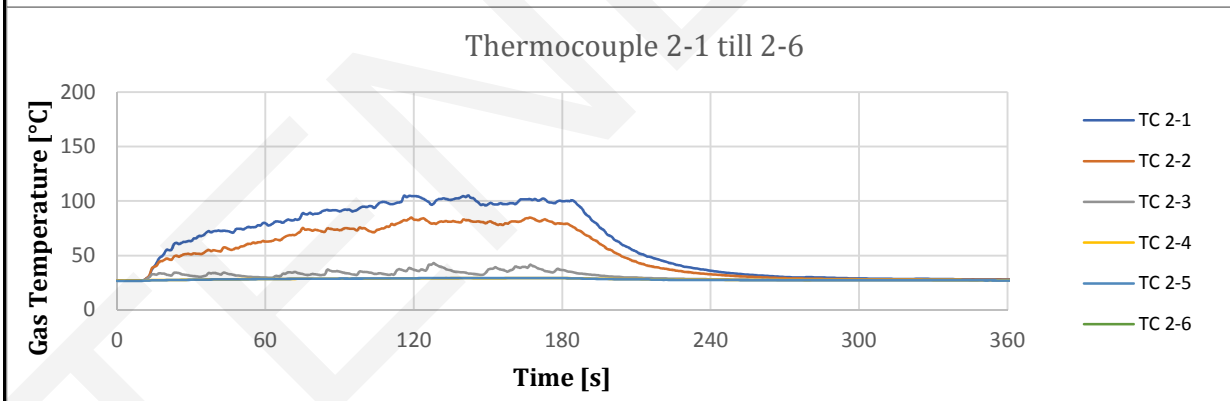

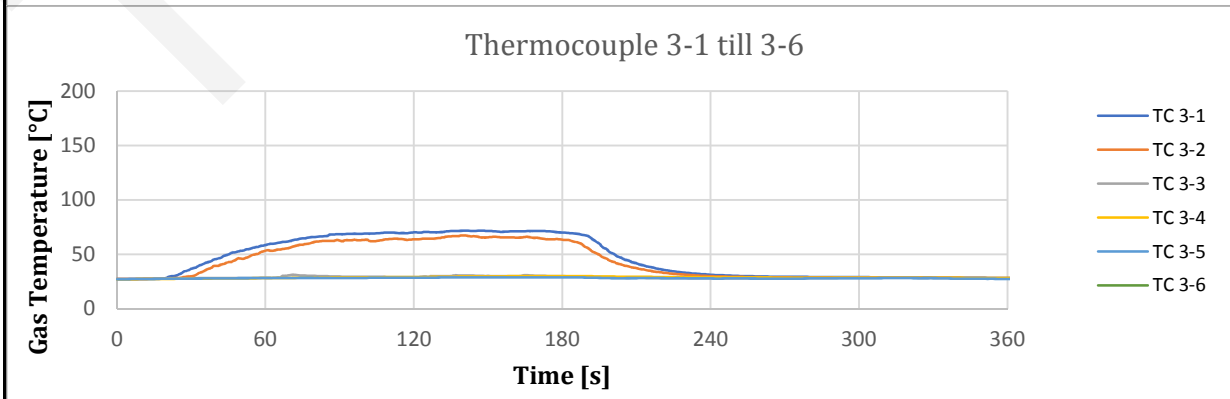

Name experiment:	Reference Heptane-Toluene 0 (RHT0)				
Date:	25-10-2017				
Ambient temperature:	17	°C			
Fire duration:	257	s			
Fuel			**Sprinkler**		
Name:	heptane-toluene (85/15)		Sprinkler activated at:		s
Surface:	0.25	m^2	Sprinkler deactivated at:		s
Weight:	1.525	kg	Operating pressure:		bar
Heat of combustion:	43.11	MJ/kg	K-factor:		L/min√bar
Theoretical THR:	65.74	MJ	Water flow rate:	0	L/min
Mass burning rate	5.934	g/s	Measured THR:	64.8	MJ
Theoretical HRR	255.8	kW	Measured avg. HRR:	279.0	kW
			Smoke layer height:	1.8-2.1	m

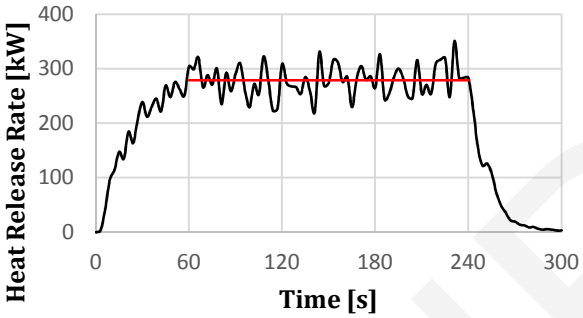

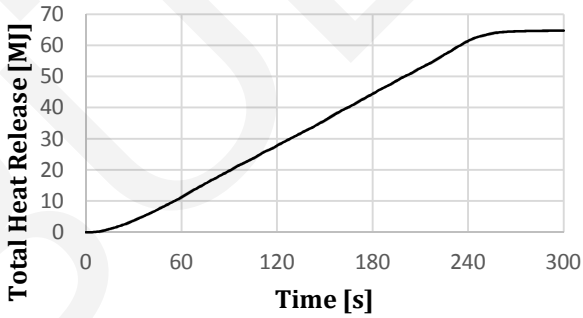

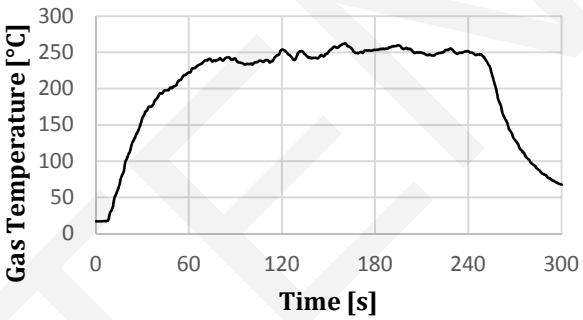

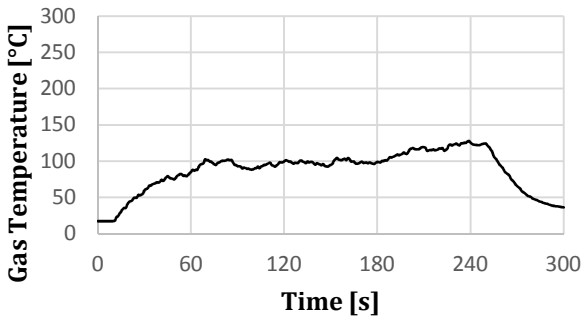

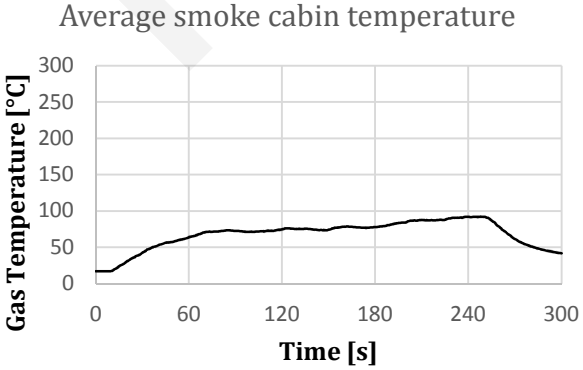

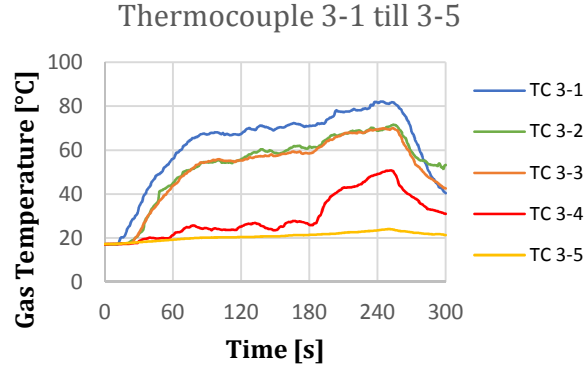

Name experiment:	Reference Heptane-Toluene 0 (RHT0)
Date:	25-10-2017
Ambient temperature:	17 °C
Fire duration:	257 s

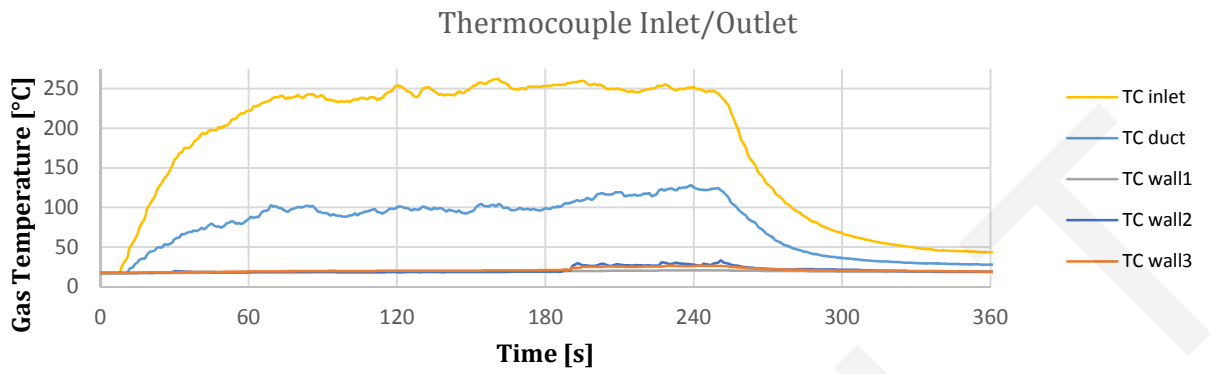

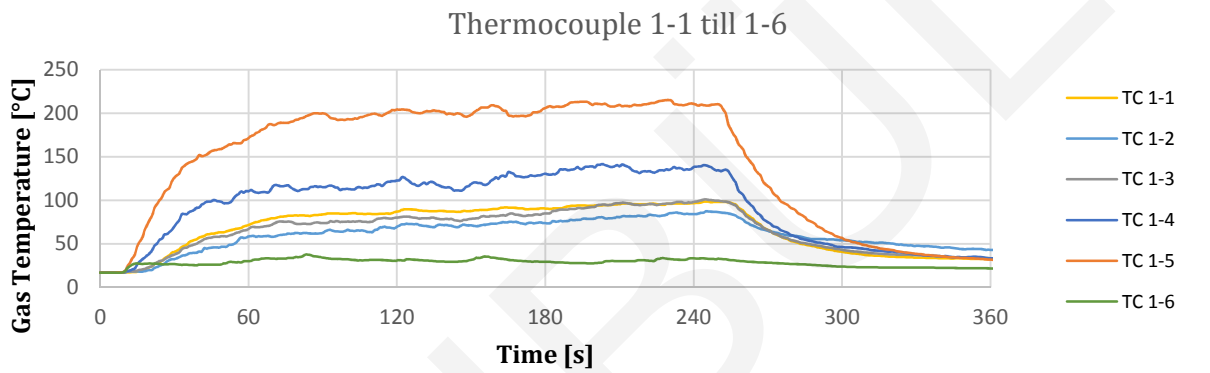

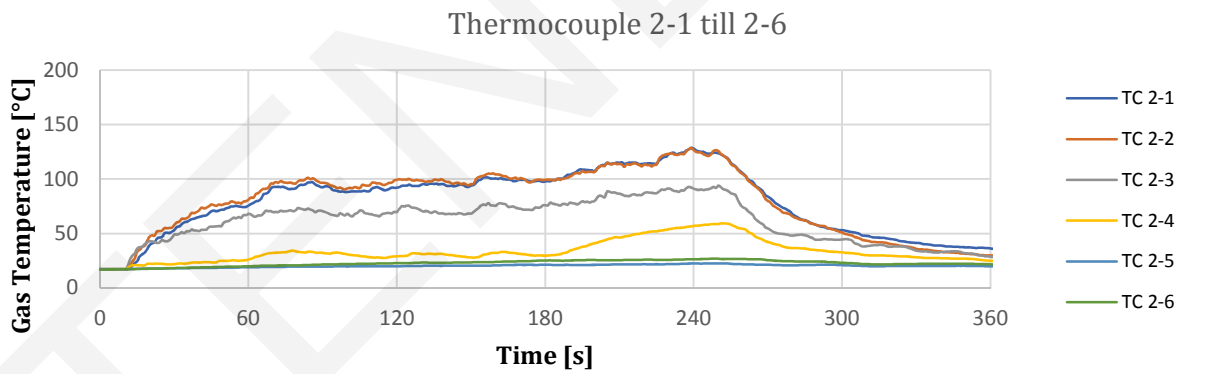

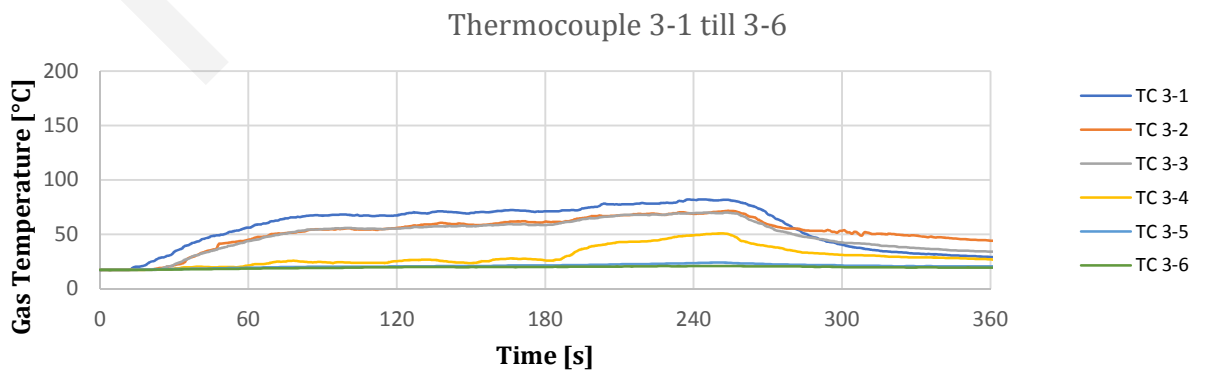

Name experiment:	Reference Heptane-Toluene 1 (RHT1)				
Date:	25-10-2017				
Ambient temperature:	17	°C			
Fire duration:	229	s			
Fuel			**Sprinkler**		
Name:	heptane-toluene (85/15)		Sprinkler activated at:		s
Surface:	0.25	m^2	Sprinkler deactivated at:		s
Weight:	1.422	kg	Operating pressure:		bar
Heat of combustion:	43.11	MJ/kg	K-factor:		L/min√bar
Theoretical THR:	61.30	MJ	Water flow rate:	0	L/min
Mass burning rate	6.210	g/s	Measured THR:	62.3	MJ
Theoretical HRR	267.7	kW	Measured avg. HRR:	291.5	kW
			Smoke layer height:	1.8-2.1	m

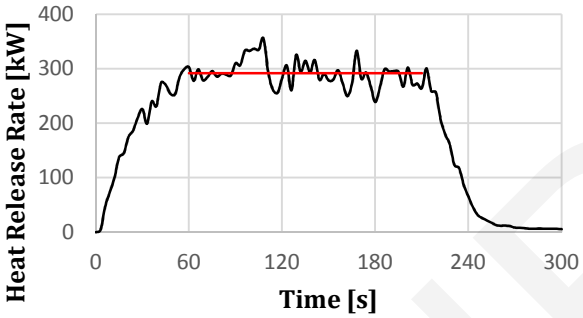

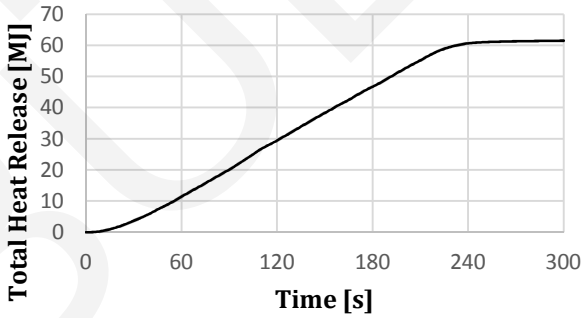

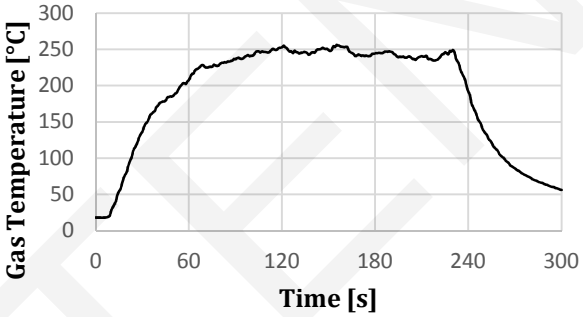

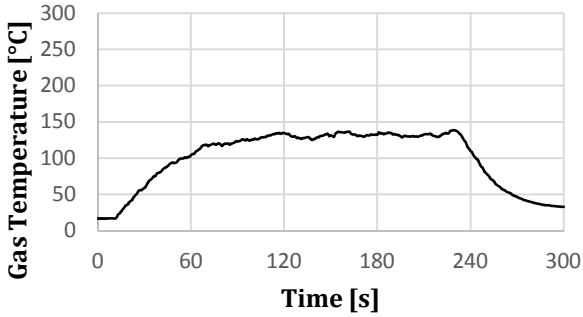

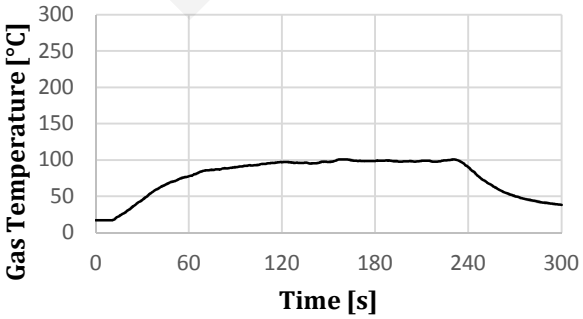

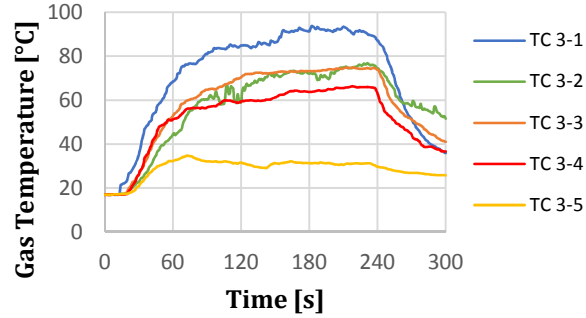

Name experiment:	Reference Heptane-Toluene 1 (RHT1)
Date:	25-10-2017
Ambient temperature:	17 °C
Fire duration:	229 s

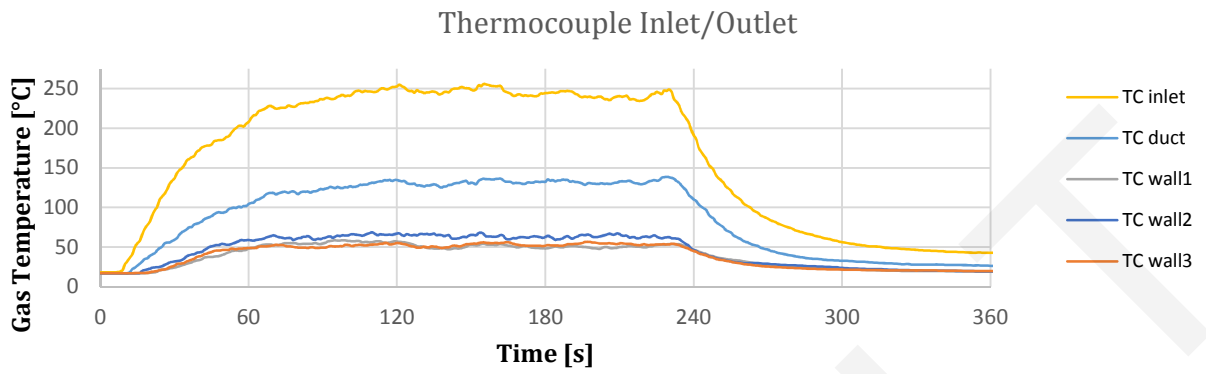

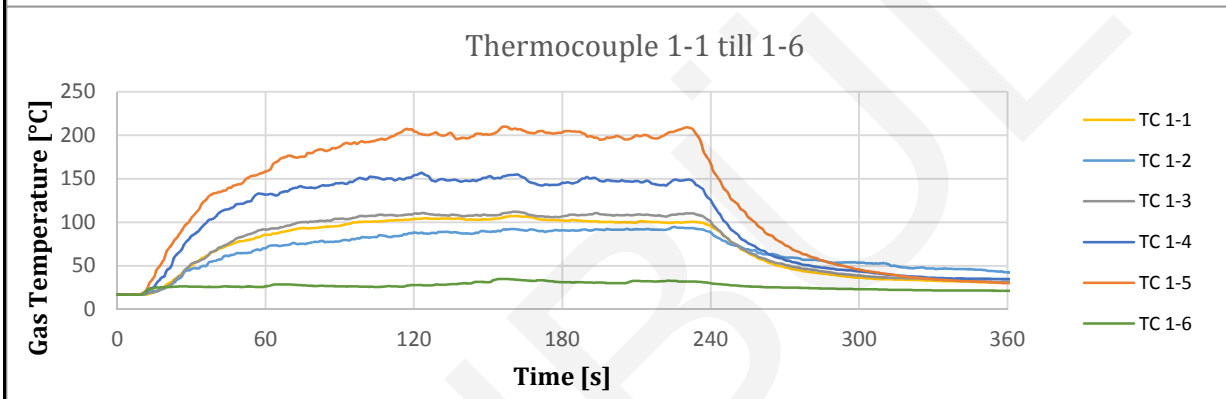

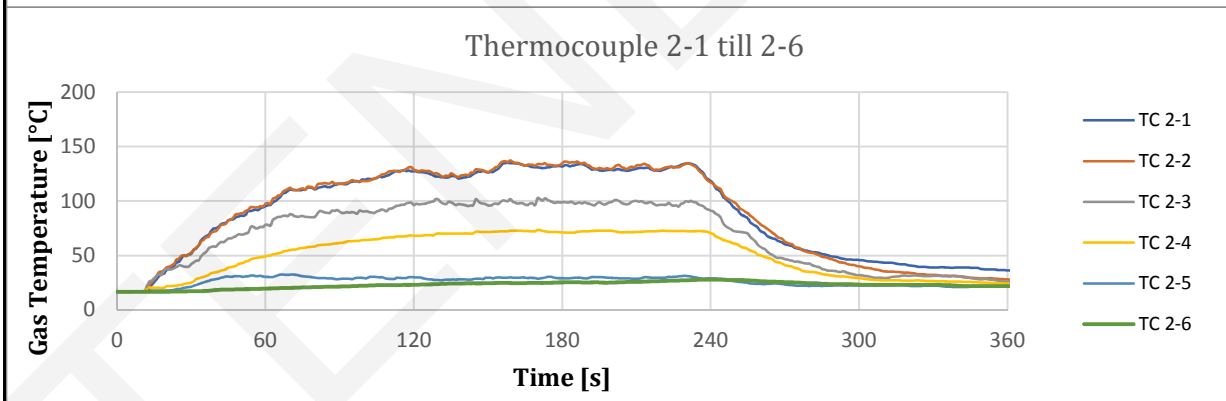

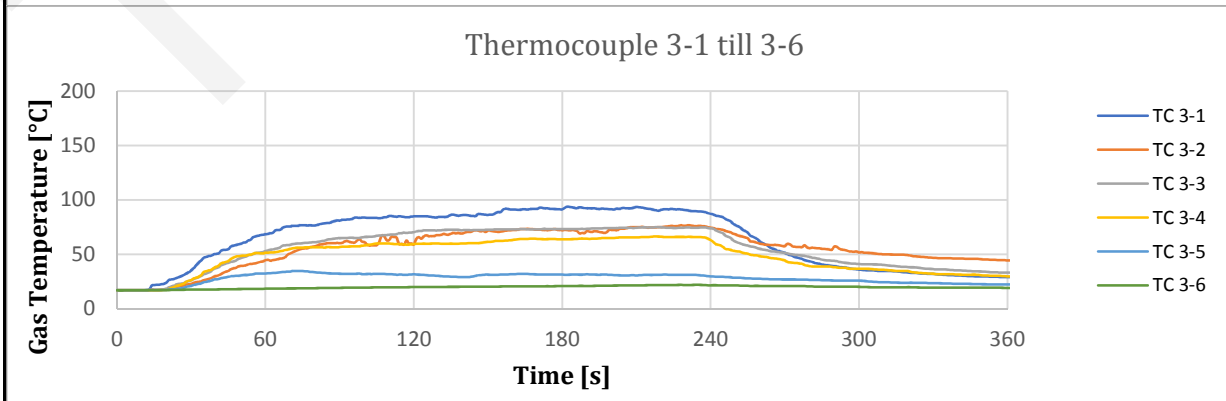

Name experiment:	Reference Heptane-Toluene 2 (RHT2)				
Date:	2-2-2018				
Ambient temperature:	14.3	°C			
Fire duration:	202	s			
Fuel			**Sprinkler**		
Name:	heptane-toluene (85/15)		Sprinkler activated at:		s
Surface:	0.35	m^2	Sprinkler deactivated at:		s
Weight:	2.98	kg	Operating pressure:		bar
Heat of combustion:	43.11	MJ/kg	K-factor:		L/min√bar
Theoretical THR:	128.47	MJ	Water flow rate:	0	L/min
Mass burning rate	14.752	g/s	Measured THR:		MJ
Theoretical HRR	636.0	kW	Measured avg. HRR:		kW
			Smoke layer height:	1.8-2.1	m

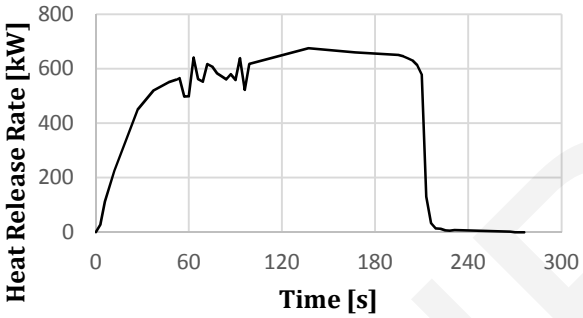

No measurement data for THR

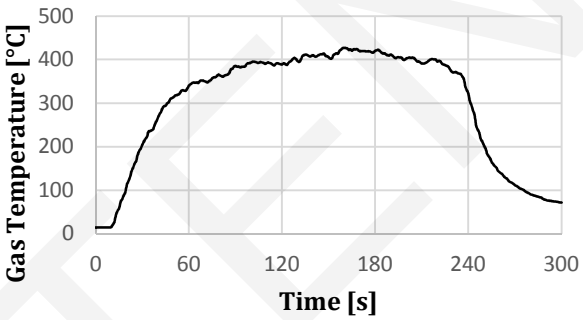

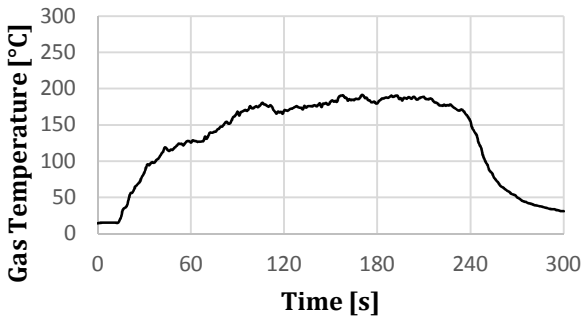

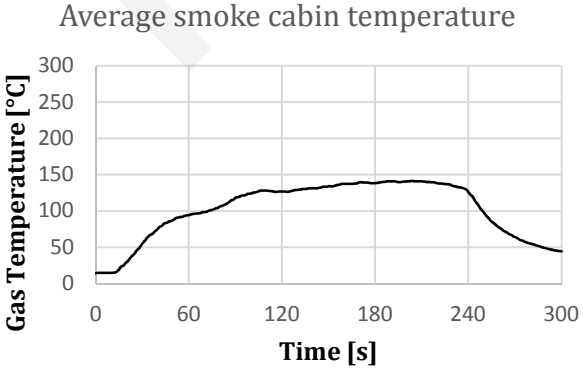

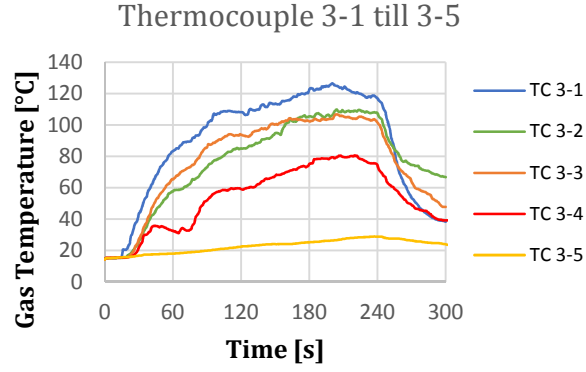

Name experiment:	Reference Heptane-Toluene 2 (RHT2)
Date:	2-2-2018
Ambient temperature:	14.3 °C
Fire duration:	229 s

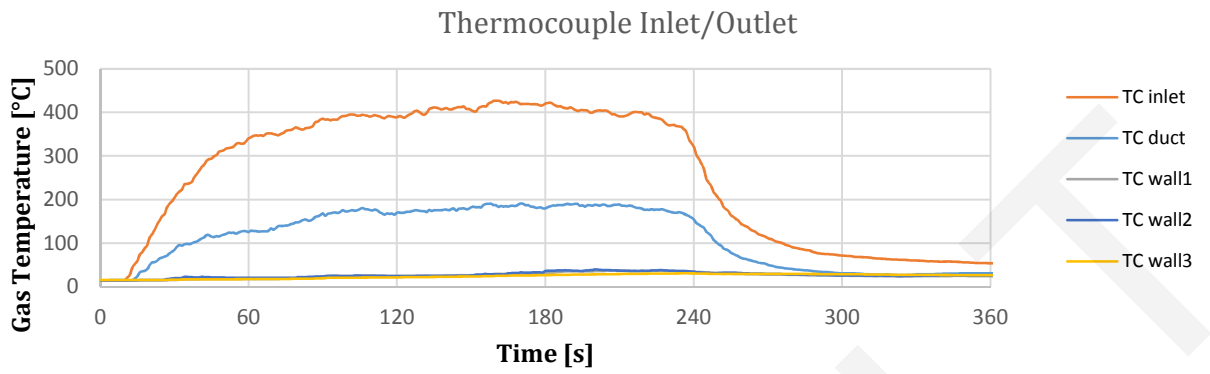

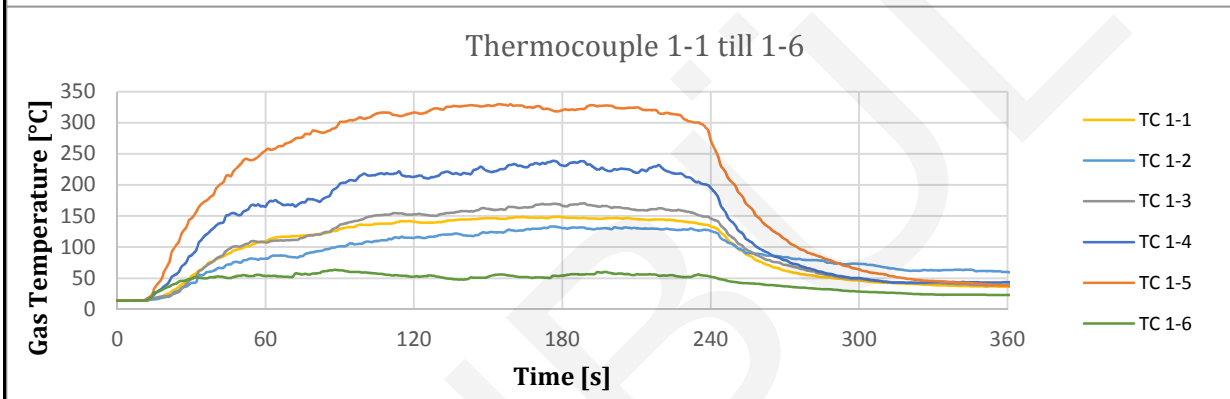

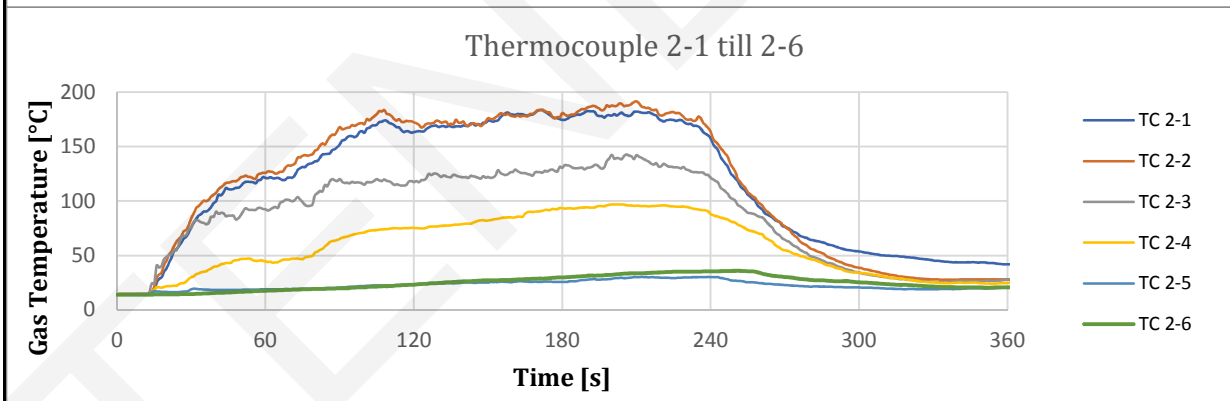

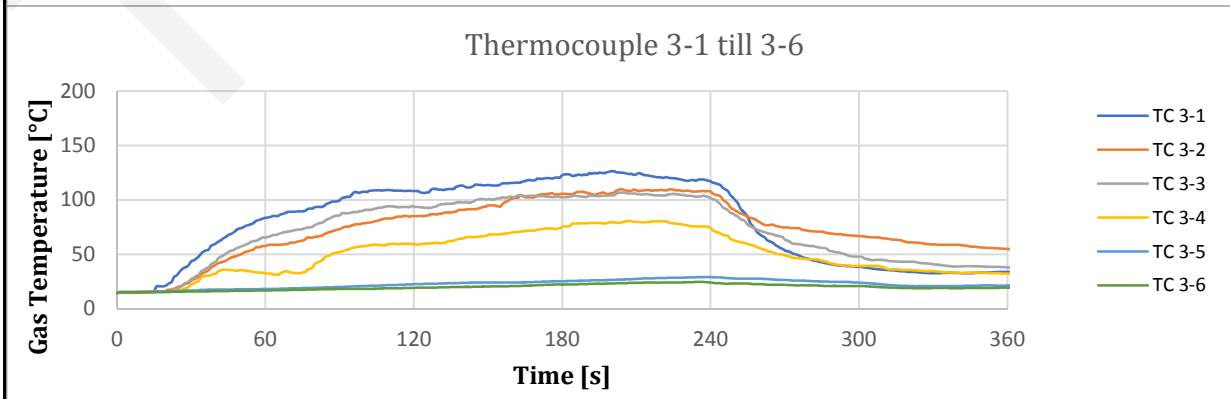

Name experiment:	Sprinkler Heptane-Toluene 1 (SHT1)				
Date:	2-2-2018				
Ambient temperature:	14	°C			
Fire duration:	221	s			
Fuel			**Sprinkler**		
Name:	heptane-toluene (85/15)		Sprinkler activated at:	154	s
Surface:	0.35	m^2	Sprinkler deactivated at:	221	s
Weight:	4	kg	Operating pressure:	0.79	bar
Heat of combustion:	43.11	MJ/kg	K-factor:	80.6	L/min√bar
Theoretical THR:	172.44	MJ	Water flow rate:	71.63885	L/min
Mass burning rate	18.100	g/s	Measured THR:	165.3	MJ
Theoretical HRR	780.3	kW	Measured peak HRR:	1081.0	kW
			Smoke layer height:	1.65	m

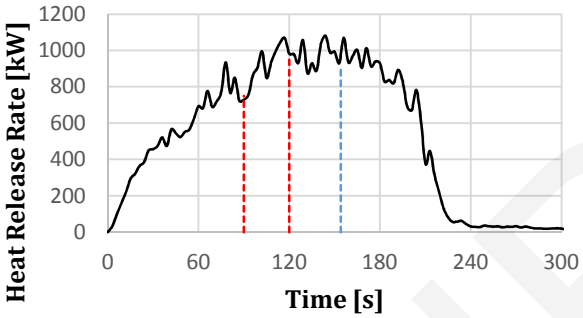

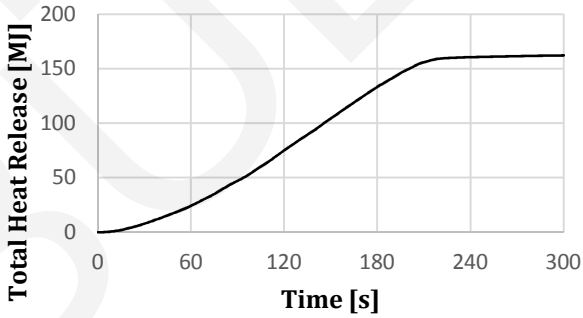

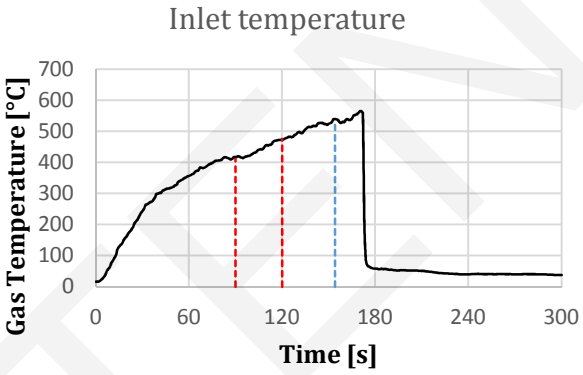

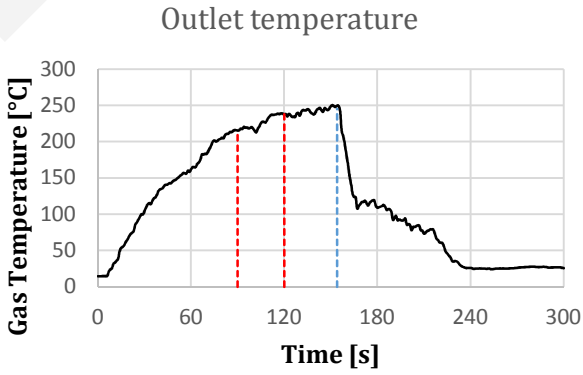

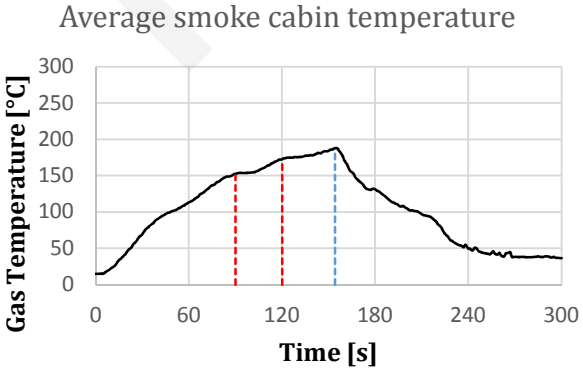

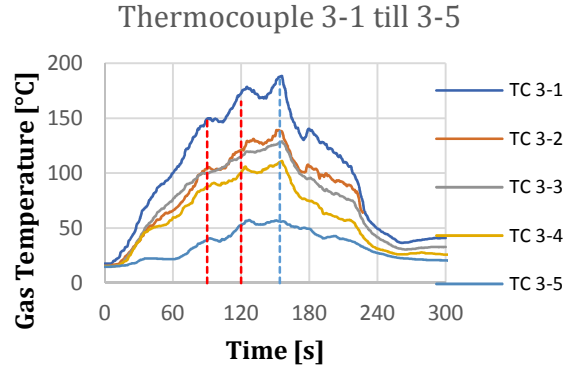

Name experiment:	Sprinkler Heptane-Toluene 1 (SHT1)	
Date:	2-2-2018	
Ambient temperature:	14 °C	90 sec. Exhaust volume flow ↑ -----
Fire duration:	221 s	120 sec. Exhaust volume flow ↑ ----
		154 sec. Sprinkler activated ----

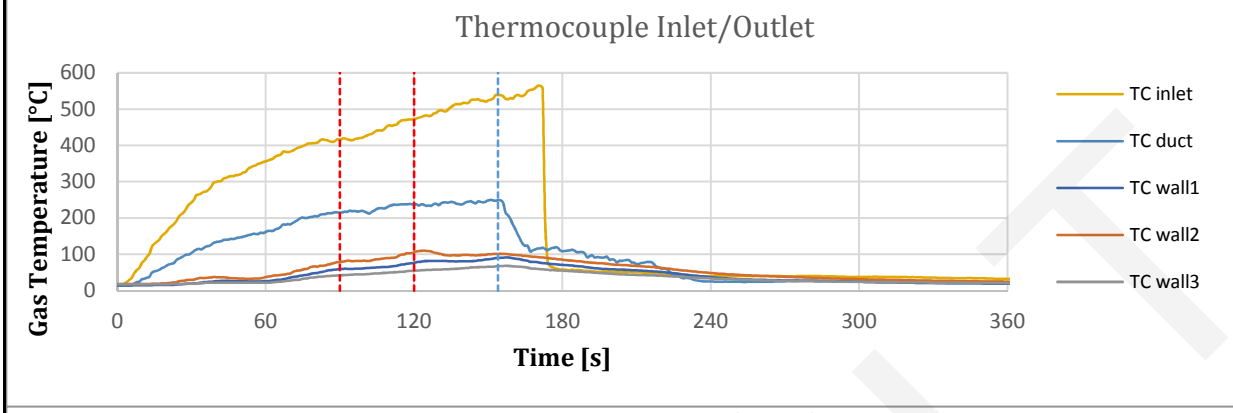

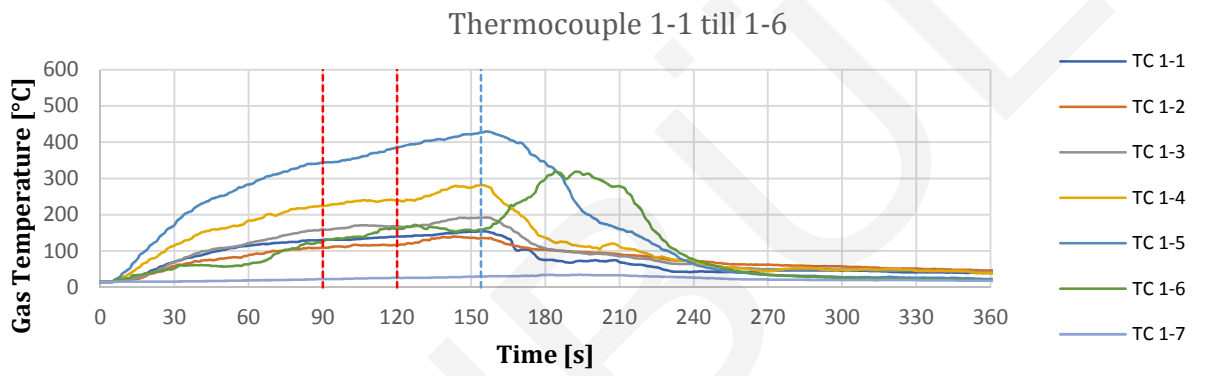

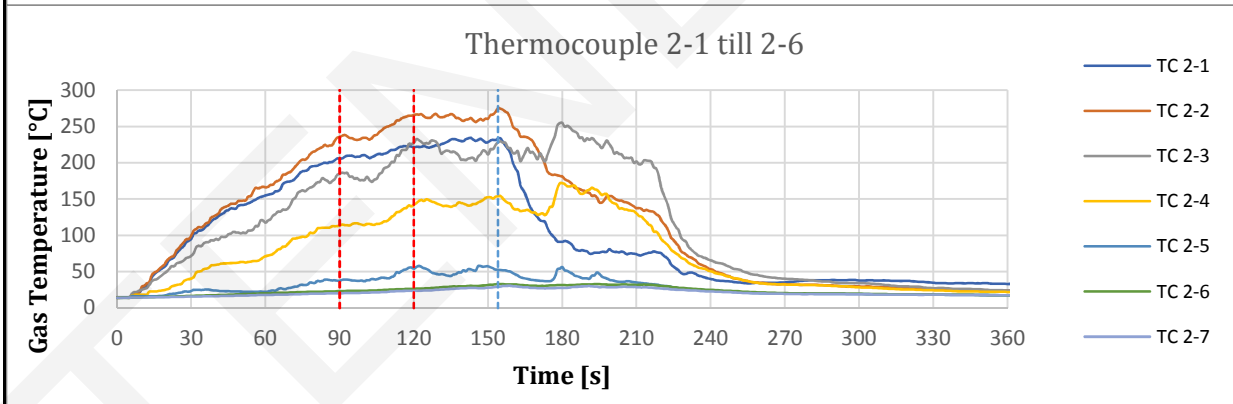

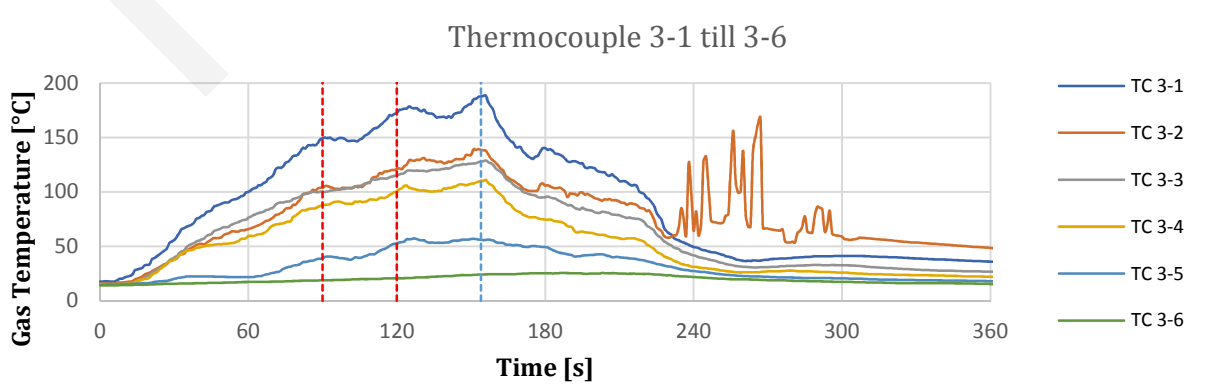

Name experiment:	Sprinkler Heptane 1 (SH1)				
Date:	27-2-2018				
Ambient temperature:	13.6	°C			
Fire duration:	242	s			
Fuel			**Sprinkler**		
Name:	Heptane		Sprinkler activated at:	96	s
Surface:	0.35	m^2	Sprinkler deactivated at:	186	s
Weight:	4	kg	Operating pressure:	0.79	bar
Heat of combustion:	44.56	MJ/kg	K-factor:	80.6	L/min√bar
Theoretical THR:	178.24	MJ	Water flow rate:	71.6	L/min
Mass burning rate	16.529	g/s	Measured THR:	198.7	MJ
Theoretical HRR	736.5	kW	Measured avg. HRR:	875.3	kW
			Smoke layer height:	1.8-2.1	m

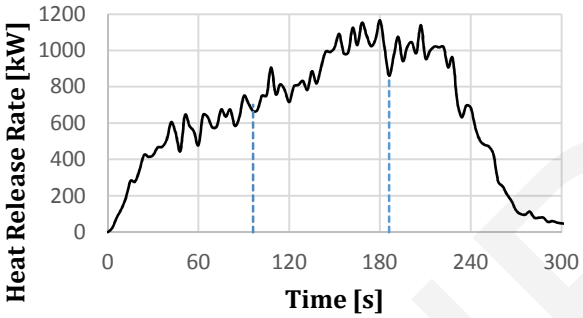

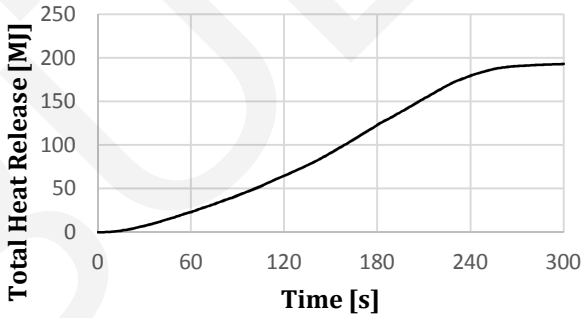

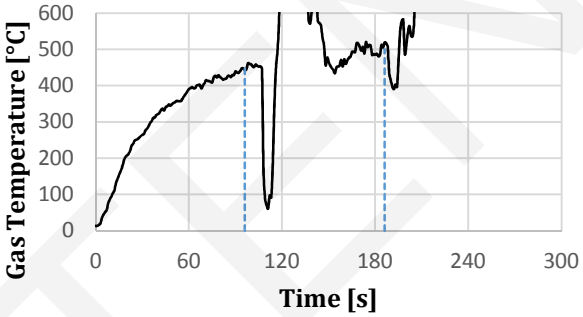

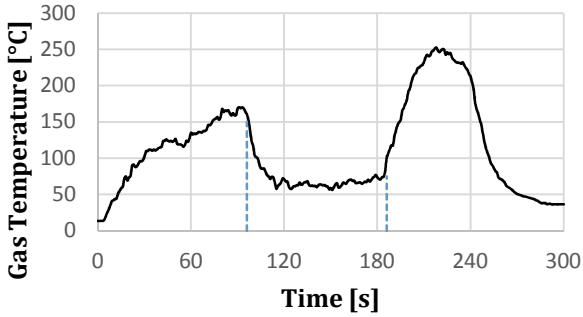

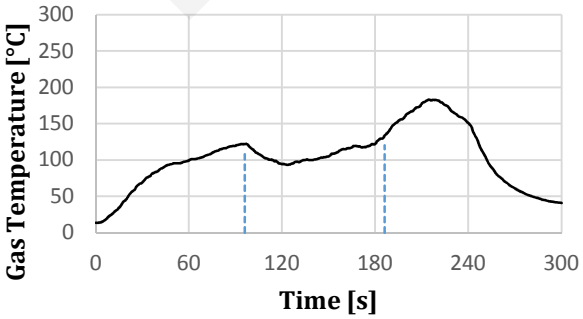

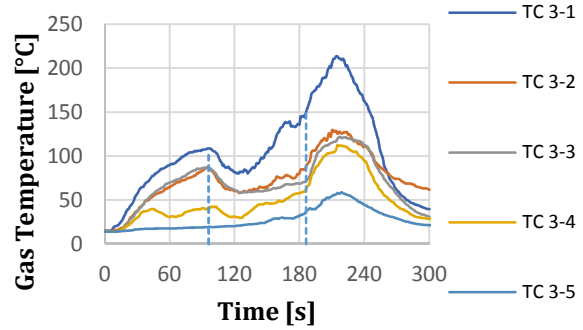

Name experiment:	Sprinkler Heptane 1 (SH1)
Date:	27-2-2018
Ambient temperature:	13.6 °C
Fire duration:	242 s

96 sec. Sprinkler activated ----
186 sec. Sprinkler deactivated ----

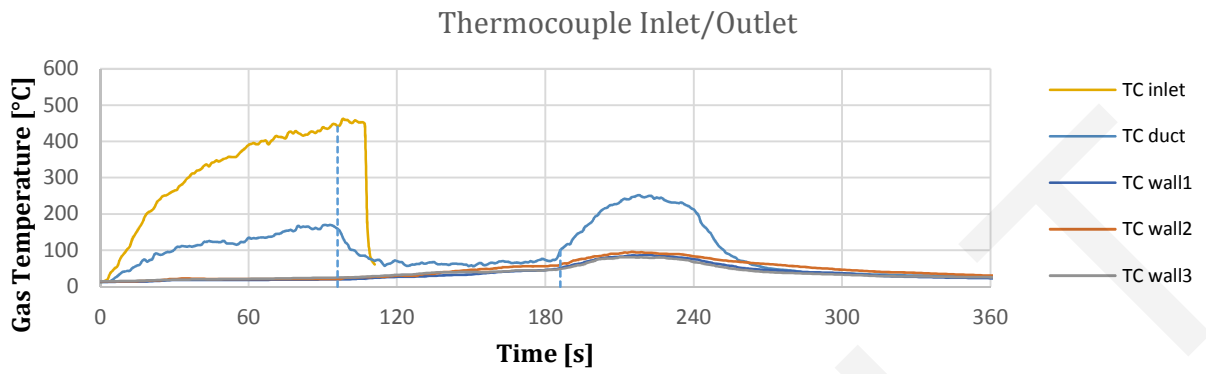

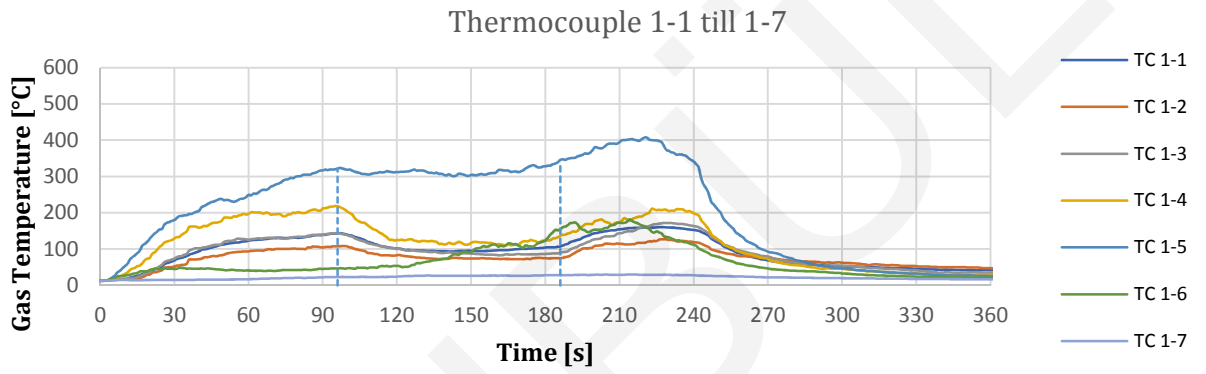

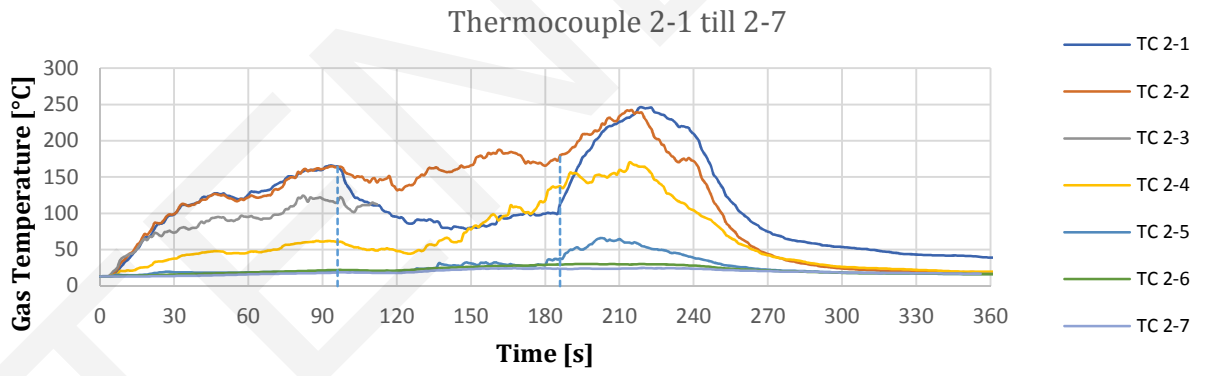

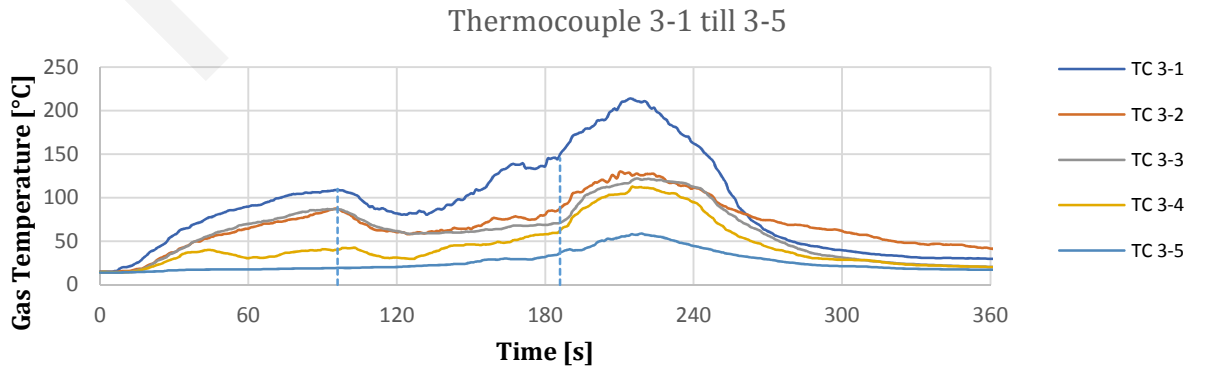

Name experiment:	Sprinkler Heptane 2 (SH2)				
Date:	7-3-2018				
Ambient temperature:	12.6	°C			
Fire duration:	290	s			
Fuel			**Sprinkler**		
Name:	Heptane		Sprinkler activated at:	118	s
Surface:	0.35	m^2	Sprinkler deactivated at:	223	s
Weight:	4.02	kg	Operating pressure:	0.4	bar
Heat of combustion:	44.56	MJ/kg	K-factor:	80.6	L/min√bar
Theoretical THR:	179.13	MJ	Water flow rate:	51.0	L/min
Mass burning rate	13.862	g/s	Measured THR:	178.3	MJ
Theoretical HRR	617.7	kW	Measured avg. HRR:	729.5	kW
			Smoke layer height:	1.8-2.1	m

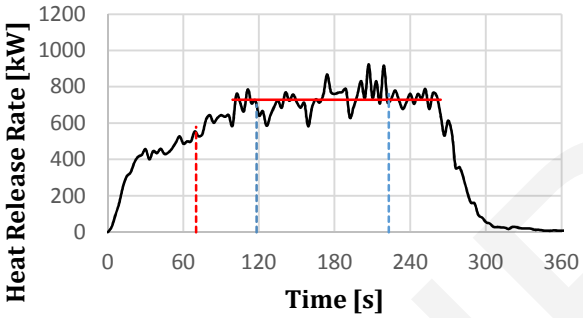

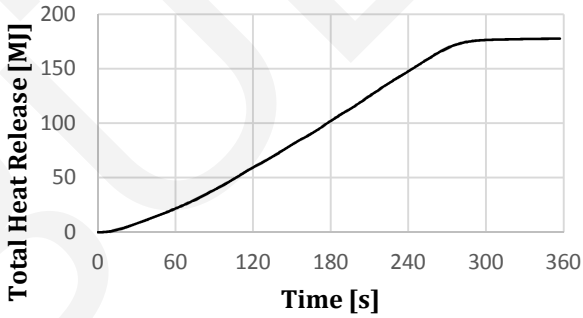

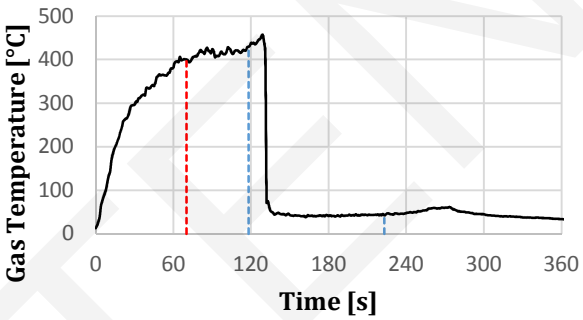

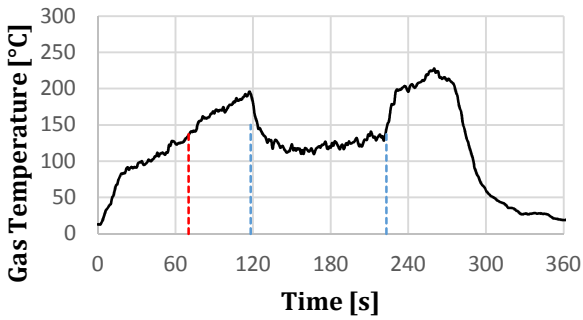

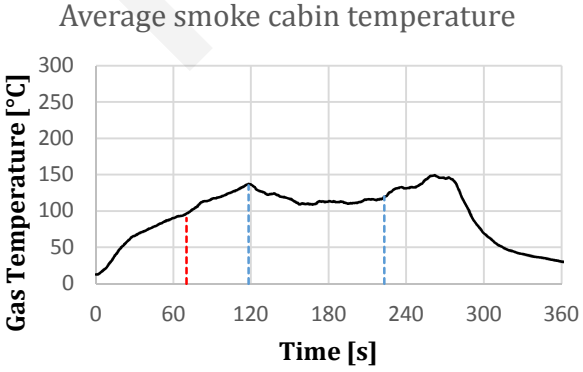

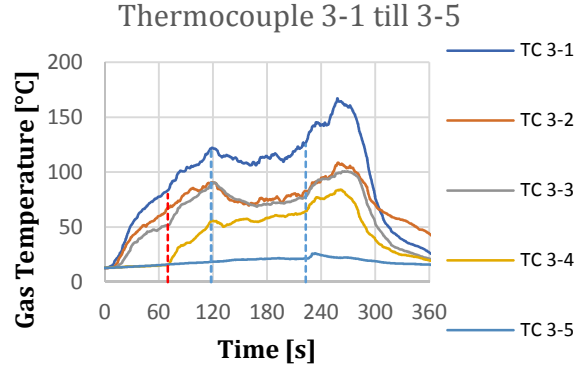

Name experiment:	Sprinkler Heptane 2 (SH2)	
Date:	7-3-2018	
Ambient temperature:	12.6 °C	70sec. Ventilation rate down
Fire duration:	310 s	118sec. Sprinkler activated ----
		223 sec. Sprinkler deactivated ----

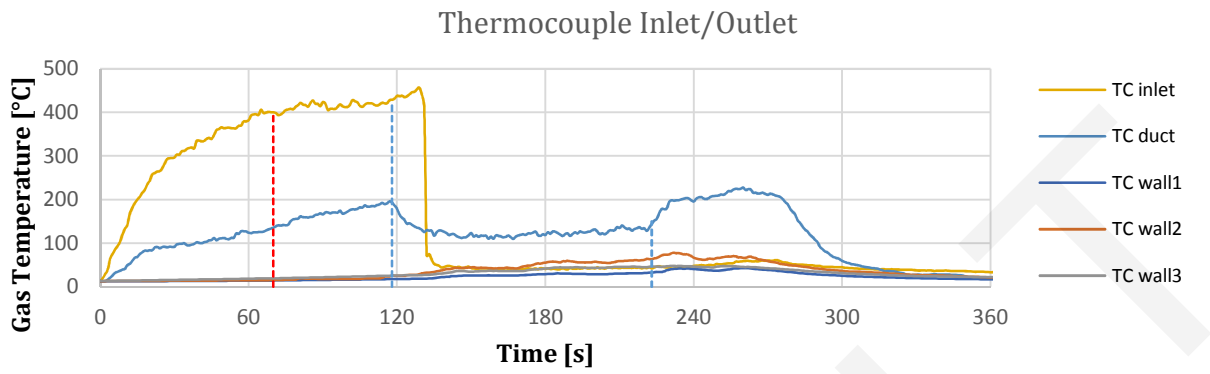

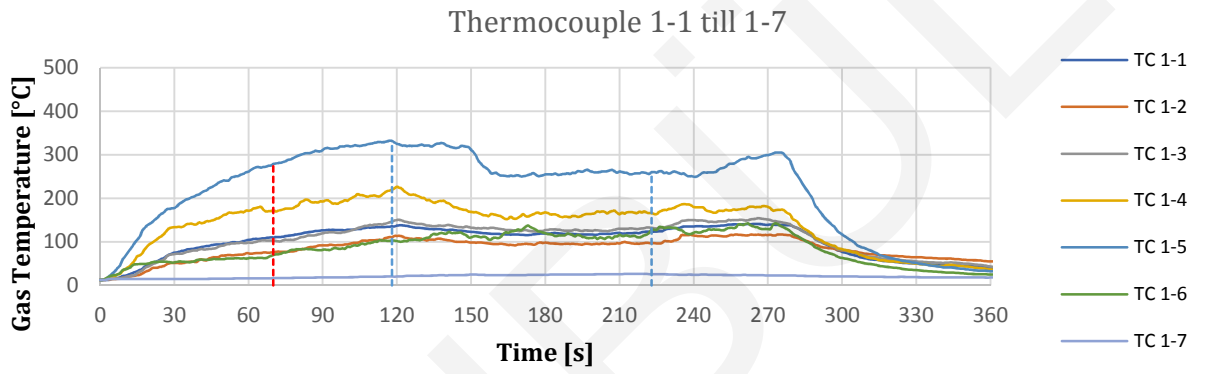

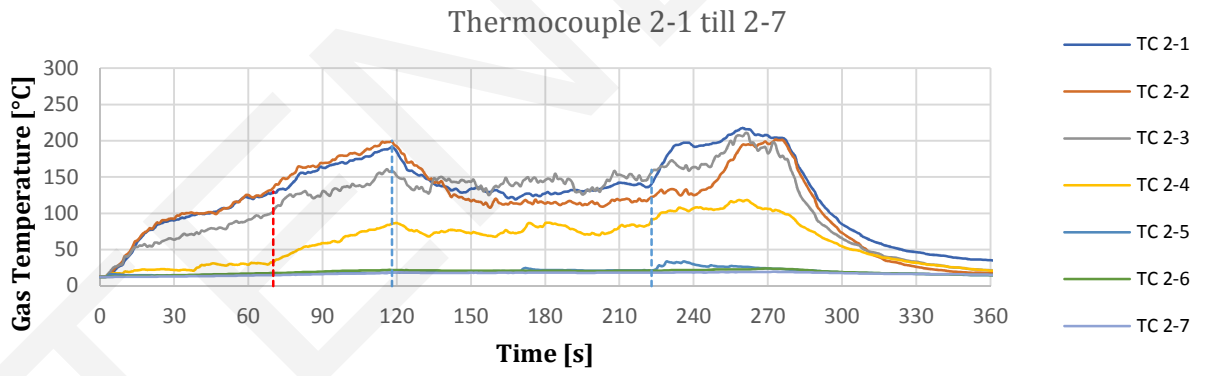

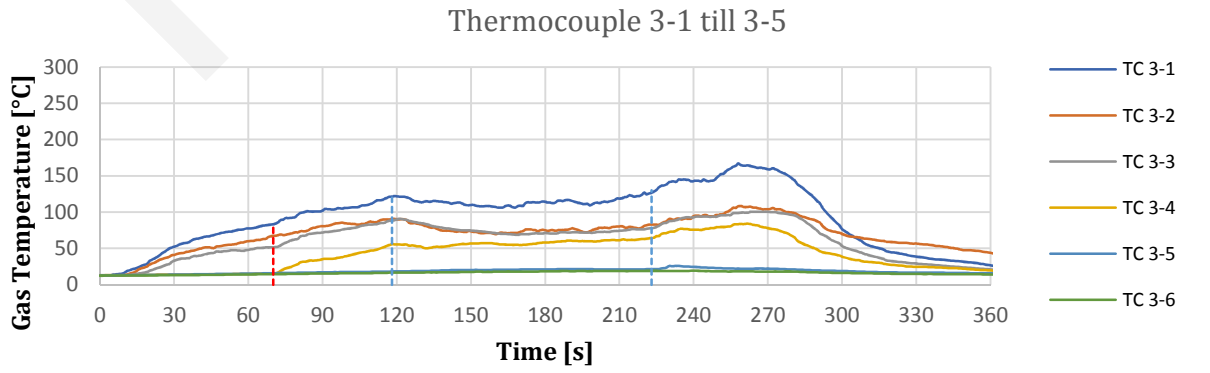

Name experiment:	Sprinkler Heptane 3 (SH3)				
Date:	7-3-2018				
Ambient temperature:	12.1	°C			
Fire duration:	260	s			
Fuel			**Sprinkler**		
Name:	Heptane		Sprinkler activated at:	120	s
Surface:	0.35	m^2	Sprinkler deactivated at:	250	s
Weight:	4.02	kg	Operating pressure:	1.34	bar
Heat of combustion:	44.56	MJ/kg	K-factor:	80.6	L/min√bar
Theoretical THR:	179.13	MJ	Water flow rate:	93.3	L/min
Mass burning rate	15.462	g/s	Measured THR:	171.1	MJ
Theoretical HRR	689.0	kW	Measured avg. HRR:	784.7	kW
			Smoke layer height:	1.8-2.1	m

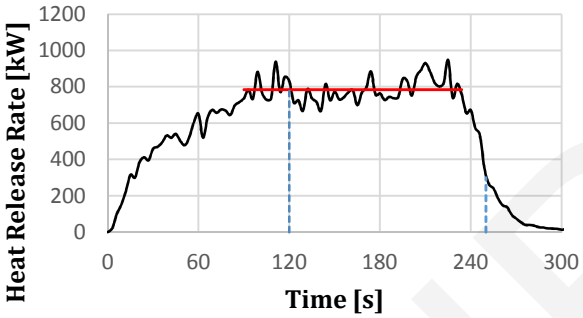

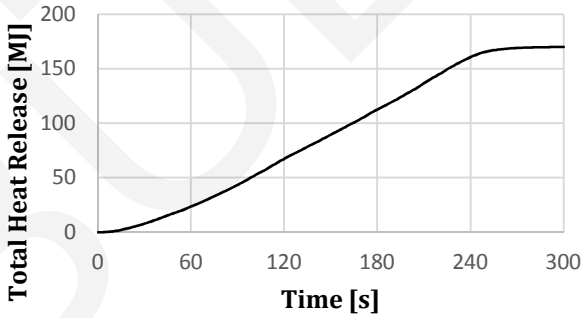

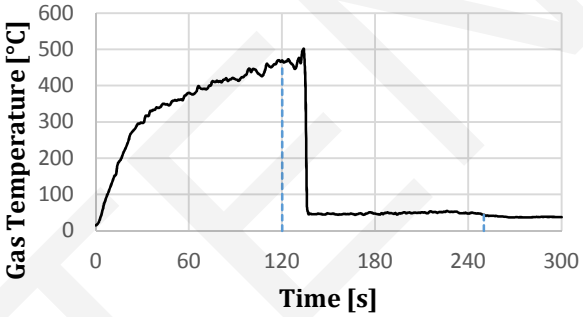

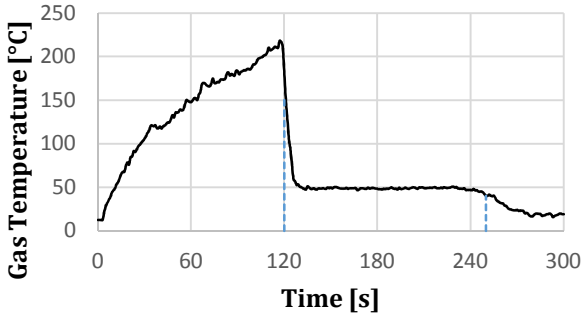

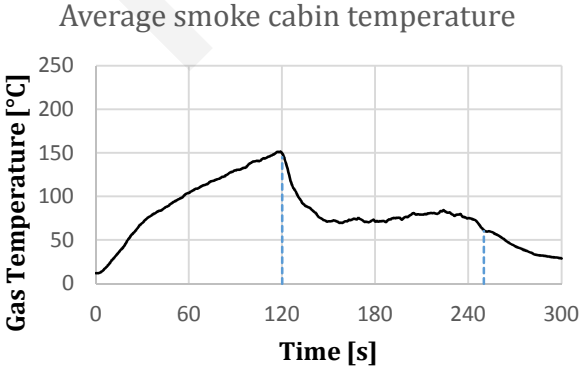

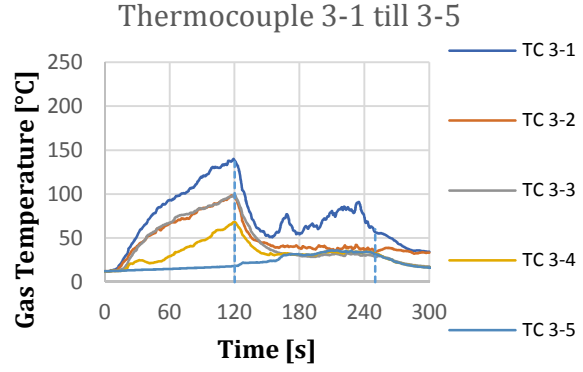

Name experiment:	Sprinkler Heptane 3(SH3)
Date:	7-3-2018
Ambient temperature:	12.1 °C
Fire duration:	260 s

120 sec. Sprinkler activated ----
250 sec. Sprinkler deactivated ----

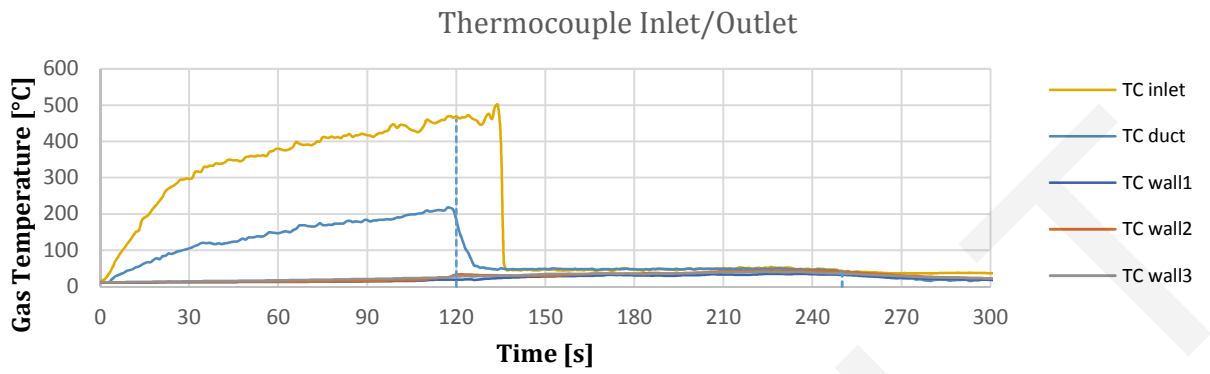

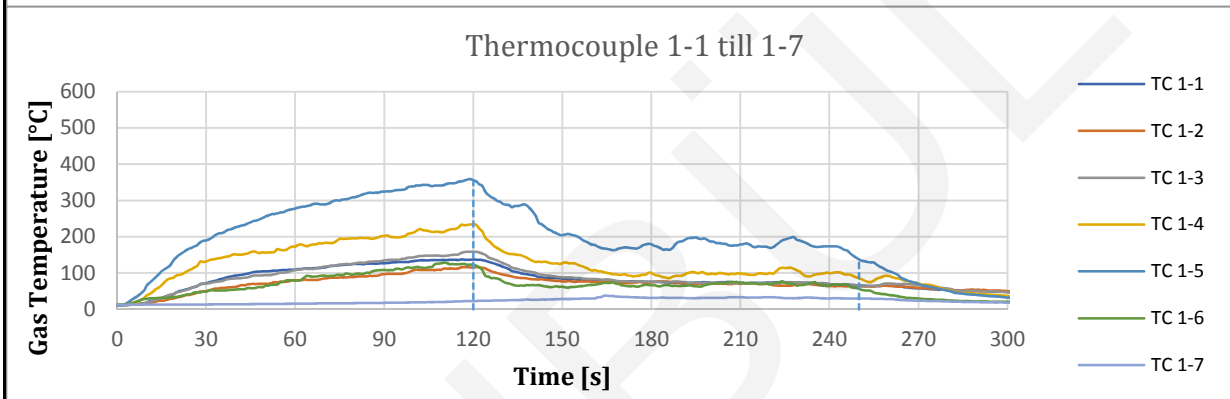

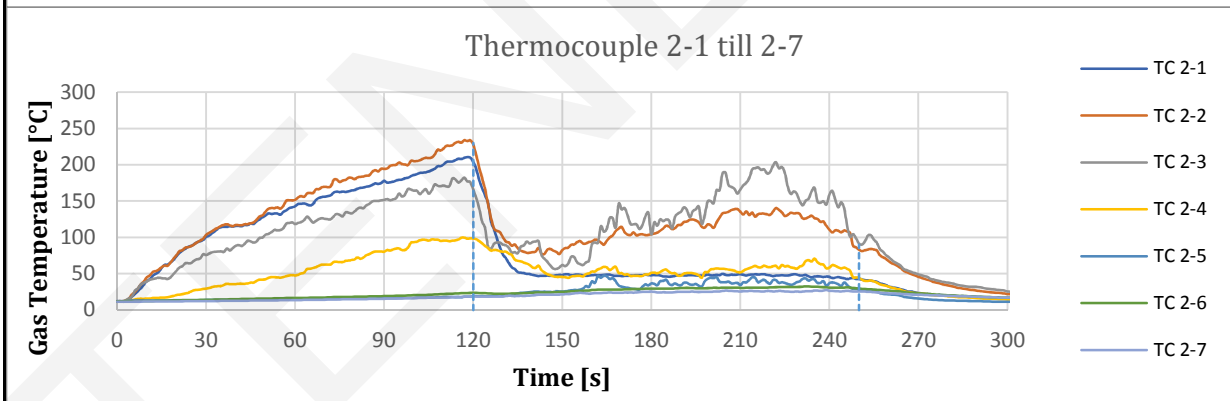

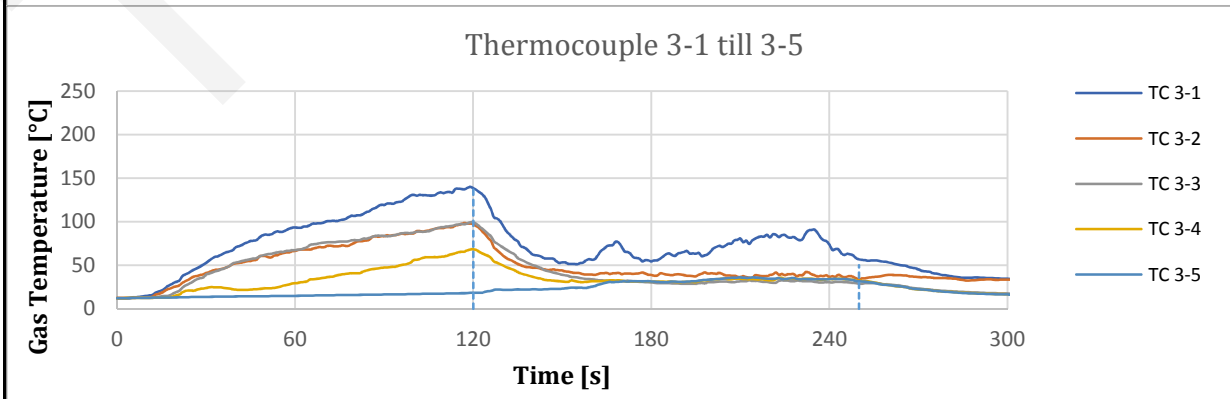

Name experiment:	Sprinkler Heptane 4 (SH4)				
Date:	30-3-2018				
Ambient temperature:	14.3	°C			
Fire duration:	250	s			
Fuel			**Sprinkler**		
Name:	Heptane		Sprinkler activated at:	123	s
Surface:	0.35	m^2	Sprinkler deactivated at:	223	s
Weight:	3.92	kg	Operating pressure:	0.79	bar
Heat of combustion:	44.56	MJ/kg	K-factor:	80.6	L/min√bar
Theoretical THR:	174.68	MJ	Water flow rate:	71.6	L/min
Mass burning rate	15.680	g/s	Measured THR:	174.8	MJ
Theoretical HRR	698.7	kW	Measured avg. HRR:	948.1	kW
			Smoke layer height:	1.6-1.9	m

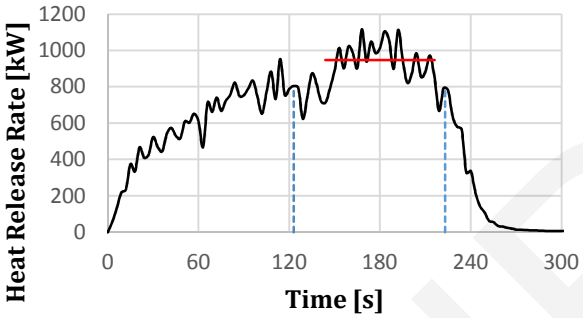

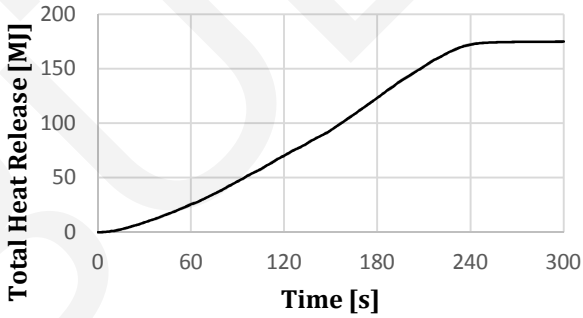

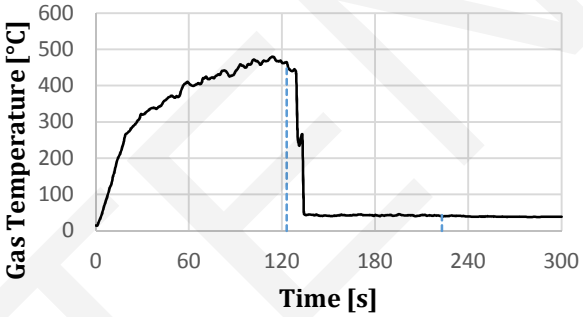

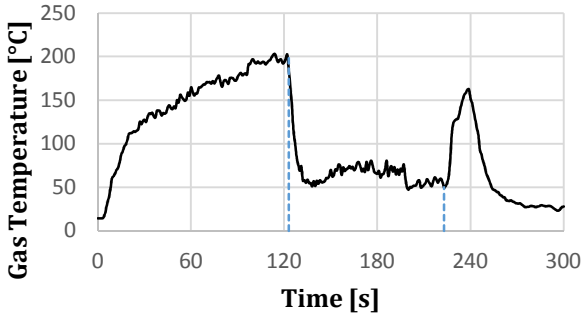

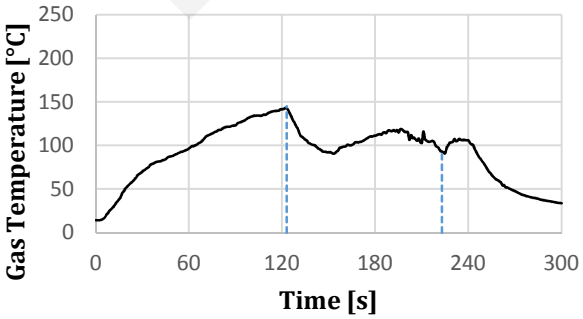

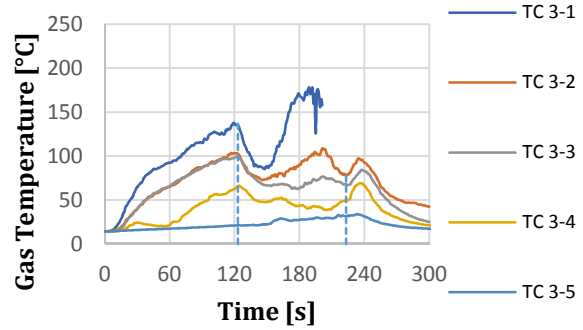

Name experiment:	Sprinkler Heptane 4 (SH4)
Date:	30-3-218
Ambient temperature:	14.3 °C
Fire duration:	250 s

123sec. Sprinkler activated ----
223 sec. Sprinkler deactivated ----

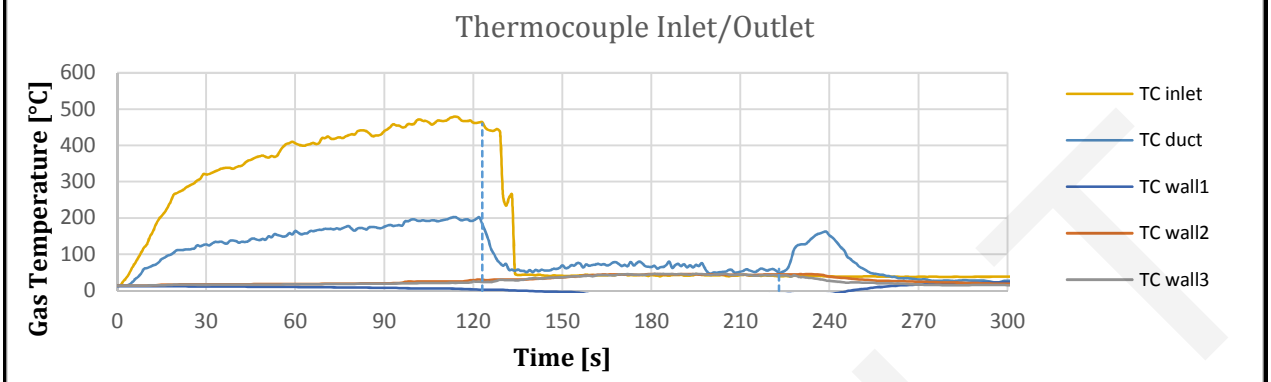

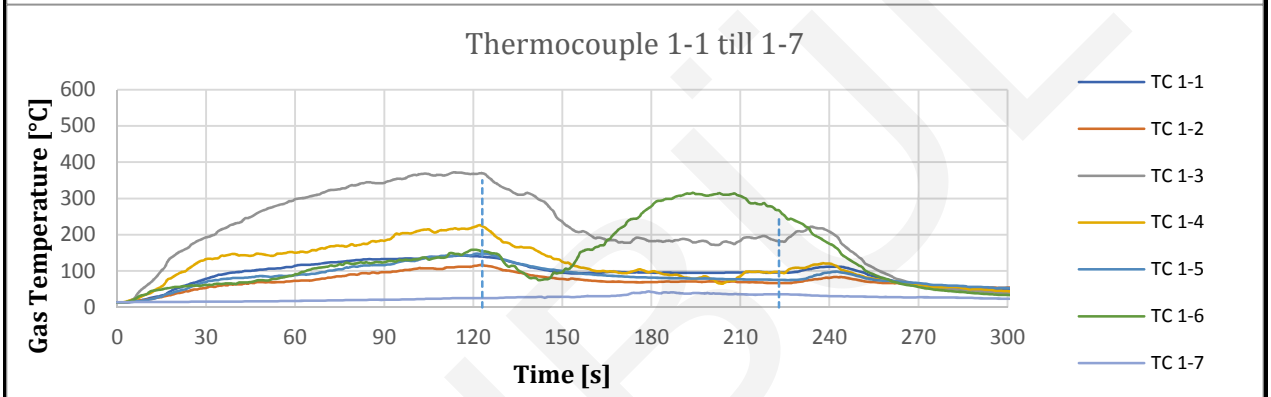

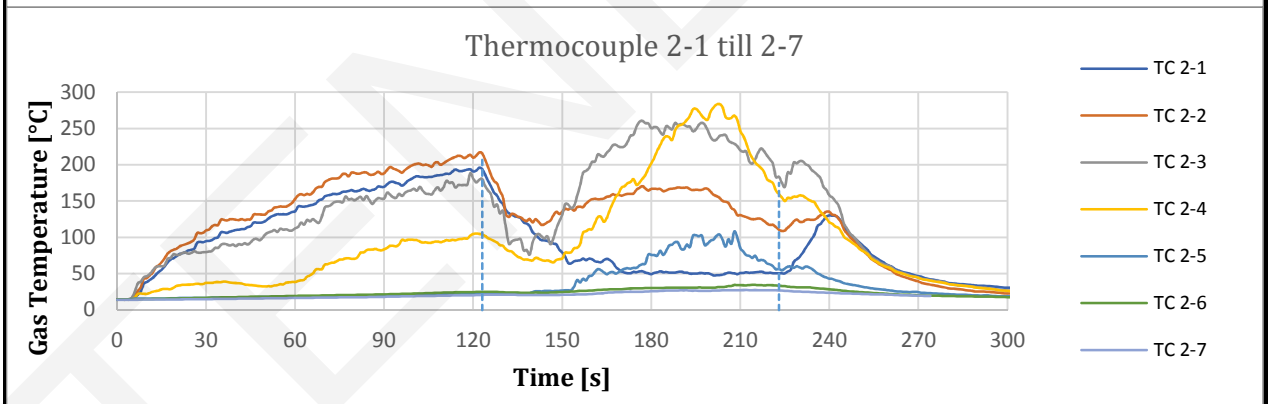

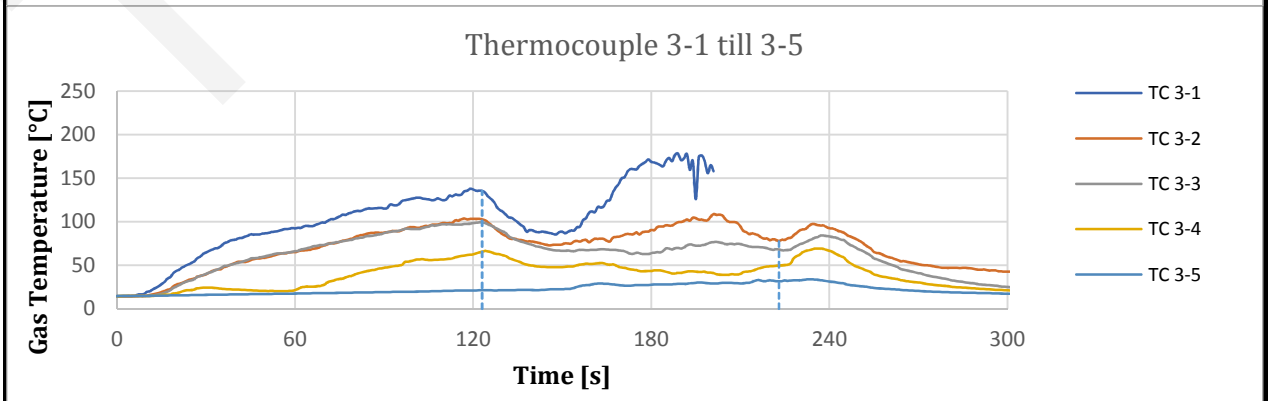

Name experiment:	Sprinkler Heptane 5 (SH5)				
Date:	30-3-2018				
Ambient temperature:	15	°C			
Fire duration:	226	s			
Fuel			**Sprinkler**		
Name:	Heptane		Sprinkler activated at:	121	s
Surface:	0.35	m^2	Sprinkler deactivated at:	221	s
Weight:	4.04	kg	Operating pressure:	1.34	bar
Heat of combustion:	44.56	MJ/kg	K-factor:	80.6	L/min√bar
Theoretical THR:	180.02	MJ	Water flow rate:	93.3	L/min
Mass burning rate	17.876	g/s	Measured THR:	167.3	MJ
Theoretical HRR	796.6	kW	Measured avg. HRR:	915.9	kW
			Smoke layer height:	1.6-1.8	m

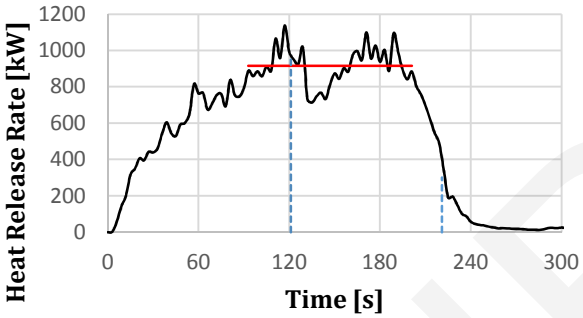

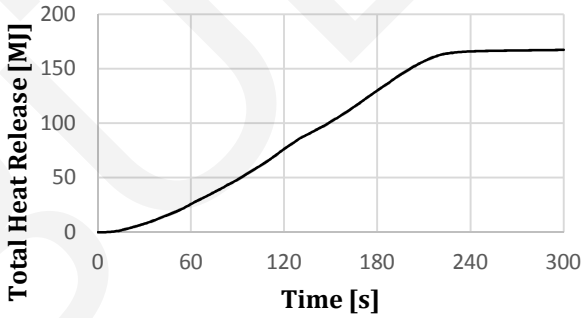

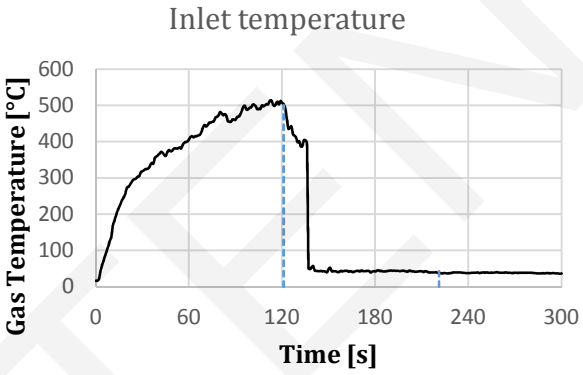

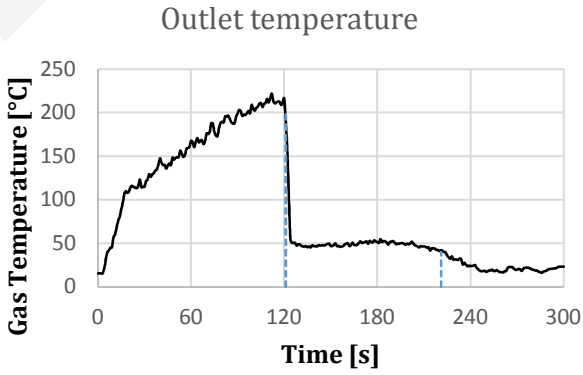

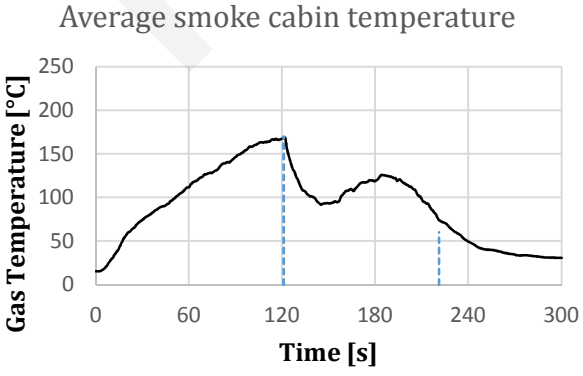

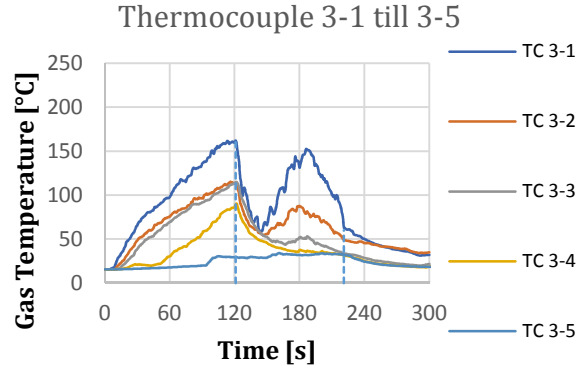

Name experiment:	Sprinkler Heptane 5 (SH5)	
Date:	30-3-2018	
Ambient temperature:	15 °C	
Fire duration:	226 s	121 sec. Sprinkler activated ----
		221sec. Sprinkler deactivated ----

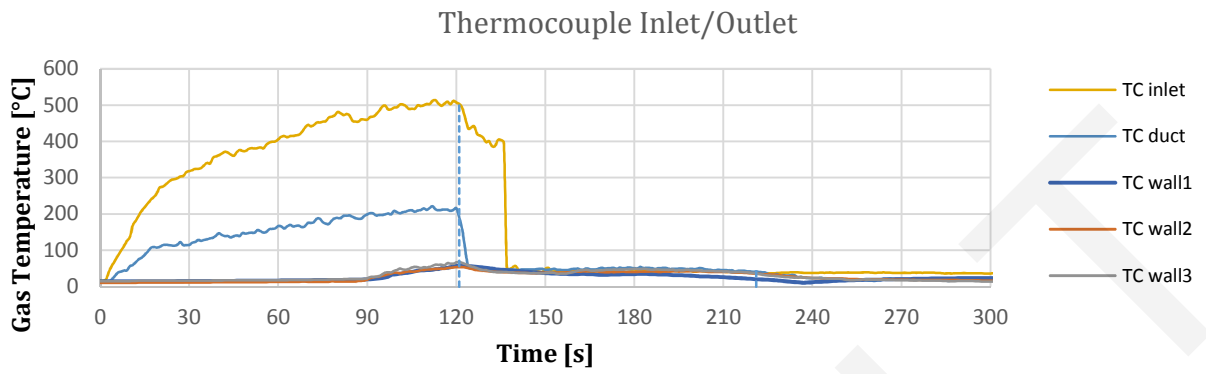

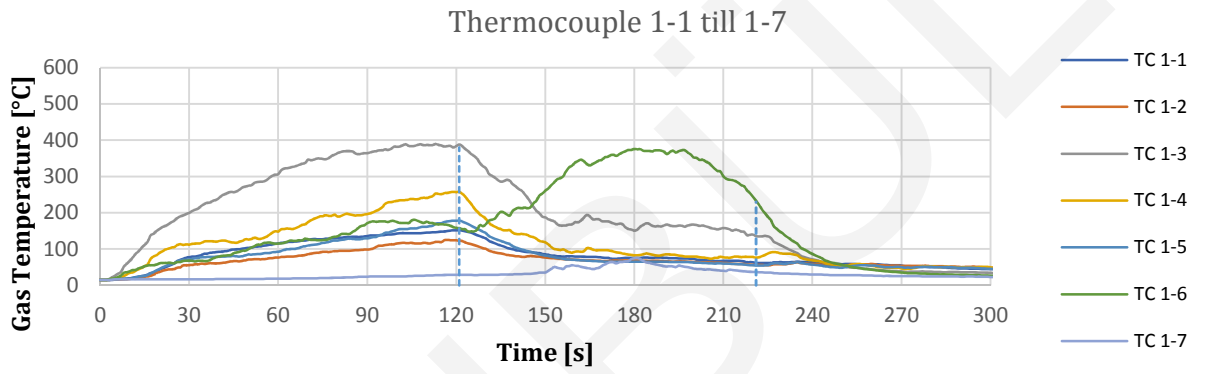

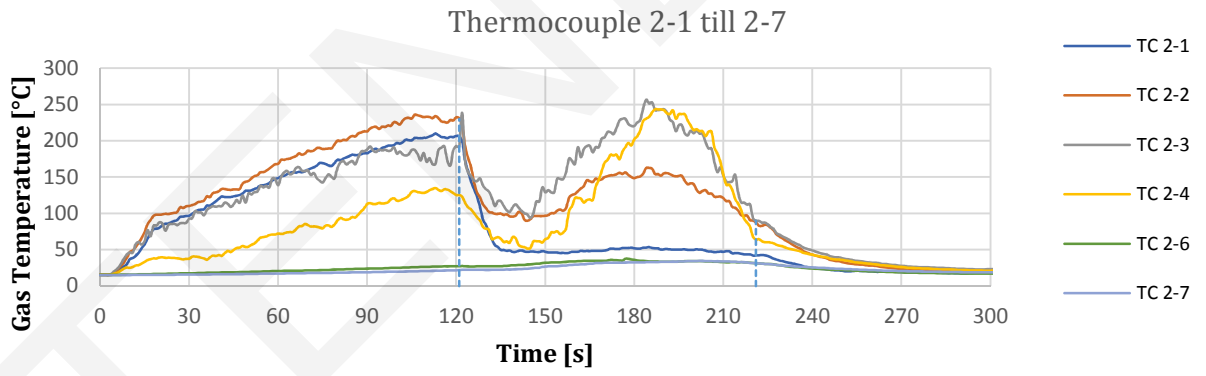

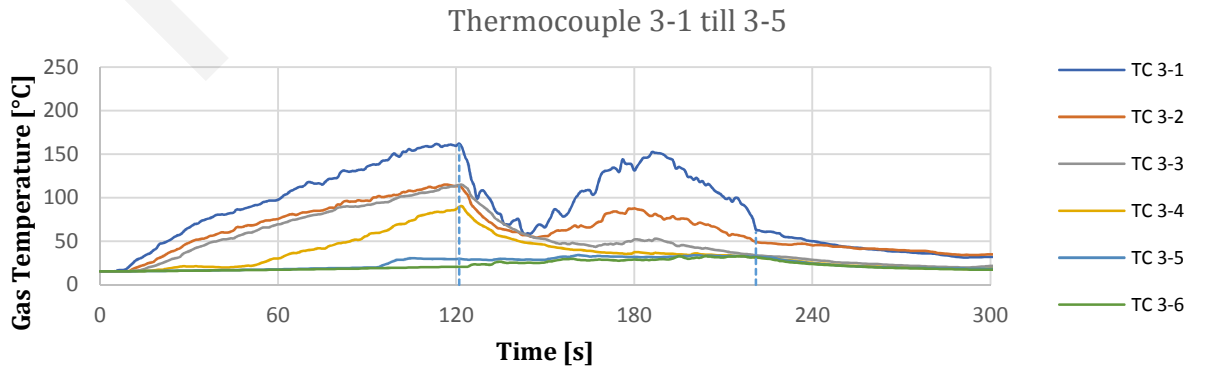

7.12 Smoke logging

Smoke logging was observed visually and smoke layer height was made clear with the rulers where every black bar represents a distance of 10cm. In Figure 1 till Figure 6 snapshots are shown of experiments SH1 and SHT1 at sprinkler activation (t_a=0), after 10 seconds and 30 seconds of sprinkler activation. The operating pressure in both experiments is 0.79 bar. It is expected that the smoke logging effect in SH1 will be larger since the smoke layer temperature at sprinkler activation (±80°C) is lower than during SHT1 (±180°C) with a larger upward buoyant force. At t_a=0 the smoke cabinet is filled with SHT1 and pulsating smoke out of the cabinet, in SH1 this effect does not occur and all smoke is kept in the cabinet. At t_a=10 the bottom of the smoke layer is diffusing in SH1. The diffuse smoke is pushed/pulled down by the water droplet till the ground surface. At t_a=30 the effect can be seen more obvious but the smoke layer remains stable. Small temperature increases were measured at the bottom thermocouples but since ambient air is entrained into the smoke layer this increase is negligible. The spill plume, however, is more affected by the water droplets. In the pictures it is difficult to see but the spill plume is bent down a little when it enters the smoke cabinet. Thereafter, it goes straight-up toward the exhaust, this middle section of the smoke cabinet is also the region with the lowest spray density. Bending of the plume is indicated by the measurement results of TC1-6, TC2-3 and TC2-4, added in Appendix 7 and 8.

For SHT1 different observations were done at t_a=10, here the smoke layer descended approximate 50cm and between the bottom of the smoke layer and the floor smoke is mixed with ambient air. At t_a=30 the smoke layer descended further to approximate 90cm below the smoke cabinet. At approximate 70cm above the floor the smoke layer remains stable. The temperatures measured at the lower thermocouples did not increase much although the smoke layer descended. Bending of the spill plume was also observed in this experiment.

The opposite of the expected events occurred during SH1 and SHT1. Although, the smoke layer temperature of SHT1 was higher smoke logging was more present than during SH1. Possible explanations for this effect are the higher soot yield of SHT1. The smoke layer contains almost twice as much soot particles as in SH1. The soot particles collide with the water droplets and are dragged down by the droplets. After the experiment the 'washed out' soot on the floor was much larger for SHT1 than was experienced after SH1.

SH1

Figure 1 - Snapshot smoke layer height SH1 after 96 seconds, activation of sprinkler

SHT1

Figure 2 - Snapshot smoke layer height SHT1 after 154 seconds, activation of sprinkler

Figure 3 - Snapshot smoke layer height SH1 after 106 seconds, sprinkler active for 10 seconds

Figure 4 - Snapshot smoke layer height SHT1 after 164 seconds, sprinkler active for 10 seconds

Figure 5 - Snapshot smoke layer height SH1 after 126 seconds, sprinkler active for 30 seconds

Figure 6 - Snapshot smoke layer height SHT1 after 184 seconds, sprinkler active for 30 seconds

In Figure 7 till Figure 12 snapshots are shown of the almost identical experiments SH3 and SH5 with an operating pressure of 1.34 bar. Both experiments show similar results, at t_a=10 diffusing of smoke is most clear between thermocouple tree number 3 (right) and the cabinet wall. Here the smoke layer temperature is slightly lower and water droplets have more effect on the buoyancy of the smoke. At t_a=30 the lower volume of the smoke cabinet is filled with diffused smoke. Although, no measurements were done regarding the optical density (OD) and visibility (Z) it can be observed in Figure 12 that the visibility is significantly reduced. The white panels placed in the back are difficult to see, indicating a visibility of 3 meters or less and an optical density of approximate 0.33 (Z=1/OD, grey smoke).

SH3

Figure 7 - Snapshot smoke layer height SH3 after 120 seconds, activation of sprinkler

SH5

Figure 8 - Snapshot smoke layer height SH5 after 121 seconds, activation of sprinkler

Figure 9 - Snapshot smoke layer height SH3 after 130 seconds, sprinkler active for 10 seconds

Figure 10 - Snapshot smoke layer height SH5 after 131 seconds, sprinkler active for 10 seconds

Figure 11 - Snapshot smoke layer height SH3 after 150 seconds, sprinkler active for 30 seconds

Figure 12 - Snapshot smoke layer height SH5 after 151 seconds, sprinkler active for 30 seconds

In Figure 13 till Figure 18 snapshots are shown of the two remaining sprinkler experiments SH2 and SH4. For experiment SH2 with an operating pressure of 0.40 bar no smoke descend or diffusing can be observed. During the experiment little diffusing was observed at the opposite site of the burner cabinet. A downward, turbulent flow could be observed which redirected upward within 1 meter. The results of SH4 are not very different from SH1, which also was performed with a sprinkler pressure of 0.79 bar.

SH2

Figure 13 - Snapshot smoke layer height SH2 after 118 seconds, activation of sprinkler

SH4

Figure 14 - Snapshot smoke layer height SH4 after 123 seconds, activation of sprinkler

Figure 15 - Snapshot smoke layer height SH2 after 128 seconds, sprinkler active for 10 seconds

Figure 16 - Snapshot smoke layer height SH4 after 133 seconds, sprinkler active for 10 seconds

Figure 17 - Snapshot smoke layer height SH2 after 148 seconds, sprinkler active for 30 seconds

Figure 18 - Snapshot smoke layer height SH4 after 153 seconds, sprinkler active for 30 seconds

Appendix 8 – FDS results

The number of thermocouples can differ per experiment. In the course of time multiple thermocouples have been added to the measurements and therefore also to the FDS models.

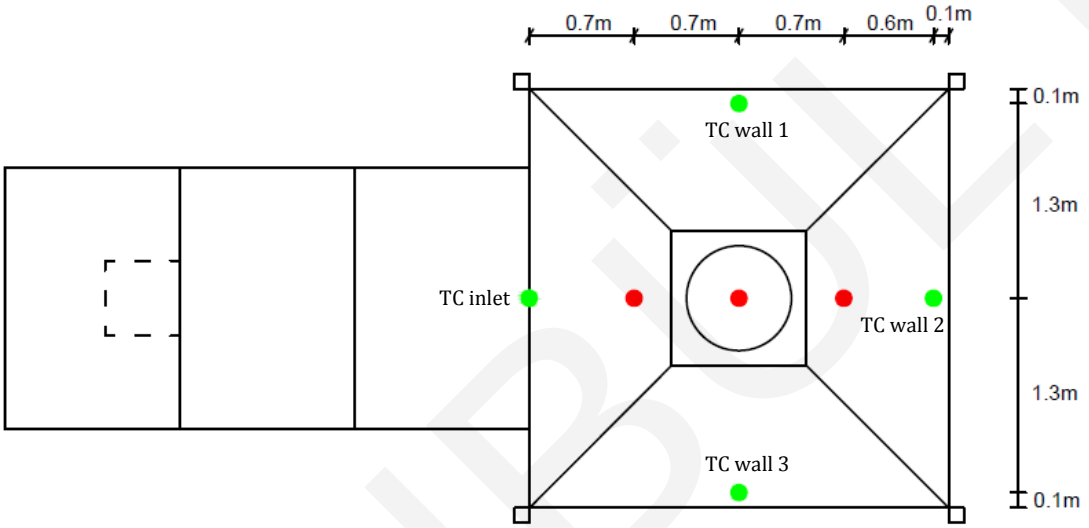

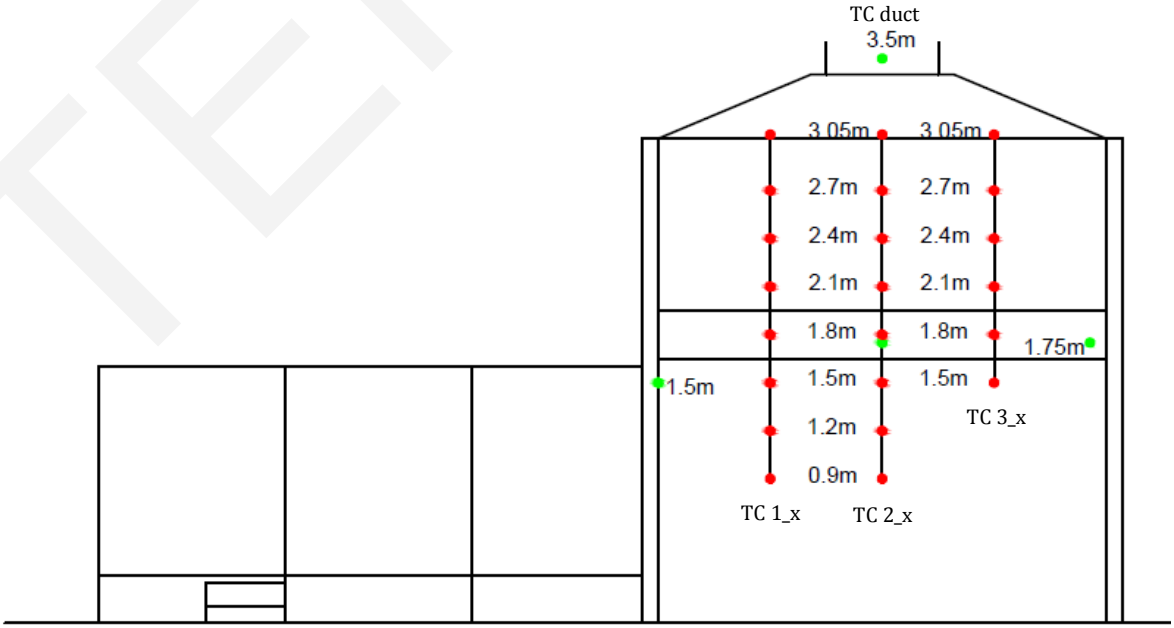

RH0 - Thermocouple Data

Date experiment: 22-8-2018

Sprinkler activation irrelevant
Sprinkler deactivation irrelevant
Operating pressure: irrelevant

Fire duration: 383 seconds

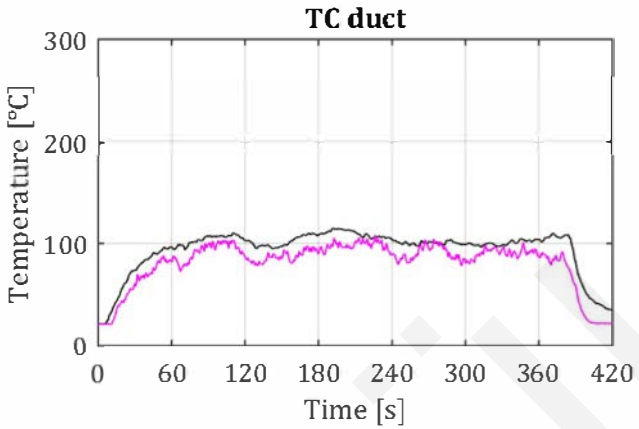

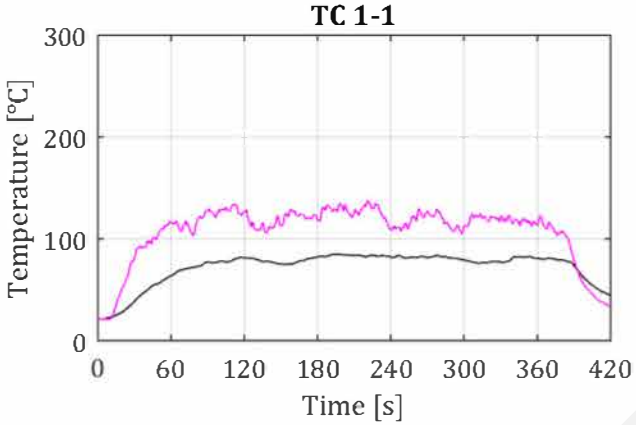

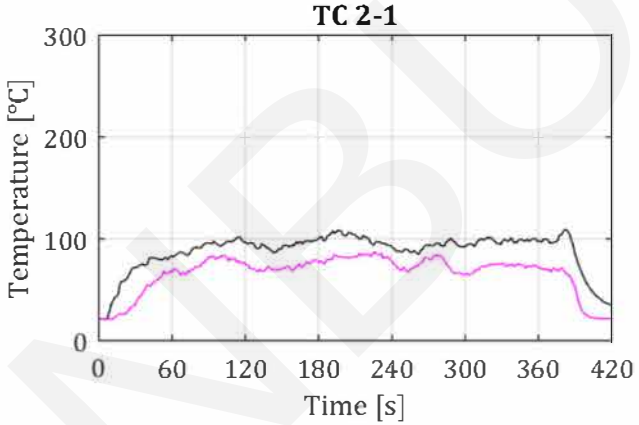

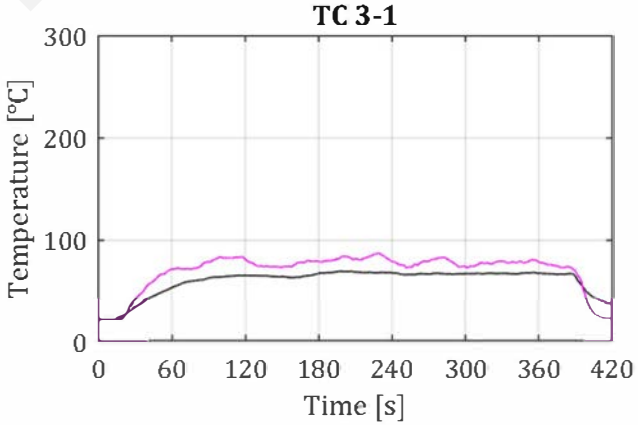

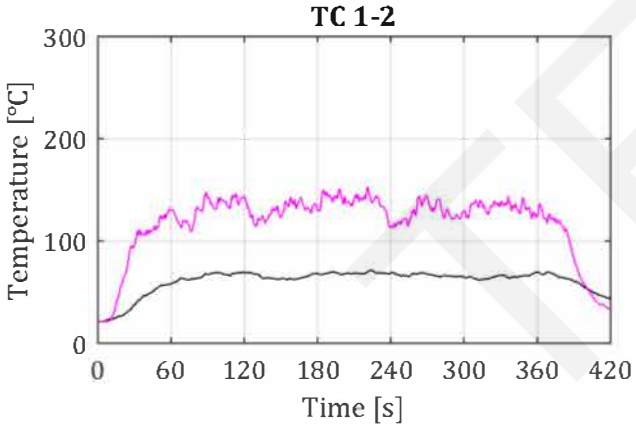

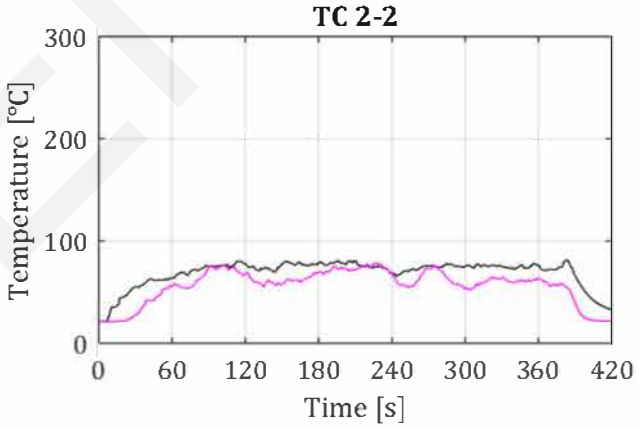

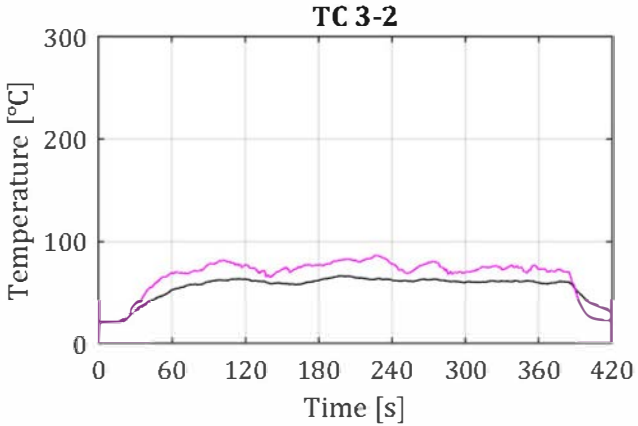

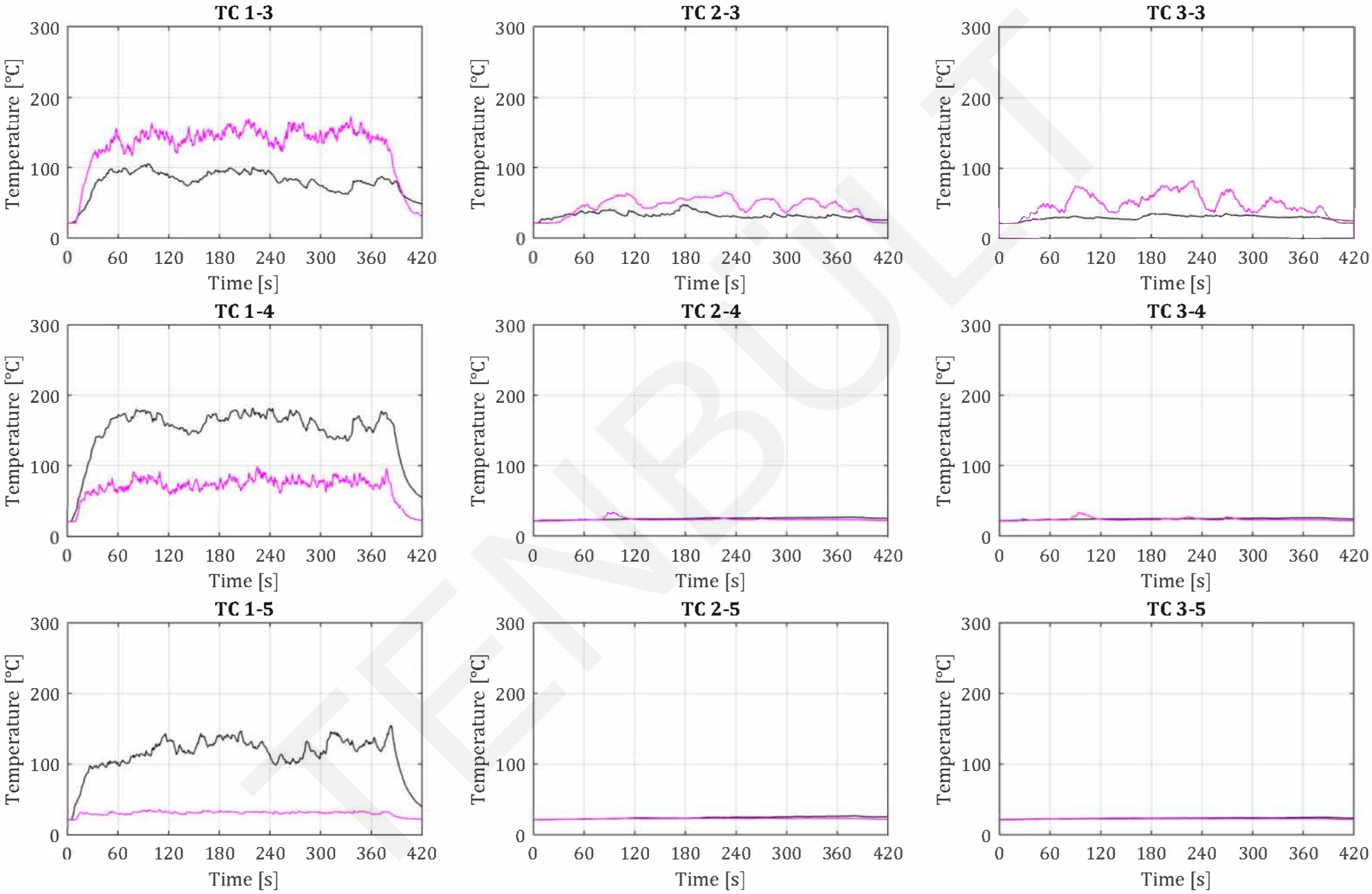
TC 1-3
TC 2-3
TC 3-3
TC 1-4
TC 2-4
TC 3-4
TC 1-5
TC 2-5
TC 3-5
Temperature [°C]
Time [s]
0
100
200
300
0
60
120
180
240
300
360
420

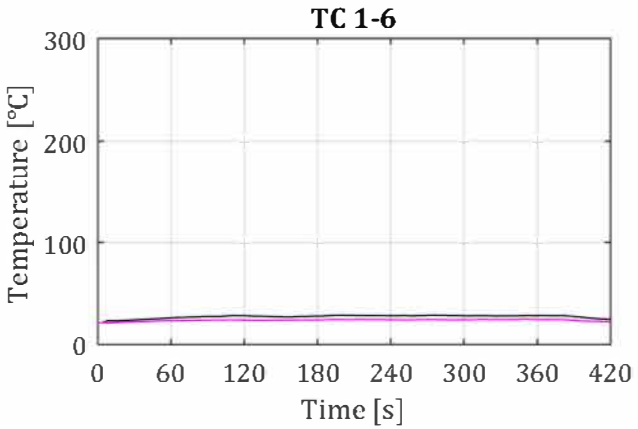
TC 1-6
Temperature [°C]
Time [s]
0
100
200
300
0
60
120
180
240
300
360
420

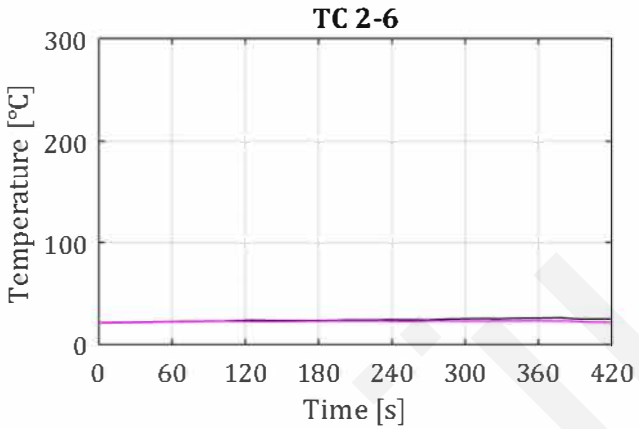
TC 2-6
Temperature [°C]
Time [s]
0
100
200
300
0
60
120
180
240
300
360
420

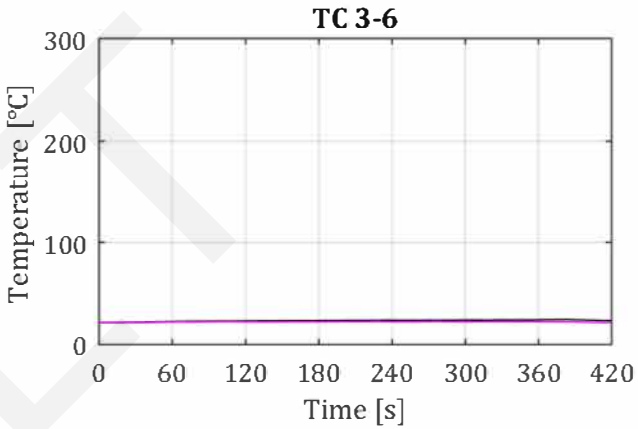
TC 3-6
Temperature [°C]
Time [s]
0
100
200
300
0
60
120
180
240
300
360
420

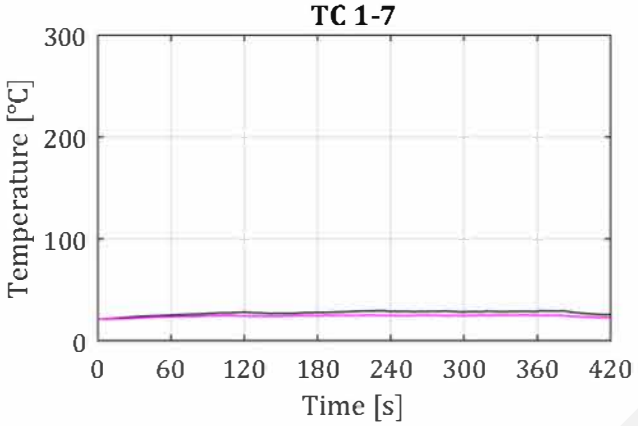
TC 1-7
Temperature [°C]
Time [s]
0
100
200
300
0
60
120
180
240
300
360
420

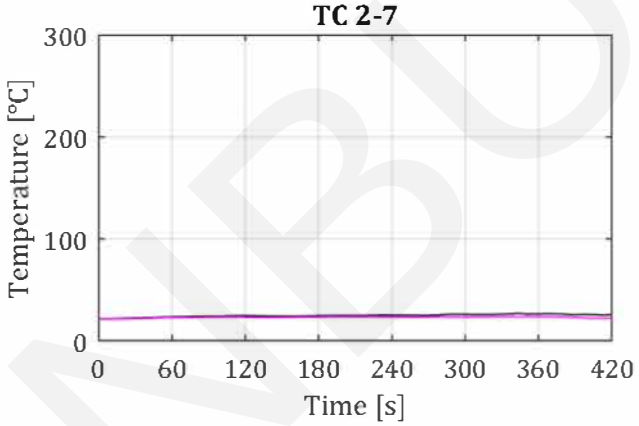
TC 2-7
Temperature [°C]
Time [s]
0
100
200
300
0
60
120
180
240
300
360
420

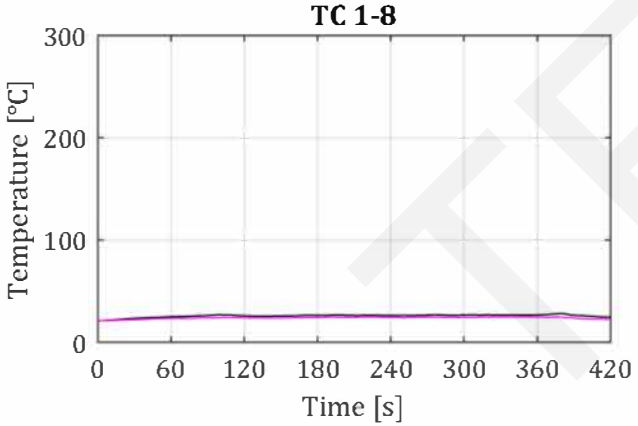
TC 1-8
Temperature [°C]
Time [s]
0
100
200
300
0
60
120
180
240
300
360
420

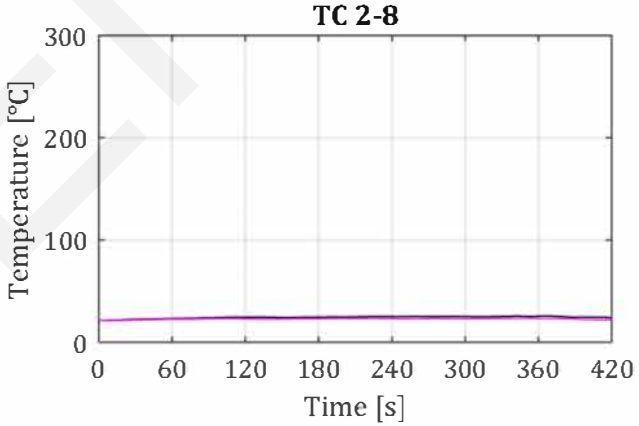
TC 2-8
Temperature [°C]
Time [s]
0
100
200
300
0
60
120
180
240
300
360
420

RH1 - Thermocouple Data

Date experiment: 29-8-2018

Sprinkler activation irrelevant
Sprinkler deactivation irrelevant
Operating pressure: irrelevant

Fire duration: 189 seconds

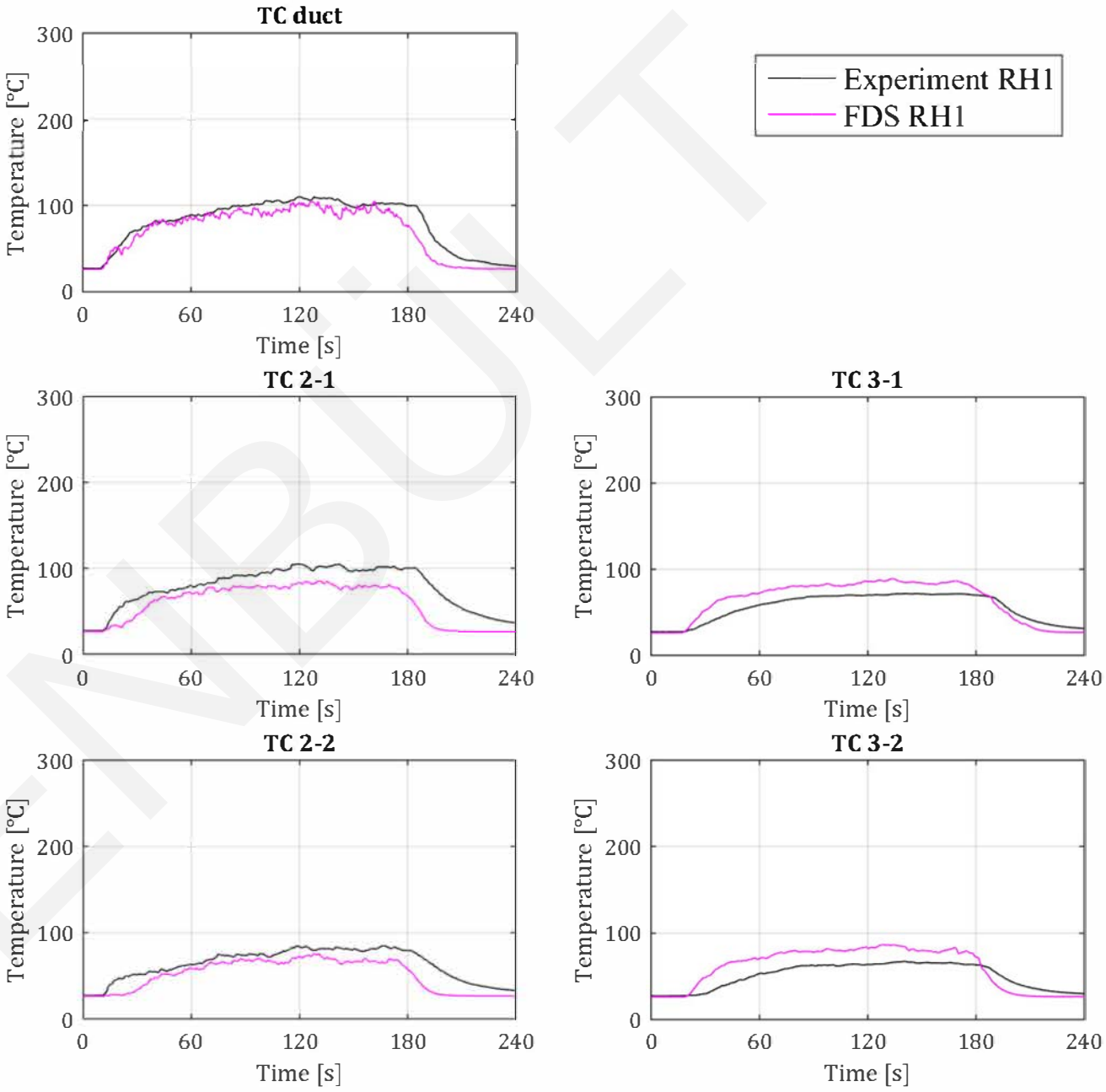

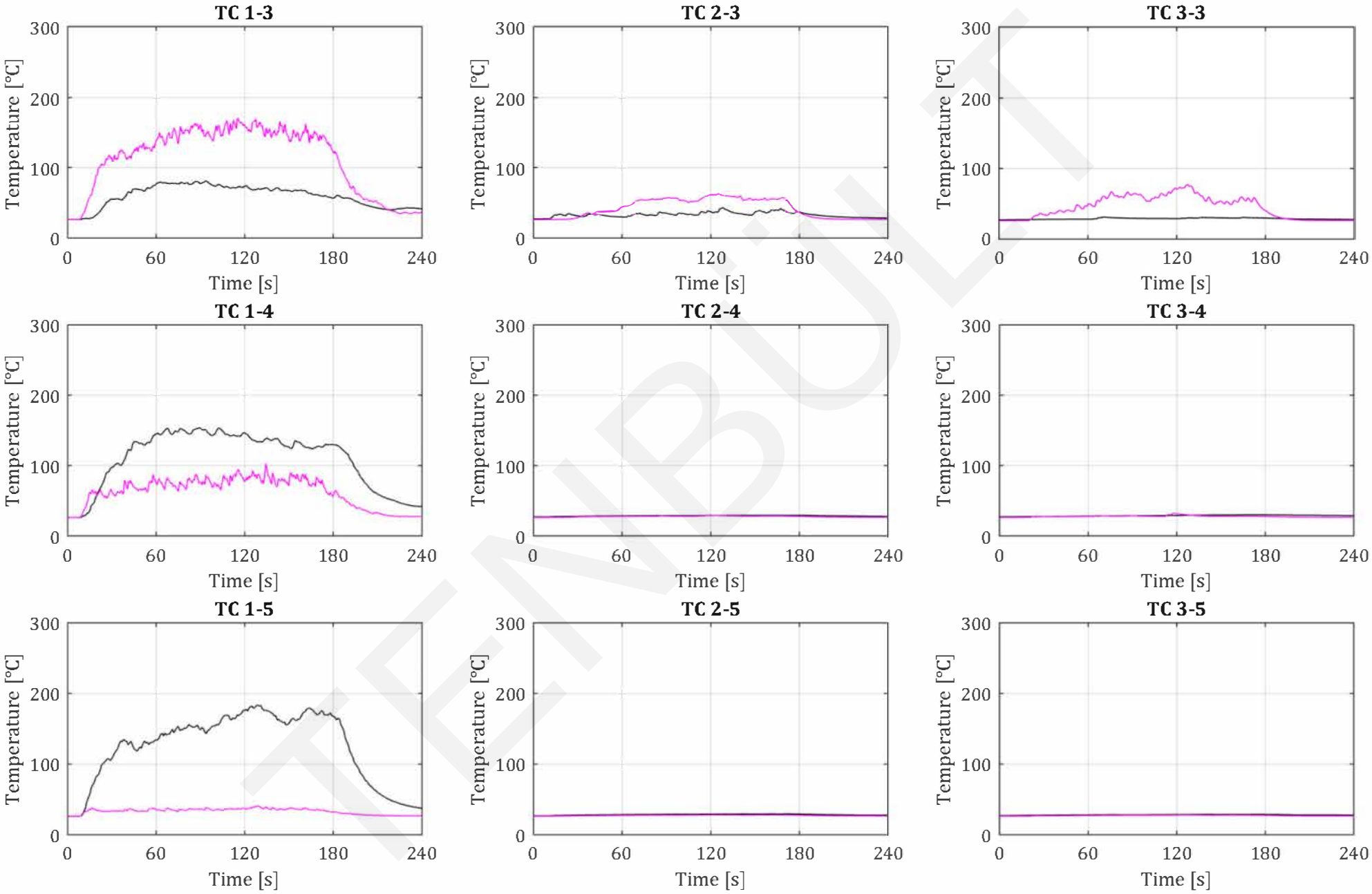
TC 1-3
TC 2-3
TC 3-3
TC 1-4
TC 2-4
TC 3-4
TC 1-5
TC 2-5
TC 3-5
Temperature [°C]
Time [s]
0
100
200
300
0
60
120
180
240

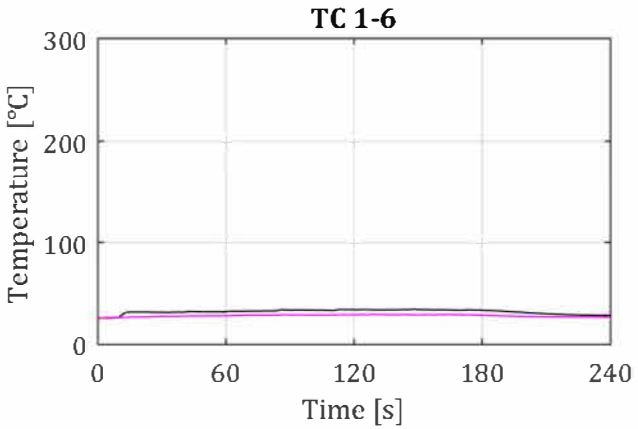
TC 1-6
Temperature [°C]
Time [s]
0
100
200
300
0
60
120
180
240

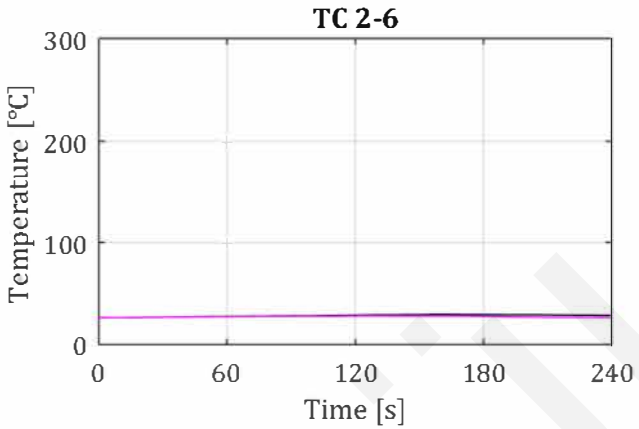
TC 2-6
Temperature [°C]
Time [s]
0
100
200
300
0
60
120
180
240

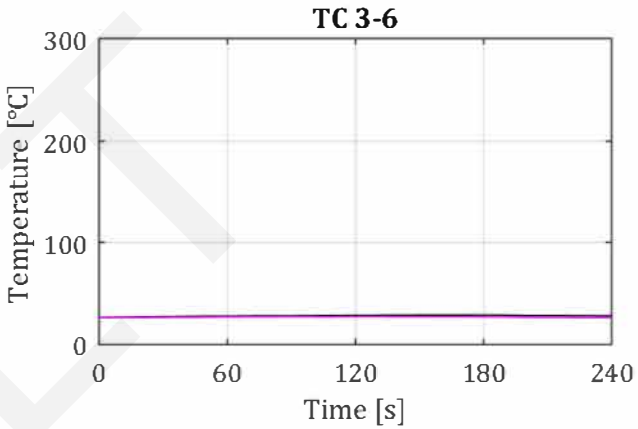
TC 3-6
Temperature [°C]
Time [s]
0
100
200
300
0
60
120
180
240

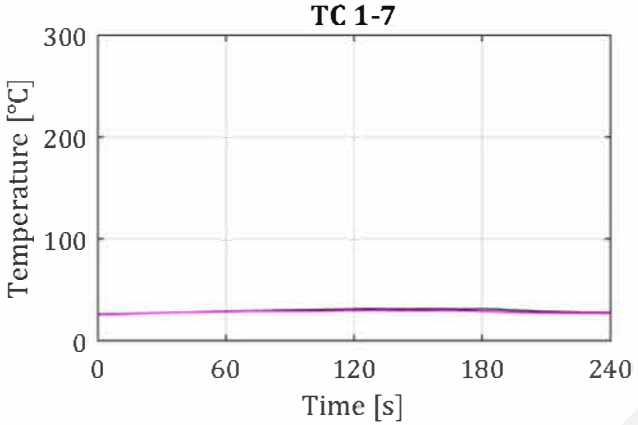
TC 1-7
Temperature [°C]
Time [s]
0
100
200
300
0
60
120
180
240

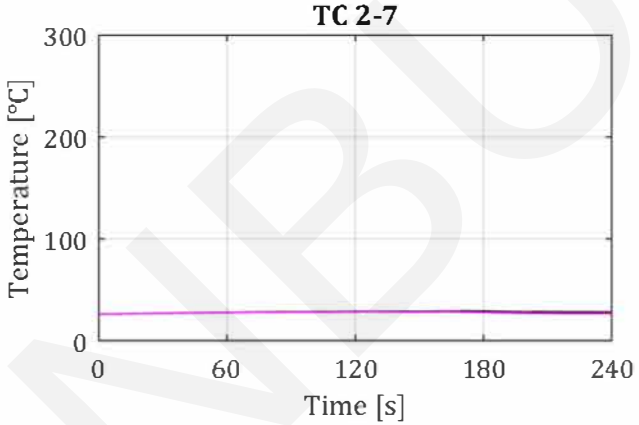
TC 2-7
Temperature [°C]
Time [s]
0
100
200
300
0
60
120
180
240

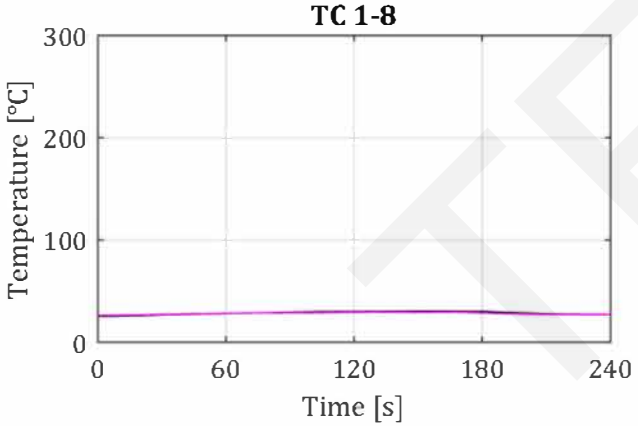
TC 1-8
Temperature [°C]
Time [s]
0
100
200
300
0
60
120
180
240

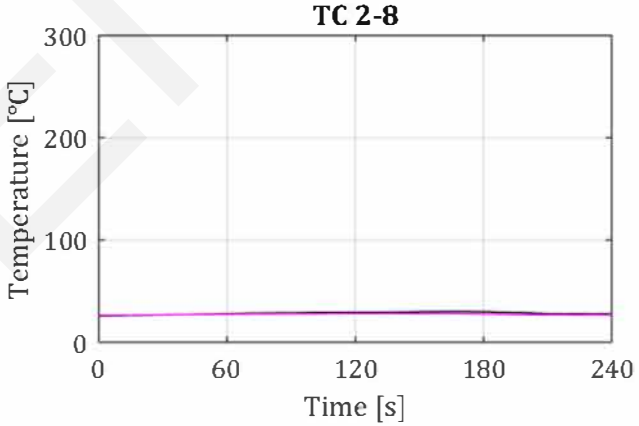
TC 2-8
Temperature [°C]
Time [s]
0
100
200
300
0
60
120
180
240

RHT2 - Thermocouple Data

Date experiment: 2-2-2018

Sprinkler activation: irrelevant
Sprinkler deactivation: irrelevant
Operating pressure: irrelevant

Fire duration: 232 seconds

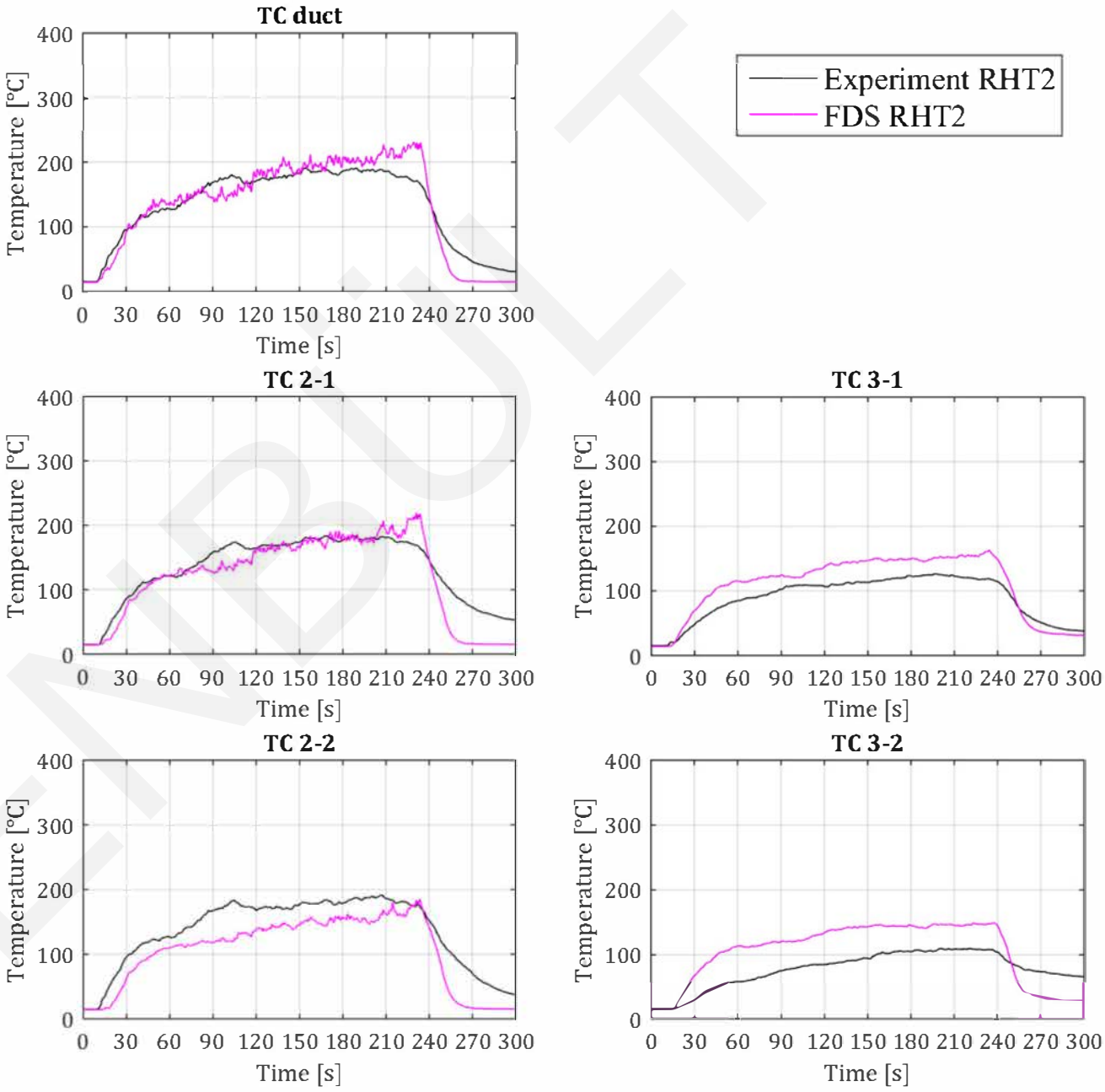

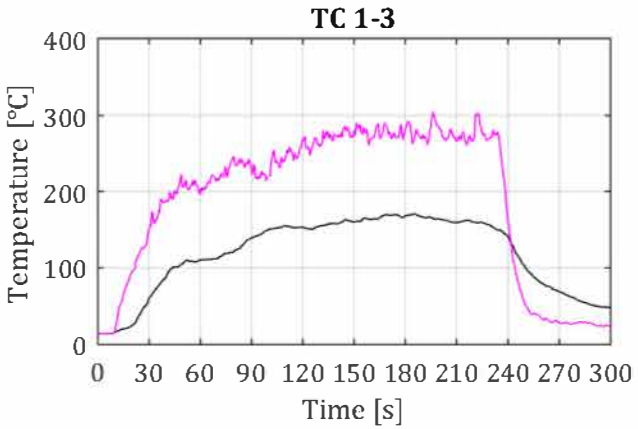
TC 1-3
Temperature [°C]
Time [s]
0
100
200
300
400
0 30 60 90 120 150 180 210 240 270 300

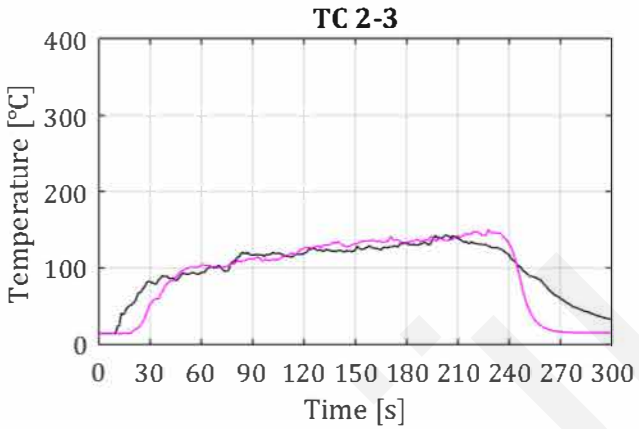
TC 2-3
Temperature [°C]
Time [s]
0
100
200
300
400
0 30 60 90 120 150 180 210 240 270 300

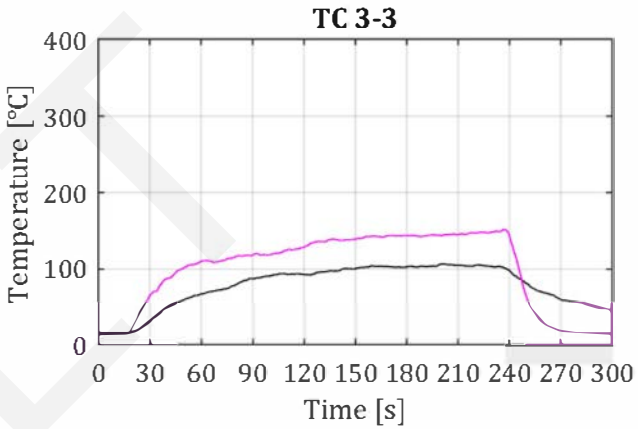
TC 3-3
Temperature [°C]
Time [s]
0
100
200
300
400
0 30 60 90 120 150 180 210 240 270 300

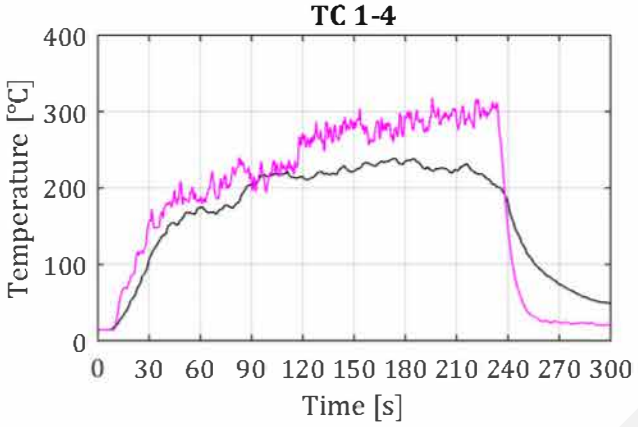
TC 1-4
Temperature [°C]
Time [s]
0
100
200
300
400
0 30 60 90 120 150 180 210 240 270 300

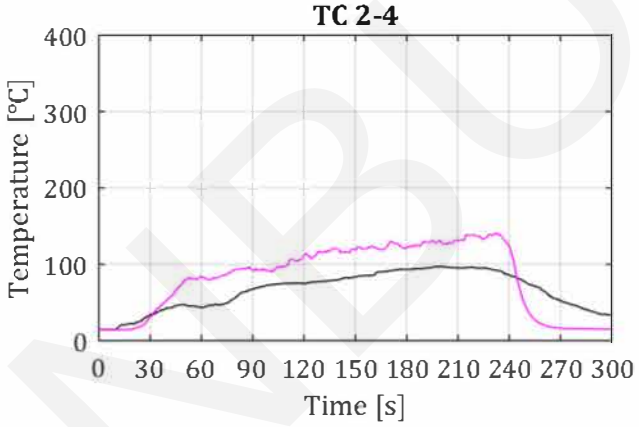
TC 2-4
Temperature [°C]
Time [s]
0
100
200
300
400
0 30 60 90 120 150 180 210 240 270 300

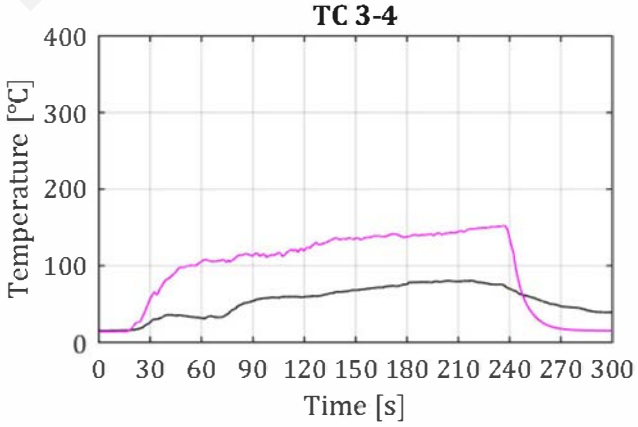
TC 3-4
Temperature [°C]
Time [s]
0
100
200
300
400
0 30 60 90 120 150 180 210 240 270 300

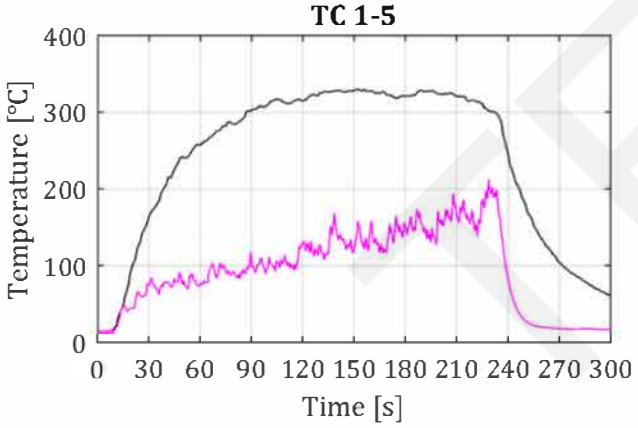
TC 1-5
Temperature [°C]
Time [s]
0
100
200
300
400
0 30 60 90 120 150 180 210 240 270 300

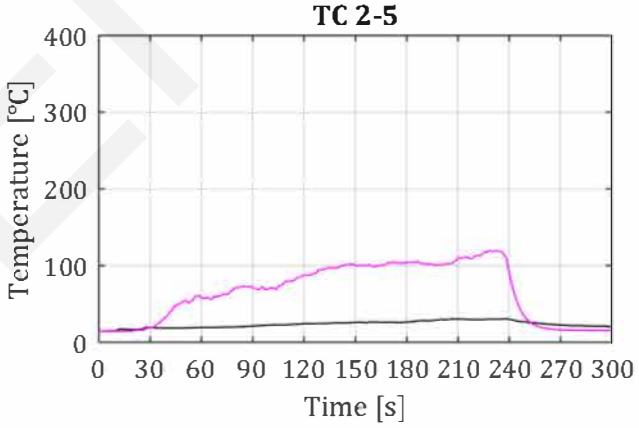
TC 2-5
Temperature [°C]
Time [s]
0
100
200
300
400
0 30 60 90 120 150 180 210 240 270 300

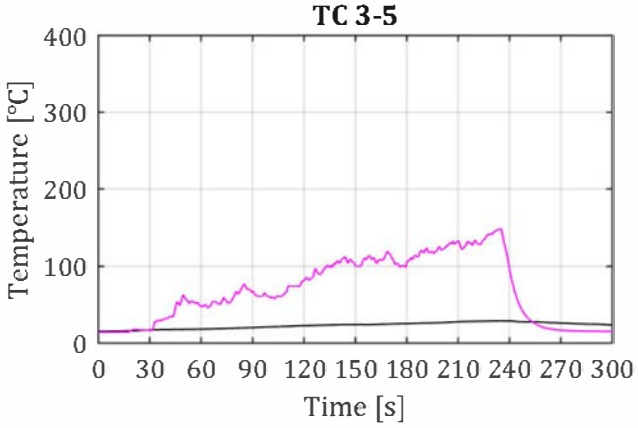
TC 3-5
Temperature [°C]
Time [s]
0
100
200
300
400
0 30 60 90 120 150 180 210 240 270 300

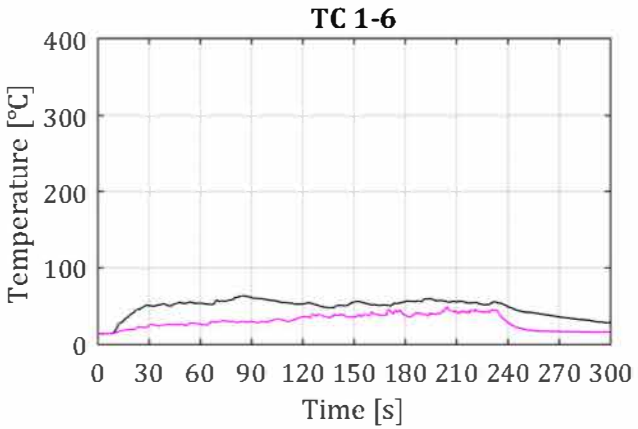
TC 1-6
Temperature [°C]
0
100
200
300
400
0 30 60 90 120 150 180 210 240 270 300
Time [s]

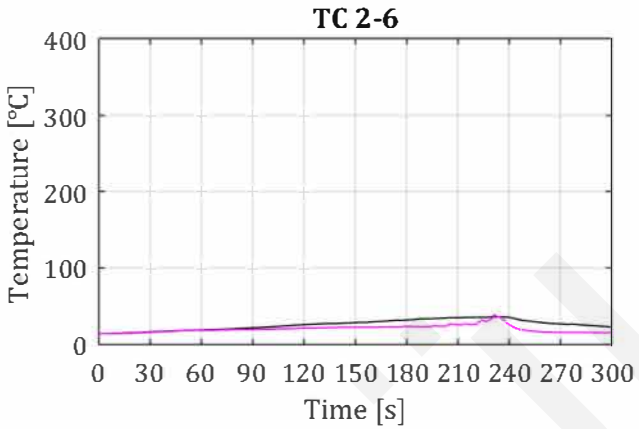
TC 2-6
Temperature [°C]
0
100
200
300
400
0 30 60 90 120 150 180 210 240 270 300
Time [s]

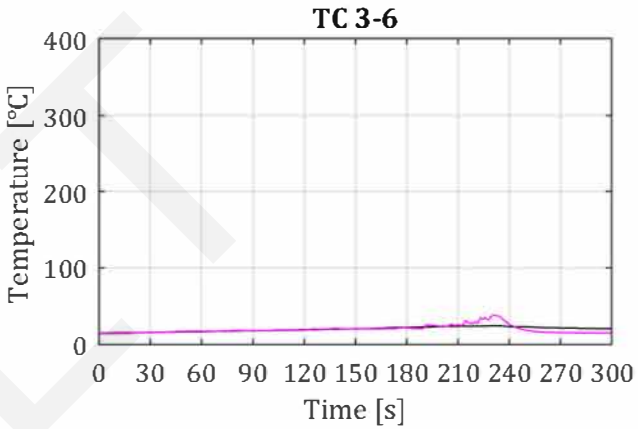
TC 3-6
Temperature [°C]
0
100
200
300
400
0 30 60 90 120 150 180 210 240 270 300
Time [s]

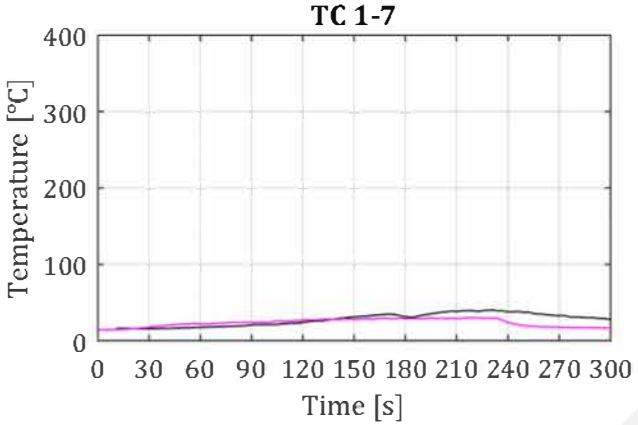
TC 1-7
Temperature [°C]
0
100
200
300
400
0 30 60 90 120 150 180 210 240 270 300
Time [s]

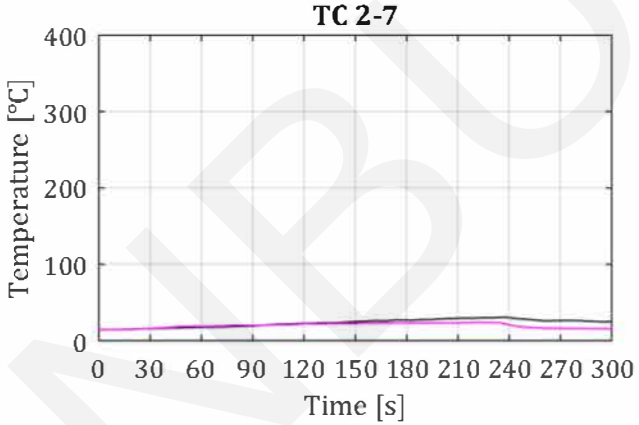
TC 2-7
Temperature [°C]
0
100
200
300
400
0 30 60 90 120 150 180 210 240 270 300
Time [s]

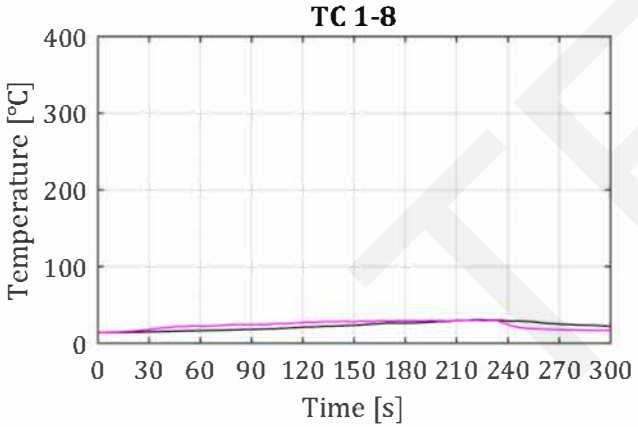
TC 1-8
Temperature [°C]
0
100
200
300
400
0 30 60 90 120 150 180 210 240 270 300
Time [s]

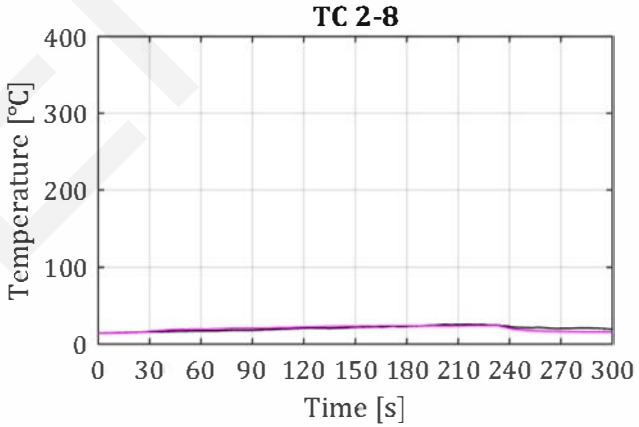
TC 2-8
Temperature [°C]
0
100
200
300
400
0 30 60 90 120 150 180 210 240 270 300
Time [s]

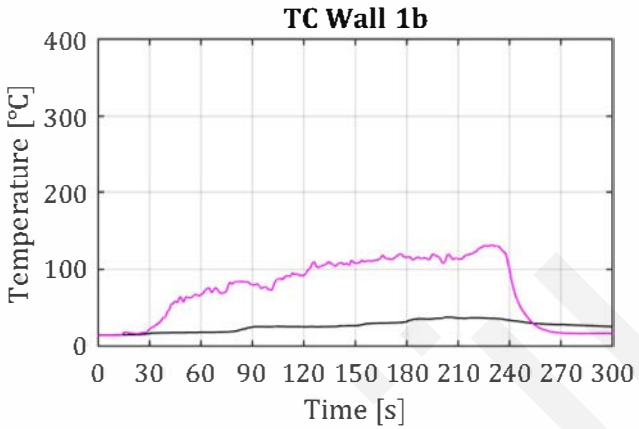
TC Wall 1b
Temperature [°C]
0
100
200
300
400
0 30 60 90 120 150 180 210 240 270 300
Time [s]

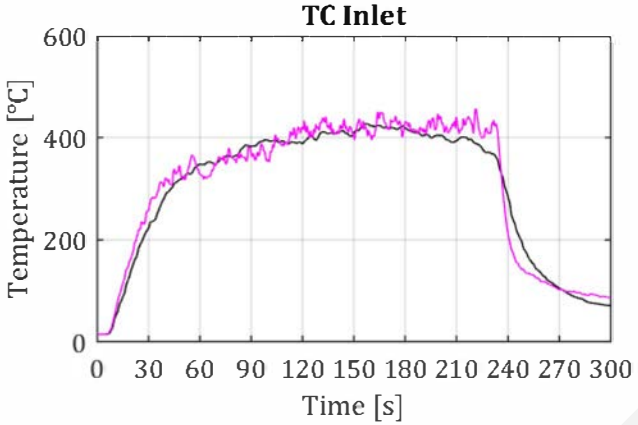
TC Inlet
Temperature [°C]
0
200
400
600
0 30 60 90 120 150 180 210 240 270 300
Time [s]

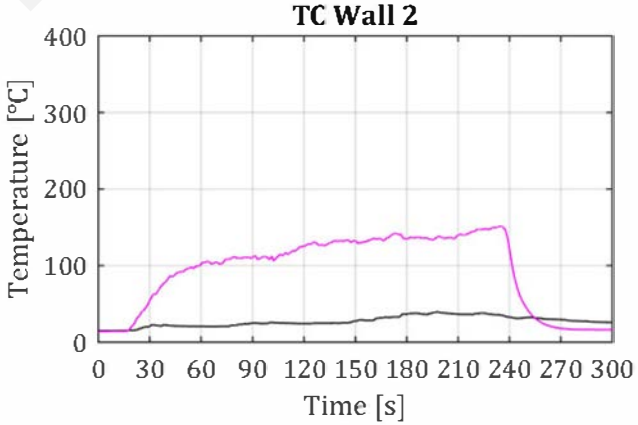
TC Wall 2
Temperature [°C]
0
100
200
300
400
0 30 60 90 120 150 180 210 240 270 300
Time [s]

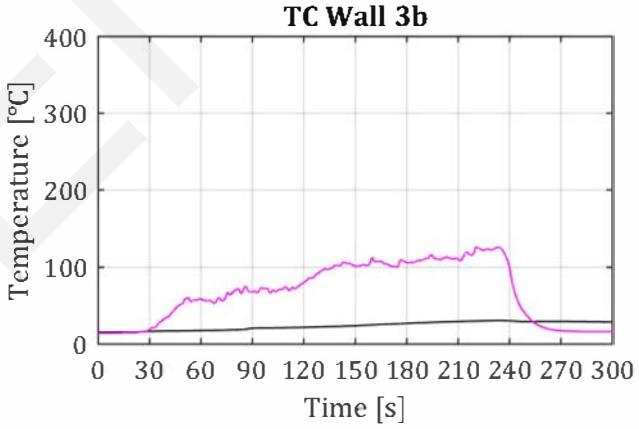
TC Wall 3b
Temperature [°C]
0
100
200
300
400
0 30 60 90 120 150 180 210 240 270 300
Time [s]

SH2 - Thermocouple Data

Date experiment: 7-3-2018

Sprinkler activation at 118 seconds
Sprinkler deactivation at 223 seconds
Operating pressure: 0.40 bar

Fire duration: 290 seconds

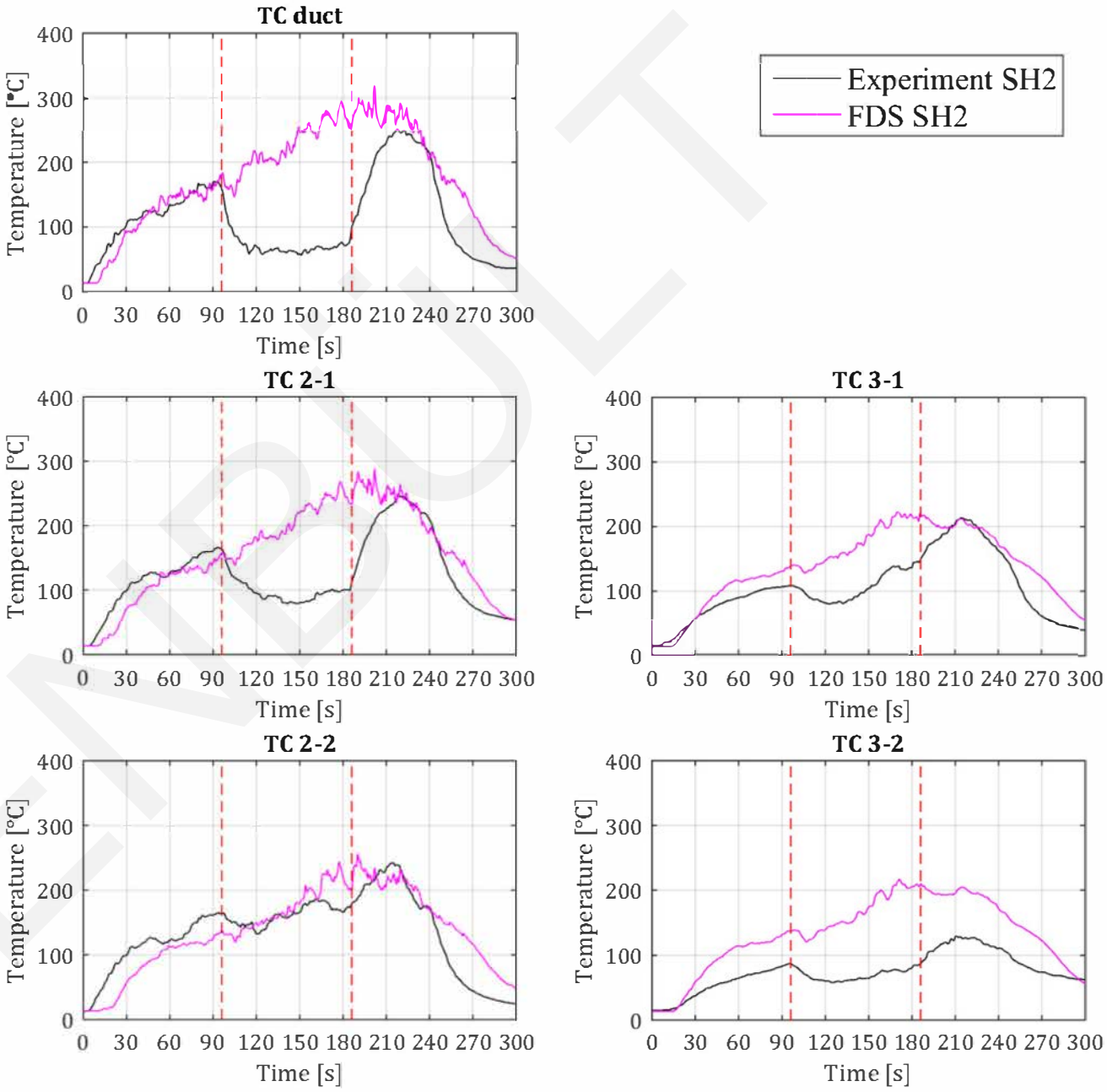

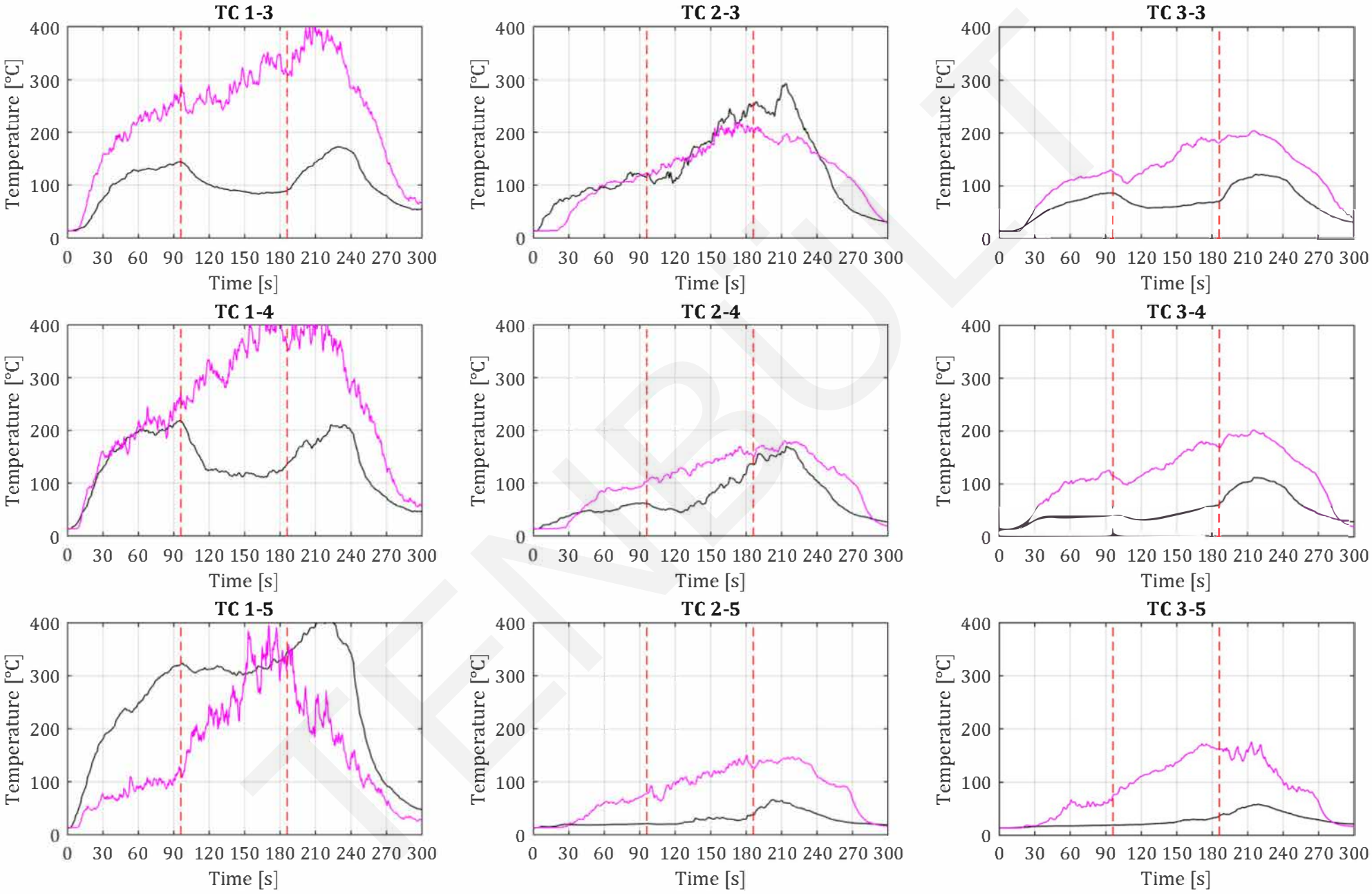
TC 1-3
TC 2-3
TC 3-3
TC 1-4
TC 2-4
TC 3-4
TC 1-5
TC 2-5
TC 3-5
Temperature [°C]
Time [s]
0
100
200
300
400
0 30 60 90 120 150 180 210 240 270 300

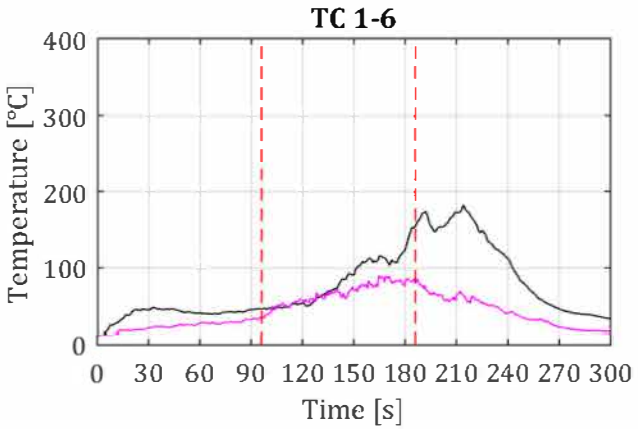
TC 1-6
Temperature [°C]
Time [s]
0
100
200
300
400
0 30 60 90 120 150 180 210 240 270 300

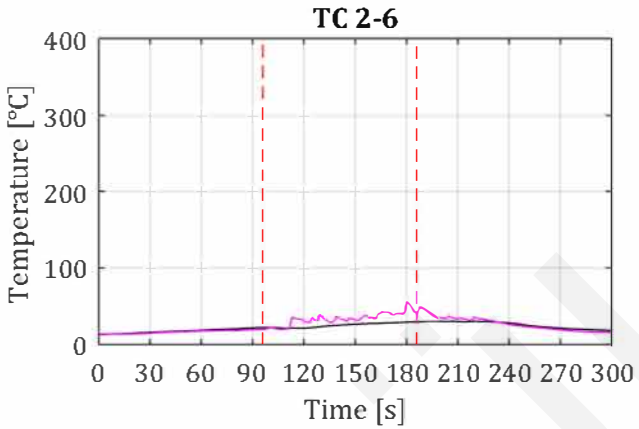
TC 2-6
Temperature [°C]
Time [s]
0
100
200
300
400
0 30 60 90 120 150 180 210 240 270 300

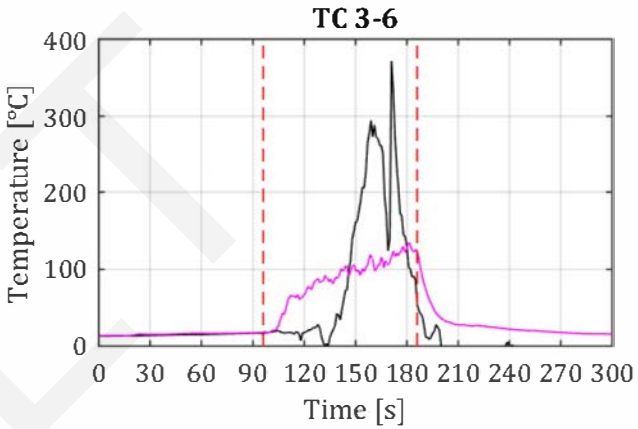
TC 3-6
Temperature [°C]
Time [s]
0
100
200
300
400
0 30 60 90 120 150 180 210 240 270 300

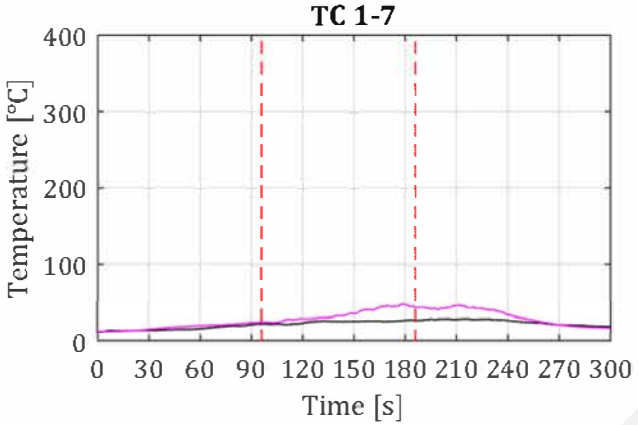
TC 1-7
Temperature [°C]
Time [s]
0
100
200
300
400
0 30 60 90 120 150 180 210 240 270 300

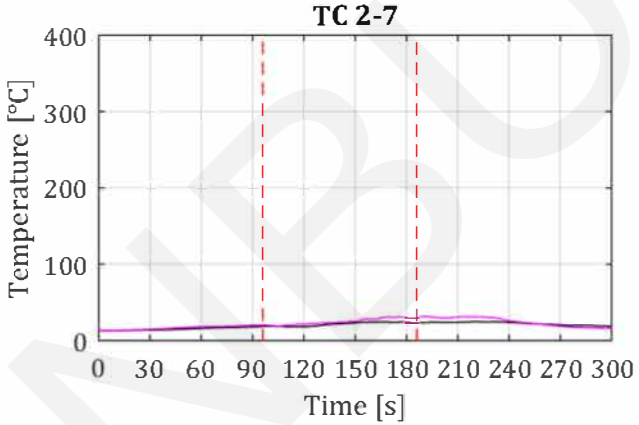
TC 2-7
Temperature [°C]
Time [s]
0
100
200
300
400
0 30 60 90 120 150 180 210 240 270 300

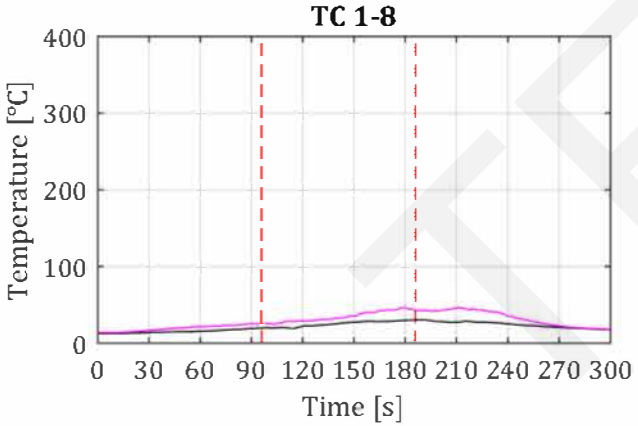
TC 1-8
Temperature [°C]
Time [s]
0
100
200
300
400
0 30 60 90 120 150 180 210 240 270 300

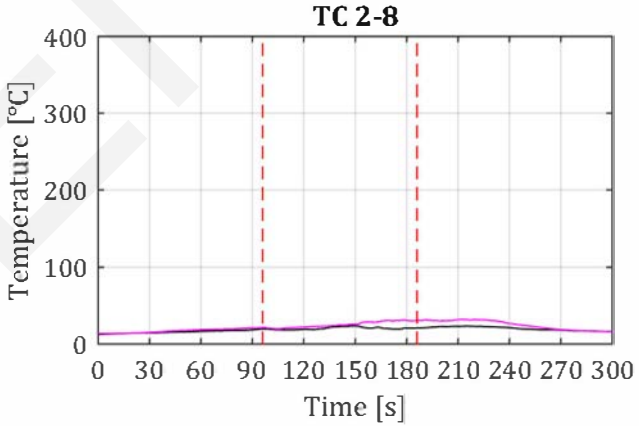
TC 2-8
Temperature [°C]
Time [s]
0
100
200
300
400
0 30 60 90 120 150 180 210 240 270 300

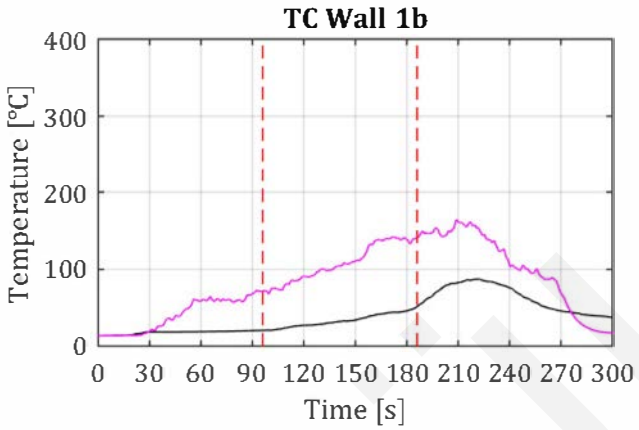
TC Wall 1b
Temperature [°C]
0
100
200
300
400
0 30 60 90 120 150 180 210 240 270 300
Time [s]

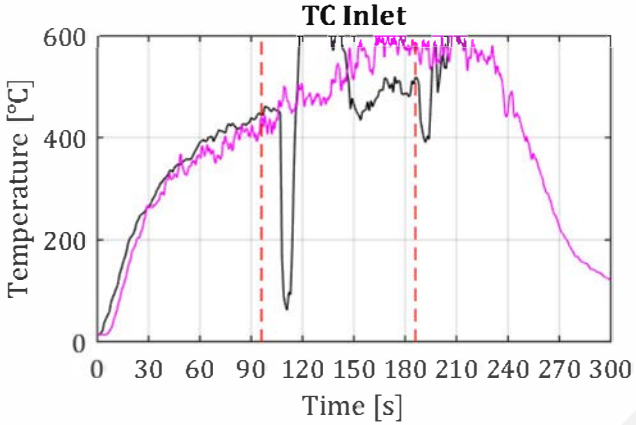
TC Inlet
Temperature [°C]
0
200
400
600
0 30 60 90 120 150 180 210 240 270 300
Time [s]

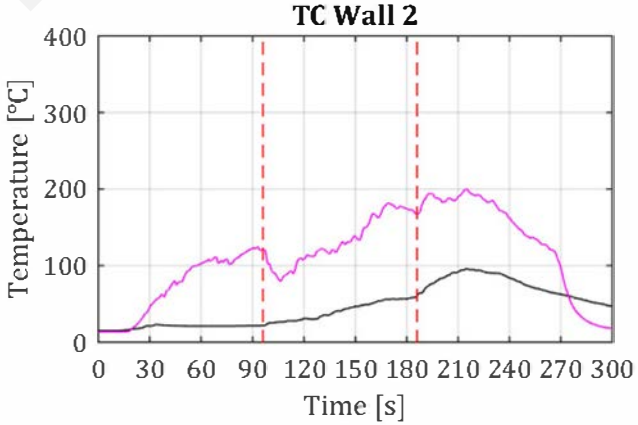
TC Wall 2
Temperature [°C]
0
100
200
300
400
0 30 60 90 120 150 180 210 240 270 300
Time [s]

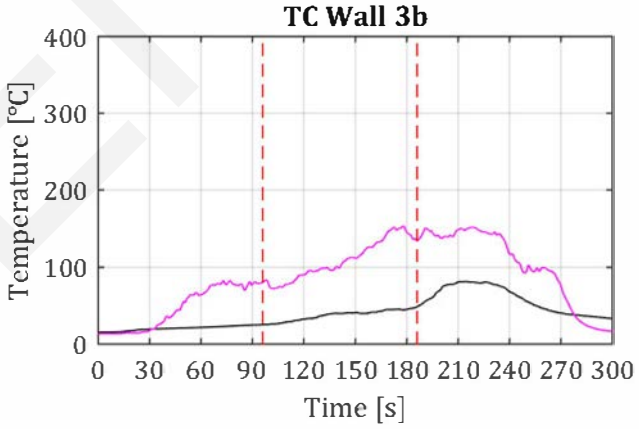
TC Wall 3b
Temperature [°C]
0
100
200
300
400
0 30 60 90 120 150 180 210 240 270 300
Time [s]

SH2 - Thermocouple Data

Date experiment: 7-3-2018

Sprinkler activation at 118 seconds
Sprinkler deactivation at 223 seconds
Operating pressure: 0.40 bar

Fire duration: 290 seconds

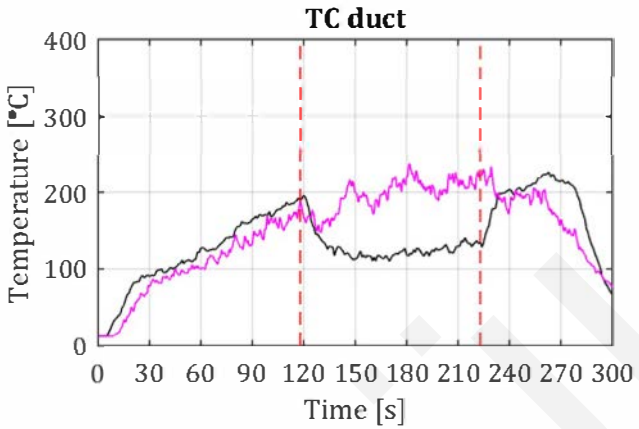

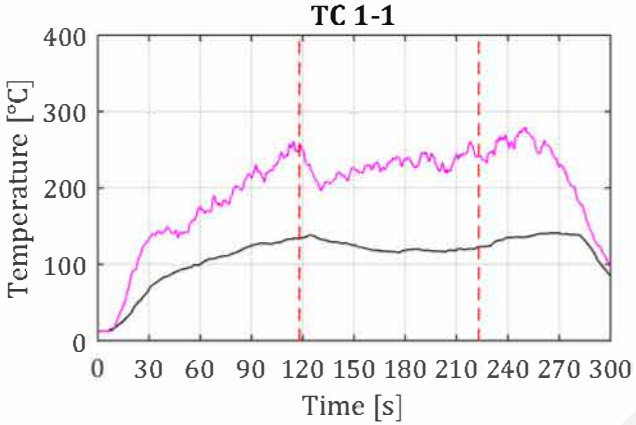

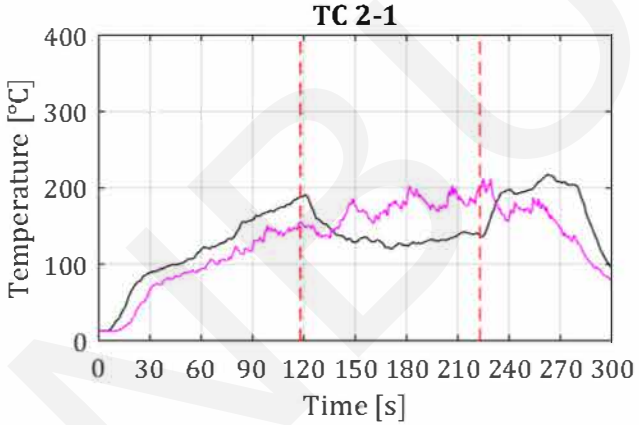

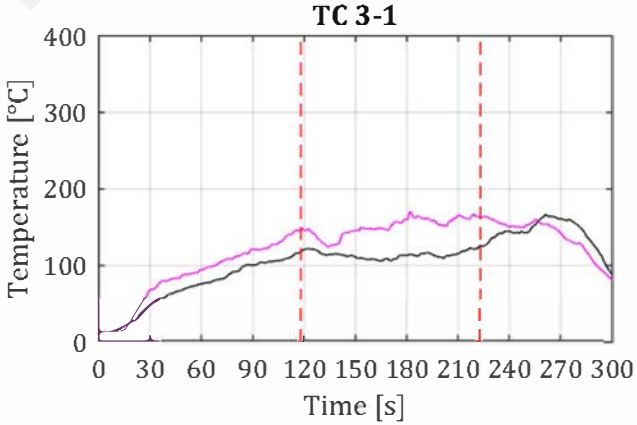

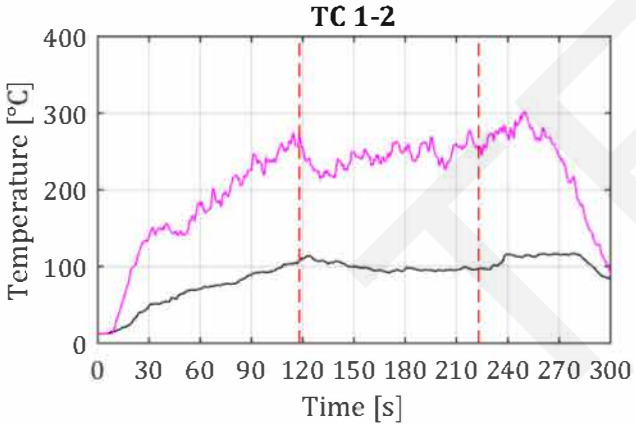

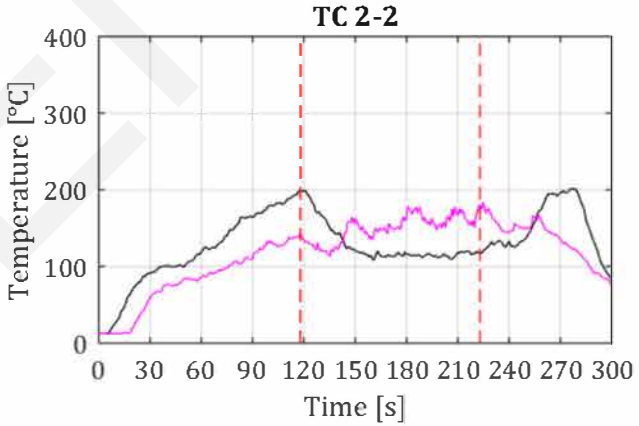

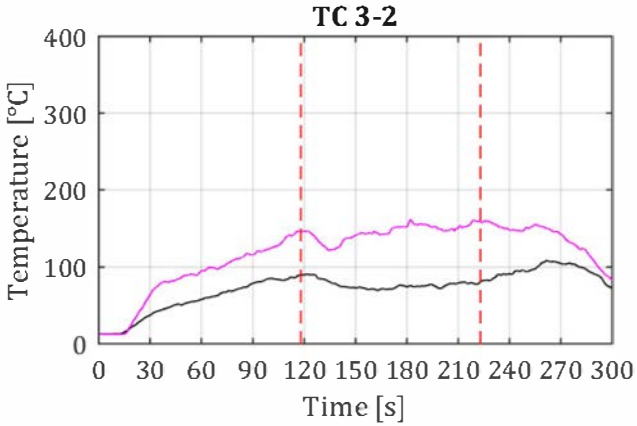

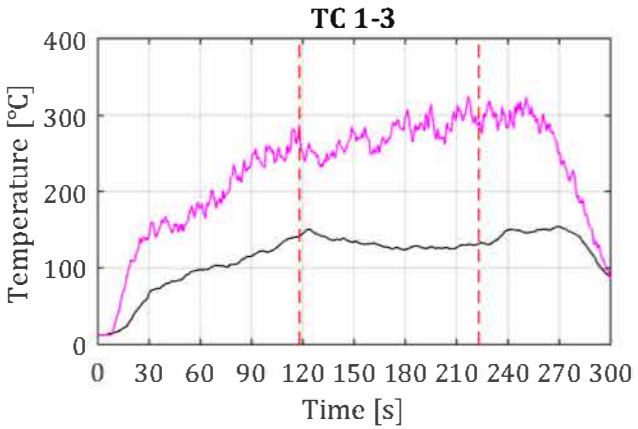
TC 1-3
Temperature [°C]
Time [s]

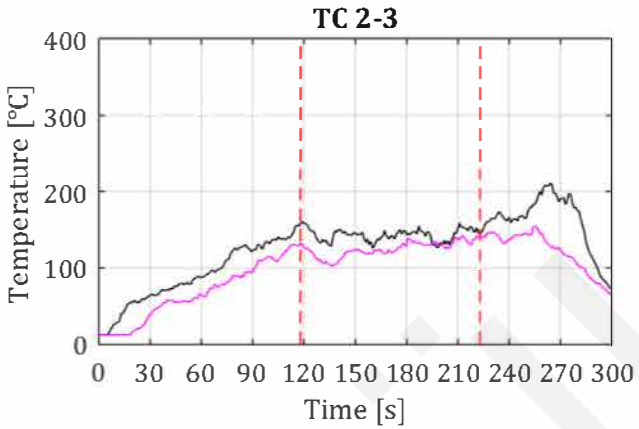
TC 2-3
Temperature [°C]
Time [s]

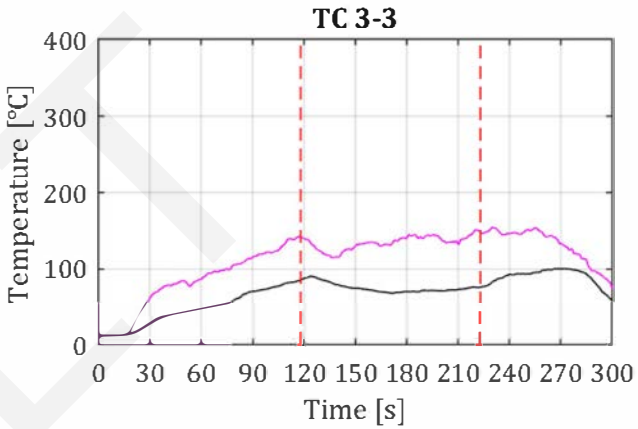
TC 3-3
Temperature [°C]
Time [s]

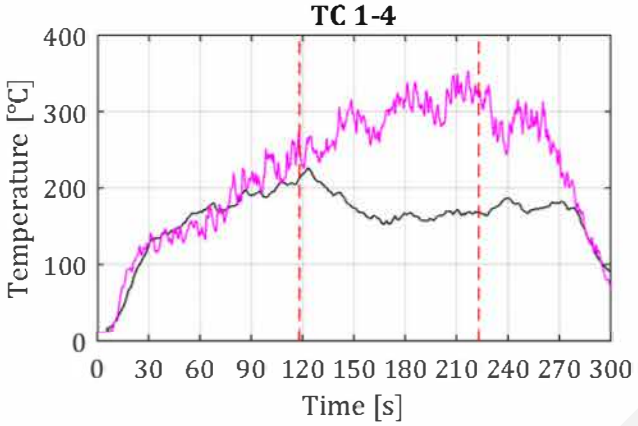
TC 1-4
Temperature [°C]
Time [s]

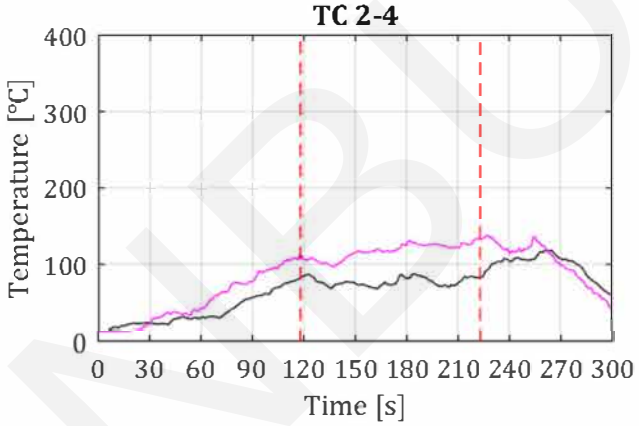
TC 2-4
Temperature [°C]
Time [s]

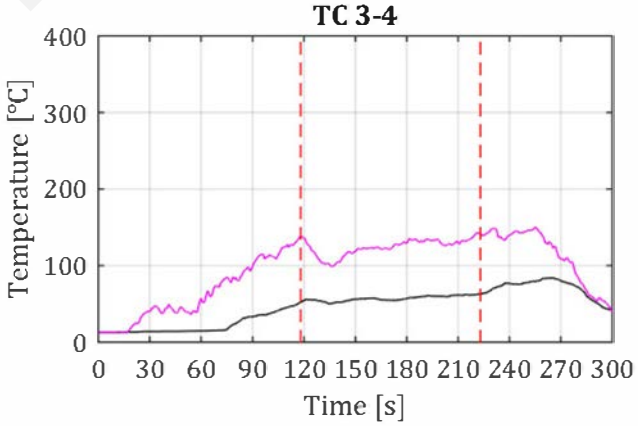
TC 3-4
Temperature [°C]
Time [s]

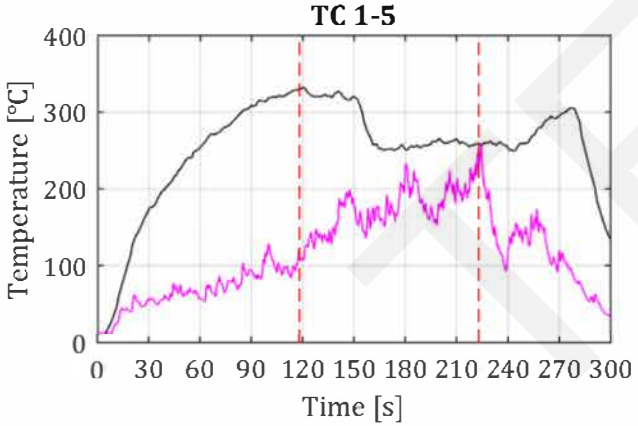
TC 1-5
Temperature [°C]
Time [s]

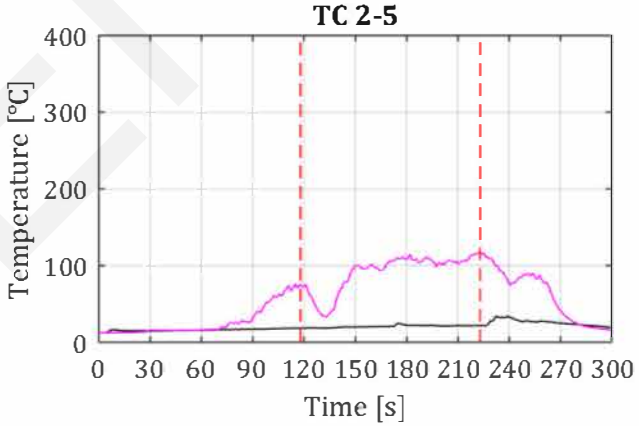
TC 2-5
Temperature [°C]
Time [s]

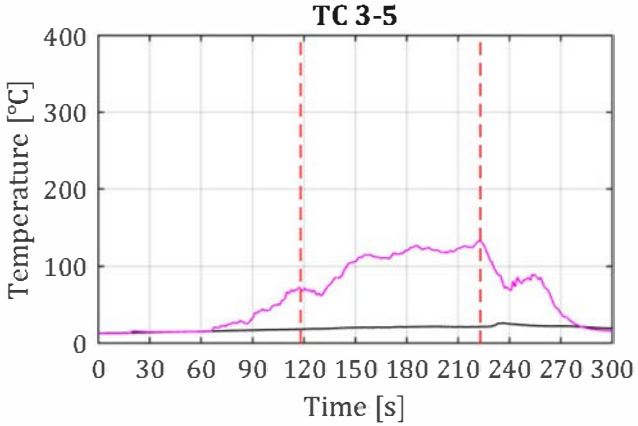
TC 3-5
Temperature [°C]
Time [s]

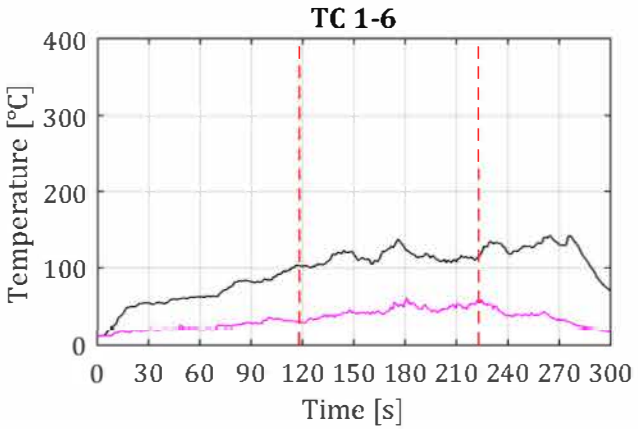
TC 1-6
Temperature [°C]
Time [s]
0
100
200
300
400
0 30 60 90 120 150 180 210 240 270 300

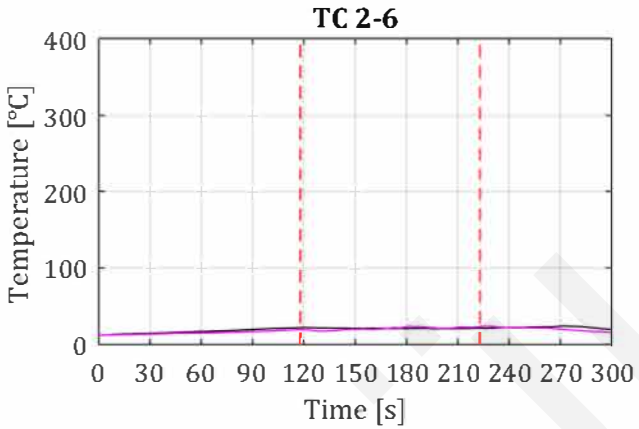
TC 2-6
Temperature [°C]
Time [s]
0
100
200
300
400
0 30 60 90 120 150 180 210 240 270 300

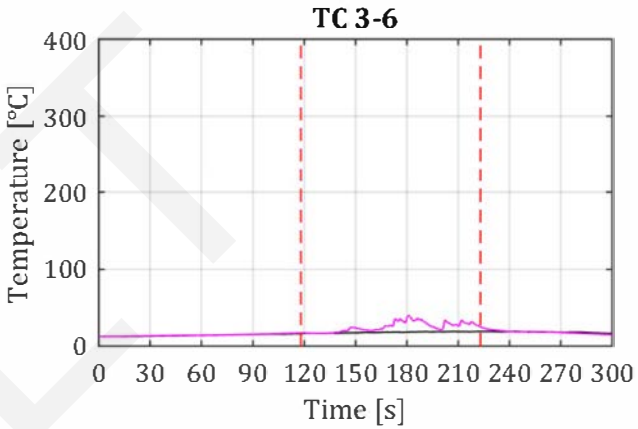
TC 3-6
Temperature [°C]
Time [s]
0
100
200
300
400
0 30 60 90 120 150 180 210 240 270 300

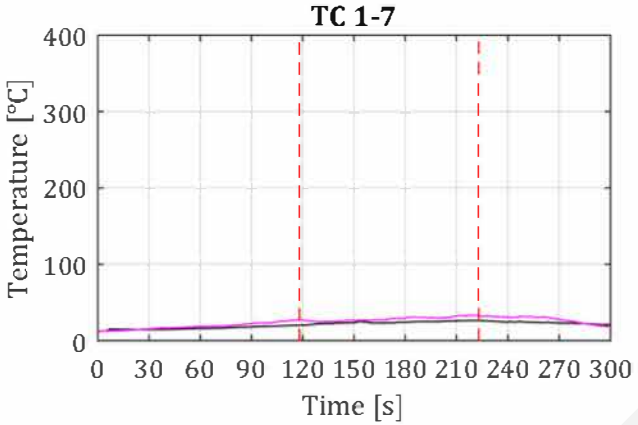
TC 1-7
Temperature [°C]
Time [s]
0
100
200
300
400
0 30 60 90 120 150 180 210 240 270 300

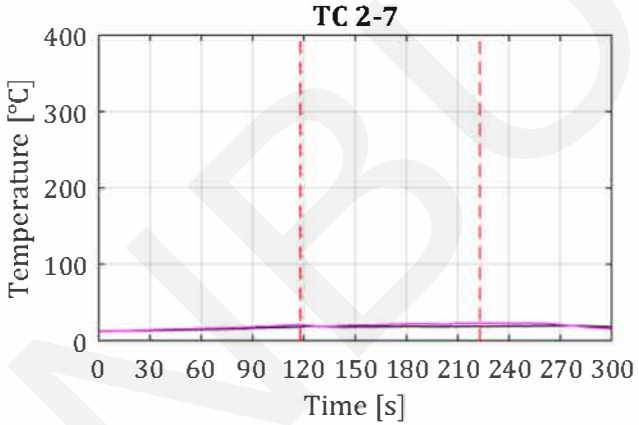
TC 2-7
Temperature [°C]
Time [s]
0
100
200
300
400
0 30 60 90 120 150 180 210 240 270 300

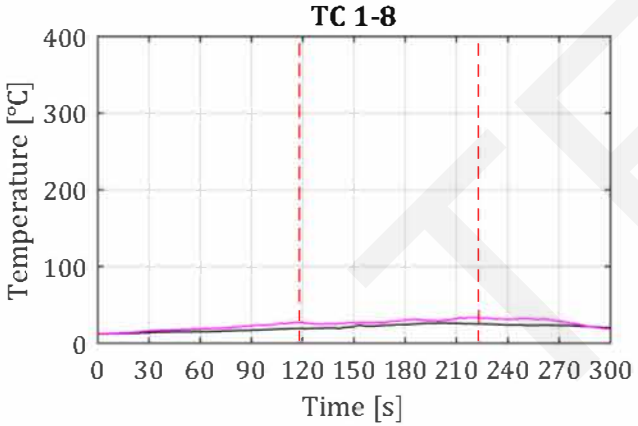
TC 1-8
Temperature [°C]
Time [s]
0
100
200
300
400
0 30 60 90 120 150 180 210 240 270 300

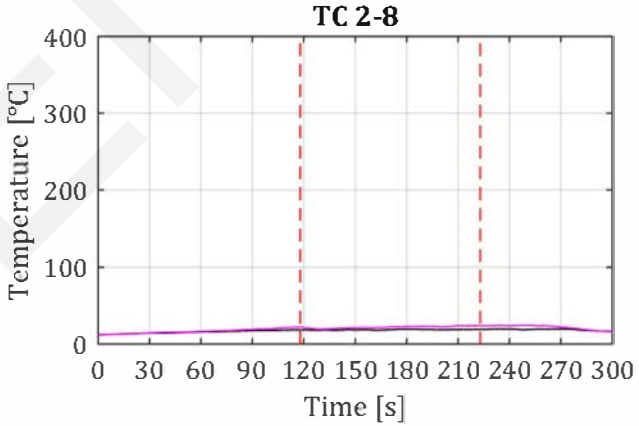
TC 2-8
Temperature [°C]
Time [s]
0
100
200
300
400
0 30 60 90 120 150 180 210 240 270 300

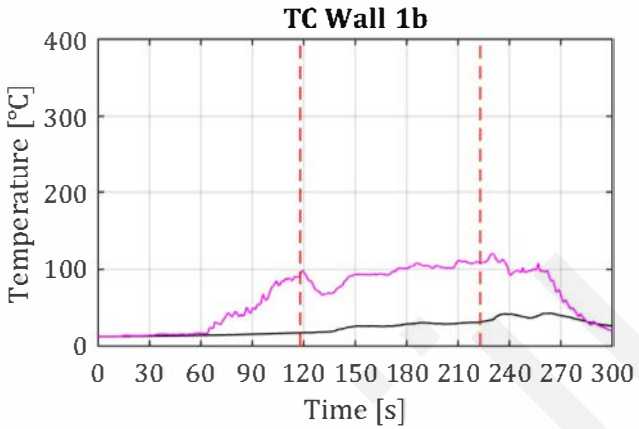
TC Wall 1b
Temperature [°C]
0
100
200
300
400
0 30 60 90 120 150 180 210 240 270 300
Time [s]

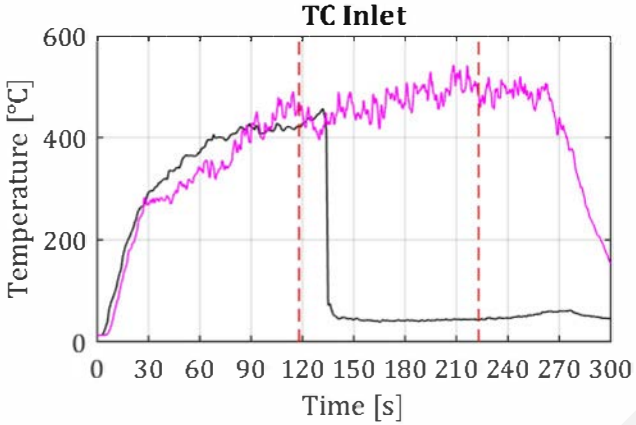
TC Inlet
Temperature [°C]
0
200
400
600
0 30 60 90 120 150 180 210 240 270 300
Time [s]

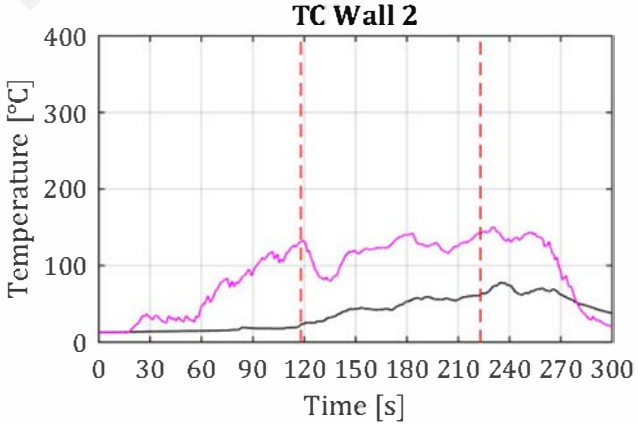
TC Wall 2
Temperature [°C]
0
100
200
300
400
0 30 60 90 120 150 180 210 240 270 300
Time [s]

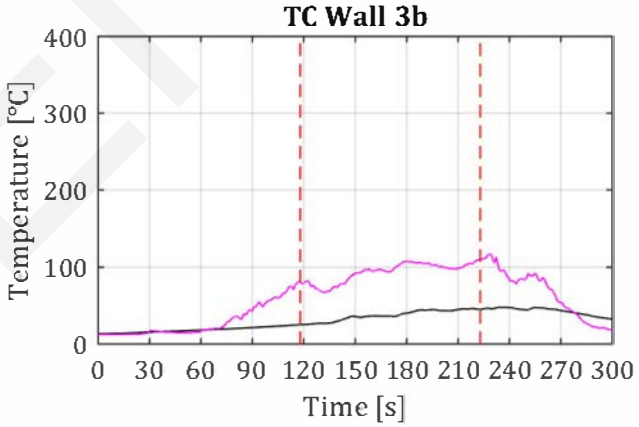
TC Wall 3b
Temperature [°C]
0
100
200
300
400
0 30 60 90 120 150 180 210 240 270 300
Time [s]

SH3 - Thermocouple Data

Date experiment: 7-3-2018

Sprinkler activation at 120 seconds
Sprinkler deactivation at 250 seconds
Operating pressure: 1.34 bar

Fire duration: 260 seconds

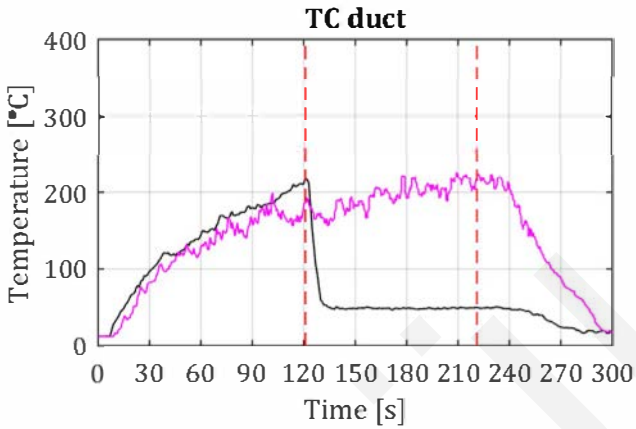

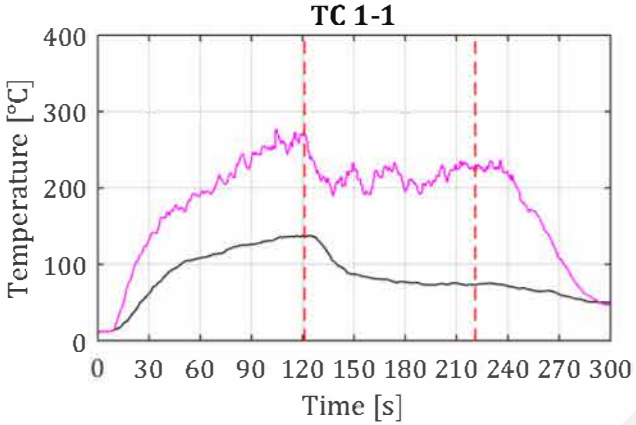

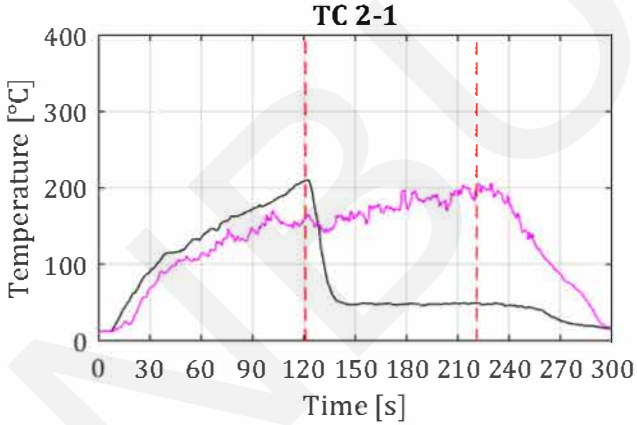

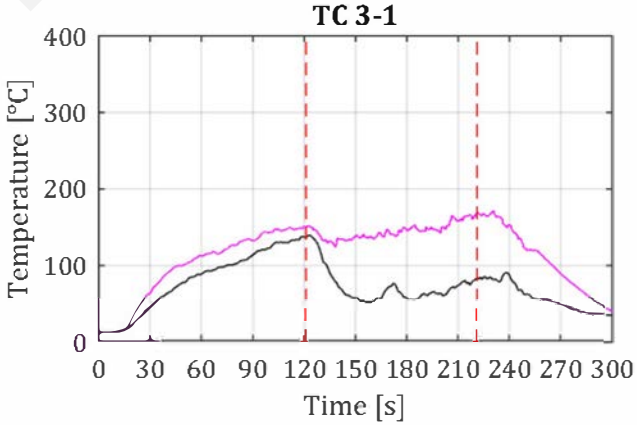

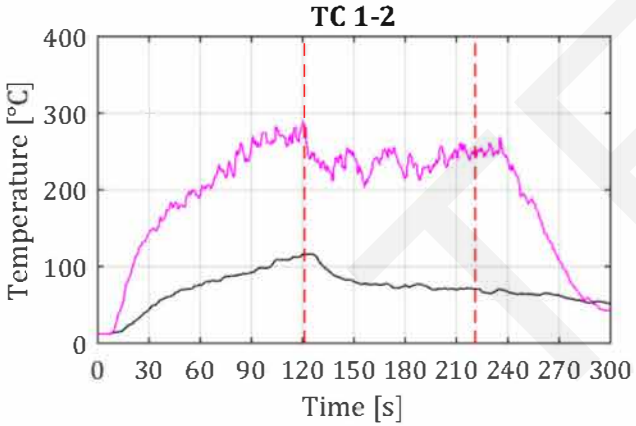

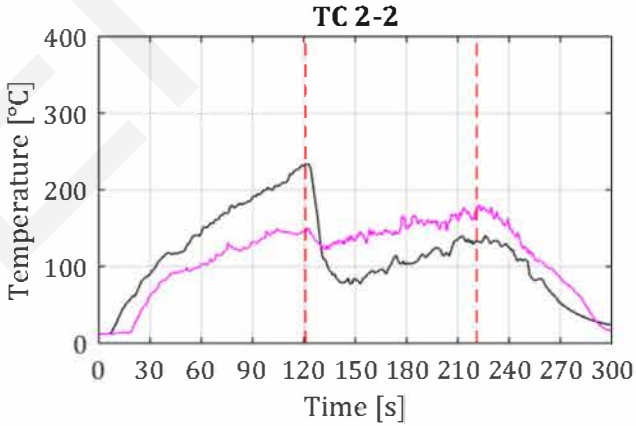

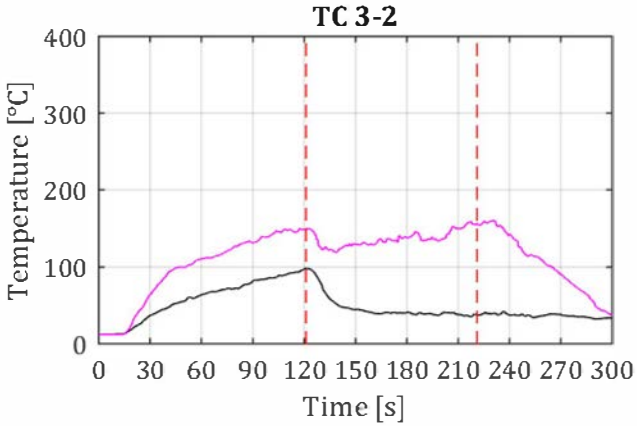

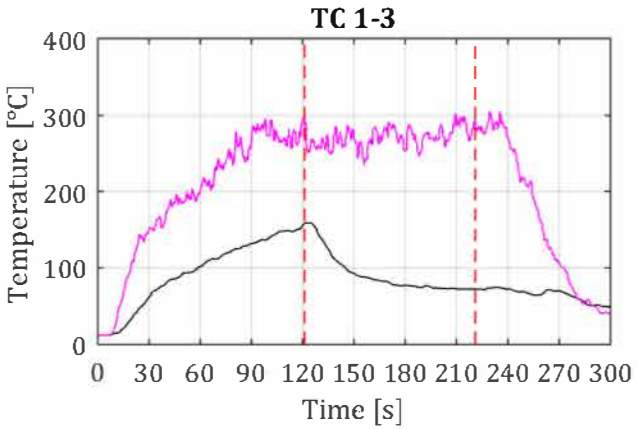
TC 1-3
Temperature [°C]
Time [s]

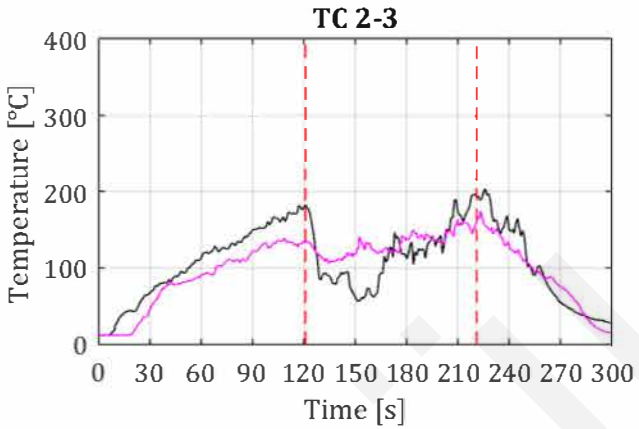
TC 2-3
Temperature [°C]
Time [s]

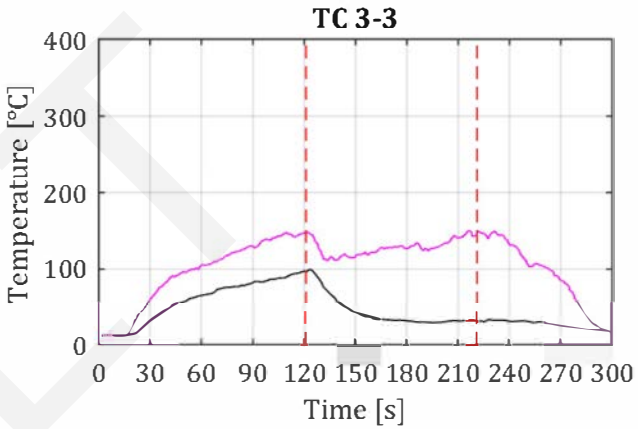
TC 3-3
Temperature [°C]
Time [s]

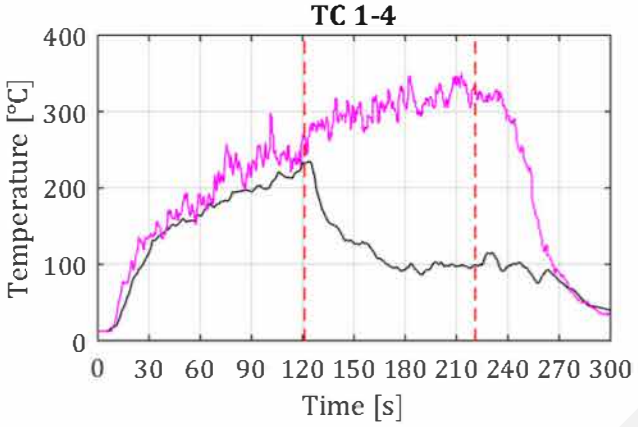
TC 1-4
Temperature [°C]
Time [s]

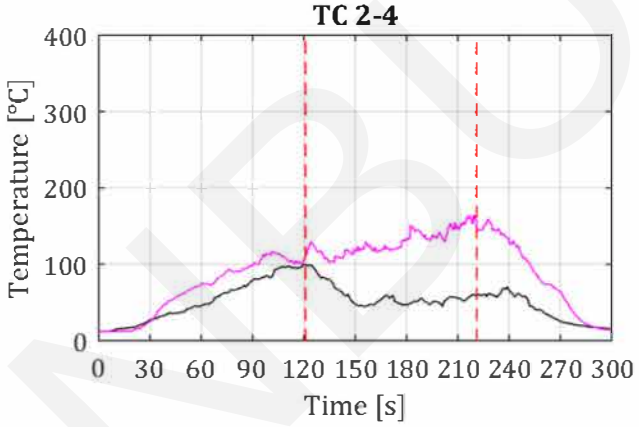
TC 2-4
Temperature [°C]
Time [s]

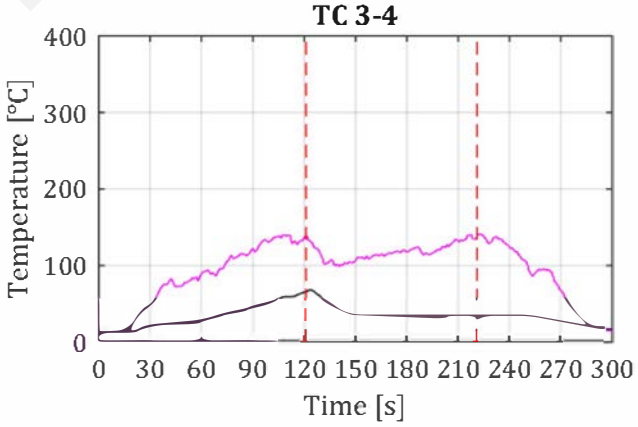
TC 3-4
Temperature [°C]
Time [s]

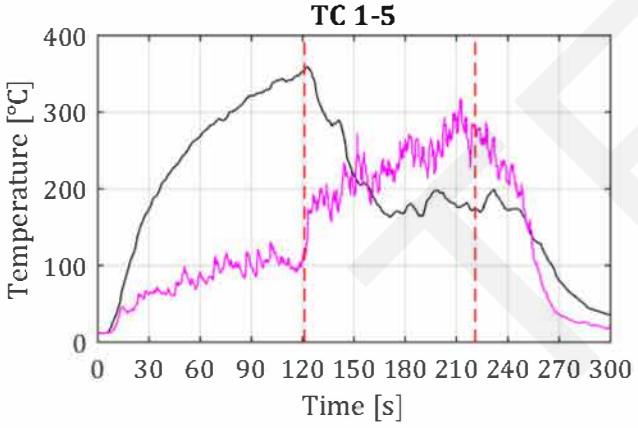
TC 1-5
Temperature [°C]
Time [s]

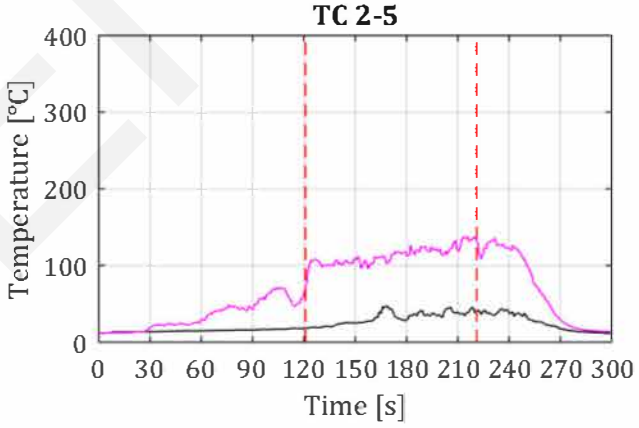
TC 2-5
Temperature [°C]
Time [s]

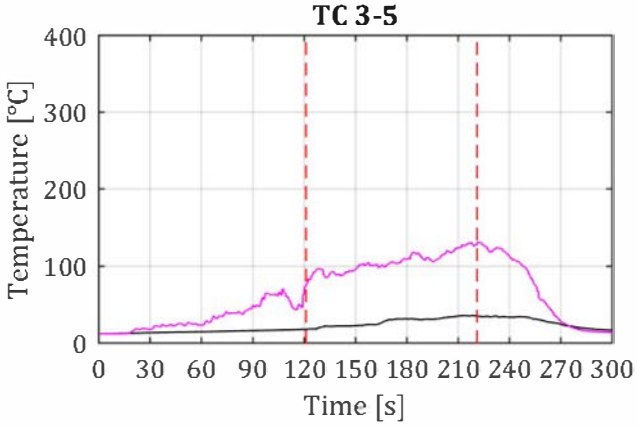
TC 3-5
Temperature [°C]
Time [s]

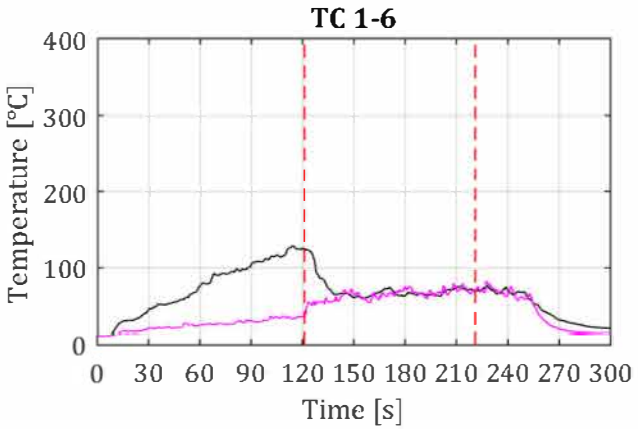
TC 1-6
Temperature [°C]
Time [s]

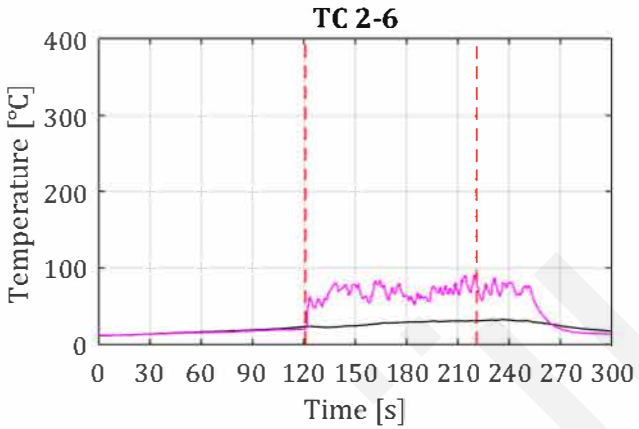
TC 2-6
Temperature [°C]
Time [s]

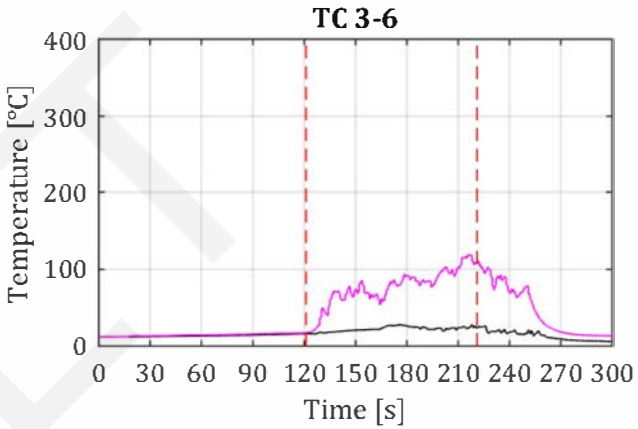
TC 3-6
Temperature [°C]
Time [s]

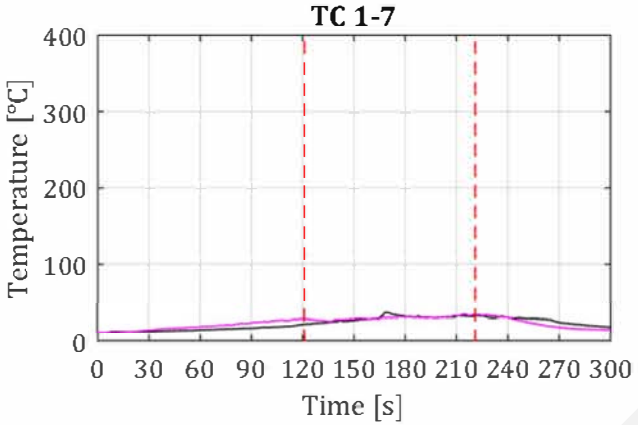
TC 1-7
Temperature [°C]
Time [s]

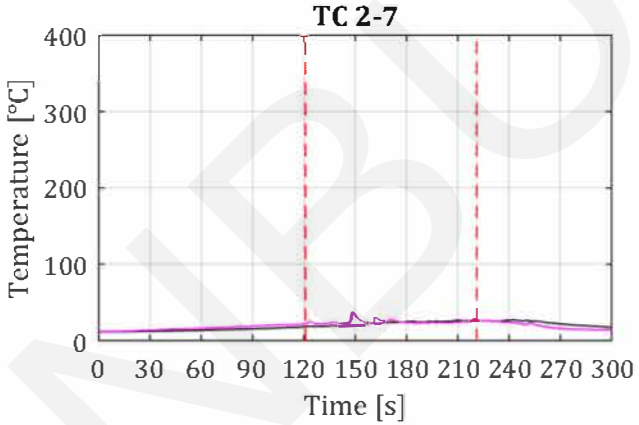
TC 2-7
Temperature [°C]
Time [s]

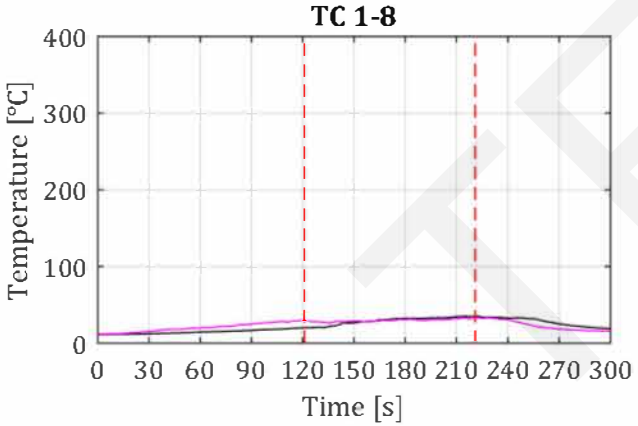
TC 1-8
Temperature [°C]
Time [s]

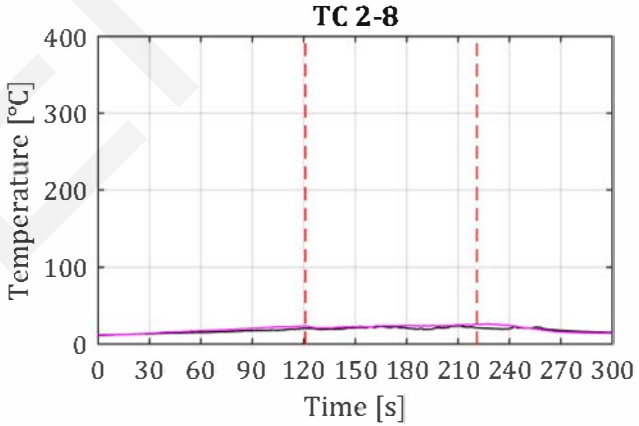
TC 2-8
Temperature [°C]
Time [s]

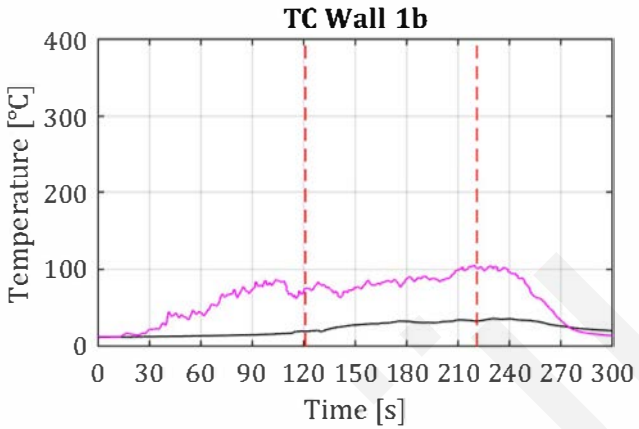
TC Wall 1b
Temperature [°C]
Time [s]
0
100
200
300
400
0 30 60 90 120 150 180 210 240 270 300

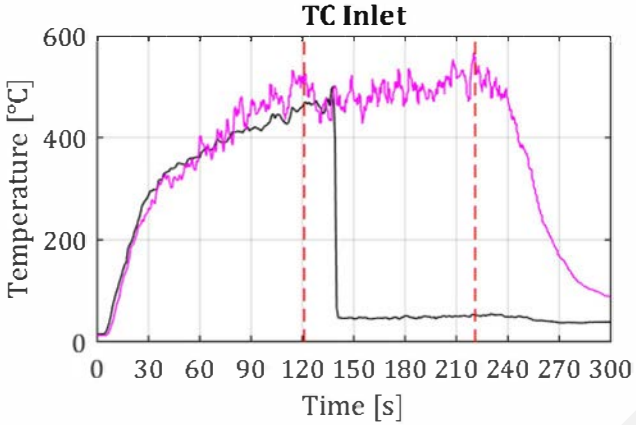
TC Inlet
Temperature [°C]
Time [s]
0
200
400
600
0 30 60 90 120 150 180 210 240 270 300

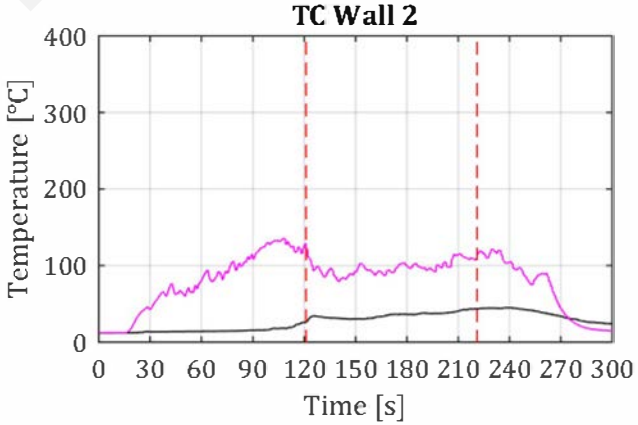
TC Wall 2
Temperature [°C]
Time [s]
0
100
200
300
400
0 30 60 90 120 150 180 210 240 270 300

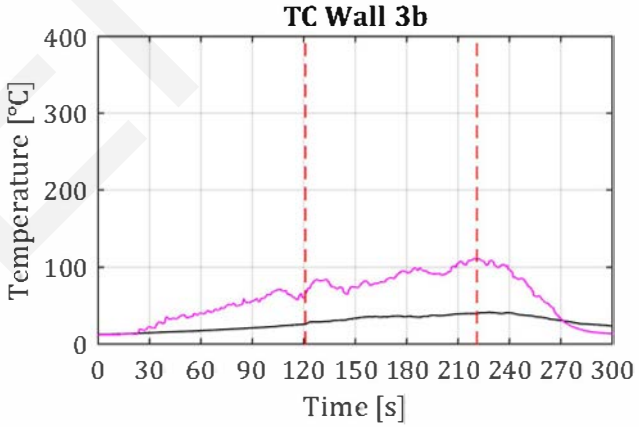
TC Wall 3b
Temperature [°C]
Time [s]
0
100
200
300
400
0 30 60 90 120 150 180 210 240 270 300

SH4 - Thermocouple Data

Date experiment: 30-3-2018

Sprinkler activation at 123 seconds
Sprinkler deactivation at 223 seconds
Operating pressure: 0.79 bar

Fire duration: 250 seconds

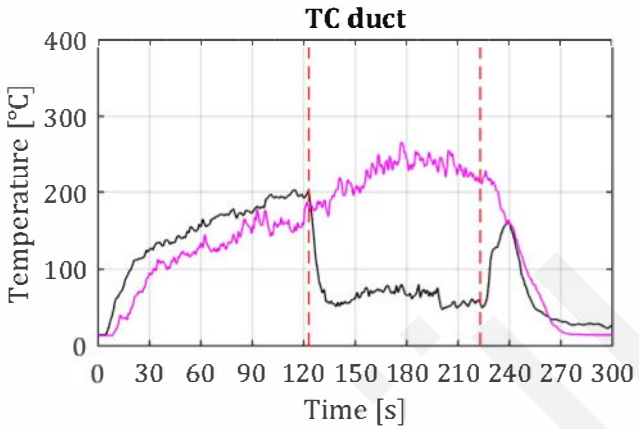

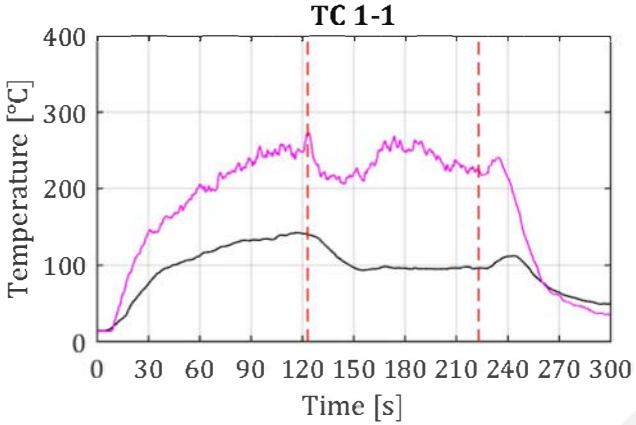

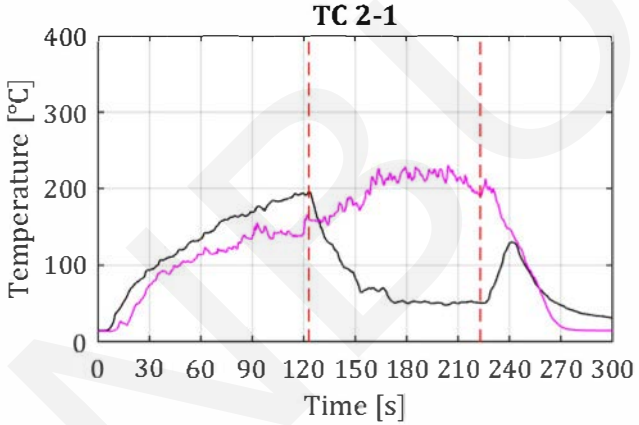

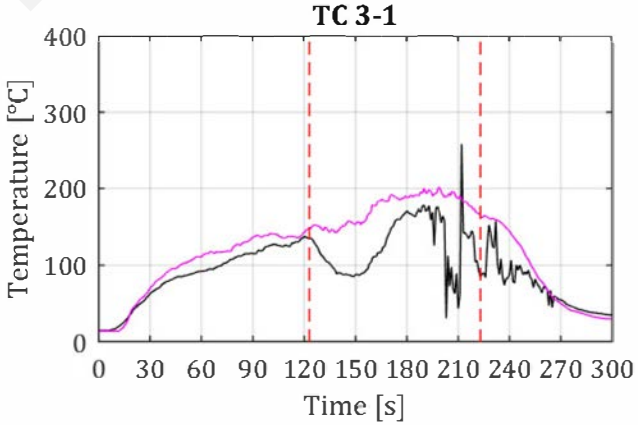

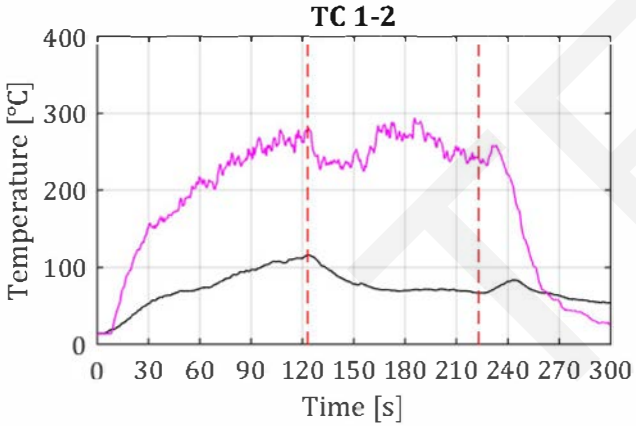

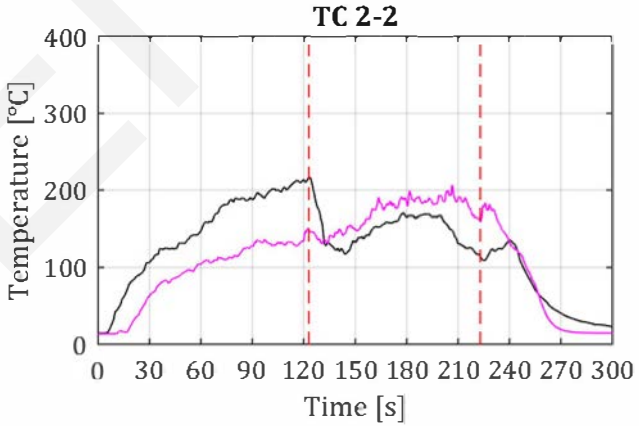

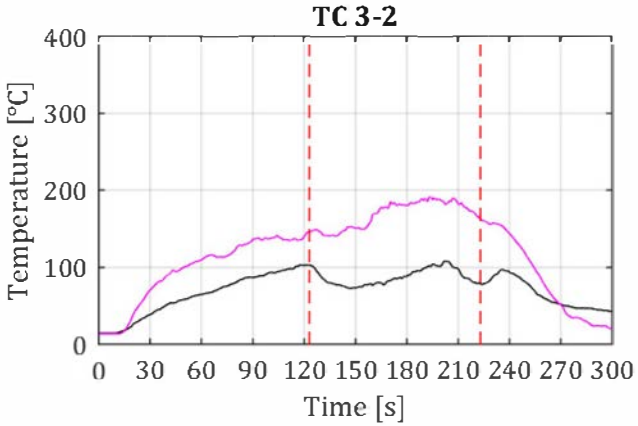

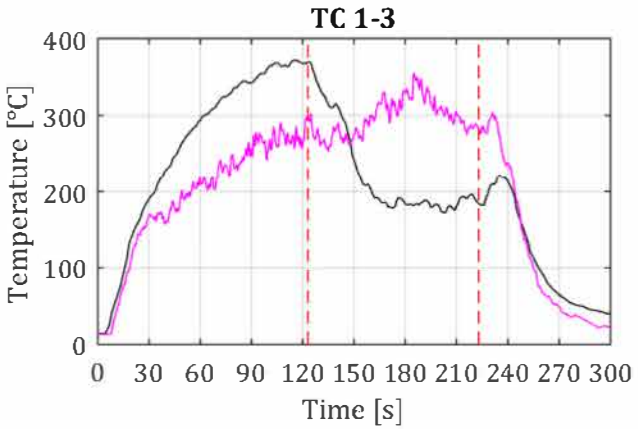
TC 1-3
Temperature [°C]
Time [s]

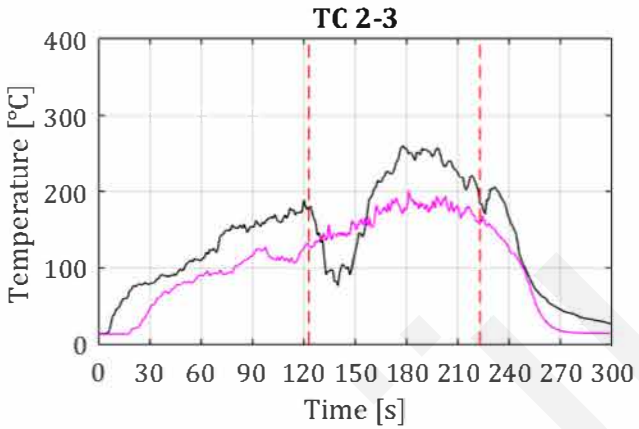
TC 2-3
Temperature [°C]
Time [s]

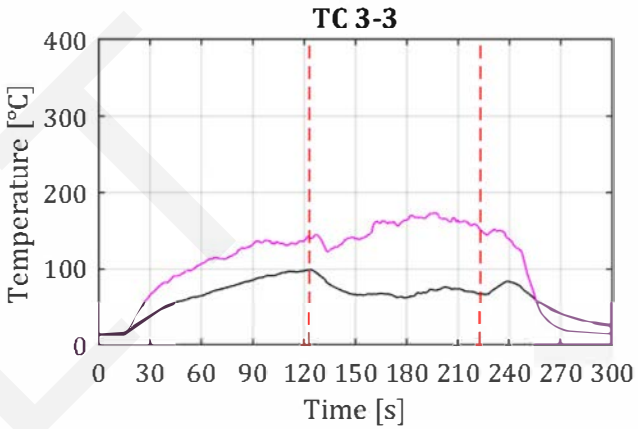
TC 3-3
Temperature [°C]
Time [s]

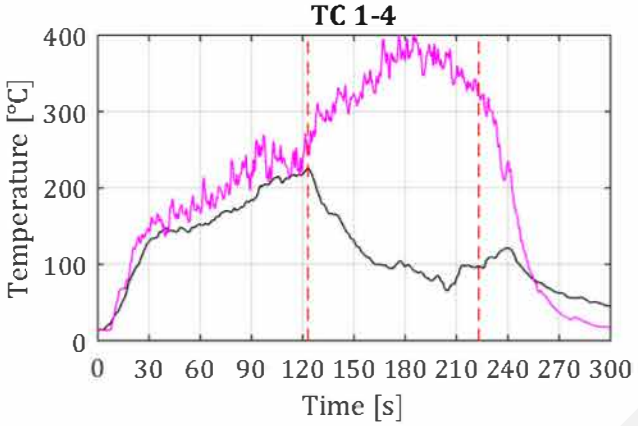
TC 1-4
Temperature [°C]
Time [s]

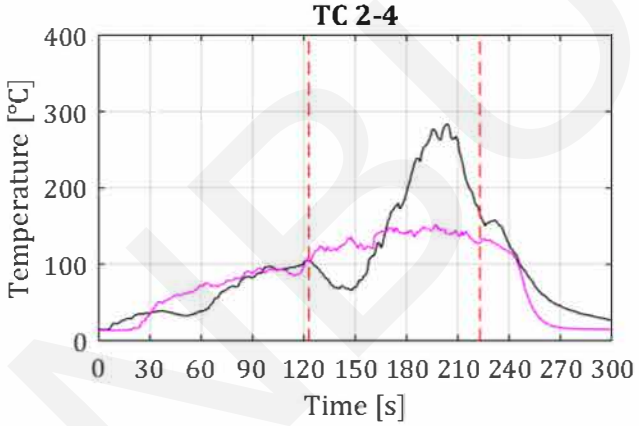
TC 2-4
Temperature [°C]
Time [s]

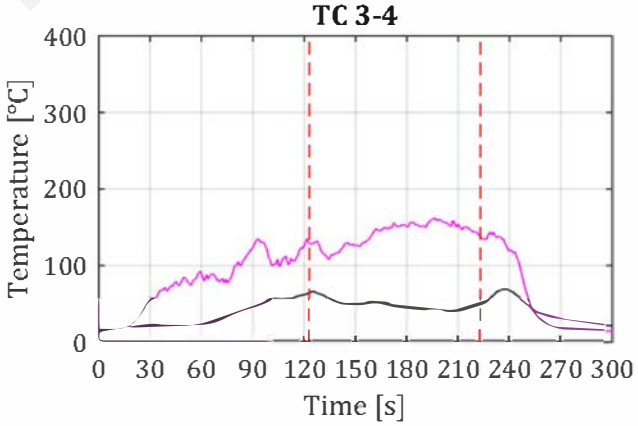
TC 3-4
Temperature [°C]
Time [s]

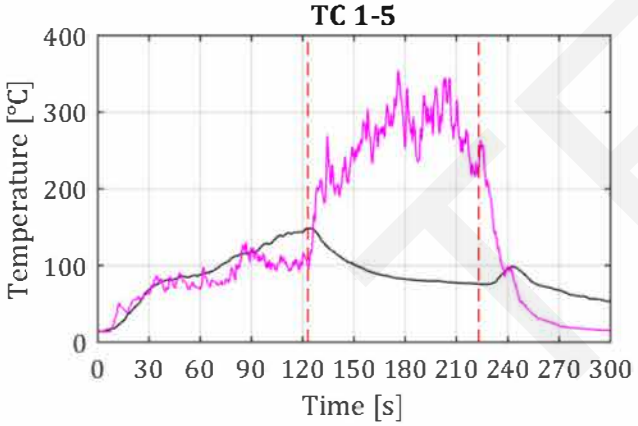
TC 1-5
Temperature [°C]
Time [s]

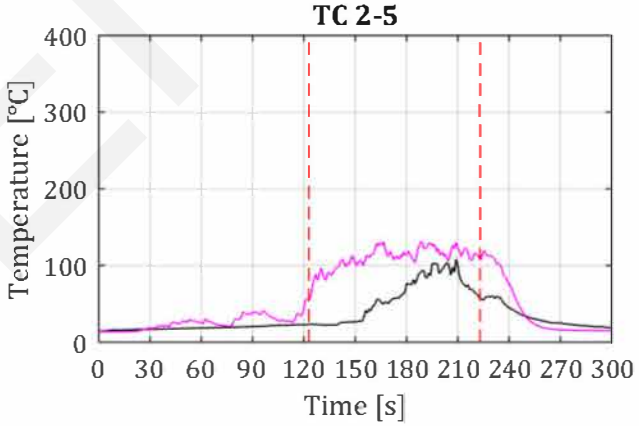
TC 2-5
Temperature [°C]
Time [s]

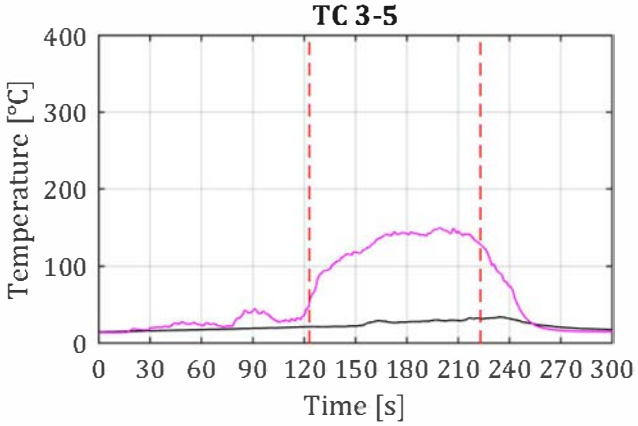
TC 3-5
Temperature [°C]
Time [s]

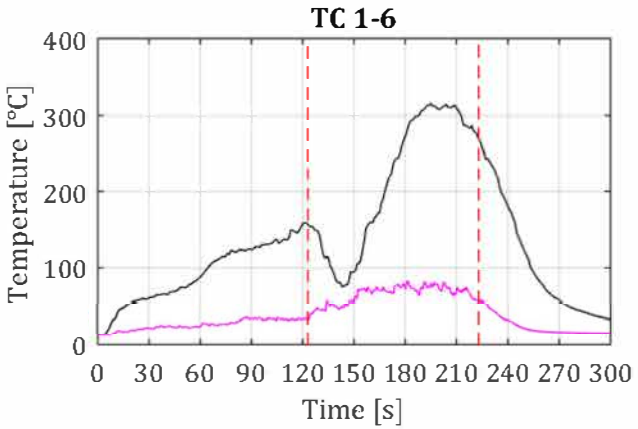
TC 1-6
Temperature [°C]
Time [s]

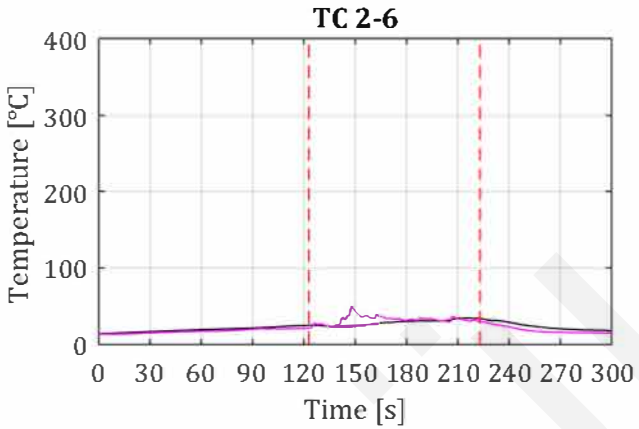
TC 2-6
Temperature [°C]
Time [s]

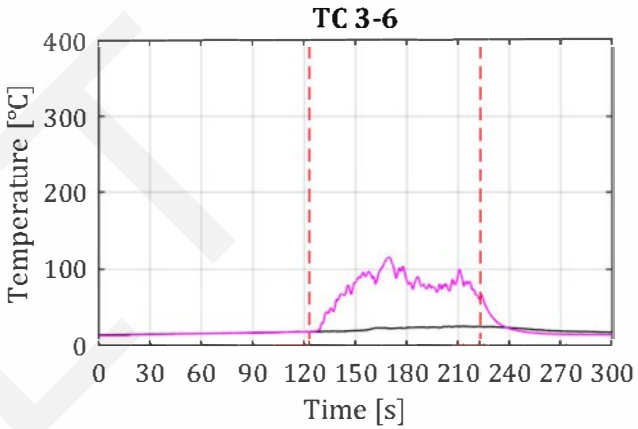
TC 3-6
Temperature [°C]
Time [s]

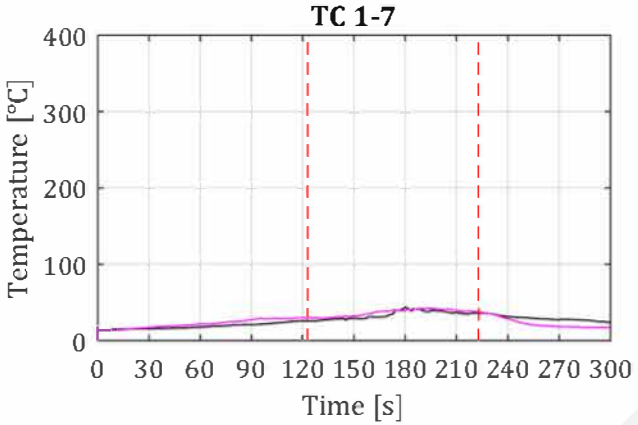
TC 1-7
Temperature [°C]
Time [s]

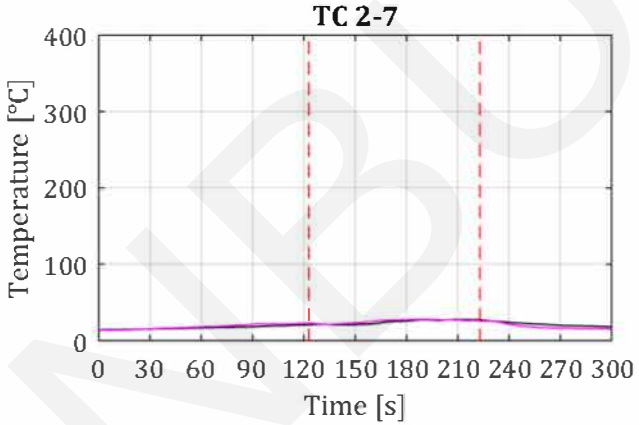
TC 2-7
Temperature [°C]
Time [s]

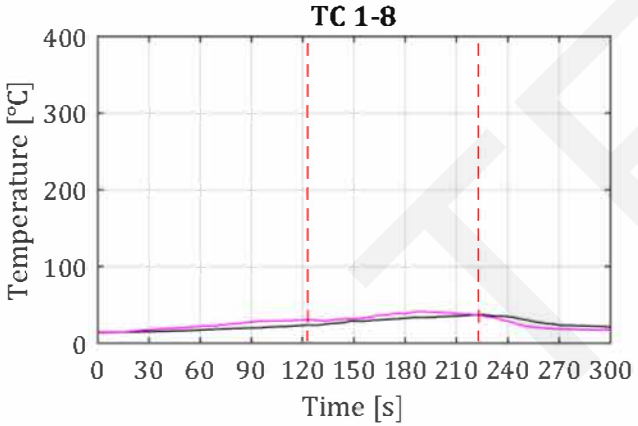
TC 1-8
Temperature [°C]
Time [s]

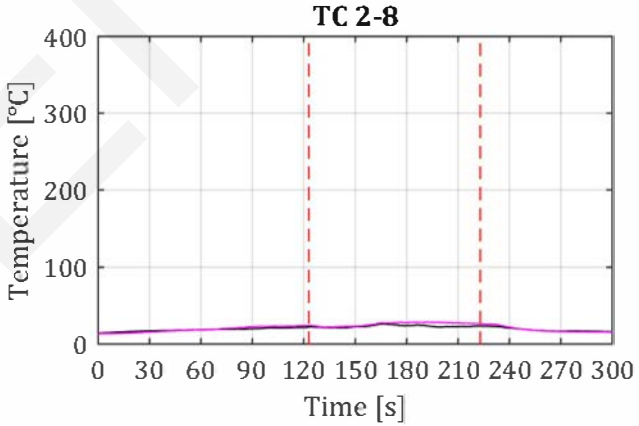
TC 2-8
Temperature [°C]
Time [s]

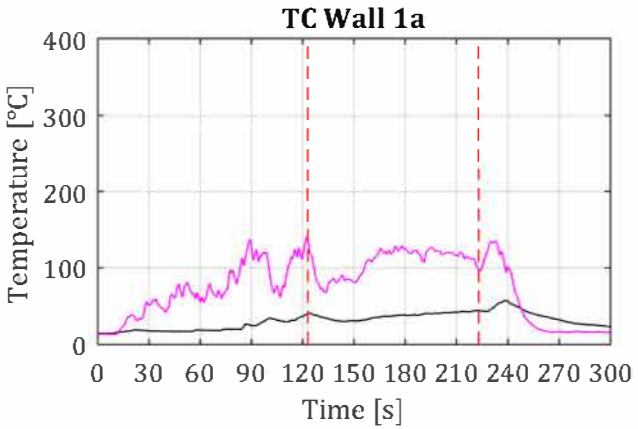
TC Wall 1a
Temperature [°C]
Time [s]

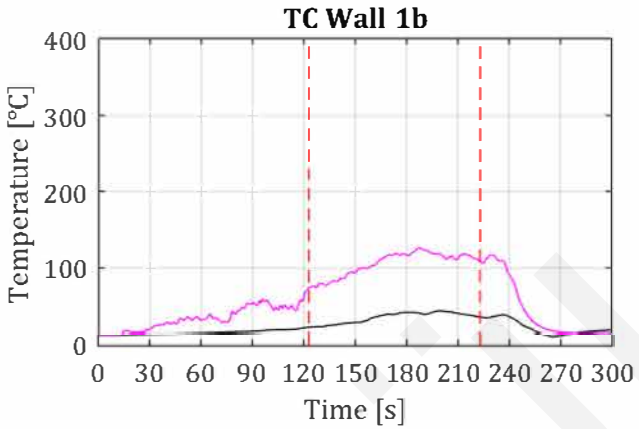
TC Wall 1b
Temperature [°C]
Time [s]

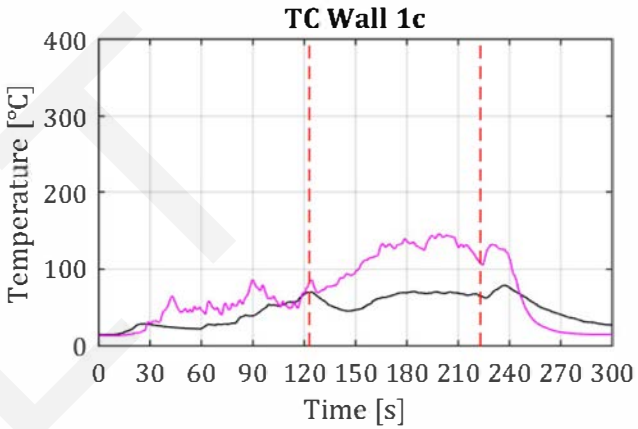
TC Wall 1c
Temperature [°C]
Time [s]

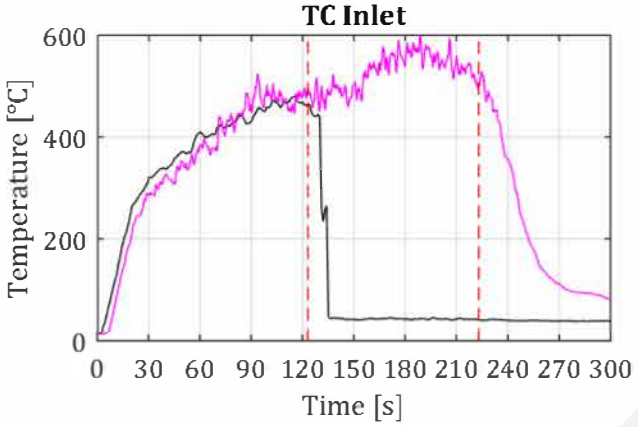
TC Inlet
Temperature [°C]
Time [s]

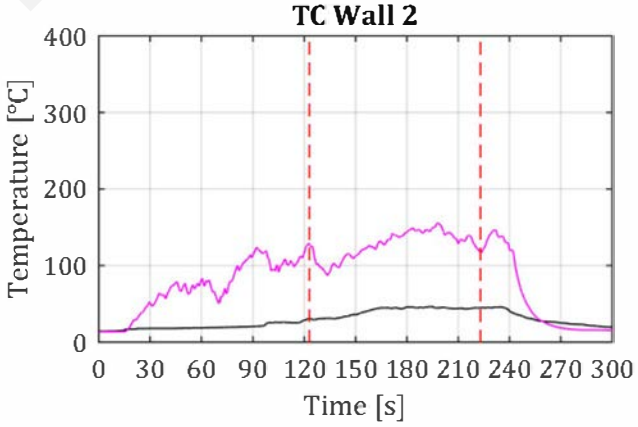
TC Wall 2
Temperature [°C]
Time [s]

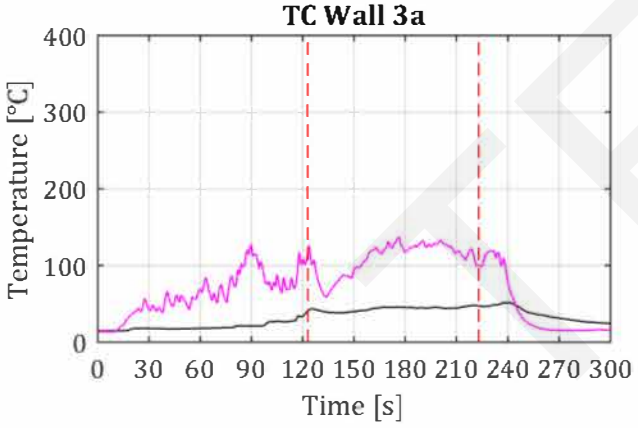
TC Wall 3a
Temperature [°C]
Time [s]

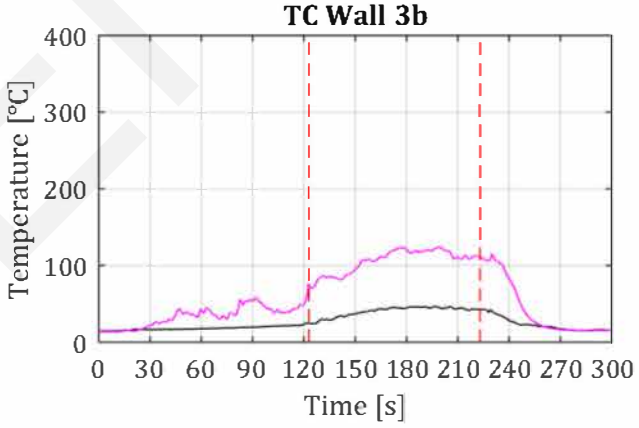
TC Wall 3b
Temperature [°C]
Time [s]

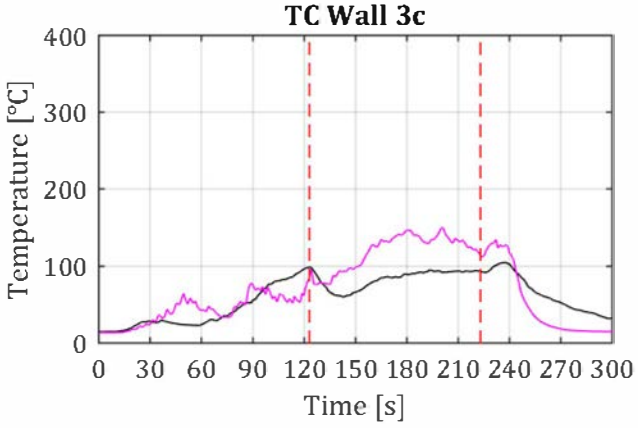
TC Wall 3c
Temperature [°C]
Time [s]

SH5 - Thermocouple Data

Date experiment: 30-3-2018

Sprinkler activation at 121 seconds
Sprinkler deactivation at 221 seconds
Operating pressure: 1.34 bar

Fire duration: 226 seconds

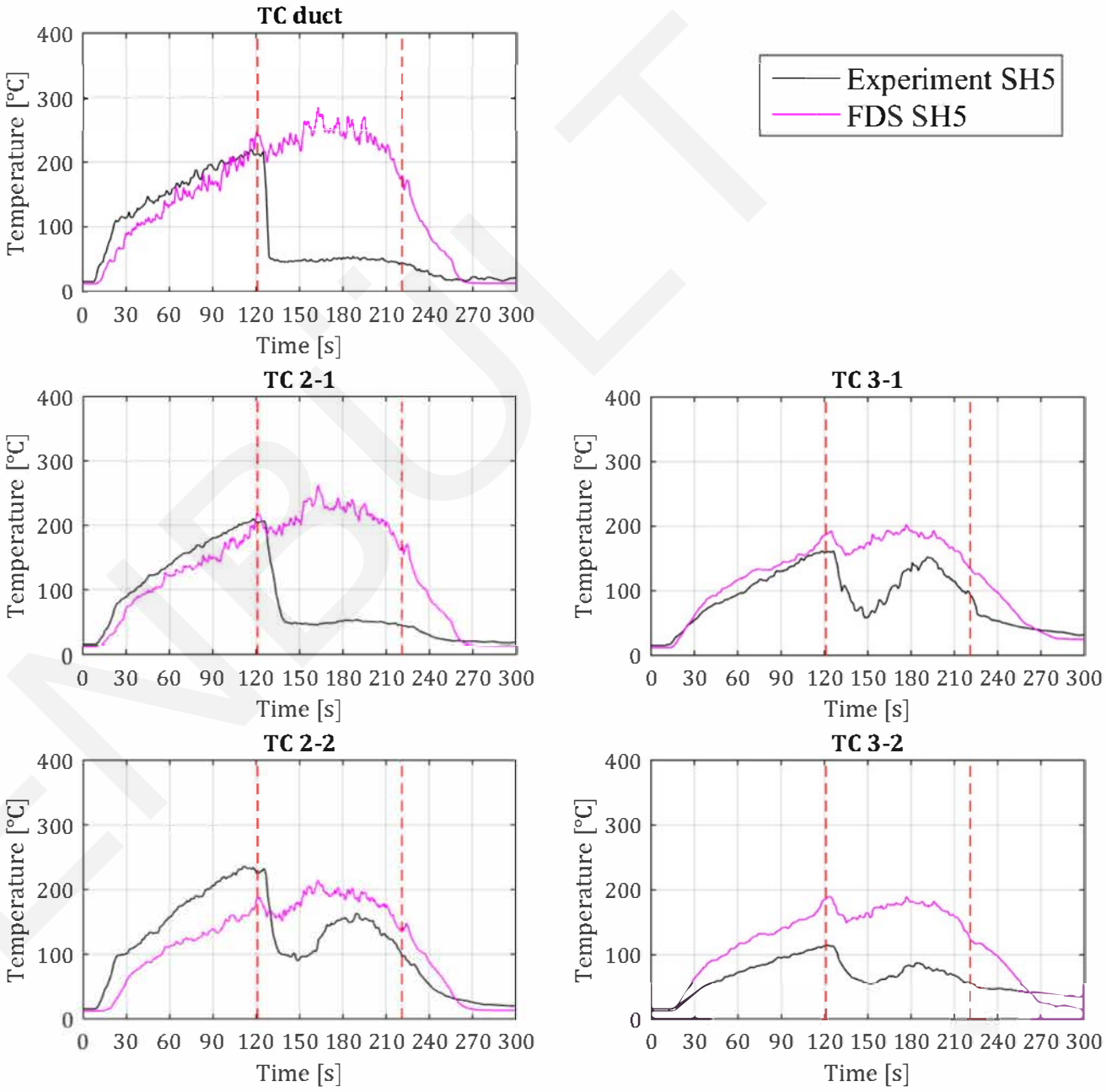

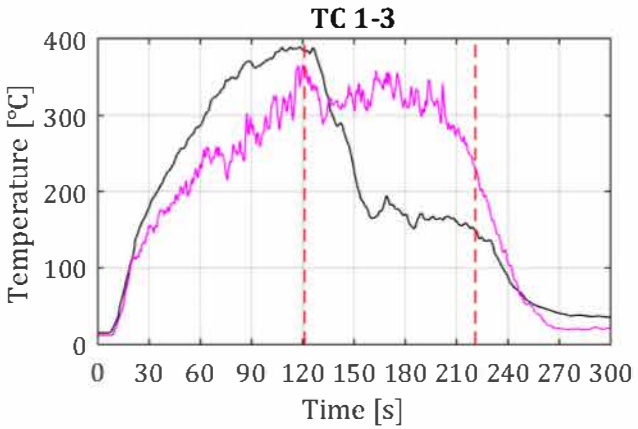
TC 1-3
Temperature [°C]
Time [s]

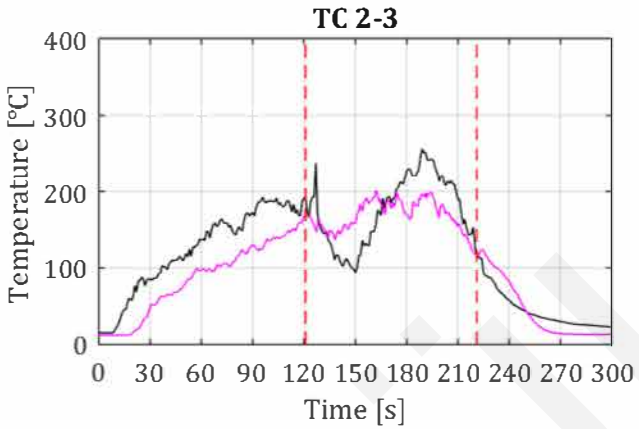
TC 2-3
Temperature [°C]
Time [s]

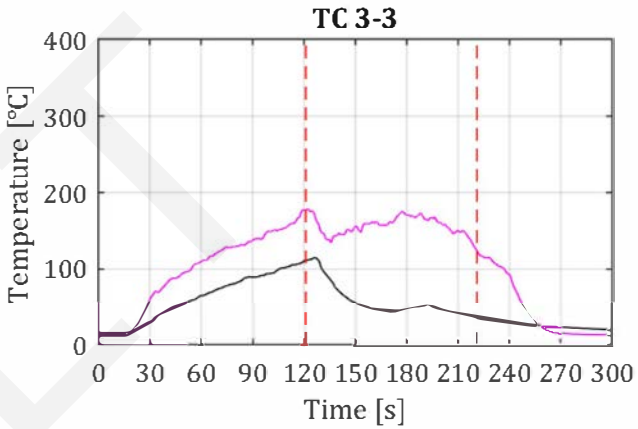
TC 3-3
Temperature [°C]
Time [s]

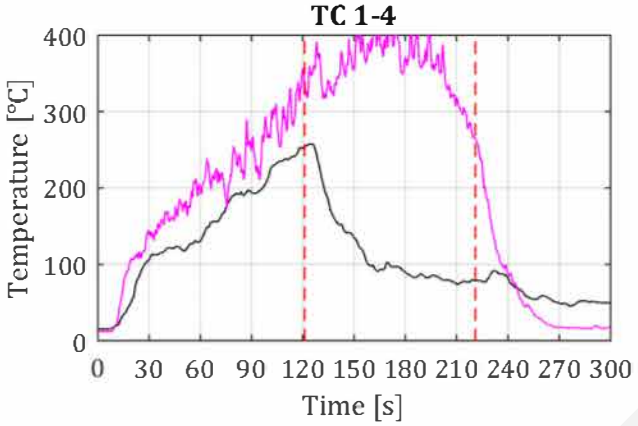
TC 1-4
Temperature [°C]
Time [s]

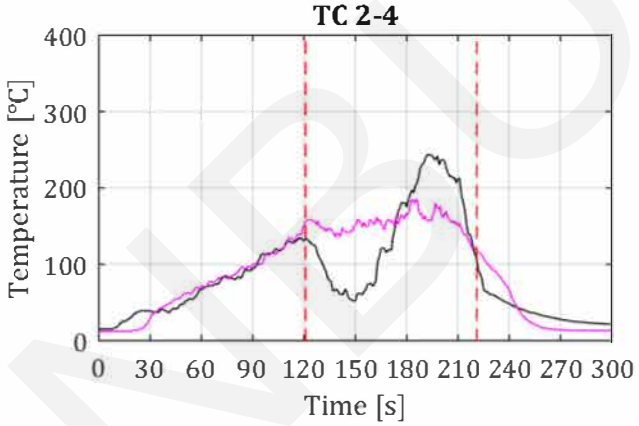
TC 2-4
Temperature [°C]
Time [s]

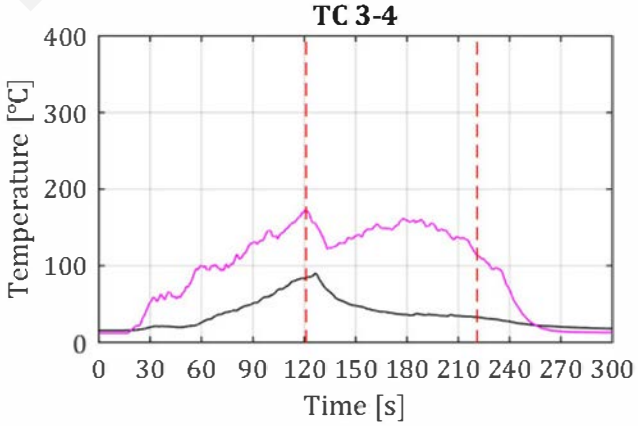
TC 3-4
Temperature [°C]
Time [s]

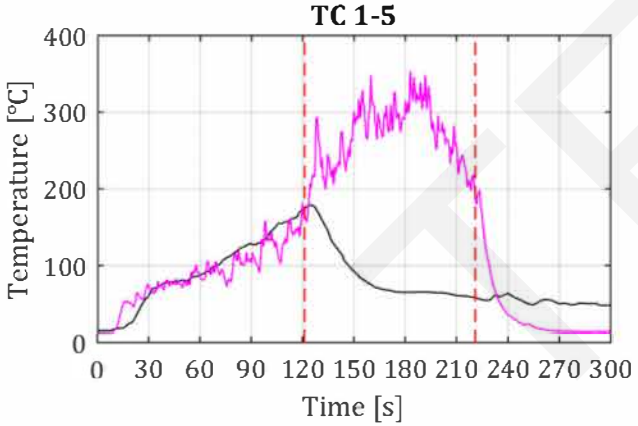
TC 1-5
Temperature [°C]
Time [s]

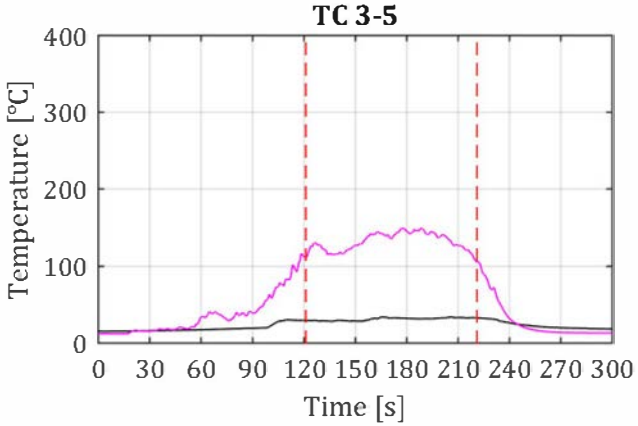
TC 3-5
Temperature [°C]
Time [s]

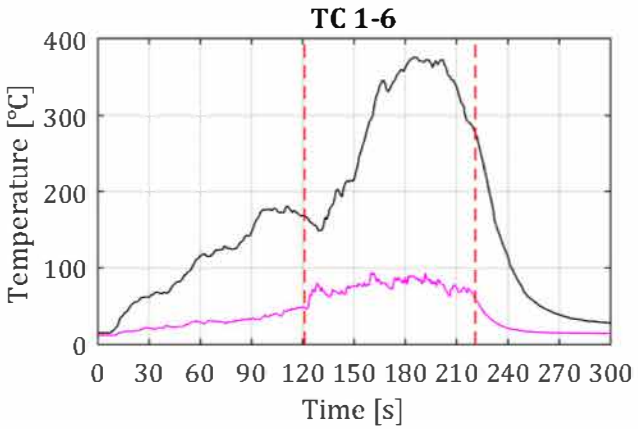
TC 1-6
Temperature [°C]
Time [s]

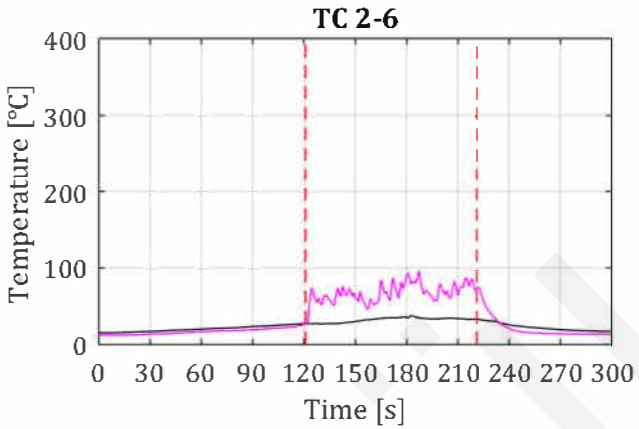
TC 2-6
Temperature [°C]
Time [s]

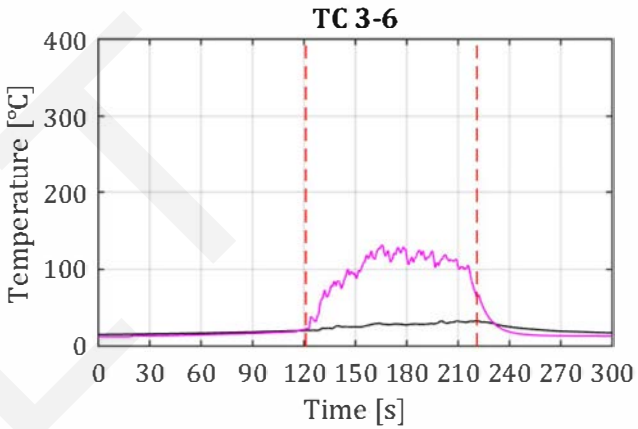
TC 3-6
Temperature [°C]
Time [s]

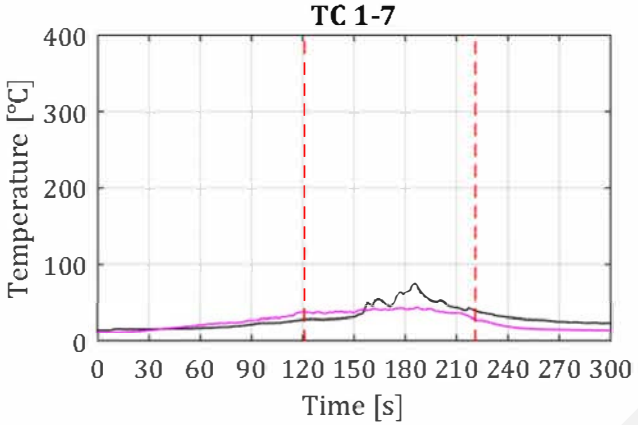
TC 1-7
Temperature [°C]
Time [s]

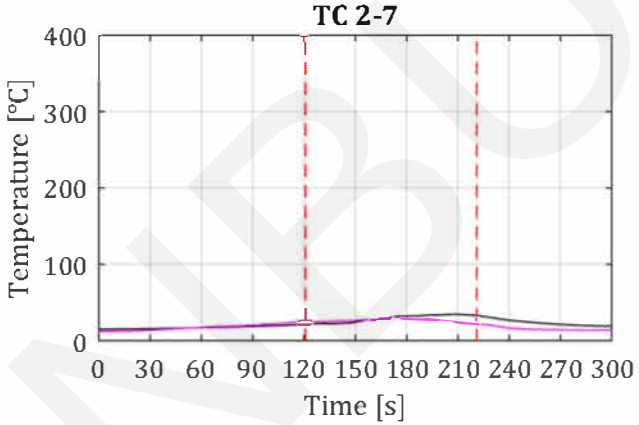
TC 2-7
Temperature [°C]
Time [s]

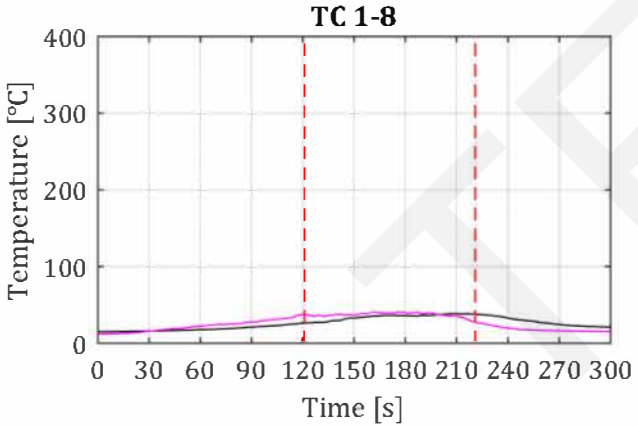
TC 1-8
Temperature [°C]
Time [s]

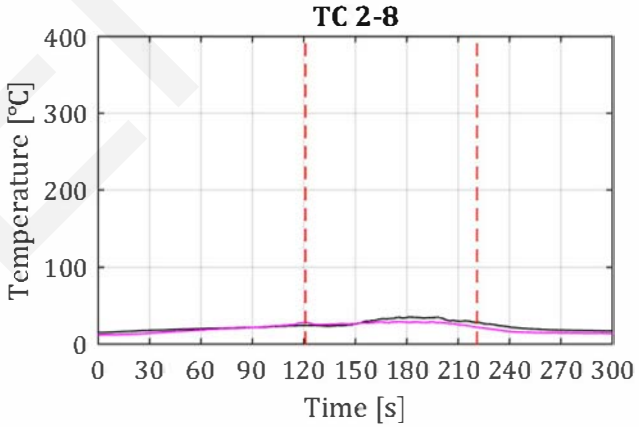
TC 2-8
Temperature [°C]
Time [s]

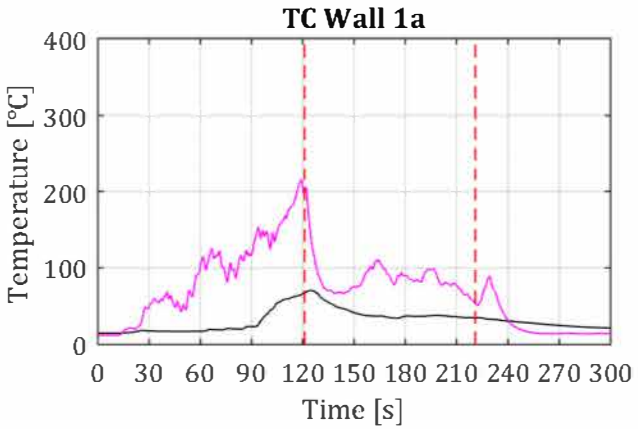
TC Wall 1a
Temperature [°C]
Time [s]

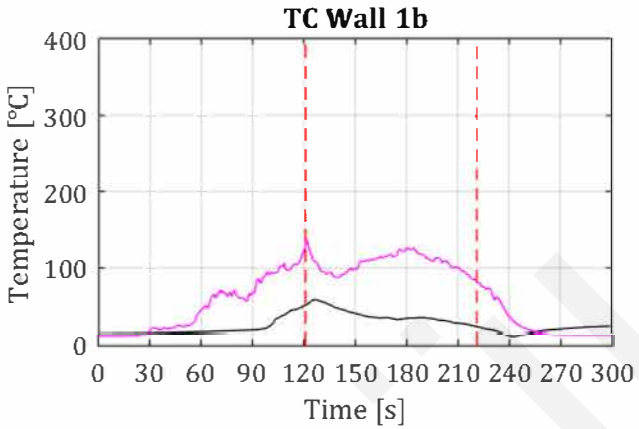
TC Wall 1b
Temperature [°C]
Time [s]

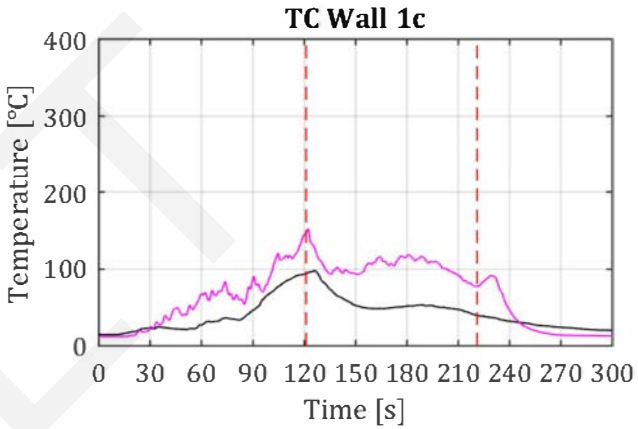
TC Wall 1c
Temperature [°C]
Time [s]

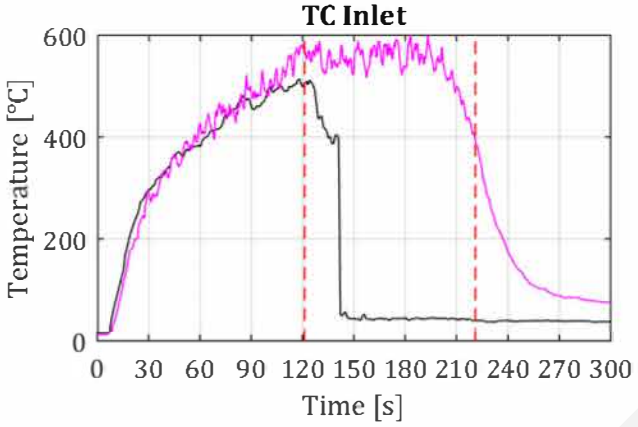
TC Inlet
Temperature [°C]
Time [s]

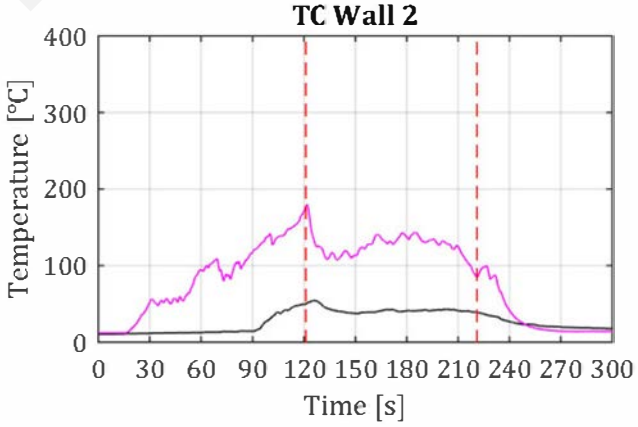
TC Wall 2
Temperature [°C]
Time [s]

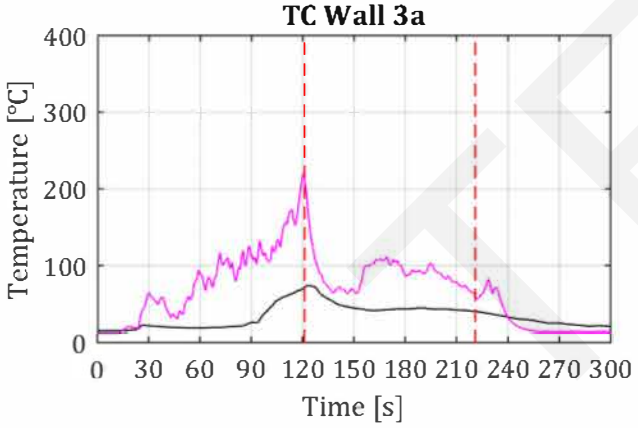
TC Wall 3a
Temperature [°C]
Time [s]

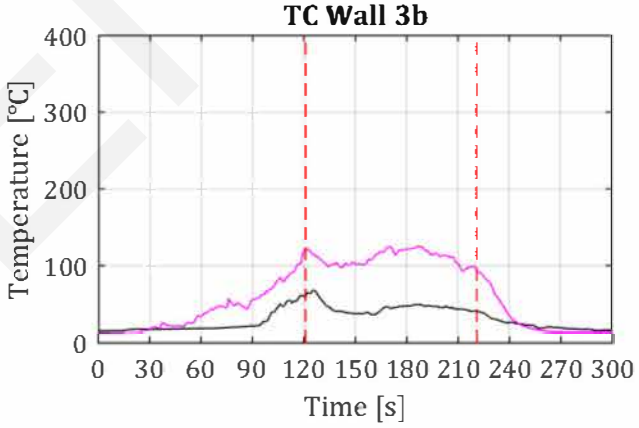
TC Wall 3b
Temperature [°C]
Time [s]

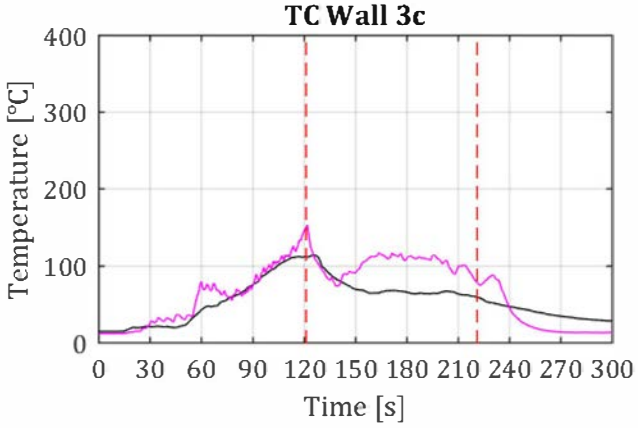
TC Wall 3c
Temperature [°C]
Time [s]

Computational time

In Table 1 an overview is given of the computational times of the models. Most simulations were done on a computer with an Intel Xeon CPU E5-2620 processor which has 6 cores and 12 threads. Also, several simulations ran on another desktop and laptop are used which have both a quad-core processor with 8 threads. The number of threads that can be assigned to a process determines the computational time of the simulation, a processor with more threads means in general more computational capacity.

The computation time is with a maximum of 30 h 40m acceptable for a CFD-model with the application of LES. However, in practice geometry of models can be much larger resulting in a much larger number of cells. Since a fine mesh is required for sprinkler modelling it is advisable to work with different scenarios and predict which sprinklers will activate first. Thereafter, the region around these sprinklers can be modelled with small cells and the other sprinkler regions which don't activate can be modelled with larger cells. This way the total number of cells can be reduced, resulting in shorter required computational time.

Table 1 - Overview computational time of FDS models

Model	**Simulation time [s]**	**HRR [kW]**	**Operating pressure [bar]**	**Computational time**		**Number of open threads per MPI process**
				With sprinkler	Without sprinkler	
RH0	420	267	NA	NA	46h 42m[a)]	1
RH1	240	266	NA	NA	21h 53m[b)]	1
RHT2	300	650	NA	NA	19h 51m	2
SH1	300	875	0.79	24h 40m	22h 3m	2
SH2	300	730	0.40	25h 33m	23h 6m	2
SH3	300	785	1.34	30h 40m	21h 51m	2
SH4	300	948	0.79	24h 12m	21h 45m	2
SH5	300	916	1.34	23h 22m	21h 1m	2
SHT1	300	978	0.79	23h 19m	20h 43m	2
SH3_simple	300	785	1.34	24h 30m	SH3	2
SH3_coarse	300	785	1.34	11h 34m[b)]	10h 57m[b)]	2
SH3_simple_coarse	300	785	1.34	11h 30m[b)]	10h 57m[b)]	2

a) Simulation is done on different pc with different processor
b) Simulation is done on a laptop with different processor

Smoke logging

In Figure 1 - Snapshot smoke layer height in FDS SH1 after 96 seconds, activation of sprinklerFigure 1 till Figure 12 snapshots are shown of the of the smoke layer height. The snapshots were taken with Smokeview 6.6.0 at the same times as the snapshots of the experiments in paragraph **Error! Reference source not found.**. Since the snapshots are only visual representations it is difficult to compare the models with the experiments. The results of models SH1 and SHT1 (both 0.79 bar) do not show much difference. The initial smoke layer at t_a=0 seems to be a little thicker for SHT1. At t_a=10 and t_a=30 the smoke layer descended about 30cm in both models and smoke is mixed with ambient air between the smoke layer and floor. Compared to the experiment the initial smoke layer is too thick in SH1 the predicted diffusing of smoke thereafter looks similar to the experiment. In SHT1 the opposite effect occurred, the initial smoke layer is similar to the experiment but

further descend of the smoke layer is not observed and smoke diffusing is underpredicted.

The initial smoke layer at t_a=0 of models SH2 (0.40) and SH3 (1.34 bar) are in good agreement with the measurements. As during the measurement almost no smoke logging is observed in the FDS model for SH2. For FDS model SH3 smoke loggings seems to be underestimated since during the experiments the visibility was significantly reduced.

The predicted smoke layer temperatures by FDS are higher than the measured temperatures which influence smoke logging. Higher smoke temperatures result in larger buoyant forces and less smoke descend and diffusing.

SH1

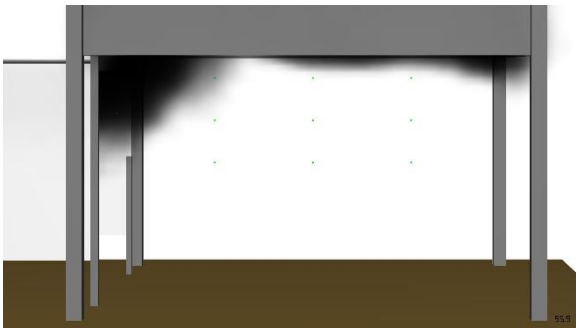

Figure 1 - Snapshot smoke layer height in FDS SH1 after 96 seconds, activation of sprinkler

SHT1

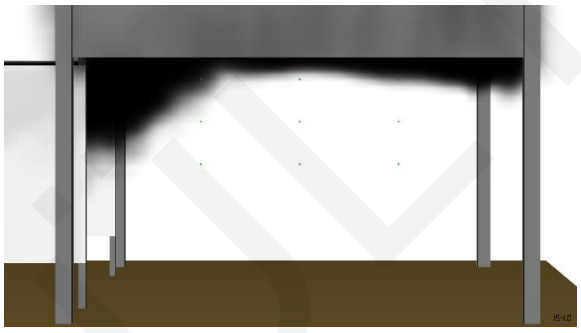

Figure 2 - Snapshot smoke layer height in FDS SHT1 after 154 seconds, activation of sprinkler

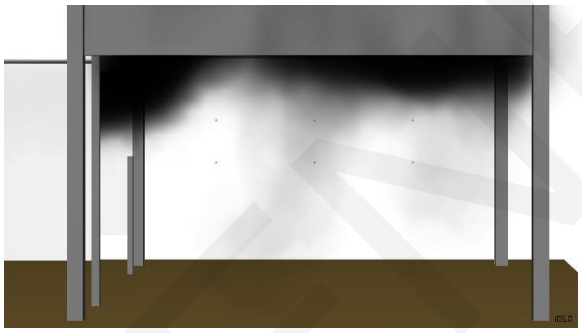

Figure 3 - Snapshot smoke layer height in FDS SH1 after 106 seconds, sprinkler active for 10 seconds

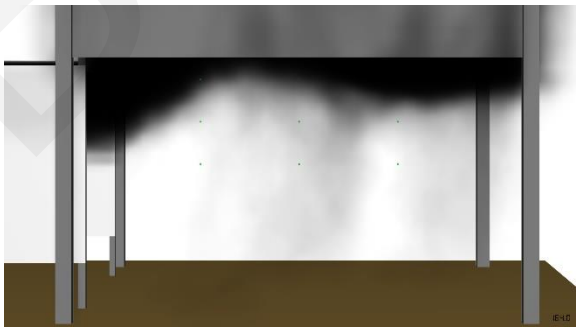

Figure 4 - Snapshot smoke layer height in FDS SHT1 after 164 seconds, sprinkler active for 10 seconds

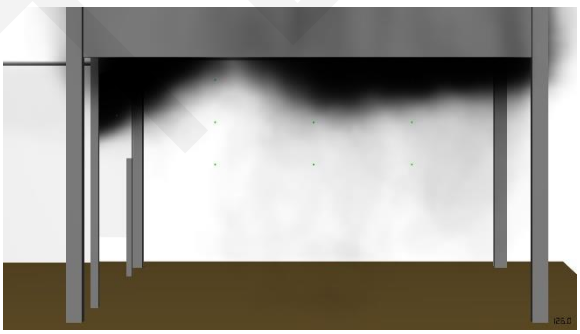

Figure 5 - Snapshot smoke layer height in FDS SH1 after 126 seconds, sprinkler active for 30 seconds

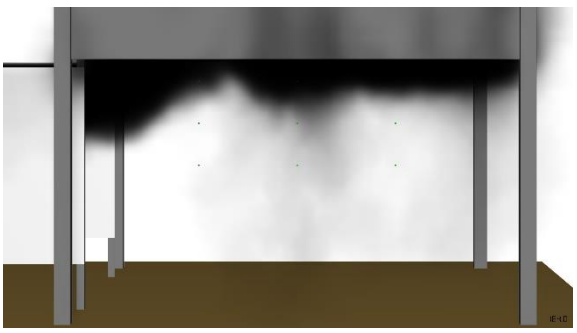

Figure 6 - Snapshot smoke layer height in FDS SHT1 after 184 seconds, sprinkler active for 30 seconds

SH2

Figure 7 - Snapshot smoke layer height in FDS SH2 after 118 seconds, activation of sprinkler

SH3

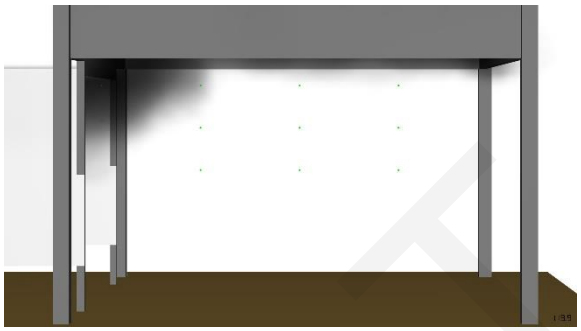

Figure 8 - Snapshot smoke layer height in FDS SH3 after 120 seconds, activation of sprinkler

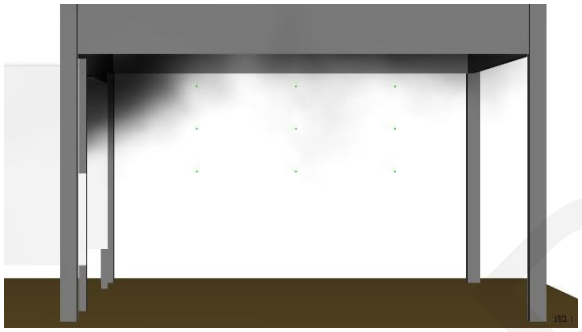

Figure 9 - Snapshot smoke layer height in FDS SH2 after 128 seconds, sprinkler active for 10 seconds

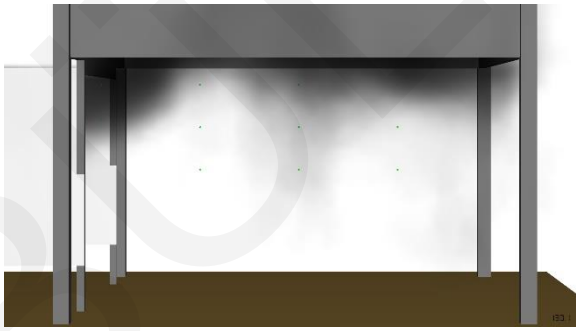

Figure 10 - Snapshot smoke layer height in FDS SH3 after 130 seconds, sprinkler active for 10 seconds

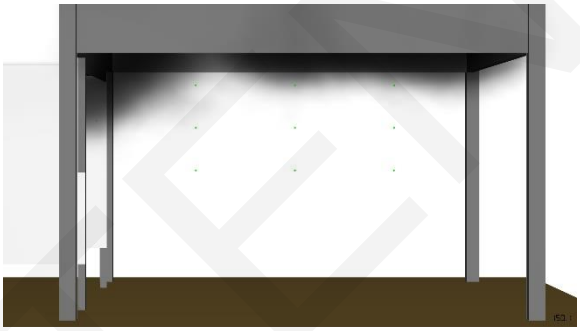

Figure 11 - Snapshot smoke layer height in FDS SH2 after 148seconds, sprinkler active for 30 seconds

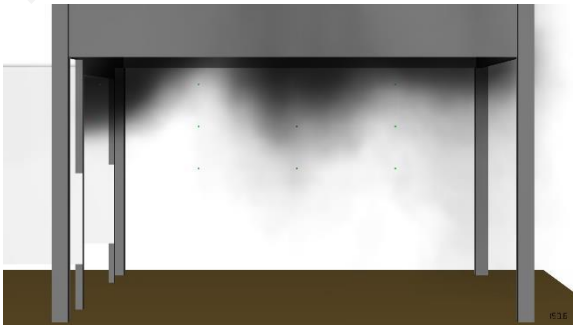

Figure 12 - Snapshot smoke layer height in FDS SH3 after 150 seconds, sprinkler active for 30 seconds

9 FDS script

Below the FDS script related to SH1 is added. Due to the excessive amount of code lines the sprinkler spray table (&TABL ID) is only given for azimuth angles 345° to 360°. For the same reason the inclined surfaces and pillars of the smoke cabinet are left out of the code below (&OBST ID).

```
SH1.fds
Generated by PyroSim - Version 2017.2.1115
16-apr-2018 10:12:30

&HEAD CHID='SH1', TITLE='Sprinkler Heptane 1'/
&TIME T_END=300.0/
&DUMP RENDER_FILE='SH1.ge1', COLUMN_DUMP_LIMIT=.TRUE./
&MISC P_INF=1.01893E5, TMPA=13.6, Y_CO2_INFTY=5.0E-4, Y_O2_INFTY=0.2095/

&MESH ID='Fine_5x5x5_S1', IJK=74,80,18, XB=1.15,4.85,0.9,4.9,2.7,3.6/
&MESH ID='Fine_5x5x5_S2', IJK=74,80,18, XB=1.15,4.85,0.9,4.9,1.8,2.7/
&MESH ID='Fine_5x5x5_S3', IJK=74,80,18, XB=1.15,4.85,0.9,4.9,0.9,1.8/
&MESH ID='Fine_5x5x5_S4', IJK=74,80,18, XB=1.15,4.85,0.9,4.9,0.0,0.9/
&MESH ID='Fine_5x5x5_B1', IJK=60,39,42, XB=1.5,4.5,6.45,8.4,0.0,2.1/
&MESH ID='Fine_5x5x5_B2', IJK=74,31,42, XB=1.15,4.85,4.9,6.45,0.0,2.1/

&ZONE ID='Hood', XB=1.6,4.4,1.5,4.3,1.65,3.05, LEAK_AREA=0.0336/

&SPEC ID='WATER VAPOR'/

&PART ID='Water',
    SPEC_ID='WATER VAPOR',
    DIAMETER=1050.6,
    MAXIMUM_DIAMETER=3000.0,
    AGE=5.0,
    SAMPLING_FACTOR=1,
    BREAKUP=.TRUE.,
    CHECK_DISTRIBUTION=.TRUE.,
    INITIAL_TEMPERATURE=11.5/

&REAC ID='HEPTANE',
    FYI='NIST NRC FDS5 Validation',
    FUEL='REAC_FUEL',
    FORMULA='C7H16',
    CO_YIELD=8.0E-3,
    SOOT_YIELD=0.015,
    HEAT_OF_COMBUSTION=4.456E4,
    RADIATIVE_FRACTION=0.4/

&RAMP ID='Control01_RAMP', T=95.75, F=-1.0/
&RAMP ID='Control01_RAMP', T=96.25, F=1.0/
&RAMP ID='Control01_RAMP', T=185.75, F=1.0/
&RAMP ID='Control01_RAMP', T=186.25, F=-1.0/

&PROP ID='Water Spray',
    PART_ID='Water',
    OFFSET=0.1,
    PARTICLES_PER_SECOND=10000,
    K_FACTOR=80.6,
    OPERATING_PRESSURE=0.79,
    SPRAY_PATTERN_TABLE='Water Spray_SPRAY_PATTERN_TABLE',
    SMOKEVIEW_ID='sprinkler_pendent'/

&TABL ID='Water Spray_SPRAY_PATTERN_TABLE', TABLE_DATA=2.0,8.0,345.0,360.0,12.3385,4.9694E-4/
&TABL ID='Water Spray_SPRAY_PATTERN_TABLE', TABLE_DATA=8.0,14.0,345.0,360.0,12.3385,1.2E-3/
&TABL ID='Water Spray_SPRAY_PATTERN_TABLE', TABLE_DATA=14.0,20.0,345.0,360.0,12.3385,2.6E-3/
&TABL ID='Water Spray_SPRAY_PATTERN_TABLE', TABLE_DATA=20.0,26.0,345.0,360.0,12.3385,4.3E-3/
&TABL ID='Water Spray_SPRAY_PATTERN_TABLE', TABLE_DATA=26.0,32.0,345.0,360.0,12.3385,5.5E-3/
&TABL ID='Water Spray_SPRAY_PATTERN_TABLE', TABLE_DATA=32.0,36.0,345.0,360.0,12.3385,5.4E-3/
&TABL ID='Water Spray_SPRAY_PATTERN_TABLE', TABLE_DATA=36.0,42.0,345.0,360.0,12.3385,4.2E-3/
&TABL ID='Water Spray_SPRAY_PATTERN_TABLE', TABLE_DATA=42.0,46.0,345.0,360.0,12.3385,3.7E-3/
```

```
&TABL ID='Water Spray_SPRAY_PATTERN_TABLE', TABLE_DATA=46.0,52.0,345.0,360.0,12.3385,4.4E-3/
&TABL ID='Water Spray_SPRAY_PATTERN_TABLE', TABLE_DATA=52.0,56.0,345.0,360.0,12.3385,5.2E-3/
&TABL ID='Water Spray_SPRAY_PATTERN_TABLE', TABLE_DATA=56.0,60.0,345.0,360.0,12.3385,5.4E-3/
&TABL ID='Water Spray_SPRAY_PATTERN_TABLE', TABLE_DATA=60.0,66.0,345.0,360.0,12.3385,4.3E-3/
&TABL ID='Water Spray_SPRAY_PATTERN_TABLE', TABLE_DATA=66.0,70.0,345.0,360.0,12.3385,2.7E-3/
&TABL ID='Water Spray_SPRAY_PATTERN_TABLE', TABLE_DATA=70.0,76.0,345.0,360.0,12.3385,1.0E-3/
&TABL ID='Water Spray_SPRAY_PATTERN_TABLE', TABLE_DATA=76.0,84.0,345.0,360.0,12.3385,2.8107E-4/
...
```

Azimuth angles 0° – 345° (with interval 15°) not shown.

```
&CTRL ID='Control01', FUNCTION_TYPE='CUSTOM', RAMP_ID='Control01_RAMP', LATCH=.FALSE., INPUT_ID='TIME'/
&DEVC ID='NOZZLE', PROP_ID='Water Spray', XYZ=3.0,2.9,2.9, ROTATION=7.5, LATCH=.FALSE., QUANTITY='CONTROL',
CTRL_ID='Control01'/

&DEVC ID='TC_1_1', QUANTITY='THERMOCOUPLE', XYZ=3.0,3.6,3.05/
&DEVC ID='TC_1_2', QUANTITY='THERMOCOUPLE', XYZ=3.0,3.6,2.7/
&DEVC ID='TC_1_3', QUANTITY='THERMOCOUPLE', XYZ=3.0,3.6,2.4/
&DEVC ID='TC_1_4', QUANTITY='THERMOCOUPLE', XYZ=3.0,3.6,2.1/
&DEVC ID='TC_1_5', QUANTITY='THERMOCOUPLE', XYZ=3.0,3.6,1.8/
&DEVC ID='TC_1_6', QUANTITY='THERMOCOUPLE', XYZ=3.0,3.6,1.5/
&DEVC ID='TC_1_7', QUANTITY='THERMOCOUPLE', XYZ=3.0,3.6,1.2/
&DEVC ID='TC_1_8', QUANTITY='THERMOCOUPLE', XYZ=3.0,3.6,0.9/
&DEVC ID='TC_2_1', QUANTITY='THERMOCOUPLE', XYZ=3.0,2.9,3.05/
&DEVC ID='TC_2_2', QUANTITY='THERMOCOUPLE', XYZ=3.0,2.9,2.7/
&DEVC ID='TC_2_3', QUANTITY='THERMOCOUPLE', XYZ=3.0,2.9,2.4/
&DEVC ID='TC_2_4', QUANTITY='THERMOCOUPLE', XYZ=3.0,2.9,2.1/
&DEVC ID='TC_2_5', QUANTITY='THERMOCOUPLE', XYZ=3.0,2.9,1.8/
&DEVC ID='TC_2_6', QUANTITY='THERMOCOUPLE', XYZ=3.0,2.9,1.5/
&DEVC ID='TC_2_7', QUANTITY='THERMOCOUPLE', XYZ=3.0,2.9,1.2/
&DEVC ID='TC_2_8', QUANTITY='THERMOCOUPLE', XYZ=3.0,2.9,0.9/
&DEVC ID='TC_3_1', QUANTITY='THERMOCOUPLE', XYZ=3.0,2.2,3.05/
&DEVC ID='TC_3_2', QUANTITY='THERMOCOUPLE', XYZ=3.0,2.2,2.7/
&DEVC ID='TC_3_3', QUANTITY='THERMOCOUPLE', XYZ=3.0,2.2,2.4/
&DEVC ID='TC_3_4', QUANTITY='THERMOCOUPLE', XYZ=3.0,2.2,2.1/
&DEVC ID='TC_3_5', QUANTITY='THERMOCOUPLE', XYZ=3.0,2.2,1.8/
&DEVC ID='TC_3_6', QUANTITY='THERMOCOUPLE', XYZ=3.0,2.2,1.5/
&DEVC ID='TC_3_7', QUANTITY='THERMOCOUPLE', XYZ=3.0,2.2,1.2/
&DEVC ID='TC_3_8', QUANTITY='THERMOCOUPLE', XYZ=3.0,2.2,0.9/
&DEVC ID='TC_wall_1b', QUANTITY='THERMOCOUPLE', XYZ=4.3,2.9,1.85/
&DEVC ID='TC_wall_2', QUANTITY='THERMOCOUPLE', XYZ=3.0,1.6,1.85/
&DEVC ID='TC_wall_3', QUANTITY='THERMOCOUPLE', XYZ=1.7,2.9,1.85/
&DEVC ID='TC_wall_01', QUANTITY='THERMOCOUPLE', XYZ=4.3,4.1,1.85/
&DEVC ID='TC_wall_1c', QUANTITY='THERMOCOUPLE', XYZ=4.3,1.7,1.85/
&DEVC ID='TC_wall_3a', QUANTITY='THERMOCOUPLE', XYZ=1.7,4.1,1.85/
&DEVC ID='TC_wall_3b', QUANTITY='THERMOCOUPLE', XYZ=1.7,1.7,1.85/
&DEVC ID='TC_duct', QUANTITY='THERMOCOUPLE', XYZ=3.0,2.9,3.35/
&DEVC ID='Velocity_inlet', QUANTITY='VELOCITY', XYZ=3.0,2.9,3.3/
&DEVC ID='Smoke_temp_inlet', QUANTITY='THERMOCOUPLE', XYZ=3.0,4.3,1.5/
&DEVC ID='SOLID', QUANTITY='WALL TEMPERATURE', XYZ=3.0,6.9,1.6, IOR=-3/
&DEVC ID='O2_fraction', QUANTITY='MASS FRACTION', SPEC_ID='OXYGEN', XYZ=3.0,2.9,3.3/
&DEVC ID='CO2_fraction', QUANTITY='MASS FRACTION', SPEC_ID='CARBON DIOXIDE', XYZ=3.0,2.9,3.3/
&DEVC ID='VolFlow_Inlet', QUANTITY='VOLUME FLOW -', XB=2.15,3.85,4.3,4.3,0.9,1.6/
&DEVC ID='HeatFlow_Exh', QUANTITY='HEAT FLOW +', XB=2.55,3.45,2.45,3.35,3.39,3.39/
&DEVC ID='HRR', QUANTITY='HRR', XB=2.15,3.85,6.45,7.8,0.0,1.6/
&DEVC ID='FLOW', QUANTITY='VOLUME FLOW +', XB=2.65,3.35,2.55,3.25,3.39,3.39/
&DEVC ID='TIME', QUANTITY='TIME', XYZ=1.15,0.9,2.7/

&MATL ID='STEEL',
    FYI='Drysdale, Intro to Fire Dynamics - ATF NIST Multi-Floor Validation',
    SPECIFIC_HEAT=0.46,
    CONDUCTIVITY=45.8,
    DENSITY=7850.0,
    EMISSIVITY=0.95/

&MATL ID='CALCIUM SILICATE',
    FYI='NBSIR 88-3752 - NBS Multi-Room Validation',
    SPECIFIC_HEAT_RAMP='CALCIUM SILICATE_SPECIFIC_HEAT_RAMP',
    CONDUCTIVITY=0.12,
    DENSITY=720.0,
    EMISSIVITY=0.83/
&RAMP ID='CALCIUM SILICATE_SPECIFIC_HEAT_RAMP', T=20.0, F=1.25/
&RAMP ID='CALCIUM SILICATE_SPECIFIC_HEAT_RAMP', T=200.0, F=1.25/
&RAMP ID='CALCIUM SILICATE_SPECIFIC_HEAT_RAMP', T=300.0, F=1.33/
&RAMP ID='CALCIUM SILICATE_SPECIFIC_HEAT_RAMP', T=600.0, F=1.55/
```

```
&SURF ID='STEEL',
    COLOR='GRAY 40',
    HEAT_TRANSFER_MODEL='LOGLAW',
    MATL_ID(1,1)='STEEL',
    MATL_MASS_FRACTION(1,1)=1.0,
    THICKNESS(1)=5.0E-3/

&SURF ID='STEEL2',
    COLOR='GRAY 40',
    LEAK_PATH=1,0,
    HEAT_TRANSFER_MODEL='LOGLAW',
    MATL_ID(1,1)='STEEL',
    MATL_MASS_FRACTION(1,1)=1.0,
    THICKNESS(1)=5.0E-3/

&SURF ID='Fire',
    COLOR='RED',
    HRRPUA=3131.0,
    RAMP_Q='Fire_RAMP_Q'/
&RAMP ID='Fire_RAMP_Q', T=0.0, F=0.0/
&RAMP ID='Fire_RAMP_Q', T=5.0, F=0.065/
&RAMP ID='Fire_RAMP_Q', T=15.0, F=0.234/
&RAMP ID='Fire_RAMP_Q', T=25.0, F=0.37/
&RAMP ID='Fire_RAMP_Q', T=35.0, F=0.437/
&RAMP ID='Fire_RAMP_Q', T=45.0, F=0.492/
&RAMP ID='Fire_RAMP_Q', T=55.0, F=0.517/
&RAMP ID='Fire_RAMP_Q', T=65.0, F=0.552/
&RAMP ID='Fire_RAMP_Q', T=75.0, F=0.579/
&RAMP ID='Fire_RAMP_Q', T=85.0, F=0.594/
&RAMP ID='Fire_RAMP_Q', T=95.0, F=0.631/
&RAMP ID='Fire_RAMP_Q', T=105.0, F=0.727/
&RAMP ID='Fire_RAMP_Q', T=115.0, F=0.706/
&RAMP ID='Fire_RAMP_Q', T=125.0, F=0.733/
&RAMP ID='Fire_RAMP_Q', T=135.0, F=0.765/
&RAMP ID='Fire_RAMP_Q', T=145.0, F=0.894/
&RAMP ID='Fire_RAMP_Q', T=155.0, F=0.936/
&RAMP ID='Fire_RAMP_Q', T=165.0, F=1.0/
&RAMP ID='Fire_RAMP_Q', T=175.0, F=0.982/
&RAMP ID='Fire_RAMP_Q', T=185.0, F=0.888/
&RAMP ID='Fire_RAMP_Q', T=195.0, F=0.923/
&RAMP ID='Fire_RAMP_Q', T=205.0, F=0.947/
&RAMP ID='Fire_RAMP_Q', T=215.0, F=0.918/
&RAMP ID='Fire_RAMP_Q', T=225.0, F=0.855/
&RAMP ID='Fire_RAMP_Q', T=235.0, F=0.62/
&RAMP ID='Fire_RAMP_Q', T=245.0, F=0.49/
&RAMP ID='Fire_RAMP_Q', T=255.0, F=0.346/
&RAMP ID='Fire_RAMP_Q', T=265.0, F=0.171/
&RAMP ID='Fire_RAMP_Q', T=275.0, F=0.095/
&RAMP ID='Fire_RAMP_Q', T=285.0, F=0.072/
&RAMP ID='Fire_RAMP_Q', T=295.0, F=0.05/
&RAMP ID='Fire_RAMP_Q', T=300.0, F=0.0/

&SURF ID='CALCIUM SILICATE',
    COLOR='GRAY 80',
    HEAT_TRANSFER_MODEL='LOGLAW',
    MATL_ID(1,1)='CALCIUM SILICATE',
    MATL_MASS_FRACTION(1,1)=1.0,
    THICKNESS(1)=0.0125/

&OBST ID='Walls_1', XB=1.55,1.6,1.5,4.3,2.7,3.05, THICKEN=.TRUE., SURF_ID='STEEL2'/
&OBST ID='Walls_1', XB=1.6,4.4,1.45,1.5,2.7,3.05, THICKEN=.TRUE., SURF_ID='STEEL2'/
&OBST ID='Walls_1', XB=1.6,4.4,4.3,4.35,2.7,3.05, THICKEN=.TRUE., SURF_ID='STEEL2'/
&OBST ID='Walls_1', XB=4.4,4.45,1.5,4.3,2.7,3.05, THICKEN=.TRUE., SURF_ID='STEEL2'/
&OBST ID='Walls_1', XB=1.55,1.6,1.5,4.3,1.8,2.7, THICKEN=.TRUE., SURF_ID='STEEL2'/
&OBST ID='Walls_1', XB=1.6,4.4,1.45,1.5,1.8,2.7, THICKEN=.TRUE., SURF_ID='STEEL2'/
&OBST ID='Walls_1', XB=1.6,4.4,4.3,4.35,1.8,2.7, THICKEN=.TRUE., SURF_ID='STEEL2'/
&OBST ID='Walls_1', XB=4.4,4.45,1.5,4.3,1.8,2.7, THICKEN=.TRUE., SURF_ID='STEEL2'/
&OBST ID='Walls_1', XB=1.55,1.6,1.5,4.3,1.65,1.8, THICKEN=.TRUE., SURF_ID='STEEL2'/
&OBST ID='Walls_1', XB=1.6,4.4,1.45,1.5,1.65,1.8, THICKEN=.TRUE., SURF_ID='STEEL2'/
&OBST ID='Walls_1', XB=1.6,4.4,4.3,4.35,1.65,1.8, THICKEN=.TRUE., SURF_ID='STEEL2'/
&OBST ID='Walls_1', XB=4.4,4.45,1.5,4.3,1.65,1.8, THICKEN=.TRUE., SURF_ID='STEEL2'/
&OBST ID='Walls_1', XB=2.15,2.15,4.3,4.9,0.9,1.6, SURF_ID='CALCIUM SILICATE'/
&OBST ID='Walls_1', XB=3.85,3.85,4.3,4.9,0.9,1.6, SURF_ID='CALCIUM SILICATE'/
&OBST ID='Walls_1', XB=2.15,2.15,4.3,4.9,0.3,0.9, SURF_ID='CALCIUM SILICATE'/
```

```
&OBST ID='Walls_1', XB=3.85,3.85,4.3,4.9,0.3,0.9, SURF_ID='CALCIUM SILICATE'/
&OBST ID='Walls_1', XB=2.15,3.85,7.8,7.8,0.3,1.6, SURF_ID='CALCIUM SILICATE'/
&OBST ID='Walls_1', XB=2.15,2.15,6.45,7.8,0.3,1.6, SURF_ID='CALCIUM SILICATE'/
&OBST ID='Walls_1', XB=3.85,3.85,6.45,7.8,0.3,1.6, SURF_ID='CALCIUM SILICATE'/
&OBST ID='Walls_1', XB=2.15,2.15,4.9,6.45,0.3,1.6, SURF_ID='CALCIUM SILICATE'/
&OBST ID='Walls_1', XB=3.85,3.85,4.9,6.45,0.3,1.6, SURF_ID='CALCIUM SILICATE'/
&OBST ID='Top_b', XB=2.15,3.85,4.3,4.9,1.6,1.6, SURF_ID='CALCIUM SILICATE'/
&OBST ID='Top_b', XB=2.15,3.85,6.45,7.8,1.6,1.6, SURF_ID='CALCIUM SILICATE'/
&OBST ID='Top_b', XB=2.15,3.85,4.9,6.45,1.6,1.6, SURF_ID='CALCIUM SILICATE'/
...
```

Inclined surfaces and pillars smoke cabinet are not shown.

```
&VENT ID='Mesh Vent: Fine_5x5x5_S1 [XMAX]', SURF_ID='OPEN', XB=4.85,4.85,0.9,4.9,2.7,3.6/
&VENT ID='Mesh Vent: Fine_5x5x5_S1 [XMIN]', SURF_ID='OPEN', XB=1.15,1.15,0.9,4.9,2.7,3.6/
&VENT ID='Mesh Vent: Fine_5x5x5_S1 [YMAX]', SURF_ID='OPEN', XB=1.15,4.85,4.9,4.9,2.7,3.6/
&VENT ID='Mesh Vent: Fine_5x5x5_S1 [YMIN]', SURF_ID='OPEN', XB=1.15,4.85,0.9,0.9,2.7,3.6/
&VENT ID='Mesh Vent: Fine_5x5x5_S1 [ZMAX]', SURF_ID='OPEN', XB=1.15,4.85,0.9,4.9,3.6,3.6/
&VENT ID='Mesh Vent: Fine_5x5x5_S2 [XMAX]', SURF_ID='OPEN', XB=4.85,4.85,0.9,4.9,1.8,2.7/
&VENT ID='Mesh Vent: Fine_5x5x5_S2 [XMIN]', SURF_ID='OPEN', XB=1.15,1.15,0.9,4.9,1.8,2.7/
&VENT ID='Mesh Vent: Fine_5x5x5_S2 [YMAX]', SURF_ID='OPEN', XB=1.15,4.85,4.9,4.9,2.1,2.7/
&VENT ID='Mesh Vent: Fine_5x5x5_S2 [YMIN]', SURF_ID='OPEN', XB=1.15,4.85,0.9,0.9,1.8,2.7/
&VENT ID='Mesh Vent: Fine_5x5x5_S3 [XMAX]', SURF_ID='OPEN', XB=4.85,4.85,0.9,4.9,0.9,1.8/
&VENT ID='Mesh Vent: Fine_5x5x5_S3 [XMIN]', SURF_ID='OPEN', XB=1.15,1.15,0.9,4.9,0.9,1.8/
&VENT ID='Mesh Vent: Fine_5x5x5_S3 [YMIN]', SURF_ID='OPEN', XB=1.15,4.85,0.9,0.9,0.9,1.8/
&VENT ID='Mesh Vent: Fine_5x5x5_S4 [XMAX]', SURF_ID='OPEN', XB=4.85,4.85,0.9,4.9,0.0,0.9/
&VENT ID='Mesh Vent: Fine_5x5x5_S4 [XMIN]', SURF_ID='OPEN', XB=1.15,1.15,0.9,4.9,0.0,0.9/
&VENT ID='Mesh Vent: Fine_5x5x5_S4 [YMIN]', SURF_ID='OPEN', XB=1.15,4.85,0.9,0.9,0.0,0.9/
&VENT ID='Mesh Vent: Fine_5x5x5_B1 [XMAX]', SURF_ID='OPEN', XB=4.5,4.5,6.45,8.4,0.0,2.1/
&VENT ID='Mesh Vent: Fine_5x5x5_B1 [XMIN]', SURF_ID='OPEN', XB=1.5,1.5,6.45,8.4,0.0,2.1/
&VENT ID='Mesh Vent: Fine_5x5x5_B1 [YMAX]', SURF_ID='OPEN', XB=1.5,4.5,8.4,8.4,0.0,2.1/
&VENT ID='Mesh Vent: Fine_5x5x5_B1 [ZMAX]', SURF_ID='OPEN', XB=1.5,4.5,6.45,8.4,2.1,2.1/
&VENT ID='Mesh Vent: Fine_5x5x5_B2 [XMAX]', SURF_ID='OPEN', XB=4.85,4.85,4.9,6.45,0.0,2.1/
&VENT ID='Mesh Vent: Fine_5x5x5_B2 [XMIN]', SURF_ID='OPEN', XB=1.15,1.15,4.9,6.45,0.0,2.1/
&VENT ID='Mesh Vent: Fine_5x5x5_B2 [YMAX]', SURF_ID='OPEN', XB=4.5,4.85,6.45,6.45,0.0,2.1/
&VENT ID='Mesh Vent: Fine_5x5x5_B2 [YMAX]', SURF_ID='OPEN', XB=1.15,1.5,6.45,6.45,0.0,2.1/
&VENT ID='Mesh Vent: Fine_5x5x5_B2 [ZMAX]', SURF_ID='OPEN', XB=1.15,4.85,4.9,6.45,2.1,2.1/
&VENT ID='Vent', SURF_ID='HVAC', XB=2.65,3.35,2.55,3.25,3.4,3.4, RGB=240,2,255, RADIUS=0.35, XYZ=3.0,2.9,3.4/

&HVAC ID='Duct', TYPE_ID='DUCT', DIAMETER=0.7, VOLUME_FLOW=2.77, RAMP_ID='Duct_RAMP_ID', NODE_ID='Air_inlet','Outlet',
ROUGHNESS=1.0E-3/
&HVAC ID='Air_inlet', TYPE_ID='NODE', DUCT_ID='Duct', VENT_ID='Vent'/
&HVAC ID='Outlet', TYPE_ID='NODE', DUCT_ID='Duct', AMBIENT=.TRUE., XYZ=3.0,2.9,3.6/
&RAMP ID='Duct_RAMP_ID', T=0.0, F=0.511/
&RAMP ID='Duct_RAMP_ID', T=7.5, F=0.617/
&RAMP ID='Duct_RAMP_ID', T=22.5, F=0.732/
&RAMP ID='Duct_RAMP_ID', T=37.5, F=0.808/
&RAMP ID='Duct_RAMP_ID', T=52.5, F=0.785/
&RAMP ID='Duct_RAMP_ID', T=67.5, F=0.872/
&RAMP ID='Duct_RAMP_ID', T=82.5, F=0.885/
&RAMP ID='Duct_RAMP_ID', T=97.5, F=0.859/
&RAMP ID='Duct_RAMP_ID', T=112.5, F=0.699/
&RAMP ID='Duct_RAMP_ID', T=127.5, F=0.697/
&RAMP ID='Duct_RAMP_ID', T=142.5, F=0.694/
&RAMP ID='Duct_RAMP_ID', T=157.5, F=0.656/
&RAMP ID='Duct_RAMP_ID', T=172.5, F=0.684/
&RAMP ID='Duct_RAMP_ID', T=187.5, F=0.763/
&RAMP ID='Duct_RAMP_ID', T=202.5, F=0.948/
&RAMP ID='Duct_RAMP_ID', T=217.5, F=0.94/
&RAMP ID='Duct_RAMP_ID', T=232.5, F=1.0/
&RAMP ID='Duct_RAMP_ID', T=247.5, F=0.836/
&RAMP ID='Duct_RAMP_ID', T=262.5, F=0.643/
&RAMP ID='Duct_RAMP_ID', T=277.5, F=0.64/
&RAMP ID='Duct_RAMP_ID', T=292.5, F=0.586/

&BNDF QUANTITY='AMPUA', PART_ID='Water'/
&BNDF QUANTITY='MPUA', PART_ID='Water'/
&BNDF QUANTITY='WALL TEMPERATURE'/

&SLCF QUANTITY='TEMPERATURE', PBY=2.9/
&SLCF QUANTITY='VELOCITY', VECTOR=.TRUE., PBY=2.9/
&SLCF QUANTITY='TEMPERATURE', PBX=3.0/
&SLCF QUANTITY='VELOCITY', VECTOR=.TRUE., PBX=3.0/
&SLCF QUANTITY='PARTICLE FLUX Z', PART_ID='Water', PBZ=0.05/
&SLCF QUANTITY='PRESSURE', PBY=2.9/
```

```
&SLCF QUANTITY='PRESSURE', PBX=3.0/
&SLCF QUANTITY='DENSITY', PBY=2.9/
&SLCF QUANTITY='DENSITY', PBX=3.0/
&SLCF QUANTITY='MIXTURE FRACTION', PBY=2.9/
&SLCF QUANTITY='MIXTURE FRACTION', PBX=3.0/
&SLCF QUANTITY='OPTICAL DENSITY', PBY=2.9/
&SLCF QUANTITY='OPTICAL DENSITY', PBX=3.0/

&DEVC ID='Temperature_MEAN', QUANTITY='TEMPERATURE', STATISTICS='MEAN', XB=1.6,4.4,1.5,2.9,1.8,2.7/
&DEVC ID='Temperature_MIN', QUANTITY='TEMPERATURE', STATISTICS='MIN', XB=1.6,4.4,1.5,2.9,1.8,2.7/
&DEVC ID='Temperature_MAX', QUANTITY='TEMPERATURE', STATISTICS='MAX', XB=1.6,4.4,1.5,2.9,1.8,2.7/
&DEVC ID='Temp 3.0m_MEAN', QUANTITY='TEMPERATURE', STATISTICS='MEAN', XB=1.6,4.4,1.5,4.3,3.0,3.0/
&DEVC ID='Temp 3.0m_MIN', QUANTITY='TEMPERATURE', STATISTICS='MIN', XB=1.6,4.4,1.5,4.3,3.0,3.0/
&DEVC ID='Temp 3.0m_MAX', QUANTITY='TEMPERATURE', STATISTICS='MAX', XB=1.6,4.4,1.5,4.3,3.0,3.0/
&DEVC ID='Temp 2.7m_MEAN', QUANTITY='TEMPERATURE', STATISTICS='MEAN', XB=1.6,4.4,1.5,4.3,2.7,2.7/
&DEVC ID='Temp 2.7m_MIN', QUANTITY='TEMPERATURE', STATISTICS='MIN', XB=1.6,4.4,1.5,4.3,2.7,2.7/
&DEVC ID='Temp 2.7m_MAX', QUANTITY='TEMPERATURE', STATISTICS='MAX', XB=1.6,4.4,1.5,4.3,2.7,2.7/
&DEVC ID='Temp 2.4m_MEAN', QUANTITY='TEMPERATURE', STATISTICS='MEAN', XB=1.6,4.4,1.5,4.3,2.4,2.4/
&DEVC ID='Temp 2.4m_MIN', QUANTITY='TEMPERATURE', STATISTICS='MIN', XB=1.6,4.4,1.5,4.3,2.4,2.4/
&DEVC ID='Temp 2.4m_MAX', QUANTITY='TEMPERATURE', STATISTICS='MAX', XB=1.6,4.4,1.5,4.3,2.4,2.4/
&DEVC ID='Temp 2.1m_MEAN', QUANTITY='TEMPERATURE', STATISTICS='MEAN', XB=1.6,4.4,1.5,4.3,2.1,2.1/
&DEVC ID='Temp 2.1m_MIN', QUANTITY='TEMPERATURE', STATISTICS='MIN', XB=1.6,4.4,1.5,4.3,2.1,2.1/
&DEVC ID='Temp 2.1m_MAX', QUANTITY='TEMPERATURE', STATISTICS='MAX', XB=1.6,4.4,1.5,4.3,2.1,2.1/
&DEVC ID='Temp 1.8m_MEAN', QUANTITY='TEMPERATURE', STATISTICS='MEAN', XB=1.6,4.4,1.5,4.3,1.8,1.8/
&DEVC ID='Temp 1.8m_MIN', QUANTITY='TEMPERATURE', STATISTICS='MIN', XB=1.6,4.4,1.5,4.3,1.8,1.8/
&DEVC ID='Temp 1.8m_MAX', QUANTITY='TEMPERATURE', STATISTICS='MAX', XB=1.6,4.4,1.5,4.3,1.8,1.8/
&DEVC ID='Temp 1.5m_MEAN', QUANTITY='TEMPERATURE', STATISTICS='MEAN', XB=1.6,4.4,1.5,4.3,1.5,1.5/
&DEVC ID='Temp 1.5m_MIN', QUANTITY='TEMPERATURE', STATISTICS='MIN', XB=1.6,4.4,1.5,4.3,1.5,1.5/
&DEVC ID='Temp 1.5m_MAX', QUANTITY='TEMPERATURE', STATISTICS='MAX', XB=1.6,4.4,1.5,4.3,1.5,1.5/
&DEVC ID='Temp 1.2m_MEAN', QUANTITY='TEMPERATURE', STATISTICS='MEAN', XB=1.6,4.4,1.5,4.3,1.2,1.2/
&DEVC ID='Temp 1.2m_MIN', QUANTITY='TEMPERATURE', STATISTICS='MIN', XB=1.6,4.4,1.5,4.3,1.2,1.2/
&DEVC ID='Temp 1.2m_MAX', QUANTITY='TEMPERATURE', STATISTICS='MAX', XB=1.6,4.4,1.5,4.3,1.2,1.2/


&TAIL /
```

10 MATLAB script

Below the Matlab script is given which can be used to calculate the input for the spray pattern table. The measurement data of the bucket test is translated into a mass fraction table for azimuth angles from 0° to 360° with an interval of 15° and 15 buckets per interval. Therefore the, input-file with measurement data must contain a 15x24 matrix. Hereby is each number a mass fraction of the total water flow. The sum of all values with the matrix must be ≤1.

```
clear all
close all

% in the model the volume median diameter is assumed for the droplet size.
% the trajectories are only calculated for one single droplet size
% the injection velocity vtot(0)is assumed to be the same for all
% directions (injection angles)
% the input file must contain 15 rows (buckets) and 24 columns (mass
% fractions for azimuth ranges of 15°). the sum of all cells must be equal to 1.

%input
P           = 0.40;          %Bar
g           = 9.81;          %m/s2
Tamb        = 286;           %K
visk        = 1.49*10.^-5*0.518*(Tamb/293)*((Tamb/293+1.55).^0.7); %m2/s
rho_air     = 1.23;          %kg/m3
L_max       = 3.975;         %midpoint of last bucket
W_buck      = 0.266;         %width of one bucket
rb = W_buck/2:W_buck:L_max;  %calculate horizontal distance r from each bucket until
                             %the sprinkler nozzle
rb=rb';
mass_table=importdata('0_40bar_mass.txt');  %import measurement data
%mass_table=importdata('0_79bar_mass.txt'); %import measurement data
%mass_table=importdata('1_34bar_mass.txt'); %import measurement data

%discretization parameters
dt_input    = 0.01;     %step size in time[s]
ds          = 10;       %step size between droplets [micro m]
d_max       = 10e3;     %maximum droplet size [micro m]

%water properties
sigma_water = 72.8e-3;      %N/m       Surface tension
rho_water   = 1000;         %kg/m3     Density
cp_water    = 4200;         %J/(kgK)   Heat capacity

%sprinkler parameters:
sp.Cm       = 2.7;          %Lawson(1988) SSP (Standard Sprinkler Pendent) 11mm
                            %orifice
sp.c        = 80.6;         %k-factor (L/min(sqrt(P))
sp.dn       = 11.1e-3;      %m
sp.alpha    = 1.0;          %ratio velocity nozzle and initial velocity of droplets
height      = 2.90;         %m Sprinkler height

%calculate spray characteristics
V    = (sp.c*sqrt(P))/60/1000;          %flow rate [m3/s]
U    = V/(pi/4*sp.dn^2);                %velocity at sprinkler nozzle[m/s]
We   = (rho_water*U^2*sp.dn)/sigma_water;   %Weber getal
dm   = sp.Cm*We^(-1/3)*sp.dn;               %volume median droplet diameter[m]
%dm=10e-4;                                  %OPTION TO CHANGE DROPLET SIZE IN MODEL
da=2;               %step size between elevation angles
amax=110;           %maximum elevation angle
amin=0;             %minimal elevation angle
```

```
a=amin:da:amax;     %distribution of elevation angles

vra   = sp.alpha*U*sin(a/180*pi);   % initial velocity horizontal [m/s]
vza   = sp.alpha*U*cos(a/180*pi);   % initial velocity vertical [m/s]

size_dist  = (ds:ds:5000)/1e6;    %droplet sizes

i_d = 1;                          %iteration in droplet size

for s=size_dist

    dt=dt_input;                  %delta t (time)
    i=0;                          %start value
    t=0;                          %start value

    n=(amax-amin)/da+1;           % number of angles
    for e=1:1:n
    vtot(e)=sqrt(vra(e).^2+vza(e).^2);  %set initial velocity for all angles
    x(e)=0;     %set initial horizontal displacement to 0 for all angles
    y(e)=0;     %set initial vertical displacement to 0 for all angles
    end

    %iteration droplet size
    m(i_d)  = 4/3*pi*(s/2)^3*rho_water; %mass of droplets size distribution, NOT
                                        %IMPLEMENTED any further
    Ad(i_d) = 4*pi*(s/2)^2;             %surface of droplets size distribution,
                                        %NOT IMPLEMENTED any further

    i_d=i_d+1;
end

    de=200;     %total number of iterations, if one of the droplets does not reach
                %the floor (h=0) within the number of iterations this number should
be
                %increased
    i=1;
    for i=1:1:de

        for c=1:1:n

        %Drag coefficient Cd for all iterations and different trajectories
        %by angles
        Re(i,c)   = (vtot(i,c)*dm)/visk;    % calculate Reynolds number

        if Re(i,c)<1
        Cd(i,c) = 24/Re(i,c);
        elseif Re(i,c)<800
        Cd(i,c) = 12.6/Re(i,c).^0.5;
        elseif Re(i,c)>800
        Cd(i,c) = 0.44;
        end

        % velocity
        vtot(i,c)=sqrt(vra(i,c).^2+vza(i,c).^2); %velocity by horizontal
                                                 %velocity vra and vertical vza


dvzdt(i,c)=g                                                                    -
3/4*((Cd(i,c)*sqrt(vra(i,c).^2+vza(i,c).^2)*vza(i,c))/(rho_water*dm));    %vertical
velocity increase/decrease per time step (i) for all angles (c)
dvrdt(i,c)= - 3/4*((Cd(i,c)*sqrt(vra(i,c).^2+vza(i,c).^2)*vra(i,c))/(rho_water*dm));
%horizontal velocity increase/decrease per time step (i) for all angles (c)

        vra(i+1,c)=vra(i,c)+dvrdt(i,c)*dt;  %horizontal velocity after iteration
        vza(i+1,c)=vza(i,c)+dvzdt(i,c)*dt;  %vertical velocity after iteration
```

```
        vtot(i+1,c)=sqrt(vza(i,c).^2+vra(i,c).^2);  %total velocity after iteration

        % execute iteration forward Euler
        x(i+1,c) = x(i,c) + vra(i,c)*dt;    %horizontal displacement after iteration
        y(i+1,c) = y(i,c) + vza(i,c)*dt;    %vertical displacement after iteration

        h=2.9-y;        %height of the droplet after iteration

        H2=[];
        for c=1:1:n     %find for every angle cell at which h<0
        H=(h<0);
        H1=find(H(:,c),1,'first');
        H2{c}=H1;
        end

        z=1:1:n;

        end
        c=c+1;

     end
     i=i+1;
    H3=cell2mat(H2);            %convert cell data into matrix
    IND=zeros([de+1,n]);        %create matrix with all zeros for height at all
                                %iterations (row) per angle (column)
    lin_ind=sub2ind(size(IND),H3,z);%convert sub-indices into indices to select
                                %iterations at which h<0
    r=x(lin_ind);               %radius at floor for all different elevation angles

nb=size(mass_table,1);              %number of buckets
lim=4.108:-0.266:(4.108-0.266*nb);  %edges of bucket as distance to center
LIM=fliplr(lim);                    %flip the values of the row (low>high)

upp=LIM(2:nb+1);    %outer edge of the buckets
low=LIM(1:nb);      %inner edge of the buckets

upp=upp';           %transpose outer edges into column
low=low';           %transpose inner edges into column

%calculate the minimal error to find the angle corresponding to every position
%outer angles of buckets
for b=1:size(upp,1)
    er=abs(r-abs(upp(b)));
    index = find(er==min(er));
    spray_angle(b)=a(index);
end

%inner angels of buckets
    for b1=1:size(low,1)
        er1=abs(r-abs(low(b1)));
        index1 = find(er1==min(er1));
        spray_angle_low(b1)=a(index1);
    end
spr_angle_low=spray_angle_low';     %transpose inner angles into column
spr_angle=spray_angle';             %transpose outer angles into column

az1=345:-15:0;                     %create row for inner azimuth angles, 15° spacing
az1=az1';                           %transpose row inner angles into column
az2=360:-15:15;                    %create row for outer azimuth angles, 15° spacing
az2=az2';                           %transpose row outer azimuth into column

Lat1=repmat(spr_angle_low,24,1);    %create column with latitude1 angles, repetition
                                    %for n buckets
Lat2=repmat(spr_angle,24,1);        %create column with latitude2 angles, repetition
                                    %for n buckets
```

```
vel=ones(360,1)*vtot(1);            %create column with equal velocities

for lp=1:1:24
    Lg1(:,lp)=repmat(az1(lp),15,1); %create matrix with inner longitude angles with
                                    %columns nx15°

end
Long1 = reshape(Lg1,[360,1]);         %reshape the matrix with n columns into one
column

for lp=1:1:24
    Lg2(:,lp)=repmat(az2(lp),15,1); %create matrix with outer longitude angles with
                                    %columns nx15°

end
Long2 = reshape(Lg2,[360,1]);         %reshape the matrix with n columns into one
column

mass_f=reshape(mass_table,[360,1]); %create column with 360rows from mass_table
sum_mass_f=sum(mass_f');            %total mass, must be =1 or <1
%%

% % %plotting of the results
f = figure;
p = uipanel('Parent',f,'BorderType','none');
p.BackgroundColor = [1 1 1];
set(gcf, 'Units', 'Normalized', 'OuterPosition', [0, 0.04, 1, 0.96]);

subplot(2,2,1,'Parent',p)
plot(upp,spray_angle,'*');
hold on
plot(low,spray_angle_low,'o');
hold on
title('Bucket edges and corresponding elevation angles droplet injection')
xlabel('Horizontal distance from nozzle at floor [m]');
ylabel('corresponding spray angle (latitude) [°]')
ylim([0 110])
legend('outer edge bucket', 'inner edge bucket','Location','northwest')
grid on
grid minor
ax = gca;
ax.YTick = [0:10:120];

subplot(2,2,3,'Parent',p)
plot (x,h)
ylim ([0,3.5])
title('Elevation angles droplet injection \delta\theta = 2°, \thetamax=110°')
xlabel('Horizontal distance from nozzle at floor[m]');
ylabel('Height [m]')
%legend('delta angle=2°')

TABLE = [mass_f vel Lat1 Lat2 Long1 Long2];
indices = find(TABLE(:,1)==0);
    TABLE(indices,:) = [];

%subplot(2,2,2,'Parent',p)
table = uitable(p);
table.Data = TABLE;
table.Units='Normalized';
table.Position = [0.55 0 0.4 1];
table.ColumnName = {'Flow fraction','Velocity
(m/s)','Lat1(°)','Lat2(°)','Long1(°)','Long2(°)'};
```